UNIVERSITAT DE BARCELONA

# WT1 in heart and gonad development: a crucial gene for cell plasticity and differentiation

Alejo Torres Cano

# WT1 IN HEART AND GONAD DEVELOPMENT: A CRUCIAL GENE FOR CELL PLASTICITY AND DIFFERENTIATION

**Alejo Torres Cano**

**Barcelona, March 2021**


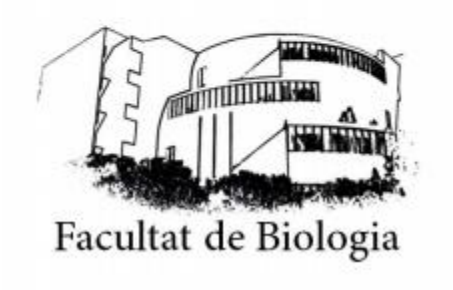


**Department of Cell Biology, Physiology and Immunology**

**Doctoral programme in Biomedicine**

Dissertation submitted by

Alejo Torres Cano

To apply for a doctorate from the "Universitat de Barcelona"

This work, titled*, Wt1 in heart and gonad development: a crucial gene for cell plasticity and differentiation*, was performed at Celltec-UB lab, in the department of Cell biology, Physiology and Immunology, in the Faculty of Biology from the Universitat de Barcelona under the supervision of Dr. Ofelia M. Martínez Estrada and Dr. Manuel Reina del Pozo.

| Director, | Co-director and tutor, | Student, |
|---|---|---|
| Ofelia M. Martínez Estrada | Manuel Reina del Pozo | Alejo Torres Cano |

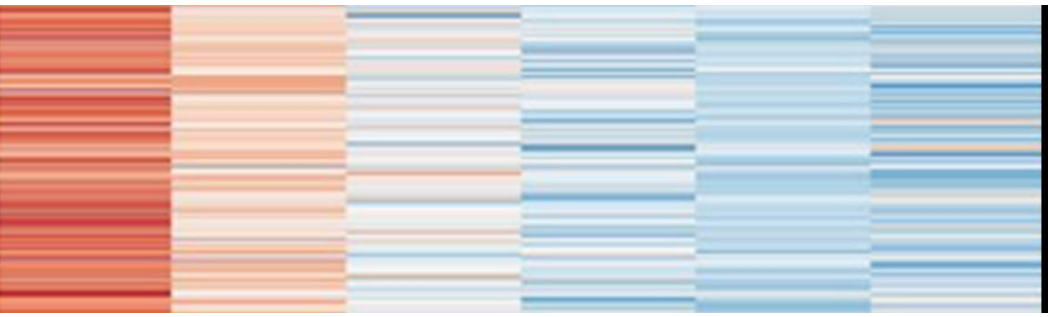

# ABSTRACT

*Wt1* is a complex gene that encodes a protein whose best described function is to act as a transcription factor. *Wt1* plays a crucial role in several organ developments, including kidneys, liver, heart or gonads. Moreover, *Wt1* is implicated in the etiology of a set of syndromes and diseases ranging from cancer to disorders of sex development (DSD). Additionally, *Wt1* has been described to play a role in adult homeostasis. In this thesis, I focused on *Wt1* role in development, specifically in gonad and heart morphogenesis. For this purpose, I used two previously described *Cre* mouse models to generate two different *Wt1KOs*.

The heart is the first organ being formed and it is primarily composed of three layers: the endocardium, the myocardium and the epicardium. The epicardium is a mesothelial layer of cells covering the vertebrate heart surface. Epicardial cells give rise to epicardial derived cells (EPDCs), progenitors of crucial cell types in heart development like vascular smooth muscle cells and cardiac fibroblasts. Moreover, the epicardium contributes to heart morphogenesis by secreting paracrine factors. After myocardial infarction, the epicardium embryonic genetic signature is reactivated. Thus, understanding the mechanisms behind epicardial development constitutes a topic of general interest.

The epicardial genetic program has been previously characterized and the *Wt1* role in the regulation of this program has been established. One of the pathways modulated during epicardium development is the BMP4 pathway. The results of this thesis demonstrate that WT1 directly regulates *Bmp4* expression. Additionally, exposed results demonstrate how the BMP4 pathway is crucial for epicardial cell maturation, through the regulation of cell morphology, from a cuboidal to a squamous cell shape, epicardial proliferation, and transcriptomic changes. Finally, the data shown in this work indicated that changes and mechanisms described for epicardium may be a phenomenon extrapolated to other mesotheliums like the lung mesothelium.

To better study Wt1 role in the development of other organs, we have characterized the recombination activity of a $Wt1^{Cre}$ mouse model using two different reporter mouse models, the $R26R^{mTmG}$ and the $R26R^{tdRFP}$. Results demonstrated that $Wt1^{Cre}$ is efficiently activated in hearts and gonads but not in other organs generated from the genital ridge, like the kidney or the adrenal gland. Taking advantage of this, the $Wt1^{Cre}$ mouse model was used to generate a new *Wt1KO*: the $Wt1^{Cre}; Wt1^{Loxp/GFP}$. $Wt1^{Cre}; Wt1^{Loxp/GFP}$ mice show a partial embryonic lethality, potentially caused by defects in heart development, but some of them reach adulthood, becoming an ideal model to investigate *Wt1* role from embryonic to adult stages. Therefore, we decided to study *Wt1*role in gonad development in $Wt1^{Cre}; Wt1^{Loxp/GFP}$ mice.

Sex development is a complex and coordinated process that starts with the differentiation of the bipotential gonads. *WT1* mutations or haploinsufficiency have been reported in different syndromes and conditions linked to DSD. The study of WT1 role in embryonic development and the impact on adult sex development has been hampered by the complete gonadal agenesis or embryonic lethality presented by other Wt1KO mouse models.

The results presented demonstrate a sharp reduction in *Wt1* levels in $Wt1^{Cre}; Wt1^{Loxp/GFP}$ gonads since the bipotential stage. This causes, in the adult, the formation of small, atrophic gonads, a hermaphroditism of the genital tract and external ambiguous genitalia. Besides, the data reported in this thesis demonstrates that $Wt1^{Cre}; Wt1^{Loxp/GFP}$ mice present an impaired gonad embryonic development due to the lack of differentiation of the main cell lineages responsible for gonad development and function: supportive cells, steroidogenic cells and primordial germ cells (PGCs).

Finally, the observed sub-lethality in $Wt1^{Cre}; Wt1^{Loxp/GFP}$ mice is explained by the observation of a severe heart developmental impairment in a portion of $Wt1^{Cre}; Wt1^{Loxp/GFP}$ embryos, whereas others show no apparent heart defects at embryonic stages. Equally, an histological study performed on $Wt1^{Cre}; Wt1^{Loxp/GFP}$ mice also described changes in the spleen and brown adipose tissue.

In summary, our results indicate the importance of morphological changes epicardial cells undergo during development, a process regulated by *Wt1* modulation of the BMP4 pathway. In addition, the generation and characterization of the $Wt1^{Cre}; Wt1^{Loxp/GFP}$ mouse renders an informative and useful tool to study *Wt1* role beyond embryonic stages and provide a more accurate frame for the understanding of results previously obtained when using the $Wt1^{Cre}$ mouse model.

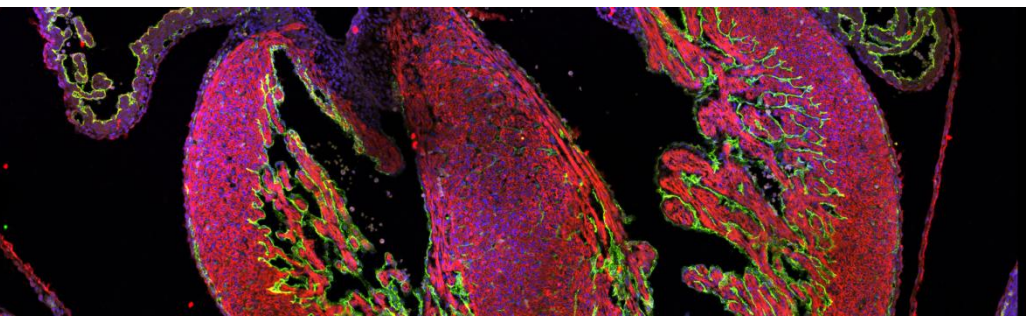

# ACKNOWLEDGMENTS

*Sería demasiado largo agradecer como merecen a todas las personas que de una u otra forma han contribuido a que esta tesis llegue a su fin. Basten las siguientes líneas como muestra del sincero agradecimiento que les debo.*

*En primer lugar debo agradecer a Ofelia haberme aceptado como su estudiante, ya en aquellos lejanos tiempos en que terminaba el grado y luego como estudiante de máster y de doctorado. A lo largo de estos años he aprendido de ti lo que sé de ciencia. Gracias por haber estado siempre dispuesta a ayudarme: cuando los tiempos se apuraban y llegaban horas intempestivas, cuando parecía que nada salía adelante; cuando en momentos en que desfallecía, fuiste comprensiva.*

*En segundo lugar, gracias a Manuel. Gracias por encontrar, sin poner nunca ningún reparo, el dinero necesario para permitirme terminar la tesis, por esforzarte en buscar para todos oportunidades que complementaran el doctorado. Gracias por enseñarme cómo la exigencia puede compaginarse con la empatía y cómo una ética de trabajador incansable no implica olvidarse de lo demás. Gracias por tu interés sincero y por tu compromiso.*

*En las neveras del laboratorio hay repartidas varias fotos. Son los recuerdos que quedan de tantos momentos de verdadera alegría. En ellas estamos todos: Ana, Marina, Marc, Raquel, Adrián, Sergi, Rubén, Claudia. Cuando vuelva la vista atrás tal vez no recuerde los pormenores de esta tesis, pero espero no olvidar jamás las historias que cuentan esas fotografías. Gracias a todos por haber sido el verdadero soporte de estos años en el laboratorio.*

*Gracias a Ángel y Marigel por su cariño y su generosidad.*

*Gracias a mis padres, por estar desde el principio, por no faltarme nunca, por todo lo que nunca seré capaz de agradecer suficiente. Gracias a mi hermano, porque por mucho que nos pinchemos, sé que siempre podré contar con él.*

*Y a ti, Leti, por todo, por tanto.*

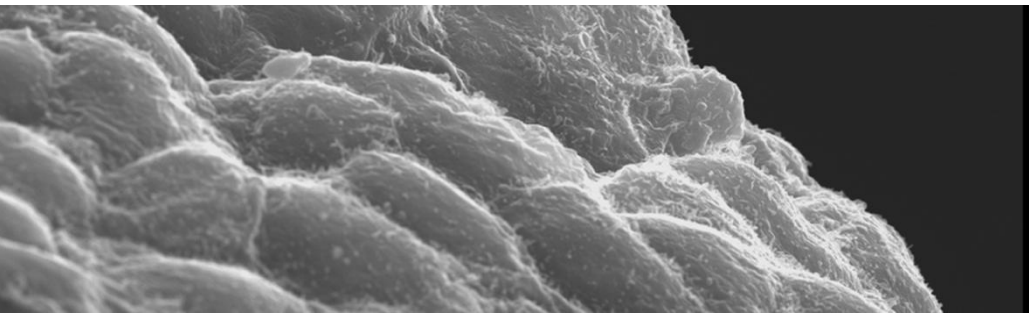

# TABLE OF CONTENTS

# LIST OF ABBREVIATIONS

| | |
|---|---|
| µm | Micrometers |
| µl | Microliters |
| AGP | Adrenogonadal primordium |
| APS | Ammonium persulfate |
| AR | Aspect ratio |
| A.U. | Arbitrary units |
| BAT | Brown adipose tissue |
| BAC | Bacterial artificial chromosome |
| BMP | Bone morphogenetic protein |
| BSA | Bovine Serum Albumin |
| BrDU | Bromodeoxyuridine |
| ChIP | Chromatin immunoprecipitation |
| DAPI | 4’,6-diamidino-2-phenylindole |
| DDS | Denys-Drash syndrome |
| Dm | Dorsomorphin |
| DMEM | Dulbecco's Modified Eagle Medium |
| DMSO | Dimethyl sulfoxide |
| DNA | Deoxyribonucleic acid |
| DSD | Disorders of sex development |
| tDSD | Testicular disorders of sex development. |
| ECM | Extracellular matrix |
| EDTA | Ethylenediaminetetraacetic acid |
| EMT | Epithelial mesencymal transition |
| FACS | Fluorescence-activated cell sorting |
| FBS | Fetal bovine serum |
| GAPDH | Glyceraldehyde 3-phosphate dehydrogenase |
| GC | Guanine Cytosyne |
| GFP | Green fluorescent protein |
| H&E | Haematoxylin and eosin |
| HBSS | Hanks' Balanced Salt Solution |
| IPF | Idiopathic pulmonary fibrosis |
| IRES | Internal ribosome entry site |
| Kb | Kilobase |
| KO | Knockout |
| KTS | Lysine-Threonine-Serine |
| L-Gln | L-Glutamine |
| LPM | Lateral Plate mesoderm |
| Mf20 | Sarcomeric myosin heavy chain |
| Min | Minutes |
| MI | Myocardial infarction |
| mRNA | Messenger RNA |
| MRTFs | Myocardin-related transcription factors |
| ON | Overnight |
| PE | Proepicardium |
| P/S | Penicillin/Streptomycin |
| PB | Phosphate buffer |
| PBS | Phosphate-buffered saline |
| PCR | Polymerase chain reaction |
| PFA | Paraformaldehyde |
| PGCs | Primordial germ cells |
| PVDF | Polyvinylidene fluoride |
| RA | Retinoic acid |

| | |
|---|---|
| RXR | Retinoid X receptor |
| RFP | Red fluorescent protein |
| RNA | Ribonucleic acid |
| SEM | Scanning electron microscopy |
| SDS | Sodium dodecyl sulfate |
| Tβ4 | Thymosine β4 |
| tdRFP | Tandem-dimer red fluorescent protein |
| TEM | Transmission electron microscopy |
| TEMED | Tetramethylethylenediamine |
| UTR | Untranslated region |
| WAGR | Wilms' tumour, aniridia, genitourinary anomalies and retardation syndrome |
| WAT | White adipose tissue |
| Wt1 | Wilm's tumour 1 |
| YAC | Yeast artificial chromosome |
| ZF | Zinc-finger |

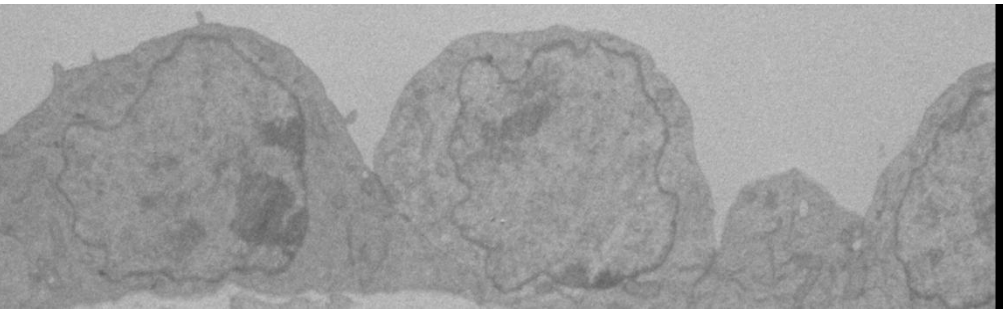

# INTRODUCTION

## 5.1 Wilm's tumour 1 gene (*WT1*).

### 5.1.1 *WT1* genetic and molecular characteristics.

The discovery of Wilms' tumour gene or WT1 transcription factor (*WT1*), in the decade of the 90s as a potential candidate for Wilm's tumors, a pediatric cancer present in 1 of every 10000 kids, opened a vast field of study that reaches our days[1–3]. Since then, *WT1* has revealed himself as a crucial gene not only in cancer but also in development, adult homeostasis or disease[4].

*WT1* gene is placed in the 11p13 chromosomic region and it spans about 50kb of the genome. *WT1* is encoded by 10 exons, and it can give rise up to 36 different isoforms[1,2,5,6]. This multiplicity is the result of the combination of different alternative splicing regions, transcription start sites and RNA editing phenomena (Fig. 1).

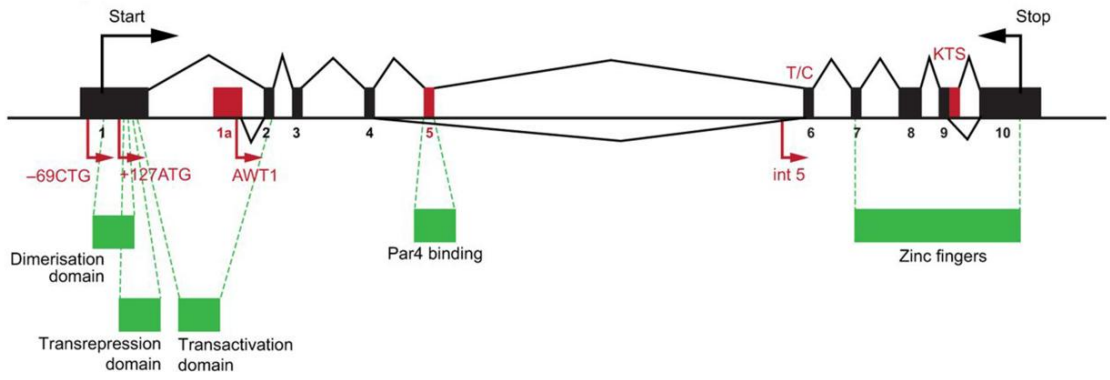


**Figure 1. Structure of the mammalian *WT1* gene**. Depiction of *WT1* exons. In red, different transcriptional and translational start sites, alternative splices and RNA editing sites. The multiple combinations of these events can give rise up to 36 different isoforms. Adapted from N. D. Hastie, 2017.

The most important and studied isoforms, transcripts about 3kb long, are the four isoforms resulting from the presence of two alternative splicing regions. The first pair is created by the insertion or deletion of the 17 amino acids encoded by exon 5. The second pair is the result of the presence or absence of the exon 9 nucleotides that give rise to a KTS (lysine, threonine, serine) aminoacid sequence[5,6]. Apart from that, the existence of two additional transcription start sites in introns 1 and 5 allows the transcription of isoforms with a truncated N-terminal domain[7,8]. Furthermore, three alternative start codons generate extra isoforms, some of them longer than the most abundant ones. The combination of all these particularities leads to the fact that, theoretically, *WT1* can give rise up to 36 different isoforms so far. The search for new

isoforms stills proceeds: for example, in 2015, Yusuke Oji described a new isoform that shows an extended (153 extra-base pair) exon 4[9].

The most relevant isoforms of *WT1* generate a protein whose best described function is to act as a transcription factor[4]. The N-terminal region includes a domain rich in prolines and glutamines implicated in transcriptional regulation, auto-association, and RNA recognition processes. The C-terminal domain is mainly composed of 5 Zn-finger (exons 7 to 10) of C2-H2 'Krüppel' type. The function of this region is to allow the binding of WT1 protein to GC rich sequences of DNA and RNA [10–12].

Once the protein has been generated, a couple of post-translational modifications have been described to alter WT1. WT1 can be SUMOylated at two residues in the N-terminal domain; this modification has been suggested to regulate WT1 nuclear localization. However, the function of WT1 SUMOylation still is not clear[13]. Phosphorylation of WT1 residues in Zn-fingers from exons 3 and 4 by PKC or PKA has also been described. WT1 phosporilation results in cytoplasmic accumulation of WT1 and inhibition of WT1 DNA-binding. Therefore, leading to the decreasing of Wt1 transcriptional activity capacity[14,15].

It is not clear whether *WT1* is present in invertebrates. However, several studies have found *WT1* isoforms in all vertebrates. It is interesting to notice that nonmammalian vertebrates express only + and – KTS isoforms, while mammals show a complex panoply of different isoforms depending on the species. For example, isoforms generated through RNA editing have been described only in mouse and human samples[4].

### 5.1.2 WT1 molecular functions.

The most relevant function of WT1 is transcriptional regulation. WT1 has been demonstrated to exert opposed roles depending on the context, sometimes acting as an activator and others as a repressor of transcription. As a partial explanation, the N-terminal region of the protein includes a transactivator domain and also a transrepressor domain. However, there are a couple of factors implicated in this decision: the cellular context, the protein levels, the isoform or the interacting partners[16,17].

WT1 can interact with several proteins. In some contexts, depending on this interaction, WT1 can act in one sense or the opposite. In the presence of p53, WT1 is a transcriptional repressor of *EGR1*. However when p53 is absent, WT1 turns into a transcriptional activator of this gene[18,19]. Another similar case is p73 binding to WT1 Zn-fingers to abrogate its transcriptional activation capacity[20]. Apart from other transcription factors, WT1 transcriptional activity is also

conditioned by the presence of different co-factors. Probably, the most well-known of these co-factors are BASP1[21] and WTIP[22], which act as cosuppressors of WT1, but also, other proteins like CBP[23] or PAR4[24,25] have shown this capacity.

If we look in more detail at the molecular characteristics of WT1, it will be easier to understand the versatility and functionality of this gene. First of all, Zn-fingers 2-4 allow WT1 binding to DNA and RNA sequences but the first one of the Zn-fingers, while it does not directly bind these sequences, helps to anchor WT1 to DNA[26]. On the other hand, the presence or absence of KTS amino acids between zinc-fingers 3 and 4 can also modulate the way WT1 binds DNA[27,28].

Indeed, + and – KTS isoforms show a different preference in their sequence binding. –KTS isoforms preferentially act as transcription factors while +KTS isoforms preferentially play roles in post-transcriptional regulation. However, despite this apparent dichotomy, both of them can actually participate in transcriptional and post-transcriptional processes[16].

One of the main goals in the study of WT1 has been the finding of its transcriptional targets. In the past decades, the efforts of several groups have generated a large amount of information about the targets of WT1 in different contexts. In 2014, Eneda Toska and Stefan G.E. Roberts attempted to gather in one publication all WT1 targets described until then[16]. Briefly, what they did was to cluster all these genes in 8 categories: genes involved in growth and development (like *BMP4*, *Vegfa* or *Sox11*), genes implicated in differentiation (*Snai2*, *CSF1* or *HOXA10*), cytoskeleton organization and cell adhesion (*Col4a1*, *Actn1* or *CDH1*), WNT signaling (*JUN*, *Wnt4* or *NLK*), MAPK signaling (*DUSP6* or *RRAS2*), apoptosis (*BCL2* or *c-MYC*), epigenetic regulation (for example *DNMT3a*) and a final category that included everything else (genes like *STIM1*, *Nos2* or *MMP9*). Since then, new studies have come to broaden this list, and the use of ChIP-seq experiments has allowed identifying new WT1 targets[29–31]. Although most of these studies have been performed on renal podocytes, restricting the relevance of the data for other fields, WT1 regulation of many of the described targets has been confirmed in other cell types. Despite this limitation, it is clear from the available data that WT1 can regulate a large number of genes implicated in a vast set of genetic, cellular, and physiological processes[16].

Beyond its role in transcriptional regulation, WT1 has been described to be implicated in other regulatory steps. As mentioned before, +KTS isoforms show a predisposition to bind RNA molecules. Additionally, WT1 has been demonstrated to play a role in translation and epigenetic regulation in some contexts[4].

Appart from DNA binding, WT1 can also bind RNA through its Zn-fingers[32,33]. Moreover, using structural studies, an RNA recognition motif has been found in the WT1 N-terminal domain[34]. Further evidence of WT1 function in post-transcriptional events is supported by a support a long series of observations showing either the binding of WT1 to spliceosome or the ability of all WT1 isoforms to shuttle from the nucleus to cytoplasm[35–37]. However, the precise role of WT1 in this process is still not clear. A recent study has demonstrated that WT1 can bind to different kinds of RNA (protein-coding RNAs, lncRNAs, miRNAs, and snoRNAs) in 5' or 3' end of transcripts, and also in UTRs of these RNAs, helping to stabilize these RNAs. The list of WT1 RNA targets provided by this study has helped to elucidate WT1 role in RNA metabolism[38].

In the last decade, some examples of WT1 regulating the epigenetic landscape have revealed a new field for WT1 action. An epigenetic function of WT1 has been described in WT1 regulation of *Wnt4* [17]. This case is also interesting because it offers a paradigmatic example of WT1 dual function depending on the context. In the kidney mesenchyme, WT1 binding to *Wnt4* locus switches the chromatin to an activated state. In contrast, WT1 binding to the same *Wnt4* locus in the epicardium leads to a repressive chromatin[17]. In kidney, WT1 is regulating a MET, while in the epicardium, it is regulating an EMT. The authors of this study proposed WT1 was regulating *Wnt4* by switching the chromatin structure of *Wnt4* locus in a way they named "chromatin flip-flop".

In hematopoietic cells from some cases of acute myeloid leukemia, *WT1* mutations result in the impossibility for TET2, a translocation enzyme able to convert 5-methylcytosine to 5-hydroxymethylcytosine (which in turn, increases gene expression), to bind to DNA[39,40].

## 5.2 WT1 in disease.

One of the reasons *WT1* has generated a huge interest since its discovery is the fact that it is implicated in a large (and increasing) number of syndromes and diseases. The comprehension of WT1 molecular characteristics and the understanding of how WT1 plays a role in these diseases has led not only to a better and more precise knowledge of them but also, in some cases, to treatments for those diseases[4,41].

### 5.2.1 WT1 in cancer.

The possibility of *WT1* playing a role in some cancers was an idea that was clear since its discovery. As I wrote previously, *WT1* was discovered in a type of pediatric cancer[1–3]. Wilm's tumor, or nephroblastoma, as it is also known, is the most common renal malignancy[42]. So far,

it is thought that Wilm's tumor arises due to defects during fetal nephrogenesis. Of all Wilm's tumor cases, about 10-20% can be related to mutations in the *WT1* gene[43]. In these tumors, *WT1* acts as a tumor suppressor gene.

Despite being a tumor suppressor gene in Wilm's tumours, the *WT1* gene is also overexpressed in some adult cancers[44]. In leukemias, *WT1* has been found to act in some cases as an oncogene and others as a tumor suppressor gene. WT1 has also been found in a series of adult solid cancers like mesotheliomas, breast cancers, brain tumors, or renal carcinomas[44]. However, the role that WT1 is playing in these cancers stills remains to be elucidated, and the proposal of *WT1* as an oncogene is not yet settled. Despite this, *WT1* has been used as a target to develop treatments for these cancers[43,45].

### 5.2.2 WT1 related diseases.

There is a group of human syndromes related to germline *WT1* mutations or *WT1* haploinsufficiency. The first of those syndromes is WAGR syndrome (Wilm's tumour, aniridia, genitourinary anomalies, and retardation syndrome). This syndrome results from the deletion of 11p13 chromosomic region[46,47], which includes the *WT1* gene. Most cases of WAGR syndrome lead to Wilm's tumors and, in males, to the absence of one or both testes. Gonadal defects caused by this syndrome are much less frequent in female patients. Interestingly, in some WAGR syndrome patients, it has been observed the presence of ambiguous genitalia[48].

The second of these syndromes is DDS (Denys-Drash syndrome). DDS is caused by heterozygous missense mutations that take place in the exons encoding WT1 Zn-fingers[49]. This syndrome is characterized by early life appearance of kidney disease, a very probable manifestation of Wilm's tumors and gonadal dysgenesis. DDS male patients present ambiguous external genitalia or even external sex-reversed genitalia. Internal genitalia of these patients present a wide range of defects that include testis dysgenesis, absence of Wolffian structures or cryptorchidism. Again, most female (XX patients) do not present a gonadal phenotype[50–52].

Frasier syndrome arises because of mutations in the donor splice in *WT1* intron 9 that allows the formation of +KTS isoforms[53]. Affected individuals show focal segmental glomerulosclerosis, which finally leads to kidney failure. Male patients also present ambiguous external genitalia and streak gonads[53].

A fourth syndrome needs to be taken into account. Meacham syndrome is an extremely rare disease (15 cases reported worldwide so far) that also can be related to *WT1* mutations (some

of them also observed in DDS patients)[54]. Again, these patients present ambiguous genitalia (and, in this case, also abnormal internal female genitalia). However, they do not present kidney defects. These patients also show congenital heart defects and congenital diaphragmatic hernia[55–57].

Finally, in a recent study, it was described that in a subset of patients with 46, XX testicular DSD (disorder/differences of sex development) or ovotesticular DSD, the phenotype could be related to a heterozygous mutation in the ZF4 of WT1[58]. The authors of this work suggested that this phenotype could be arising from WT1 mutated protein ability to sequester β-CATENIN, a key pro-ovary factor, leading to a masculinization of XX gonads[58]. The significance of this work consists of being the first reported case in which WT1 is not implicated in the feminization of XY gonads but the opposite.

It is worth to recapitulate that most of these syndromes include renal abnormalities and that all of them include some kind of "sex-reversed" or gonadal malformation phenotype.

### 5.2.3 WT1 in fibrosis.

Fibrosis is a feature of many chronic degenerative disorders. It normally consists on the progressive accumulation of extracellular matrix (ECM) by myofibroblats. There are a couple of diseases related to WT1 and involving some kind of fibrosis.

One of them is Idiopathic pulmonary fibrosis (IPF). IPF is a severe chronic fibrotic lung condition[59]. In IPF mesenchymal cell genes are dysregulated, leading to an uncontrolled fibrotic signaling which ultimately causes an impaired lung function. *WT1* expression is upregulated in mesothelial and mesenchymal cells of IPF lungs[60]. And WT1 upregulation has been described to regulate profibrotic processes, like proliferation, myofibroblast transformation and ECM production[61].

In fibrotic liver injury, activated hepatic stellate cells are the main responsibles for orchestrating fibrosis. A subset of the quiescent stellate cells arise from the *Wt1*-expressing hepatic mesothelium[62]. Additionally, *Wt1* deletion has proved to result in an enhanced fibrotic response in the liver[63].

## 5.3 WT1 in development.

WT1 plays a role in the embryonic development of several organs and tissues[4]. The function of WT1 in each organ most of the times cannot be inferred from other tissues data. Moreover,

new functions of WT1 are described every year. Recently, for example, a WT1 role in nervous system (where it was never detected until then) has been discovered[64]. Therefore, trying to offer a complete and exhaustive view of WT1 role in development is far beyond the intentions and possibilities of this introduction. I will focus, then, in the two organs in which my research has been done: heart and gonads. However, to provide a better understanding of the results presented I will also make a brief introduction of WT1 in other organs development.

### 5.3.1 WT1 in gonads.

One of the seminal articles that first described *WT1,* did so in WAGR syndrome patients[2]. As I have mentioned, these patients present, among other symptoms, genito-urinary abnormalities. While this was the first evidence of the participation of WT1 in gonadal development, now we have a more comprehensive view of the role of WT1 in mouse gonad development.

#### *5.3.1.1 Gonad embryogenesis.*

In the mouse, the initial step in gonad development is the formation of the structures termed genital ridges, the bipotential gonad that appears about E10.5[65]. The process of formation of this intermediate implies the stratification of the single-layered coelomic epithelium placed over the mesonephros. While this thickening occurs, Primordial Germ Cells (PGCs), precursors of gametes, migrate into the genital ridges[65]. At this point, there is no morphological difference between males and females.

The bipotential gonad arises from the intermediate mesoderm[66]. However, the mechanism implicated in the specification of the region giving rise to the bipotential gonad is not well characterized. In chicken embryos, Sonic Hedgehog and BMP4 signaling are implicated in this process but whether this can be applied to mammals remains to be determined[67]. There are a couple of genes crucial for the formation of the bipotential gonad. GATA4 is one of the first transcription factor expressed specifically in the genital ridge[68]. GATA4 expression is necessary for the coelomic epithelium thickening and regulates the expression genes implicated in this process, like *Lhx9* and *Sf1* (Steroidogenic factor 1), also known as *Nr5a1*[68]. EMX2 and LHX9 are two transcription factors also implicated in this process, and their lack prevents gonad formation[69,70]. LHX9 regulates *Sf1*, another transcription factor necessary for gonad and adrenal gland formation[71,72]. CBX2 is a member of the polycomb multiprotein complex, necessary to maintain a repressed transcriptional state of many genes during development. *Cbx2KO* mice show a delay in gonad formation and male to female sex reversal[73]. WT1 plays an

important role during these initial steps. WT1, in cooperation with other transcription factors, regulates *Sf1*[74,75], and the lack of either of these factors prevents gonad and adrenal gland formation[72,76]. These genes will be then crucial for regulating the genes determining male or female fates. Importantly, *in silico* reconstruction of cell fate trajectories in embryonic gonads suggested that coelomic epithelial cells are a common progenitor of the most abundant lineages in developing gonads: supporting and interstitial cells[77,78].

At this point, sexual differentiation starts, and the development of the gonad takes then a different road depending on the presence of chromosome Y (Fig. 2). This decision occurs when *Sry* (Sex determining region of the Y chromosome) is expressed in a subset of gonad cells[79–81]. The cells expressing this gene will be Sertoli cells, supportive somatic cells that guide PGC.

*Sry* has been described to be regulated by CBX2[82]. Additionally, it has been suggested that WT1 could be directly regulating *Sry* expression. In mice lacking +KTS isoforms, XY gonads show a reduction in the number of cells expressing *Sry* and also a reduction of *Sry* levels in those cells expressing it[83]. In fact, this direct regulation has been proved in humans[84].

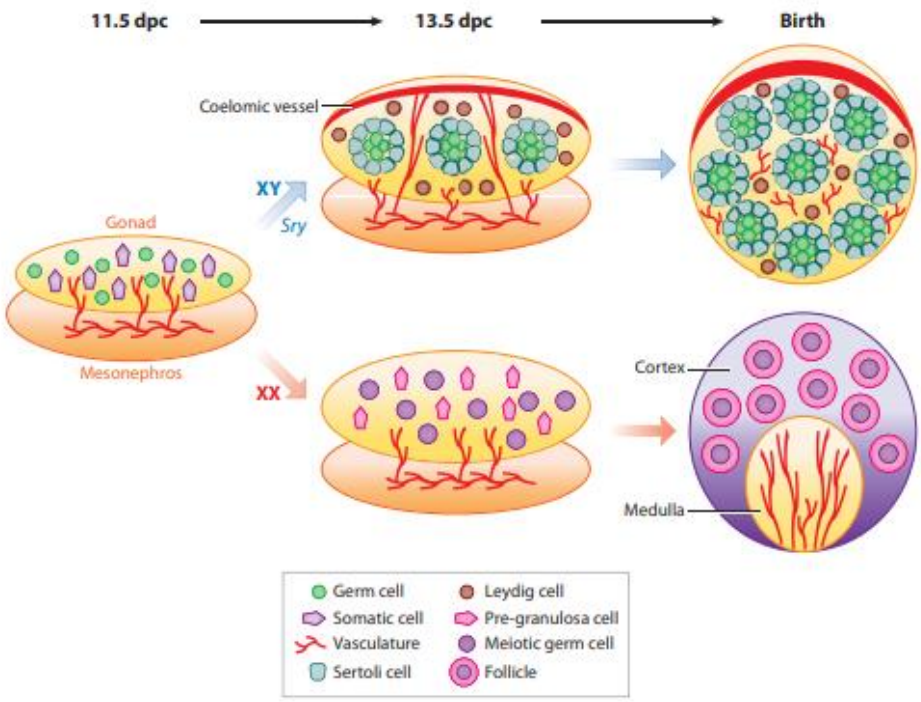


**Figure 2. Overview of mouse gonad morphogenesis.** At E11.5, *Sry* expression initiates testis differentiation: testis cords are formed, Leydig cells differentiate and the coelomic arterial vessel is formed. In female gonads, PGCs enter meiosis, medullary and cortical domains are established and folliculogenesis starts. Image obtained from DeFalco & Blanche Capel, 2009.

SRY activates *Sox9*[85], sufficient to induce whole male development[86,87] (Fig 3). The cells expressing this gene differentiate into Sertoli cells[85]. Indeed, abrogation of *Sox9* expression

leads to ovaries development in XY mice[88], while SOX9 overexpression results in testes development in XX mice[87,89]. WT1 +KTS KO mutants show a reduced expression of *Sox9* and also *Fgf9*[83], a gene downstream *Sox9*, needed for male gonad proliferation and recruitment of progenitors[90].

After *Sox9* activation in males, three main processes orchestrate testis development: 1) around E11.5, coelomic epithelial cells of the gonads start to proliferate[91], and some of them delaminate and give rise first to Sertoli cells and second to interstitial cells[66]. At E12.5-E13.5, some of the interstitial cells differentiate into Leydig cells, the steroidogenic cells of the testis. Leydig cells will then cluster next to the vasculature, from where they will secrete the hormones responsible for male virilization; 2) the second of these events is the formation of testis cords. At E12.5, Sertoli cells and PGCs aggregate to form solid testis cords surrounded by a basal lamina. Next, PGCs will enter mitotic arrest and will continue in this state until after birth. During the rest of the development, testis cords keep developing. Finally they give rise to the seminiferous tubules from adult testis[65]. 3) in parallel to these phenomena, endothelial cells from the mesonephros migrate into the gonads, where they mainly generate the vasculature network needed to support testis cords development (Fig. 2)[92,93].

In Sertoli cells, downstream SOX9, a large list of genes have been described to be implicated in testis development. Apart from *Fgf9*, previously mentioned, *Amh*, which is one of the first hormones produced in the testis, is responsible for the regression of female Müllerian ducts[94]. DAX1 is a nuclear receptor required for correct testis determination[95]. However, DAX1 overexpression has been described to antagonize testis development[96]. Other genes implicated in testis formation are *Gata4* and *Zfpm2* (*Fog2*), a GATA4 cofactor. The KOs of these genes show severe testis anomalies or a sex reversal phenotype[97,98]. These two genes have also been described to regulate *Sry* expression[97].

*Wt1* deletion prior to sex determination abrogates the correct formation of male somatic cells, and the genes responsible for the male genetic program are downregulated (*Sox9*, *Fgf9*, *Amh*)[99]. Once sex determination starts, WT1 is expressed in Sertoli cells during all development and adulthood. Two different works in which *Wt1* was either downregulated[100] or ablated[101] in Sertoli cells, demonstrated that *Wt1* expression in Sertoli cells is necessary for testis development. *Sox9* and *Amh* expression are downregulated in the absence of WT1, leading to the loss of testis architecture and ultimately to reduced sperm motility. *Wt1* ablation in Sertoli cells, also results in stabilization of β-CATENIN pathway[102], responsible for ovary development, suggesting an explanation for the sex-reversal phenotype present in WT1-linked syndromes.

Additionally, *Wt1* ablation in Sertoli cells results in PGCs loss. In Leydig cells, as soon as they differentiate, *Wt1* expression is shut down. Indeed, ablation of *Wt1* after sex determination leads to an anticipated and higher differentiation of Leydig cells[99]. Both Leydig and Sertoli cells have been described to originate from *Wt1*-expressing cells[99] and *Wt1* inhibition in ones and maintenance in the others is key for their correct differentiation. In fact, it has been described that either WT1 overexpression in Leydig cells or downregulation in Sertoli cells leads to a cell reprogramming to the other cell type[103].

Mesonephric cell migration is needed for correct testis cord formation[104,105]. Most mesonephric migrating cells are endothelial cells[93]. In male mesonephros, endothelial cells migrate from the mesonephric vascular plexus into the gonads and subdivide them into 10 regions that will later become the seminiferous tubes[106,107]. There are several genes implicated in this process: first of all, a genetic male background is needed to trigger mesonephric migration and indeed, *Sry* is needed to initiate it[106,108]. It has also been described that female associated genes as *Wnt4* must be downregulated to allow migration from mesonephros[109]. Interestingly, ablation of male genes *Sf1* and *Cited2* expression induces ectopic migration in female mesonephros[110], while *Rspo1* male *KOs* fail to induce the characteristic XY vasculature[111]. VEGF inhibition prevents endothelial cell migration in the testis and results in the absence of testis cords[112,113]. Besides, it has been described that mesonephric vascular migration may depend on other signaling factors like PDGF[114], Neurotrophin 3[115] or AMH[116].

In the case of females, *Sry* is not expressed and, as a consequence, female gonad development takes place (Fig. 2). Similar to male development, somatic cells from XX gonads differentiate into granulosa cells and Theca cells, the steroidogenic cells from female gonads[65]. It has been suggested that both types of cells arise from progenitors of the coelomic epithelium. PGCs, opposite to what happens in males, remain dispersed and, due to retinoic acid activity, enter meiosis at E13.5[117]. From this point, until a few days after birth, few changes in the morphology of female gonads have been characterized. Then, PGCs placed on the medullary region undergone apoptosis[118] and, in a process termed folliculogenesis, cortical PGCs generate cyst-like structures formed by adhered PGCs surrounded by somatic cells[119]. These will be primary follicles, which are the basic unit of the ovary: oocytes surrounded by somatic cells. Additionally, by this stage, vasculature, connective tissue and other somatic cells concentrate in the medullary region[65].

Ovary determination is not as well characterized as it is for testis[120]. However, there is a group of genes whose expression we know is necessary for correct ovary development (Fig. 3). FOXL2

is a transcription factor and is one of the earliest genes to be upregulated in the ovary[121]. Mice lacking FOXL2 show gonadal anomalies and activate the somatic testis determination program[121]. Moreover, *Foxl2* expression is necessary to maintain the ovary identity throughout life in mammals[122]. Female mice lacking RSPO1, a signaling molecule of the WNT/β-CATENIN pathway, show masculinized gonads and it has been proposed that RSPO1 acts by inducing *Wnt4* expression and β-CATENIN patwhay[123,124]. WNT4 is another protein that equally acts by activating β-CATENIN pathway. In accordance with this, *Wnt4* KO female mice show some male gonads[125]. β-CATENIN expression inhibits *Sox9* and *Fgf9* and drives ovary development by inducing the expression of key female genes as *Fst* or *Wnt4*[124,126].

Although the role of WT1 in male gonad development is well studied, WT1 importance on female gonad development is not so well understood. *Wt1* deletion prior to sex determination abrogates the correct formation of female somatic cells, and the genes responsible for the female genetic program are downregulated (*Wnt4*, *Rspo1*, *Foxl2*)[99]. Additionally, *Wt1* deletion after sex determination also resulted in the ectopic appearance of steroidogenic cells in XX gonads[99]. What this suggests is that, similarly to what happens in males, *Wt1* expression is necessary for female somatic cell maintenance while, on the other hand, *Wt1* inhibition is necessary for female steroidogenic cell differentiation. It is not known whether WT1 directly regulates *Wnt4* and *Rspo1* in gonads. However, it has been described that it does so in kidneys[17,127].

Traditionally it has been believed that the female pathway is activated by default, and the male pathway needs to be actively induced. However, in the past decades, this assumption has become outdated[120]. The current view on this topic is that both fates are tightly regulated and that each of the pathways exerts inhibiting actions on the other. FOXL2, for example, inhibits *Sox9* expression[122]. *Sf1* is initially both expressed in male and female gonads, but then it is upregulated only in males. This male-specific expression is maintained by WT1 and LHX9. In females, FOXL2 can antagonize WT1 activity, leading to an *Sf1* downregulation[128]. FGF9 maintains *Sox9* expression during male development and both inhibit *Wnt4* expression. WNT4, in turn, inhibits *Fgf9* expression. Moreover, WNT4, through the activation of the β-CATENIN pathway, also inhibits *Sox9* expression[129,130]. This mutual suppression is maintained in mature gonads. As I have mentioned, FOXL2 prevents the induction of the male pathway and maintains the ovary identity through adult life[122]. In mature males, the transcription factor DMRT1 keeps testis identity while inhibiting female pathway genes like *Foxl2* or Retinoic acid[131,132].

These examples illustrate two important concepts in sexual differentiation: 1) sexual differentiation is a tightly regulated process with delimitated windows and levels of gene expression, and 2) it is not only important to induce male genetic programs but also to inhibit female differentiation processes.

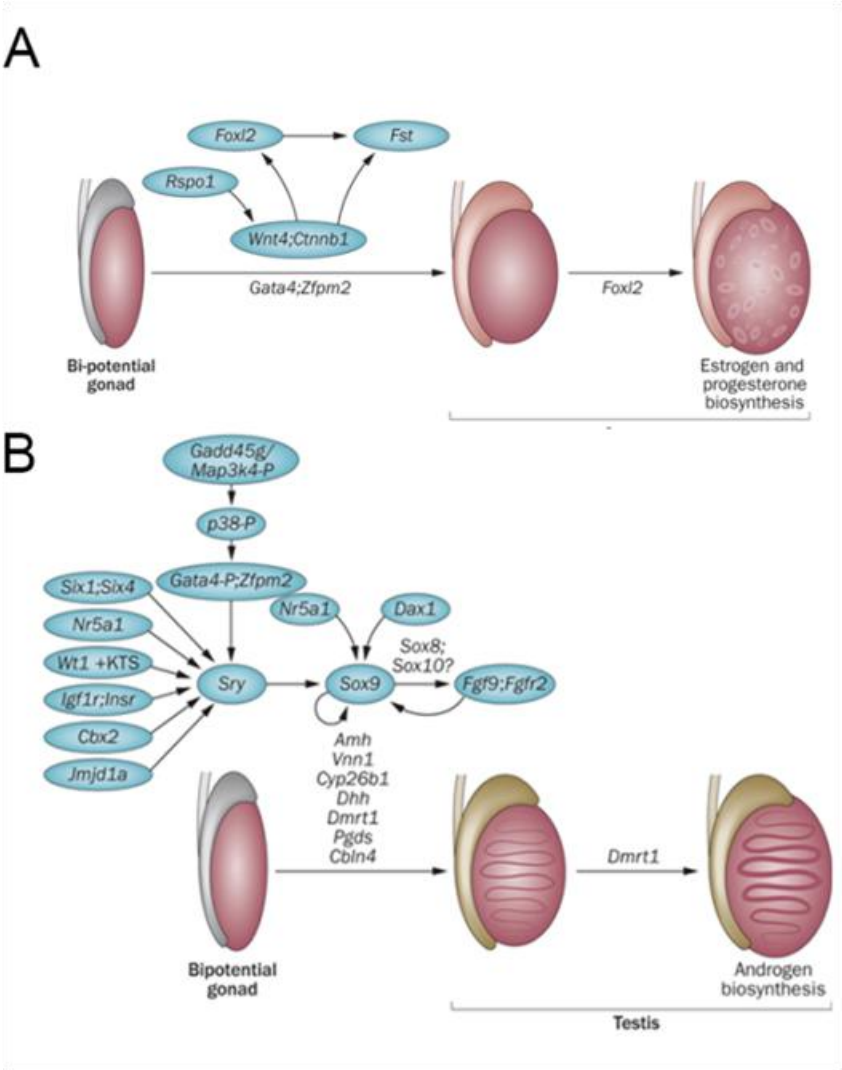


**Figure 3. Genes and pathways required for ovary and testis development and differentiation.** A) In XX mice, *Rspo1*, *Wnt4* and *Foxl2* are expressed during ovary development. *Rspo1*$^{-/-}$ ovaries show reduced levels of *Wnt4* expression, suggesting that *Rspo1* acts upstream of *Wnt4*. *Wnt4* and RSPO1 cooperation in activating *Ctnnb1* has also been suggested. FOXL2, RSPO1 and WNT4 activate *Fst*. In addition, GATA4 is implicated in ovary formation. In the adult, FOXL2 is required for tissue maintenance and follicle maturation. B) *Nr5a1*, *Six1*, *Six4*, *Wt1*, *Igf1r*, *Insr*, *Cbx2*, *Jmjd1a*, and the *Gadd45g–Map3k4P–p38P–Gata4–Zfpm2* induce *Sry* expression. In XY mice, *Sry* is transiently expressed in the bipotential gonad. Sry expression induces *Sox9* expression, which then stimulates *Fgf9*. *Fgf9* and *Sox9* act in a positive feedback loop to further upregulate *Sox9*. Nr5a1 is involved, together with *Dax1,* in the regulation of *Sox9* expression. *Sox8–Sox10*, *Fgfr2*, *Amh*, *Vnn1*, *Cyp26b1*, *Dhh*, *Pgds* and *Cbln4* are necessary for the regulation and maintenance of this crucial testis pathway. *Dmrt1* is required for the maintenance of the differentiated testis and is also crucial for preventing female reprogramming in postnatal mouse testis. Modified from Eggers et al., 2014.

### *5.3.1.2 Wolffian and Müllerian ducts development*

In parallel to testis or ovary development, male or female reproductive tract morphogenesis occurs (Fig. 4). Wolffian ducts will give rise to the epididymis, vas deferens and seminal vesicles, while Müllerian ducts are the embryonic progenitors of future fallopian tubes, uterus and upper part of the vagina[133,134].

Both structures are nephric ducts present in the mesonephros. These structures, as development progress, contact the developing gonads. At early embryogenesis, Wolffian and Müllerian ducts are present both in males and females and both develop in close association. At later stages of development, the duct from the other sex will regress, allowing the formation of the respective reproductive tract[133,134].

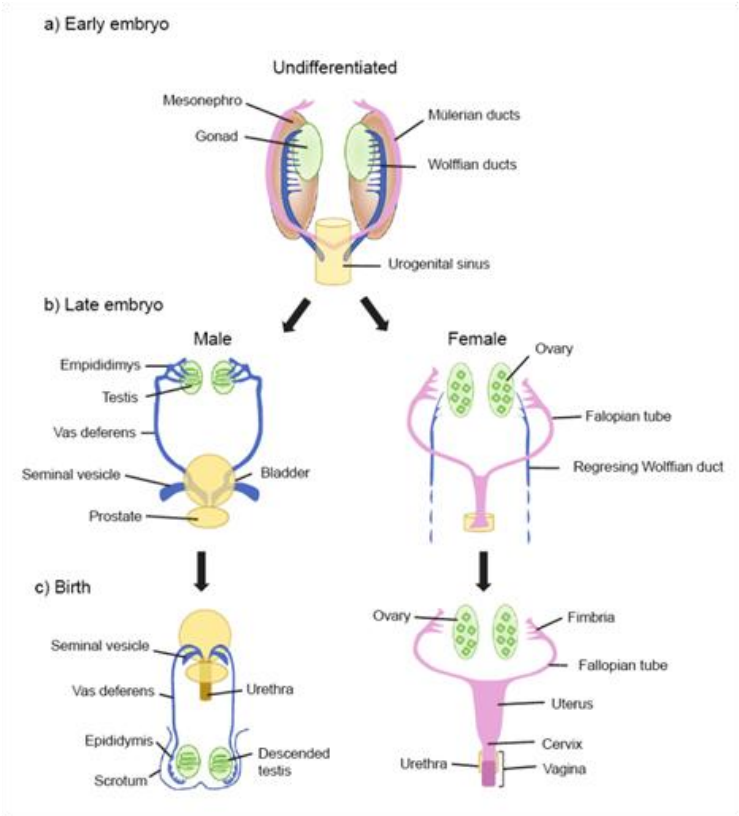


**Figure 4. Schematic view of urogenital system development.** (a) At the undifferentiated stage, gonads develop on ventromedial surface of the mesonephric kidneys. Two pairs of ducts form, Wolffian and Müllerian ducts. (b) Later in development, AMH in males leads to Müllerian duct regression, while testosterone stimulates differentiation of the Wolffian ducts into male structures (vas deferens, epididymis and seminal vesicles). In the female, lack of these hormones leads to Müllerian duct differentiation into female structures (fallopian tubes) and regression of the Wolffian ducts. The mesonephros regress in both sexes. c) By birth, the paired testes and associated male ducts descend into the scrotum. In females, the fallopian tubes fuse caudally, giving rise to the uterus and upper portion of the vagina. (Bladder omited in the female for clarity). Modified from Roly et al., 2018.

In males, regression of Müllerian duct at E13-14 is triggered by AMH. Indeed *Amh*KO mice show female reproductive organs[94]. AMH signals through AMHR2 and SMAD phosphorylation[135,136]. The activation of this pathway induces Müllerian duct apoptosis and regression. *Amhr2* expression is also a key point in this process and it has been described to be regulated by WT1[137] and WNT7[138]. For Wolffian duct differentiation, androgens are required[139,140]: leydig cells secrete testosterone, which stabilizes the Wolffian duct. Then, the cranial section of the Wolffian duct differentiates and gives rise to the epididymis, the central section to the vas deferens, and the distal to the seminal vesicles[133].

In females, in the absence of AMH, WNT7 induces the expression of Hox genes, which induce correct differentiation of Müllerian duct[141]. Hox gene expression is also regulated by sex steroid hormones[142]. The cranial section of the Müllerian duct differentiates and gives rise to fallopian tubes, the central section to the uterus, and the distal to the upper vagina[134].

### 5.3.2 WT1 in the heart, the epicardium.

#### *5.3.2.1 Heart embryogenesis.*

The heart is the first organ being formed. The first step in heart development is the migration of cardiac precursors through the anterior region of the primitive streak to the splanchnic lateral mesoderm (Fig. 5). There, these cells will differentiate and form the linear heart tube and the secondary heart field. The heart tube is formed by two cell layers, the myocardium, and the endocardium[143].

Then, the heart tube starts looping to the right. In parallel, the heart tube starts growing mainly thanks to the contribution of cells from the secondary heart field[143]. These cells will give rise principally the outflow tract, the right ventricle, and parts of the atria, whereas cells from the heart tube will form the left ventricle, most of the atria, and parts of the right ventricle (Fig. 5)[144].

The heart keeps growing due to cell proliferation and this allows the formation of the different heart chambers. Finally, septation of the four chambers is completed, allowing the separation of systemic and pulmonary circulatory systems (Fig. 5)[143].

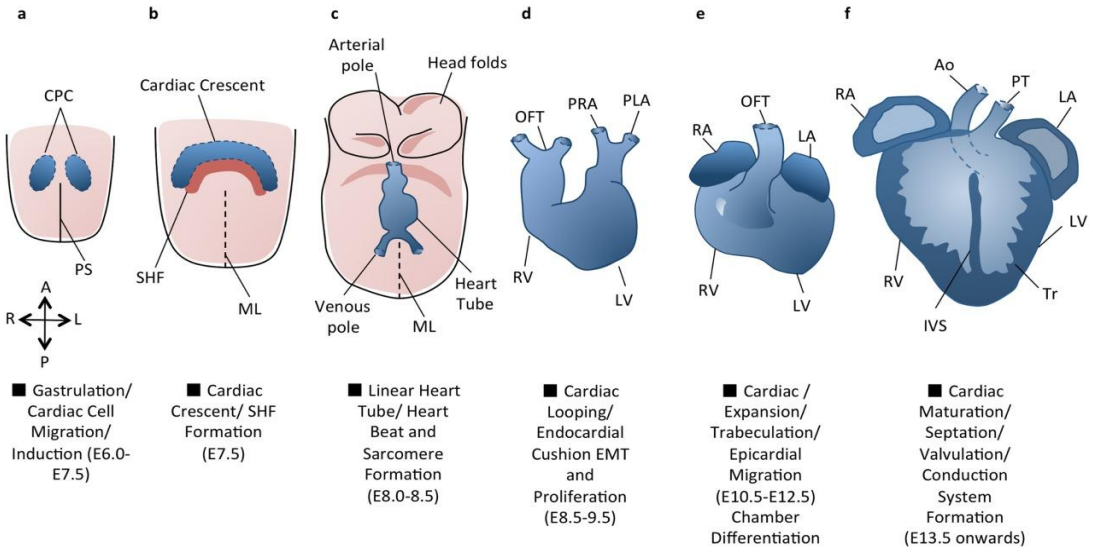


**Figure 5. Overview of the heart morphogenesis.** (a) Cardiac progenitors migrate through the primitive streak to form the cardiac crescent (b) and then the linear heart tube (c). Heart tube loops to the right (d), starts growing and forming heart chambers (e). Finally septation and formation of the valves and great vessels occurs (f). A = Anterior, Ao = Aorta, CPC = Cardiac Precursor Cells, IVS = Interventricular septum, L = Left, LA = Left Atrium, LV = Left Ventricle, ML = Midline, OFT = Outflow Tract, P = Posterior, PHF = Primary Heart Field, PLA = Primitive Left Atrium, PRA = Primitive Right Atrium, PS = Primitive Streak, PT = Pulmonary Trunk, R = Right, RA = Right Atrium, RV = Right Ventricle, SHF = Secondary Heart Field, Tr = Trabeculae. Image obtained from Clowes et al., 2014.

During heart development, besides the myocardium and the endocardium, a third layer will form. This layer, named the epicardium, is the mesothelial layer covering vertebrate hearts.

### *5.3.2.2 The epicardium, an introduction.*

The epicardium plays an essential role during heart development, and defects in the epicardium formation have been associated with impaired cardiac function[145]. Epicardial cells contribute to the formation of cardiovascular precursor cells that give rise to coronary smooth muscle cells, perivascular and cardiac interstitial fibroblasts, and a small % of cardiomyocytes and endothelial cells[145]. Since it has been suggested that epicardial cells are reactivated following myocardial infarction (MI), knowledge about the epicardium development has gained relevance during these last years[145].

The epicardium was first described more than 100 years ago[146]. Presence of this cell sheet is well conserved in vertebrates and it has been studied in human, chick, frog, mouse and zebrafish among others[147–151]. Interestingly, the evolutionary origin of the proepicardium has been proposed to be the pronephric external glomeruli, a structure composed of kidney cells found in the lampreys, the most primitive representative of the vertebrates[152,153].

The epicardium origin was one of the first debates raised by initial studies: originally, the epicardium was believed to derive from the primitive myocardium of the early embryonic heart[154]. However, this hypothesis, similarly to another one that stated that the epicardium has an endocardial origin, was refuted. Now it seems clear that the epicardium arises from an extracardiac source: the proepicardium[155].

#### *5.3.2.3 The proepicardium.*

The proepicardium is a cell structure, generally described to show a grape or cauliflower-like shape. It appears at early embryonic stages at the base of the venous inflow tract, where the primitive myocardium and the posterior lateral plate mesenchyme join in what is called the *septum transversum*[155]. Differences in the composition and structure of the proepicardium have been described between species. In the dogfish (*Scyliorhinus canicula*), the most primitive species in which the epicardium is present, the proepicardium is a simple clump of mesothelial cells, with little extracellular matrix between them[156]. On the other side, in mammals, the proepicardium is a bilateral protrusion formed by a layer of mesothelial cells surrounding a group of mesenchymal cells, embedded in a large amount of extracellular matrix[155]

The mechanism of proepicardium induction is not really understood[155]. From the data obtained in different animal models, it has been suggested that there are two actors implicated in PE formation and induction. The first one is the lateral plate mesoderm (LPM) and its derived structures: the first and second heart fields. And the second one, the endoderm derived liver bud[155]. Lineage tracing experiments have demonstrated that PE cells derive from *Nkx2-5* and *Isl1* expressing cells (two markers expressed in the cardiac crescent)[157]. However, only *Nkx2-5* loss impaired PE formation[157]. Other Cre directed by the promoters of cardiac transcription factors, or lateral plate mesoderm markers like *Hand1*[158] or *Mesp1*[159], have been used to support this idea. Moreover, the deletion of some of the markers of LPM, or the cardiac crescent, like *Gata4*[160] or *Hand2*[161,162], abrogates the formation of the PE or leads to defects in the epicardium development. The proximity of the PE to the liver bud raised the possibility that it could influence PE. In fact, in quail embryos, implantation of a donor liver bud leads to ectopic expression of PE markers like *Wt1* or *Tbx18*[163].

There are a couple of pathways or genes implicated in maintaining PE identity. *Bmp4* is expressed in the proepicardium, whereas *Bmp2* and other BMP proteins are expressed in the concomitant region of the inflow tract myocardium[164–166]. Precise regulation of this pathway has been proposed to be essential for PE specification, and distortion of BMP signaling results in a loss of PE identity toward the myocardial lineage[162,164–166]. Interestingly, BMP4 is necessary

for *Gata4* expression[167], which, as I have mentioned, is necessary for PE formation[160]. Although Notch signaling is not needed for PE formation, it is necessary for maintaining PE identity through the regulation of BMP signaling[166,168]. In cooperation with BMP, FGF signaling also regulates PE specification and identity. FGF2 and FGF10 are present in the PE, as well as several FGF receptors[164,165,169]. FGF signaling role is not clear: it has been proposed that FGF signaling is necessary for PE survival and proliferation but not for PE specification[169,170]. However, other authors have claimed that FGF, through BMP signaling inhibition, in fact, helps driving PE specification[171]. Finally, WNT signals also play a role in PE. WNT2a, WNT5b, and several Frizzled receptors are expressed in the PE[172]. WNT pathway has also been proposed to be implicated in the decision between myocardial and proepicardial linage specification[172] and *Dkk1* and *Dkk2* mutants (two inhibitors of the canonical WNT pathway) show an over-specification of PE cells[173].

Next, proepicardial cells migrate to the myocardial surface, where they form the epicardium(Fig. 6). As I described for its composition and formation, different mechanisms of cell transfer have been described in different organisms: in Xenopus[148] and chick[151,174], proepicardial cells reach the heart through a tissue bridge connecting both structures. In mice, a tissue bridge has also been described[175] but other studies have claimed the presence of free-floating vesicles that travel through the pericardial cavity and attach to the heart, creating epicardial islands[176,177].

The transmission of PE cells to the heart surface occurs in two ways. Cells from PE can form a cell bridge connecting both structures. In this process, the extracellular matrix plays a key role not only by guiding PE cells[178] but also accumulating "attracting" signals from the myocardium, as Bmp2[179]. In the PE, TBX5 overexpression or Knockdown leads to PE incapacity to generate the epicardium, suggesting a role for this transcription factor in this step[180]. Additionally, the deletion of adhesion molecules expressed in the PE like α4-INTEGRIN or in the myocardium, VCAM-1, resulted in the absence of the epicardium in mutant hearts[181,182]. Apart from the cell matrix bridge, PE cells have been described to attach to the myocardium through the formation of cysts. In this process, adhesion molecules like the integrin α4β1 are also needed[177]. Other studies also indicate a role for planar cell polarity proteins in this process[150,176]. Interestingly, in a study performed on zebrafish, it was demonstrated that heartbeat generates movements in the pericardial fluid that help PE cells to reach the myocardium, influencing their place of attachment[183].

Once proepicardial cells reach the myocardial surface, around E9.5 in mice, they start to spread like a wave. Proepicardial cells cover the whole heart surface at E11.5, thus setting the confluent cell layer we call the epicardium[145].

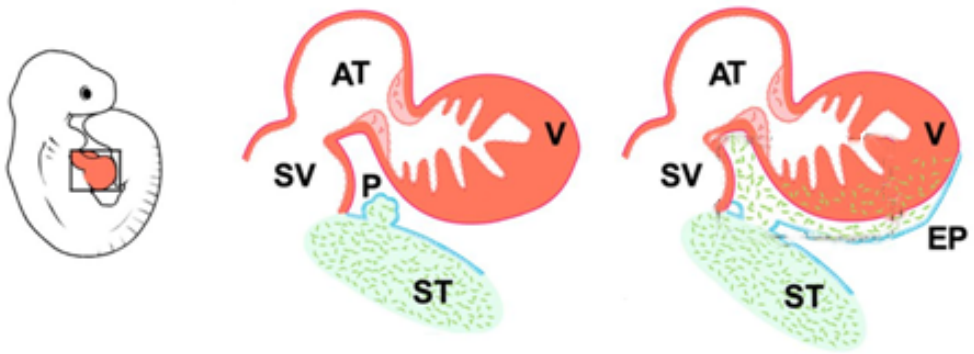


**Figure 6. The epicardium development**. The proepicardium forms in the Septum Transversum (ST), in the base of the sinus venosus (SV), as a cell protuberance. Proepicardial cells migrate to the myocardium surface, where they cover the whole heart surface by E11.5. AT, Atrium; V, ventricle; P, proepicardium; EP, epicardium. Modified form Cano et al., 2016.

### *5.3.2.4 The epicardium: relevance, roles, and molecular pathways.*

**The relevance of the epicardium**

The epicardium contributes to heart development in several ways[145]. At E13.5, some epicardial cells migrate into the subepicardial space giving rise to epicardial derived cells (EPDCs). The fate of these cells has been a matter of intense debate since they were described[145]. Additionally, epicardial cells secrete a set of growth factors and other paracrine factors that establich a crosstalk with the adjacent myocardium[145].

The relevance of these events is reflected on the phenotypes of the multiple KO models generated to perturb epicardium formation or the mentioned processes. Most conventional and conditional KOs presenting defects in epicardium formation share defects in coronary vessels development and a thin myocardium. The usual consequence is an embryonic or postnatal lethality caused by cardiac failure. Putting aside the idoneity and specificity of the used Cre models, the phenotypes af all epicardium-conditional KOs (Table 1) generated so far (to our knowledge), are a clear indication of the importance of the epicardium during heart embryogenesis. The reasons leading to those phenotypes will be next explained as I develop the process and mechanisms implicated in epicardium development.

| KO model | Phenotype | Reference |
|---|---|---|
| *Gata5$^{Cre}$; RXRα$^{fl/fl}$* | Thin myocardium, embryonic lethality | Merki et al., 2005[184] |
| *Gata5$^{Cre}$; β-catenin$^{fl/fl}$* | Impaired coronary formation, embryonic lethality | Zamora, Männer &Ruiz-Lozano, 2007[185] |
| *Gata5$^{Cre}$; PDGFRβ$^{fl/-}$* | Defects in coronary vessels, thin myocardium | Mellgren et al., 2008[186] |
| *Gata5$^{Cre}$; Alk$^{fl/fl}$* | Thin myocardium, ventral body wall closure defect | Sridurongrit et al., 2008[187] |
| *Gata5$^{Cre}$; Cnb$^{fl/fl}$* | No phenotype | Zeini et al., 2009[188] |
| *Wt1$^{GFPCre}$;Fog$^{ll/fl}$* | Thin myocardium, endocardial cushion defects, perinatal lethality | Zhou et al., 2009[189] |
| *Gata5$^{Cre}$; Wt1$^{fl/GFP}$* | Cardiac faliure, embryonic lethality | Martínez-Estrada et al., 2010[190] |
| *Gata5$^{Cre}$; Dicer$^{fl/GFP}$* | Abnormal coronary vasculature, hemorrage in pericardial space, perinatal lethality | M. K. Singh et al., 2011[191] |
| Wt1$^{Cre}$; *Nfatc1$^{fl/fl}$* | Abnormal coronary vasculature, bifid apex, no heartbeat, prenatal lethality | Combs et al., 2011[192] |
| *Gata5$^{Cre}$; Nfatc1$^{fl/fl}$* | Abnormal coronary vasculature, bifid apex, no heartbeat, prenatal lethality | Combs et al., 2011[192] |
| *Gata5$^{Cre}$; PDGFRβ$^{fl/fl}$ PDGFRα$^{fl/-}$* | Hemorrhaging | Smith et al., 2011[193] |
| *Wt1$^{Cre}$; Notch$^{fl/fl}$* | Body and pericardial hemorrhages, embryonic lethality | Del Monte et al., 2011[166] |
| *Tbx18$^{Cre}$; Rbpj$^{fl/fl}$* | Abnormal coronary vessels | Grieskamp et al., 2011[168] |
| *Wt1$^{CreERT2/GFPCre}$* | Cutaneous edema, pericardial effusion, bifid apex, embryonic lethality | von Gise et al., 2011[194] |
| *Wt1$^{CreERT2}$; Ctnnb1$^{fl/fl}$* | Peripheral edema | von Gise et al., 2011[194] |
| *Wt1$^{Cre}$; Fgfr1/2$^{fl/fl}$* | Thin myocardium | Vega-Hernandez. et al., 2011[195] |
| *Gata5$^{Cre}$; Nf1$^{fl/fl}$* | Increased epicardial EMT | Tallquist & Baek, 2012[196] |
| Wt1$^{Cre}$; *Nf1$^{fl/fl}$* | Increased epicardial EMT | Tallquist & Baek, 2012[196] |
| Wt1$^{CreERT2}$; *Nf1$^{fl/fl}$* | Increased epicardial EMT | Tallquist & Baek, 2012[196] |
| *Tbx18$^{Cre}$; Ctnnb1$^{fl/fl}$* | No heart phenotype | Rudat et al., 2013[197] |
| *Tbx18$^{Cre}$; Smo$^{fl/fl}$* | No heart phenotype | Rudat et al., 2013[197] |
| *Tbx18$^{Cre}$; Fgfr1$^{fl/fl}$ Fgfr2$^{fl/fl}$* | No heart phenotype | Rudat et al., 2013[197] |
| *Tbx18$^{Cre}$; Pdgfra1$^{fl/fl}$* | Impaired cardiac fibroblast differentiation | Rudat et al., 2013[197] |
| *Gata5$^{Cre}$; Rbpj$^{fl/fl}$* | Shorteded lifespan, cardiac hypertrophy | Wei et al., 2015[198] |
| *Wt1$^{CreERT2}$; Mrtfb$^{fl/fl}$ Mrtfa$^{-/-}$* | Sub-epicardial hemorrhage | Trembley et al., 2015[199] |
| *Wt1$^{Cre}$;Mrtfb$^{fl/fl}$ Mrtfa$^{-/-}$* | Sub-epicardial hemorrhage, postnatal lethality | Trembley et al., 2015[199] |
| *Sema3d$^{GFPCre}$; Yap$^{fl/fl}$ Taz$^{fl/fl}$* | Cardiovascular isufficiency, embryonic lethality | A. Singh et al., 2016[200] |
| *Wt1$^{CreERT2}$; Yap$^{fl/fl}$ Taz$^{fl/fl}$* | Disrupted coronary development, embryonic lethality | A. Singh et al., 2016[200] |
| *Gata5$^{Cre}$; Pkr1$^{fl/fl}$* | Thin ventricular wall; postnatal lethality (heart failure) | Arora et al., 2016[201] |
| Wt1$^{Cre}$; *Pkr1$^{fl/fl}$* | Thin myocardium, septal defects, bifid apex; embryonic lethality | Arora et al., 2016[201] |
| *Wt1$^{CreERT2}$; Crim1$^{fl/fl}$* | Increased epicardial migration | Iyer et al., 2016[202] |
| *Tbx18$^{Cre/GFP}$; Tbx2$^{fl/fl}$* | No phenotype | Greulich. et al., 2016[203] |
| *Gata5$^{Cre}$;Brj1j$^{fl/fl}$* | Small, under-developed hearts, embryonic | Vieira et al., 2017[204] |

| | | |
|---|---|---|
| | lethality | |
| *Wt1*$^{CreERT2}$; *Brj1*$^{fl/fl}$ | Reduced cornonary vessels | Vieira et al., 2017[204] |
| *Wt1*$^{CreERT2}$; *Yap*$^{fl/fl}$ *Taz*$^{fl/fl}$ (after MI) | Post-MI pericardial inflammation and myocardial fibrosis. Cardiomyopathy and death. | Ramjee et al., 2017[205] |
| *Wt1*$^{CreERT2}$; *Wdpcp*$^{m/fl}$ | Coronary artery defects | Liu et al., 2018[206] |
| *Wt1*$^{CreERT2}$; *Lats1/2*$^{fl/fl}$ | Smaller hearts, less compacted myocardium, defectiv coronary vessels, embryonic lethality | Xiao. et al., 2018[207] |
| *Wt1*$^{Cre}$; *Mrtfb*$^{fl/fl}$ *Mrtfa*$^{-/-}$ | Protection against cardiac fibrosism dyastolic dysfunction | Quijada et al., 2019[208] |
| *Wt1*$^{Cre}$; *Srf*$^{fl/fl}$ | Protection against cardiac fibrosism dyastolic dysfunction | Quijada et al., 2019[208] |

Table 1. Epicardial conditional KO models and phenotypes.

**Epicardial cell fate and secretome**

Epicardial cells can either become EPDC, and then one of the differentiated cells they can give rise, or stay as epicardial cells and act as heart mesothelial cells. This decision is not yet understood. However, it has been proposed that β-CATENIN, an adherent junction component, and NUMB, an intracellular adaptor protein, regulate epicardial spindle orientation. This, in turn, controls cell entry into the myocardium: perpendicular cell division drives the cell to the myocardium, whereas parallel cell division keeps the cell in the epicardium[209]. Despite this interesting proposal, this question remains to be truly answered. Whereas cells are predetermined to become EPDC and one of its descendant lineages before or after they reach the epicardium is also unknown yet.

EPDC fates have been characterized using cell lineage experiments. Several reasons make lineage tracing studies troublesome. Many of these problems are related to the fact that in the last years, the scientific community has realized that the presumptive specificity of some markers used to trace fate is not as specific as it was initially believed. Additionally, some of those markers are acually expressed in some of the traced cell types. In the case of EPDCs and the cellular types they give rise to it is even more difficult since it is not clear whether cell fate is decided during the proepicardium, the epicardium, or EPDCs stages[210]. Also, some studies have claimed that the epicardium is not a homogeneous population but rather composed of different populations with subtly different profiles of expression[211–214].

It is well accepted that EPDC can give rise to vascular smooth muscle cells, cardiac fibroblasts, and pericytes (studies in the chick embryo, mice, and zebrafish have reached similar conclusions) (Fig. 7). Not so clear is that they can derive into endothelial cells and cardiomyocytes[145]. EPDC differentiation to cardiac fibroblasts, vascular smooth muscle cells, and pericytes has been demonstrated by different lineage tracing experiments in mice using G2-Gata4$^{Cre}$ [215] Gata5$^{Cre}$ [184], and different *Tbx18*$^{Cre}$ [216–218], and *Tcf21*$^{Cre}$ [219,220]. Additionally, two

different *Wt1-Cre* mice (*Wt1*$^{CreERT2}$ and *Wt1*$^{Cre}$)[221–223] used for lineage tracing experiments have come to similar conclusions.

In the case of endothelial cells, the hypothesis is supported mainly by Wt1$^{Cre}$ lineage tracing experiments. However, Wt1$^{Cre}$ animal models have been demonstrated not to be an accurate tool to prove this[224,225]. Moreover, neither Tcf21$^{Cre}$[219] nor Tbx18$^{Cre}$[226] lineage tracing experiments (two classic epicardial cell markers) succeeded in finding epicardial endothelial-derived cells. An article published in 2012 proposed that the proepicardium is formed by different cell compartments that can give rise to different cell types[212]. This affirmation, however, has been confronted by a recent publication that, using RNAscope, claims not to find these different cell types[227]. In this sense, the results observed by Cano and colleagues when using a *G2-Gata4*$^{Cre}$: that coronary endothelial cells derive from a proepicardial/*septum transversum* compartment, could be limited to a *septum transversum* population[215]. Also, recently, a study comparing *Gata5*$^{Cre}$, *Wt1*$^{Cre}$, *G2-Gata4*$^{Cre}$, and *cTnT*$^{Cre}$ lineage contribution to the total CD31 heart population was published. At E17.5-19.5, the later stages analysed, this contribution ranged from 3.6 to 6.9% of total CD31 heart cells (except for the *G2-Gata4* contribution, which reached 19.5%). The authors conclude that EPDC generate as much as 4% of all cardiac endothelial cells during gestation[228]. In any case, the contribution of the epicardium to the endothelial lineage should be carefully considered, as those constitutive Cre models may be already active in traced cells.

Even less clear is that EPCDs can derive into cardiomyocytes. Although initial experiments using lineage tracing experiments suggested this possibility[216,229], some publications have questioned it[225]. Also, it has been suggested that even before the epicardium colonizes the heart surface, there is a preexistent WT1 expressing population of cardiomyocytes in the myocardium[230]. This result shadows every conclusion obtained using *Wt1-Cre* transgenic lines.

The epicardium has also been described to contribute to epicardial adipose tissue, the layer of fat surrounding the heart[231]. This small fat depot has been described to influence the heart by endocrine, paracrine, and vasocrine effects. Morevover, it plays a role in heart-related pathologies like heart failure and coronary artery disease[232].

Finally, during development, a subset of fetal yolk sac macrophages colonizes the space within and immediately below the epicardium. Ablation of the epicardium reduced the number of fetal heart macrophages[233]. CD45+ hematopoietic cells arising from the hemogenic endothelium also contributes to the epicardium from E10.5 onward[234].

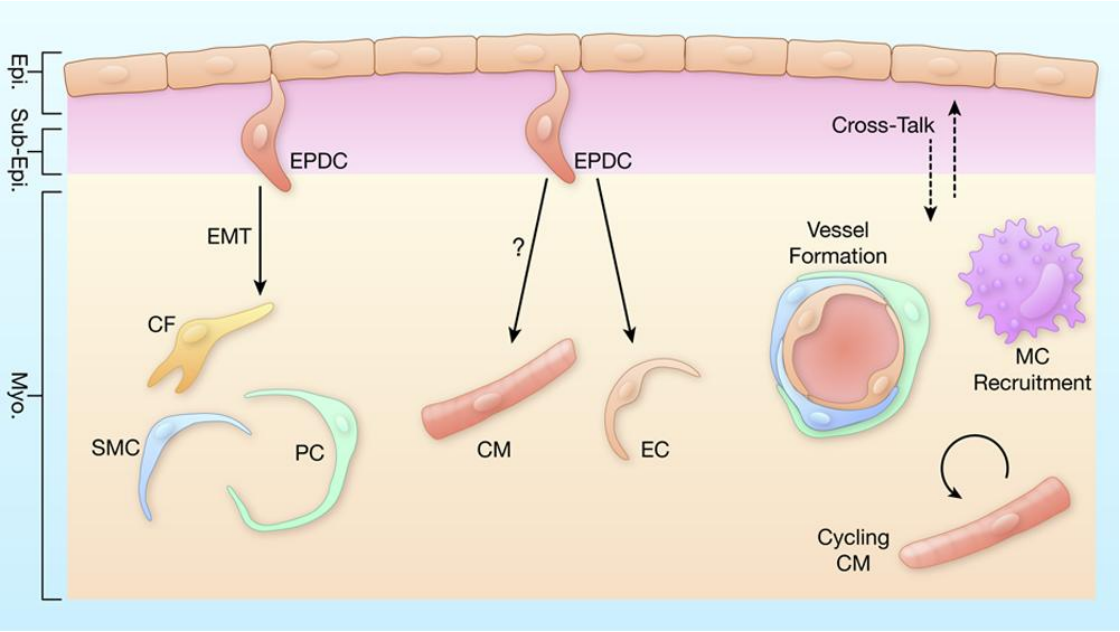


**Figure 7. Epicardial derived cell fates.** EPDCs (Epicardium-derived progenitor cells) contribute to various cardiac lineages, such as cardiac fibroblasts (CFs), smooth muscle cells (SMCs), and pericytes (PCs). The ability of EPDCs to differentiate into endothelial cells (ECs) in vivo is limited, and cardiomyocytes (CMs) are not generally thought to derive from EPDCs. In addition to cellular contributions, the epicardium participates in reciprocal paracrine signaling (dashed arrows) to stimulate CM proliferation, macrophage (MC) recruitment and coronary vessel growth and maturation. Epi indicates the epicardium; myo, myocardium; and subepi, subepicardium. Image obtained from Pearl Quijada et al., 2020 Illustration credit: Ben Smith.

Apart from EPDCs, the epicardium has also been described to contribute to heart development by secreting a set of growth factors and other paracrine factors. Epicardial cells express CXCL10 and CCL5, two chemokines that, *in vitro*, have been described to regulate epicardial cell migration and cardiomyocyte proliferation, respectively[235]. Secreted erythropoietin in the liver seems to induce IGF2 production by epicardial cells. IGF2 goes then to the myocardium, where it also stimulates cardiomyocyte proliferation[236,237]. The epicardium expresses different FGF proteins, including FGF2, FGF9 or FGF16. Some of them, specially FGF9, have been described to induce myocardial proliferation[238,239]. Apart from influencing cardiomyocyte proliferation, the epicardium secretome also regulates coronary vessel patterning. Epicardial cells have been described to express VEGF and Angiopoietin-1, two well-known vascular growth factors[194].

Probably, the most relevant molecule of the epicardium secretome is retionic acid (RA). Retinoic X receptor (RXR) or retinoid acid receptors mutants die during embryonic development due to defects in heart development[240,241]. Deletion of Raldh2, the main responsible for RA synthesis, similarly leads to an embryonically lethal phenotype[242]. RA induces the secretion of several epicardial paracrine factors such as WNT-9A, FGF-2 or IGF-2[184,236]. Additionally, RXR deletion in the epicardium results in a thin myocardium and defects

in the formation of coronary arteries, indicating RA is required for a proper formation of EPDC[184]. Importantly, Raldh2 expression is induced by Wt1[243].

**Epicardial derived cells (EPDCs)**

The most important efforts in the study of the epicardium have focused on understanding the mechanisms controlling the epicardial formation of EPDCs and the consequent differentiation to the cells that contribute to heart development[145].

The formation of EPDCs occurs through a mechanism classically called epithelial-mesenchymal transition (EMT). As a brief introduction, the EMT is a process in which a cell with epithelial characteristics, an apicobasal polarity, and the presence of junctional complexes lose these features to adopt the migration and invasion behavior that is typical from a mesenchymal cell (Fig. 8)[244]. This process can go in the other way in what is called a mesenchymal-epithelial transition (MET)[245]. Although originally it was described as a shift between two well-defined states, it is now clear that, through the path, there is a wide spectrum of intermediate states in which cells can linger[246].

There are several moments and tissues during development in which EMT processes occur: during gastrulation, some blastula epithelial cells give rise to mesoderm mesenchymal cells; at the neurula stage, neural crest cells undergo an EMT process to give rise to mesenchymal cells that migrate to distant territories[244]. During heart formation, sequential rounds of EMT and MET participate in heart morphogenesis[247]; also, the formation of the vasculature of many organs like the heart or the lung is achieved by the EMT that mesothelial cells lining these organs undergo to give rise the different cell types that form the vasculature[248]. The EMT process also plays a role in many diseases and pathological situations like cancer, fibrosis, or wound healing[244,249,250].

EMT regulation is complex, operates at different levels, and it is still a matter of debate. The central process of EMT regulation is the inhibition of the adhesion molecule E-CADHERIN. There is a group of major EMT transcription factors that include SNAI1, SNAI2, ZEB1, and TWIST1[251]. Around them, an intricate network of regulatory mechanisms, including miRNAs, splicing proteins, epigenetic mechanisms, or post-translational modifications, tightly controls EMT[244,252,253].

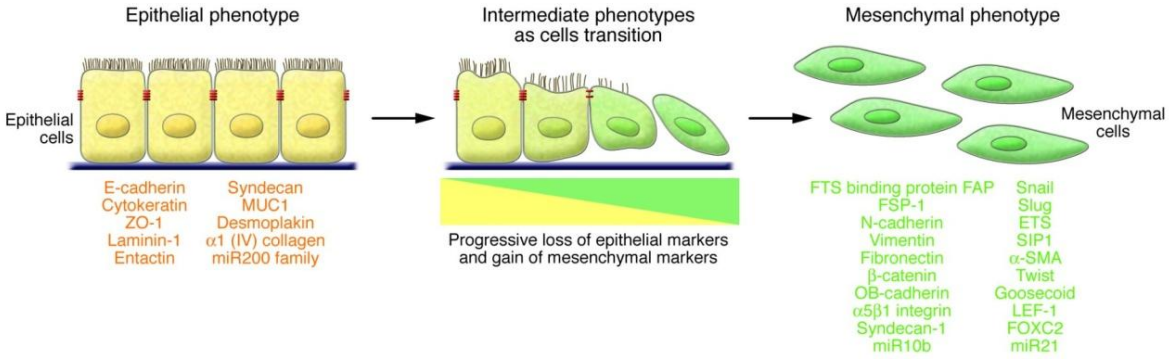


**Figure 8. EMT overview.** Epithelial to mesenchymal transition is characterized by the shift from an epithelial phenotype, characterized by an apicobasal polarity and the presence of junctional complexes to a mesenchymal one, in which cells show migratory and invasive features. Main epithelial and mesenchymal markers used to describe one or the other state are listed. Image obtained from Raghu Kalluri & Robert A. Weinberg, 2009.

Beyond the black or white paradigm defined by classic EMT or MET, today we know that there is a wider spectrum of different cellular transitions from one state to another[246]. The case of epicardial EMT is an example: the embryonic epicardium is a coelomic epithelium which, in the adult, would become a mesothelium. What this means is that epicardial cells do not show all classic properties of epithelial cells, but rather a mix between epithelial and mesenchymal cell features[248]. Therefore, the transition between epicardial cells and EPDCs cannot be considered as a canonical EMT. The term mesothelial-mesenchymal transition has already been proposed elsewhere[248]. However, as most of the literature still refers to it as an EMT, I will also talk about epicardial EMT.

There are a set of signals that seem to influence epicardial EMT (Fig 9). Transforming growth factor β (TGFβ) family members such as TGFβ1-3 or the receptor TGFβR3 are expressed in the epicardium[254,255]. Deletion of *Tgfβ3R* causes the formation of an aberrant myocardium and leads to defects in the myocardium and coronary vessel development[254]. Moreover, TGFβ1-3 growth factors have been described to modulate epicardial cell capacity for EMT[256,257]. Besides TGFβ, fibroblast growth factor (FGF) proteins are also implicated in regulating epicardial EMT[195,256,258]. *Fgf10* and *Fgfr2b* KOs have smaller hearts than wild-type embryos due to an impaired epicardial differentiation[195]. Other molecules influencing EPDC migration are Thymosinβ4[259], RA[184], and platelet-derived growth factor[186,260,261].

There are also several transcription factors whose expression has been linked to correct epicardium development. One of the most studied of these transcription factors is WT1[145]. *Wt1* is expressed in PE, the epicardium, and EPDC. *Wt1* expression is higher in the early stages of epicardium development, and then its expression is progressively reduced during epicardial development. *Wt1* conventional KO dies between E11.5 and E13.5 and shows defects in heart development caused by an impaired epicardial development[76,262]. This phenotype has been

proposed to be induced by a defective epicardial EMT leading to a thin myocardium and impaired formation of the coronary vasculature[190]. Two molecular mechanisms underlying this phenotype have been proposed. First, using a conditional *Wt1KO* in which *Wt1* was only deleted in epicardial cells, it was proposed that WT1 operates through the regulation of *Snail* and E-cadherin[190]. On the other hand, it has been suggested that WT1 regulates EPDC formation through *β-catenin* and RA pathway regulation[194]. However, while in the first work the epicardium was correctly formed, the integrity of the epicardium in the second one was not complete, thus explaining the differences observed between both[190,194].

Apart from WT1, other transcription factors have been linked to epicardial function. *Tcf21* null embryos have a detached epicardium. Moreover, the generation of epicardially derived cardiac fibroblasts is abrogated in these mutants[211,219]. YAP and TAZ are two transcription factors of the HIPPO signaling pathway. The deletion of both of them in the epicardium leads to coronary vasculature defects caused by impaired epicardial proliferation, EMT and fate determination[200]. Further evidence for the role of the Hippo pathway in the epicardium resulted from deletion of the Hippo kinases LATS1/2. LATS1/2 mutants showed defective coronary vasculature remodeling. Single-cell transcriptomic data revealed defective epicardial transcription in *Lats1/2KO* mice resulting in a reduced cardiac fibroblast differentiation[207]. NFACT1 and myocardin-related transcription factors (MRTFs) have been described to regulate EPDC migration, and their respective KOs show a reduced penetration of coronary vessels into the myocardium and downregulation of the expression of genes related to cell mobility[192,223].

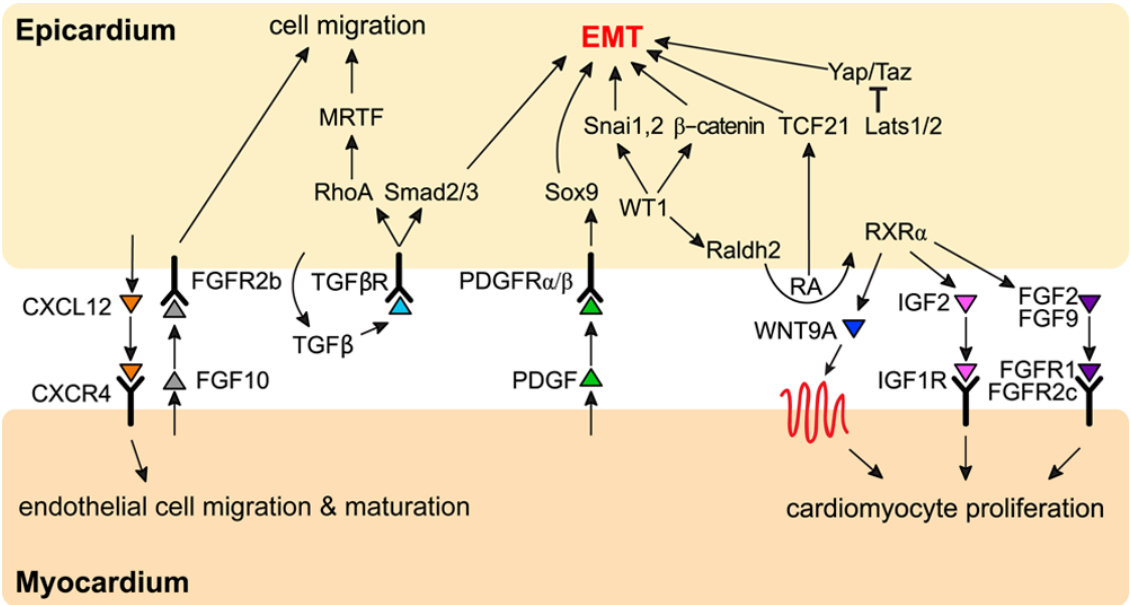


**Figure 9. Molecular control of epicardial epithelial-to-mesenchymal transition (EMT).** Intrinsic and extrinsic molecular programs regulate epicardial EMT in mice, which include the regulation of transcription factors and

molecular signaling. Cytokine-mediated signaling between the epicardium and cardiomyocytes is reported to stimulate heart growth, and epicardium-derived signals support the growing coronary vasculature. CXCL, C-X-C motif chemokine receptor-ligand; CXCR, CXC chemokines and receptor; FGF, fibroblast growth factor; IGF, insulin growth factor; MRTF, myocardin-related transcription factor; PDGFR, platelet-derived growth factor receptor; TGF, transforming growth factor; and YAP, yes associated protein 1. Image obtained from Quijada et al., 2020.

Finally, some epigenetic regulatory mechanisms have been described to be implicated in epicardium development. The chromatin remodeling complex BRG1-SWI/SNF regulates *Wt1* expression in the epicardium and the deletion of one of its components, BRG1, leads to classical epicardial EMT defects[204]. Also, it has been suggested that p300, a nuclear acetyltransferase is necessary for the epicardium formation and correct EMT[263].

#### *5.3.2.5 The embryonic program of the epicardium and Wt1 role on it.*

Although much has been said about EPDC formation and differentiation, little is known about epicardial cell development *per se*. Previously to this thesis, our group identified the epicardial cell genetic program throughout development (Fig. 10). *Wt1* is one of the most used markers of the epicardium. Taking advantage of this, *Wt1*$^{GFP}$ Knockin mice were used to isolate epicardial cells at different stages of development, from E11.5 (a stage in which the epicardium has just formed) to E16.5 (a late stage in development at which the epicardium has become quiescent). Using a transcriptomic analysis, the expression of a large set of genes was evaluated at these stages, allowing to analyse how these genes were modulated during the epicardium development[230].

The embryonic epicardial program consisted of the modulation of four groups or clusters of genes[230]. The first cluster comprehends genes with high expression at early developmental stages (E11.5-E12.5) and whose expression is downregulated progressively from E13.5 onwards. Cluster 2 genes are repressed during the E11.5-E12.4 stages, but their expression is upregulated from E13.5 onwards. Cluster 3 genes show a peak of expression between E13.5 and E14.5 stages, the period when epicardial EMT occurs. Finally, cluster 4 genes are those whose maximum expression levels were observed at E15.5 and E16.5 stages[230]. Some examples of the genes modulated in each cluster and the biological functions highlighted in each cluster can be seen in table 2.

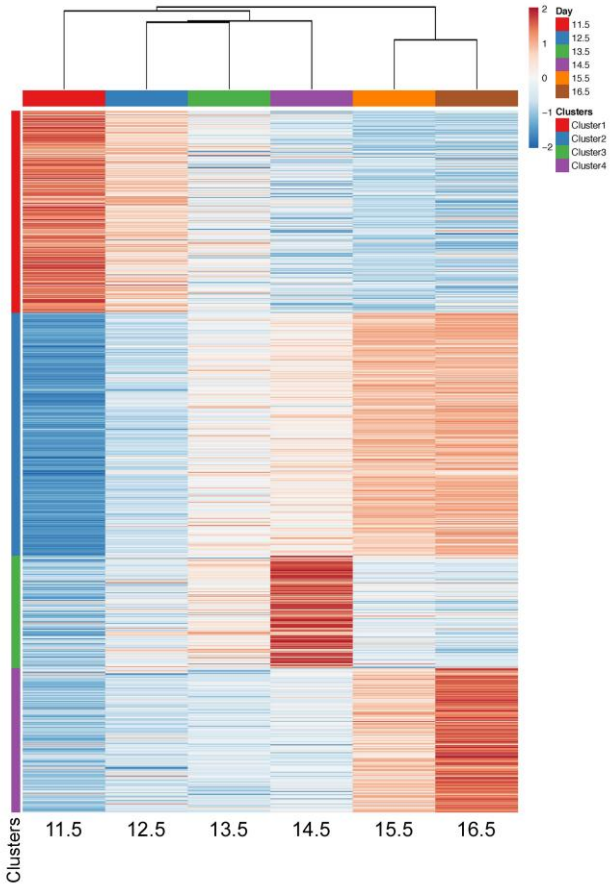


**Figure 10. Embryonic epicardial program**. Heatmap for the hierarchical clustering of the gene expression profiles of *Wt1GFP*$^{++}$ cells at different days of heart development. Red represents high gene expression and blue low gene expression. Cluster 1 genes are downregulated during epicardium development. Cluster 2 genes are upregulated from E13.5 onward. Cluster 3 genes show a peak of expression at E13.5. Cluster 4 genes maximum expression levels were observed at E15.5 and E16.5.

| Cluster | Genes | Biological function |
|---|---|---|
| 1 | *Ccnd2, Cdk4* | Cell cycle |
| | *Podxl, Alcam, Cdh3, Itga3* | Cell adhesion |
| 2 | *Meox1, Notch1, Hes1, Nfatc1* | Epicardial development |
| 3 | *Col2a1,Des, Emilin1* | Extracellular matrix |
| | *Itgb5, Ncam1, Vcam1* | Cell adhesion |
| 4 | *Msln, Cldn15, Dmkn* | Adult epicardium |

Table 2. Representative genes and functions from each cluster represented in figure 10.

The study of the genes or pathways modulated in these four clusters may offer important clues about the biology of the epicardium. To analyse the role of WT1 in the modulation and maintenance of this program, our group used a conditional epicardial *Wt1KO (epiWt1KO)* (Fig. 11). Together with the embryonic epicardial program previously mentioned, both transcriptomic data allowed to generate a precise frame to clarify the WT1 role in the epicardium development. One of the genes modulated during the embryomic epicardium development and in *epiWt1KO* is *Bmp4*.

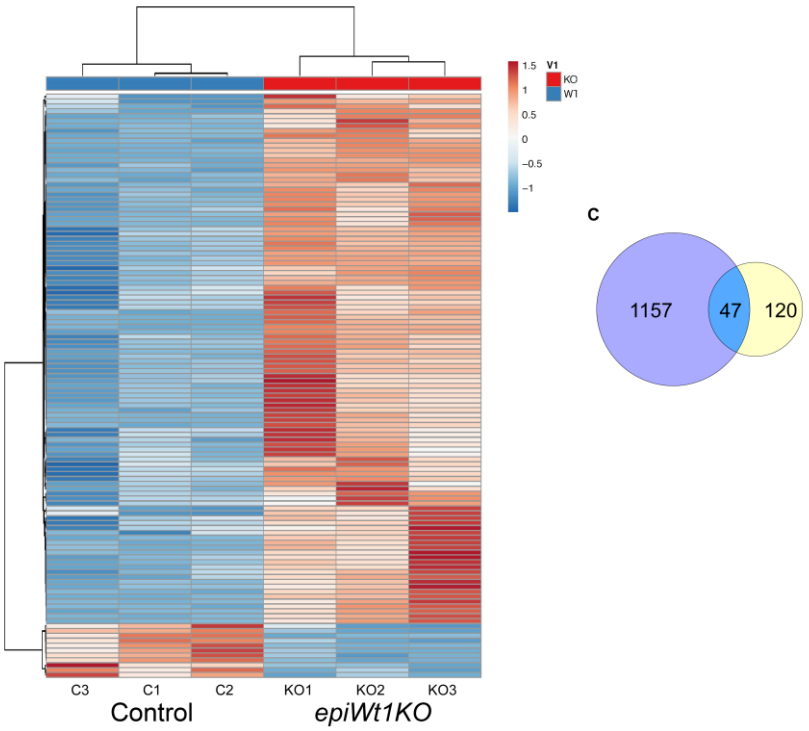


**Figure 11. Gene profiling of *Wt1*GFP$^{++}$sorted cells from control and *Gata5$^{Cre}$* *Wt1KO* mice.** (A) Heatmap of differentially expressed genes identified by transcriptomic analysis in *Wt1GFP$^{++}$* FACS-sorted cells from E13.5 control and *epiWt1KO* mice. (C) Identification of the role of *Wt1* in the embryonic epicardial program. Venn diagram showing the overlap of dynamically modulated genes during epicardial development (T1) with genes modulated in *Wt1GFP++* epicardial cells from *epiWt1KO* mice (T2). Modified from Velecela et al., 2019

### *5.3.2.6 The BMP4 pathway.*

*Bmp4* is a member of the Bone Morphogenetic Proteins (BMPs), a group of signaling molecules belonging to the Transforming Growth Factor-β (TGFβ) superfamily of proteins. While taking its name from the seminal studies describing BMP capacity to induce ectopic bone formation[264,265], BMPs have revealed as key morphogens in multiple processes during embryogenesis and development.

There are more than 15 different BMPs. According to its amino acid and nucleotide resemblance, BMPs can be clustered in 4 subgroups: BMP2/4, BMP5/6/7/8, BMP9/BMP10, and BMP12/13/14[266]. As well, there are two types of receptors binding BMPs. There are three type-I BMP receptors (BMPR-1A or ALK3, BMPR-1B or ALK6 and ActR-1A or ALK2) and three more type-II receptors (BMPR-2, ActR-2A and ActR-2B)[267]. BMP receptors form heterotetrameric complexes formed by a pair of dimers of type I and II receptors. The formation of these complexes requires the binding of a BMP to one type of receptor, and then the recruitment of the other type. In the case of BMP4, it preferentially binds type I receptors, and then recruit type II receptors[268].

Once BMPs bind to its receptor, BMPs signaling can act through canonical and non-canonical pathways (Fig. 12). BMP binding makes type II receptors phosphorylate type I receptors. Activated type I receptors can then phosphorylate three SMAD proteins (SMAD1, SMAD5 and SMAD8), forming a complex. Phosphorylated SMAD1/5/8 associates next with the co-mediator SMAD4. The resulting complex translocates then to the nucleus, where, in cooperation with different coactivators and corepressors, acts as a transcription factor. This pathway is additionally regulated by a set of inhibitory SMADS (SMAD6 and SMAD7) and a group of intracellular and extracellular modulators that include Noggin, Nbl1, DAN proteins, microRNAs, or phosphatases.

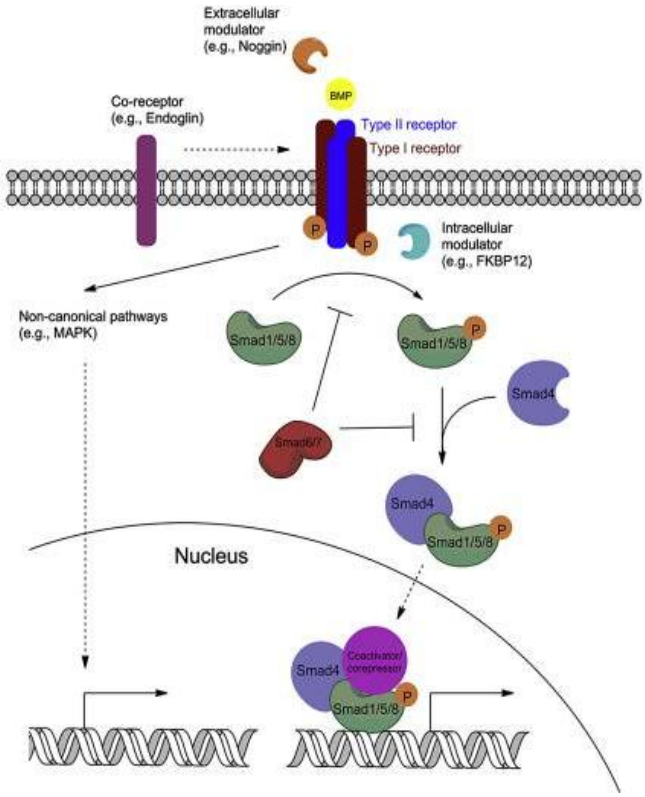

**Figure 12. BMP signaling pathway.** BMPs signal via the canonical or various non-canonical pathways. In the canonical pathway, BMPs bind to type I or type II serine/threonine kinase receptors and form a heterotetrameric complex. The constitutively active type II receptor then transphosphorylates the type I receptor, and the type I receptor phosphorylates SMAD1/5/8. Phosphorylated SMAD1/5/8 associates with the SMAD4. The complex translocates to the nucleus where it associates with coactivators or corepressors. Various non-canonical pathways can also lead to the regulation of gene expression. BMP signaling is modulated extracellularly), intracellularly and by co-receptors in the plasma membrane. Modified from Wang et al., 2014.

Besides the canonical pathway, BMPs have been described to activate other pathways, including MAPK, PI3K/Akt, P/kc, or Rho-GTPase pathways[269]. The decision of which pathway is activated largely depends on the cellular context: the extracellular microenvironment, the crosstalk with other pathways, etc.

*Bmp4* is essential for a wide range of events during development. In the absence of *Bmp4*, mesoderm is not formed[270], PGCs are not generated[271], and there is no lens induction[272]. *Bmp4* conventional KO does not surpass gastrulation (they do not differentiate mesoderm), hurdling the study of *Bmp4* role in post-gastrulation events. However, it has been described that *Bmp4* expression is needed for limb development, and it is necessary for a correct digit patterning and the apical ectodermal ridge[273].

#### *5.3.2.7 The epicardium in myocardial infarction.*

Heart failure occurs due to the damage of a wide number of cardiomyocytes, normally because of myocardial infarction (MI). Although human cardiomyocytes may be able to divide[274], the normal proliferation capacity of these cells is not enough to deal with the problems arising from MI[275]. To face this problem, different strategies have been followed. One of them has focused on the epicardium. Taking into account that epicardial cells are multipotent cardiac progenitors during development, several studies have tried to understand the epicardium's role during and after MI and then how to manipulate epicardial potency to ameliorate MI effects[145].

The regeneration capacity of the heart depends on the animal. Zebrafish hearts have the capacity to recover the lost cardiac muscle after MI[276]. Although adult mammals do not show this capacity, neonatal mouse hearts can regenerate after MI up to 7 days after birth[277]. The report of heart recovery in a newborn child after MI has suggested this regeneration window is also conserved in humans[278].

Although cardiomyocytes are the leading actors in this regenerative process, several studies have demonstrated that the epicardium also plays a role after MI. In a zebrafish transgenic animal in which epicardial cell population was ablated, cardiomyocyte proliferation was

inhibited and muscle regeneration delayed[279]. Actually, it is now clear that the epicardium is reactivated after MI, independently of the regeneration capacity of the organism in which this occurs. Epicardial hallmark embryonic genes are reexpressed (including *Wt1*), epicardial cells start to proliferate, cover the infarcted area, and through an EMT process contribute to different cell lineages in the damages zone of the heart[277,280–282].

First of all, epicardial proliferating cells cover the infarcted area[279]. It has been suggested that the triggering process for inducing epicardial cells to migrate is an increase in mechanical tension[283]. Cells covering the infarcted area start to produce ECM components that form a scaffold necessary for cardiomyocyte proliferation and correct migration[284–286]. The epicardium also modulates heart injury by secreting vascular mitogens and paracrine factors[287–289]. Furthermore, it has been demonstrated that reactivated epicardial cells can give rise to different types of cells in the damaged cell: myofibroblasts, perivascular cells, smooth muscle, and fat cells[284,290–292]. Additionally, the epicardium has also been described to modulate inflammation after MI[233,293].

Despite the epicardial contribution, it is evident that it is not enough to achieve complete heart repair. Therefore, it has been tried to stimulate the regenerative capacity of the epicardium. Thymosin β4 (Tβ4) is a G-actin monomer-binding peptide essential for embryonic epicardial EMT[259]. Tβ4 induces adult epicardial cell migration and the expression of epicardial embryonic markers[259,294]. In the adult injured heart, Tβ4 can induce epicardial embryonic gene expression, EPDC migration, and differentiation, allowing the formation of new blood vessels and cardiomyocytes[295,296].

In conclusion, the study of the embryonic epicardial mechanisms and characteristics has helped to understand how the epicardium contributes to heart regeneration. This has allowed opening the way for new potential therapies to deal with MI.

### 5.3.3 Wt1 in kidney development.

Kidney development starts when the intermediate mesoderm gives rise to two structures: the nephric duct and the metanephric mesenchyme[297]. From the nephric duct emerges the ureteric bud, which, in the end, will lead to the formation of the renal collecting system. The metanephric mesenchyme, through a process called nephrogenesis, which includes a mesothelial-epithelial transition (MET), will give rise to the functional unit of the kidney, the nephron[297].

*Wt1* expression is needed during different phases of kidney development. Deletion of *Wt1* abrogates bud outgrowth leading to a bilateral renal agenesis[76]. WT1 has also been described to be essential for initial metanephric mesenchyme survival[298] and posterior nephrogenic MET[17,299,300]. It has been proposed that WT1 exerts this function through the control of FGF and BMP-pSMAD pathways[127] and also through the regulation of *Wnt4*, a key gene in the control of embryonic kidney MET[17,299,301] . Using specific Cre models to delete *Wt1* expression after MET, it has been demonstrated that WT1 is necessary for posterior events in kidney development, as are tubule maturation and glomerulogenesis[302]. Even later, WT1 has also been described to be essential for podocyte function, and several *Wt1KO* models have been described to develop golmerulosclerosis[262,302–307].

### 5.3.4 WT1 in lung development.

During the lung development, *Wt1* is expressed in lung mesothelial cells. Through an EMT process, these mesothelial cells give rise to endothelial cells, smooth muscle cells, and other mesenchymal cells[308,309]. *Wt1KO* mice present defects during lung development: lung lobes fusion, diaphragmatic defects, and abnormal pleural cavities[309].

### 5.3.5 WT1 in pancreas development.

As in the lung, in the pancreas, *Wt1* is expressed only in mesothelial cells. Pancreatic mesothelial cells have been described to give rise to pancreatic stellate cells and endothelial cells[310]. *Wt1* germline KO die before it is possible to analyse pancreatic development but show an abnormal pancreas position. Mice in which *Wt1* has been deleted using Cre-ER tamoxifen technology showed defects in pancreas development consisting of a reduction in number and growth of acini. However, pancreatic differentiation seems to be unaffected by *Wt1* deletion[310].

### 5.3.6 WT1 in liver development.

Hepatic stellate cells are a mesenchymal type of liver cells that, although they only represent 5-8% of all liver cells, play a vital role in liver physiology and fibrogenesis. A subset of the hepatic stellate cells derive from the embryonic *Wt1* expressing mesothelium[62]. Indeed, *Wt1KO* embryos show reduced size livers with lobing anormalities, caused by an anomalous differentiation of hepatic stellate cells[311]. In the liver, as in other organs, *Wt1* has been suggested to act through the modulation of the RA pathway[311].

### 5.3.7 WT1 in fat development.

*Wt1* expression has been observed in several fat depots. It has not been observed, however, on subcutaneous WAT or BAT[312]. The developmental origin of fat depots is still not well understood. However, the use of lineage tracing strategies has proved that large percentages of adipocytes derive from WT1-positive cells in epicardial, omental, mesenteric, retroperitoneal and perirenal fat depots. But, again, not in subcutaneous WAT or BAT[313].

A role in adipocyte biology has also been described: deletion of *Wt1* on primary adipocytes using an *Adiponectin*$^{Cre}$ did not abrogate differentiation *in vitro*. However, it induced the expression of thermogenic genes like *Ucp1* or *Cidea* and the repression of pro-Inflammatory genes like *Saa3* or *Agt*[314].

## 5.4 WT1 in adult homeostasis.

In the adult, WT1 was traditionally though to be present in kidney podocytes, supporting gonadal cells, mesothelial cells lining the organs, and 1% of bone marrow cells[4]. However, WT1 in other organs in the adult have come to light in the past years[312,315]. Although traditionally believed to be a developmental gene, WT1 has proved to play a crucial role in adult homeostasis. Deletion of *Wt1* in adult tissues using a ubiquitous Cre-ER$^{TM}$ lead to severe deterioration of mice health up to the point that mice needed to be culled[312]. Kidneys from these mice presented acute glomerulosclerosis. The hematopoietic system showed aberrant defects: spleens were paler and smaller than normal spleens and mutant mice presented reduced extramedullary hematopoiesis in the red pulp compartment. Adult *Wt1KO* mice also showed atrophy in the pancreas, bone loss and fat reduction[312]. Moreover, using two different approaches to downregulate *Wt1* in adult mice, Christoph A. Gebeshuber's lab described how that lead in both cases to a focal segmental glomerulosclerosis phenotype[316], indicating that WT1 plays a crucial role in kidney homeostasis.

It has also been demonstrated that in the adult adrenal gland, a population of cells expressing *Wt1* persists. This population turned to be able to differentiate into gonadal steroidogenic cells throughout life[317]. Deletion of *Wt1* in the adult pancreas leads to the loss of normal tissue architecture by a mechanism involving the RALDH2/retinoic axis, suggesting a role for WT1 in adult pancreas homeostasis[315].

In humans, *WT1* expression in adult tissues can be analysed thanks to the effort of different platforms like the GTEx portal and the human protein atlas (Fig. 13). The data found in these

databases can be related to the phenotypes observed in adult mice. *WT1* is primarily expressed in sexual tissues (ovaries, testis, fallopian tubes, epididymis…), kidney, spleen smooth muscle, and adipose tissue[318].

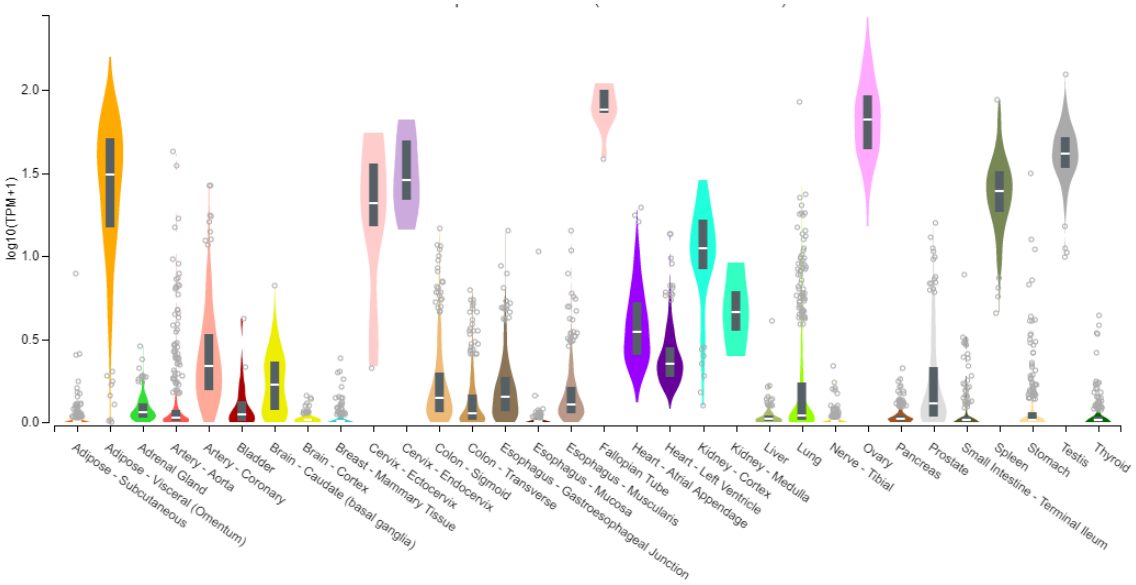


**Figure 13. Wt1 expression values in human adult tissues**. Values are expressed as the $\log^{10}$ of the measured TPM (Transcripts per million), calculated from a gene model with isoforms collapsed to a single gene. Box plots are shown as median and 25yh ant 75th percentiles. Points are displayed as outliers if they are above or below 1.5 times the interquartile range. Image obtained from GTEx Portal on 24/01/21.

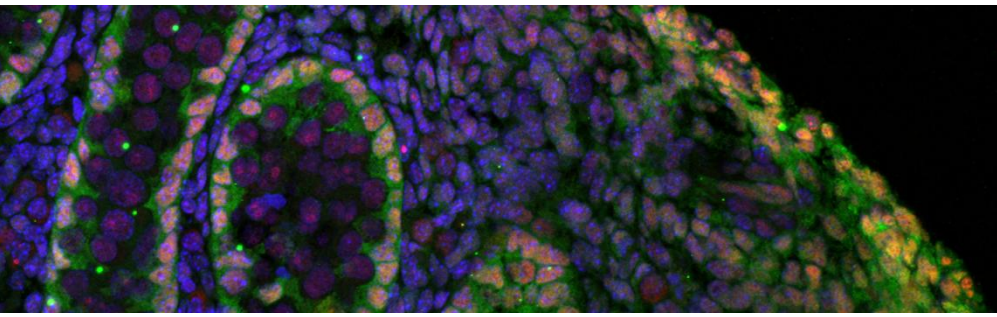

# MATERIALS AND METHODS

## 6.1 Reactives, kits and equipments.

In the following tables will be indexed the reactives, equipments, kits and other material used throughout this thesis.

### 6.1.1Cell culture media and its suplements.

| Cell culture media | Abbreviature | Manufacturer |
|---|---|---|
| Dubecco's Modified Eagle Medium 4,5g/l glucose | DMEM | Lonza BE12-914F |
| Hanks' Balanced Salt Solution | HBSS | Gibco 14025-050 |
| OptiMeM I | OptiMeM | Gibco 31985-047 |

**Table 3.** Cell culture media

| Reactive | Abbreviation | [Stock] | Manufacturer |
|---|---|---|---|
| Fetal bovine serum | FBS | 100% | Lab Clínic A15-101 |
| Penicilin/Streptomicine | P/S | 10.000U/ml - 10.000µg/ml | Lonza DE17602F |
| L-Glutamine | L-Gln | 200mM | Lonza 17905C |

**Table 4.** Cell culture media supplements.

### 6.1.2 Buffers.

| Buffer solution | Abbreviature | Composition |
|---|---|---|
| Phosphate buffered saline 1X | PBS | NaCl 1,36M; KCl 16,82M; $KH_2PO_4$ 14,69mM; $Na_2HPO_4$ 22,96 mM; pH7,2 |
| Phosphate buffer (1M) | PB | $KH_2PO_4$ 1M; $Na_2HPO_4 2H_2O$ 1M |
| Sample buffer | | Glycerol 10%; SDS 2%; β-mercaptoethanol 5%; 1M Tris pH 6,8 6%; Bromophenol blue 0,025% |
| Electrophoresis buffer 10X | SDS-Page | Glycine 1,92M; Tris base 0,25M; SDS 34,68mM |
| Transference buffer 10X | | Glycine 1,92M; Tris base 0,25M |
| WB Blocking buffer | | PBS-Tween, Skim milk 10% |
| WB Washing buffer | PBS-Tween | PBS 1X, TWEEN® 20 0,5% |
| Tris-Acetate-EDTA buffer 50X | TAE | Tris base 2M; Boric acid 1M; EDTA 50mM |
| Citrate buffer 10x | | Tri-Sodium Citrate 2-hydrate 100mM; pH 6,0 |
| Fixation buffer | PFA 4% | PB , PFA 4% |
| ChIP lysis buffer | | HEPES 5nM, KCl 85 mM , 0.5% NP-40 and |

| | | |
|---|---|---|
| | | protease inhibitor cocktail set III |
| Sonication buffer | | Tris–Cl 50 mM , EDTA 10 mM , 1% SDS and protease inhibitor cocktail set III |
| ChIP washing buffer | | HEPES 50mM, NaCl 500 mM , EDTA 1 mM , 0.1% SDS, 1% TritonX-100, 0.1% Na deoxycholate |

**Table 5.** Buffers

### 6.1.3 Enzymes.

| Reactive | Concentration | Manufacturer |
|---|---|---|
| Tripsine-EDTA | 0,5g/L-0,2g/L | Sigma T3924 |
| Collagenase Type I | 2g/L | Worthington LS004196 |

**Table 6.** Enzymes

### 6.1.4 Equipments.

| Equipment | Manufacturer |
|---|---|
| Class II type A2 Biological safety cabinet | Telstar |
| Incubator Jouan IGO150 Cell Life | Thermo Fischer Scientific |
| Refrigerate microcentrifuge | Eppendorf 5424R |
| Mili-Q® Integral Water Purification System | Millipore |
| Binocular magnifying glass StereoBlue | Euromex |
| Phase contrast microscope TS100 | Nikon |
| Phase contrast microscope Axiovert 40C | Zeiss |
| Inverted fluorescence microscope BX61 | Olympus |
| Camera DP70 | Olympus |
| Confocal microscope Zeiss 880 | Zeiss |
| Microtome RA303 | Leica Byosistems |
| Plate reader Infinite® M200PRO | Tecan |
| PCR Thermocycler | Eppendorf |
| PCR-RT Thermocycler StepOne® System | Applied Biosystems |
| Cytometer FACS Aria III | BD Biosciences |
| SensION+ pH3 | Hach |
| Mini-PROTEAN Tetra Cell | BioRad |
| Mini Trans-Blot Electrophoretic Transfer Cell | BioRad |

| | |
|---|---|
| Vivid Q | GEHealthcare |
| BP-2000 | Visitech Systems |
| HP Scanjet G2710 | HP |
| Electric pressure cooker | Palson 30622 Sapore 6L |
| Biosystems BOND RX research staining robot | Leica Biosystems |
| Diagenode bioruptor | Diagenode |

**Table 7.** Equipments.

### 6.1.5 Kits.

| Kit | Manufacturer |
|---|---|
| EZ-ECL kit | Biological Industries 20-500-120 |
| SuperscriptTM III First-Strand Synthesis SuperMix | Invitrogen 11752-50 |
| PureLink™ RNA Mini Kit | Invitrogen 12183025 |
| GoTaq® qPCR Master Mix | Promega A6002 |
| Single Cell RNA Purification Kit | Norgen 5180 |
| Quantitect® Whole Trenscriptome Kit | QIAGEN 207043 |
| GoTaq® G2 Green Master Mix | Promega M7822 |
| Cell Proliferation ELISA, BrdU | Roche 11647229001 |
| Dual-Glo® Luciferase Assay System | Promega E2920 |
| ACD Bio LS 2.5 Brown RNAscope assay kit | ACD, 401308 |

**Table 8.** Kits

### 6.1.6 Other reactives and products.

| Reactive | Abbreviation | [Stock] | Manufacturer |
|---|---|---|---|
| Ethidium bromide | | 400µg/ml | Sigma E8751 |
| Agarose | | | Sigma A2576 |
| 1kb DNA Ladder | | | Promega G571A |
| Spectra™ Multicolor Broad Range Protein Ladder | | | Thermo Scientific™ 26634 |
| Paraformaldehyde | PFA | | Sigma P6146-1KG |
| Formaldehyde | | | (Calbiochem, 344198) |
| Superfrost Plus™ Adhesion Microscope | | | Thermo Scientific™ |

| | | | |
|---|---|---|---|
| Slides | | | J1800AMNT |
| Super PAP Pen | | | Invitrogen 8899 |
| Bovine Serum Albumin | BSA | | Sigma A2153-100G |
| Tris | | 400µg/ml | Sigma E8751 |
| Glycerol | | | Sigma A2576 |
| Glycine | | | Sigma 50046-50G |
| Sodium Dodecyl Sulfate | SDS | | Sigma L5750 |
| β-mercaptoethanol | | | Sigma M6250 |
| Bromophenol blue | | | Sigma B8026 |
| Tween 20 | | | Sigma P1379 |
| Skim milk | | | Nestle Sveltesse |
| Methanol | | | PanReac Applichem UN1230 |
| Ammonium persulfate | APS | 10% | Sigma A3678-25G |
| N,N,N',N'-Tetramethylethylenediamine | TEMED | | Sigma T9281-100ML |
| Acrylamide/Bis-acrylamide, 30% solution | Acrilamide | 30% | Sigma A3574-100ML |
| Membrana Immobilon-P, PVDF | | | Merck IPVH00010 |
| Carestream® BioMax® light film | | | Kodac373508-50EA |
| ReBlot Plus Mild Antibody Stripping Solution | Stripping solution | 10X | Sigma 2502 |
| Carestream® autoradiography GBX developer/replenisher | Developer | 5x | Sigma P7042 |
| Carestream® autoradiography GBX fixer/replenisher | Fixer | 5x | Sigma P7167 |
| Magnetic Dynabeads | | | Thermo Scientific™ 1001D |
| Proteinase K | | | Sigma 1245680100 |
| Protease inhibitor cocktail set III | | | Calbiochem |
| Mayer's Haematoxylin. | | | Dako S3309 |
| DPX mounting medium | | | Cell Path Ltd SEA-0302-00A |

**Table 9.** Other reactives and products.

## 6.2 Animal models.

### 6.2.1 An introduction to the Cre technology.

The Cre-loxP system was discovered in 1986 in the bacteriophage P1[319]. Only 4 years after it was used to insert an exogenous DNA into eukaryotic cells[320]. It took merely two years more to generate the first transgenic mice with the Cre-loxP system[321,322]. Since then, a myriad of Cre mouse models has been created to generate knockouts, perform lineage tracing experiments, and, in general, modify the genome.

As the Cre-loxP system is a well-known and widely used technology, I will explain it briefly: Cre is a protein that catalyzes site-specific recombination between two loxP sequences. Therefore, to delete a region of the genome, it must be flanked by those sequences. In the presence of Cre, this region will then be cut and excised. It is possible to control the expression of Cre so that it is only expressed when and where we desire. Depending on the promoter regulating Cre expression, it will be expressed in the cells and at the time this promoter is active. Moreover, it has also been developed a tool that allows the temporal control of the activity of Cre: the Cre-estrogen receptor system. In this system, Cre, although expressed, is not active in the absence of tamoxifen. In the presence of this drug, Cre is drove to the nucleus, where it can exert its function.

For better clarity of future explanations, it may be helpful to explain also how this technology is used to perform lineage tracing experiments. In this kind of experiment, cells either do not express any fluorescent protein or express one, let's say, as an example, a red fluorescent protein. In the presence of a Cre recombinase, cells either start to express a fluorescent protein or, in case they did express one, a different one, following with the example, a green fluorescent protein. So cells in which the promoter controlling Cre expression is active and, importantly, all their descendants (no matter if the Cre is not active in them), will then express the new fluorescent protein. Therefore this system allows tracing all the descendants of a group of cells in which a specific promoter is active.

### 6.2.2 Animal husbandry.

All animals used in this thesis were housed in the animal facility of the Pharmacy faculty of the “Universitat de Barcelona”. All animal experiments were approved by the Animal Experimentation Ethics Committee (CEEA) of the University of Barcelona, thereby complying with current Spanish and European legislation.

### 6.2.3 Transgenic animal models.

During this thesis, several transgenic mouse models have been used. I will explain each of them below. In experiments where no transgenic mice were used, the CD1-IGS strain was used. CD1-IGS mice were provided by the Unit of animal experimentation of the faculty of from the Universit of Barcelona.

**a) *Wt1*$^{GFP/+}$ knock-in mice**

*Wt1*$^{GFP/+}$ mice were generated by Hosen et al. (2007)[323]. In these mice, exon 1 of one of the *Wt1* alleles has been replaced by a green fluorescent protein (GFP) sequence. Therefore GFP is expressed under the endogenous regulatory sequences of *Wt1*. As a consequence, GFP is expressed in all cells where *Wt1* is expressed, acting as a reporter of *Wt1* expression. The allele where *Wt1* exon 1 has been replaced does not generate the major isoforms of *Wt1*. However, the loss of one allele in *Wt1*$^{GFP/+}$ mice does not affect viability[323].

**b) Tg(WT1-cre)#Jbeb (*Wt1*$^{Cre}$) mice**

Wt1$^{Cre}$ mice were generated by Wessels *et al.,* (2012)[166,221]. In these mice the genome has inserted in an unknow position a BAC (RP23-266M16; https://bacpacresources.org/). This BAC contains the region of the genome ranging from -127kpb to +11.5kpb relative to *Wt1* transcription start site. 17bp downstraim of the translational start site of the Wt1 gene it is placed an IRES-EGFP-CRE cassette. As a consequence, and in theory, everywhere WT1 is expressed a Cre recombinase will be expressed allowing for lineage tracing experiments or the deletion of specific genes in *Wt1* expressing cells.

**c) Wt1 conditional line (*Wt1*$^{loxP/loxP}$)**

*Wt1* conditional mice were generated by Martínez-Estrada *et al*., (2010)[190]. In these mice the exon 1 of both *Wt1* alleles is flanked by loxP regions. Accordingly, In the presence of a Cre recombinase, the region between these loxP sites will be cut off generating a *Wt1* knockout of its major isoforms.

**d) *R26R*$^{mTmG}$ mouse line.**

*R26R*$^{mTmG}$ mouse line was generated by Mandar Deepak et al., (2007)[324]. In these mice a ROSA fluorescent protein is expressed ubiquitously. In the presence of a Cre recombinase the expression of this protein is shut down and GFP begins to be expressed in every Cre expressing

cell and therefore in all cells that come from those that once have expressed the Cre recombinase.

**e) *R26R$^{tdRFP}$* mice**

*R26R$^{tdRFP}$* mouse line was generated by Hervé Luche et al., (2007)[325]. In these mice a red fluorescent protein is the ubiquitoulsy expressed ROSA26 locus. The tdRFP is placed in an antisence orientation with respect to the ROSA26 transcription. Therefore, in the presence of a Cre recombinase the tdRFP is correctly orientiated and expressed. In Cre expressing cells and all cells deriving from them will then be RFP positive.

**f) *Gata5$^{Cre}$* mice**

*Gata5$^{Cre}$* mice were generated by Pilar Ruiz Lozano[184]. In these mice a Cre recombinase sequence lies behind the *Gata5* promoter. Details about *Gata5* expression in heart have already been published.

### 6.2.4 Matings.

Embryos were generated through timed matings, whereby females that have mated during the night were checked for plugs early the following morning. The morning on which a plug was found was considered to be E0.5.

### 6.2.5 Genotyping.

The different crossing strategies followed to generate the animals used in the experiments presented in this thesis required in many cases the genotyping of embryos or adult mice.

***DNA extraction***

First of all genomic DNA was purified from mouse ear clips or tissue fragments extracted from embryos:

1. The ear clips were first incubated with 500µl of NaOH 50µM at 100°C.
2. Tissue fragments were mechanically disaggregated with the help of a pipette.
3. 60µl of HCl 1M were added and the samples were incubated 5 additional minutes at 100°C.
4. Genomic DNA samples were then centrifuged 15 minutes at 12000g.
5. The supernatant was then transferred to a new tube.

### *PCR*

Once genomic DNA was purified, a genotyping reaction mix was prepared for each sample and gene. Each reaction mix consisted of:

| Reactive | Volume |
|---|---|
| PCR mix | 12.5 µl |
| Primers | 0.5µl/ primer |
| $H_2O$ nuclease free water | Up to complete the final 25µl of the reaction mix |
| Sample | 5 µl |

**Table 10.** Genotyping PCR mix.

Primers used for genotyping can be found in table10

| Gene | Sequence |
|---|---|
| *Cre/F* | 5'-GCATTACCGGTCGATGCAACGAGTGATGAG-3' |
| *Cre/R* | 5'-GAGTGAACGAACCTGGTCGAAATCAGTGCG-3' |
| *Fabpi200/F* | 5'-TGGACAGGACTGGACCTCTGCTTTCCTAGA-3' |
| *Fapbi200/R* | 5'-TAGAGCTTTGCCACATCACAGGTCATTCAG-3' |
| *$Wt1^{loxP}$/F* | 5'-TGGGTTCCAACCGTACCAAAGA-3' |
| *$Wt1^{loxP}$/R* | 5'-GGGCTTATCTCCTCCCATGT-3' |
| *$Wt1^{loxP}$/R2* | 5'-GTACGCGCGAACACTGACTA-3' |
| *$Wt1^{GFPm}$/F* | 5'-GCCTGAAGAACGAGATCAGC-3' |
| *$Wt1^{GFPm}$/F2* | 5'-AGCCTGAAGCTGCTCACATCC-3' |
| *$Wt1^{GFPm}$/R* | 5'-GGCAGCTTGAATTCCTCTCA-3' |
| *Rbm31 F* | 5'-CACCTTAAGAACAAGCCAATACA-3' |
| *Rbm31 R* | 5'-GGCTTGTCCTGAAAACATTTGG-3' |
| *R26g2F* | 5'-TGTTATCAGTAAGGGAGCT-3' |
| *R26g2/Rmut* | 5'-AAGACCGCGAAGAGTTTGT-3' |
| *R26g2/Rwt* | 5'-CACACCAGGTTAGCCTTTA-3' |

**Table 11.** List of primers used for genotyping.

PCR reaction mix were run in a thermocycler under the following cycling conditions:

| Cycles | Temperature | Time |
|---|---|---|
| 1 | 94°C | 3 minutes |
| 35 | 94°C | 30 seconds |
| | 58°C | 30 seconds |
| | 72°C | 1 minute |
| 1 | 72°C | 5 minutes |
| | 4°C | - |

### *PCR result visualization*

To visualize PCR results, the amplified DNA was run on 2% agarose gels. Agarose gels were run as follows:

1. Using a microwave, agarose was dissolved on TAE buffer until the solution was almost boiling.
2. Once the mix had cooled, but before solidification of the agarose, ethidium bromide was added at a final concentration of 16ng/ml.
3. The mix was placed on the appropriate recipient with a mold to generate the desired number of wells.
4. Once the mix had polymerized the gel was placed on an electrophoresis cell and samples were loaded.
5. To prepare the DNA ladder, 9µl of nuclease free water, 2µl of loading buffer and 1µl of the Promega ladder were mixed. Then it was loaded next to the samples.
6. Then the gel was run TAE buffer at a voltage of 90V until the front reached the end of the gel.
7. The result was visualized on a UV light transilluminator.

## 6.3 Western Blot.

Western blot is a semi quantitative technique that allows measuring the presence of a protein in a cellular lysate. In this thesis cellullar lysates were obtained either from embryonic tissues or cultured cells. Westerns blots were performed according the following protocol.

### 6.3.1 Protein extraction.

In the case of cultured cells:

1. Sample buffer was warmed at 95°C for 5 minutes.
2. Next, sample buffer was added to the well.
3. Using a pipette tip the surface of the well was intensely scrapped.
4. Sample buffer was then picked from the well and stored at -20°C until it was used.

In the case of tissues:

1. Embryos were dissected under a binocular magnifying glass in PBS using 2 sterile needles.
2. Dissected hearts were placed on a tube.
3. 95°C warmed sample buffer was loaded on the tube.
4. Using a pippete heart was disaggregated in the sample buffer.
5. For a better disaggregation the lysate was then warmed again at 95°C for 5 extra minutes.
6. Lysates were stored at -20°C until they were used.

### 6.3.2 Gel preparation.

Before starting the electrophoresis, 10% acrylamide gels were prepared. Gels were formed by the resolving gel and the stacking gel.

1. First the resolving gel was prepared. For 10ml:

| Component | Volume |
|---|---|
| Tris 1,5M pH 8,8 | 2,5ml |
| SDS 10% | 100µl |
| Acrilamyde 30% | 3,3ml |
| APS | 70µl |
| TEMED | 7µl |
| Mili-Q water | 4ml |

**Table 12.** Resolving gel components volumes.

2. After the resolving gel had polymerized the stacking gel mix was prepared. For 5 ml:

| Component | Volume |
|---|---|
| Tris 0,5M pH 6,8 | 1,25ml |
| SDS 10% | 50µl |
| Acrilamyde 30% | 0,65ml |
| APS | 60µl |
| TEMED | 7µl |
| Mili-Q water | 3,05ml |

**Table 13.** Stacking gel components volumes.

### 6.3.3 SDS-PAGE electrophoresis and protein transference.

1. Gels were placed in the electrophoresis system (Mini-PROTEAN Tetra Cell from Bio-Rad) and the electrophoresis buffer was loaded.
2. Before loading the samples, lysates were incubated during 5 minutes at 95°C.
3. Next lysates were loaded in the acrilamide gels. Next to them the protein ladder Spectra BR from Thermo Scientific™ was also loaded.
4. Gels were run in the electrophoresis buffer at a voltage of 100V until the protein front reached the end of the gel.
5. While the electrophoresis was running, transfer buffer was prepared. For this 700ml of mili-Q water, 200ml of methanol and 100ml of transfer buffer 10X were mixed.
6. Additionally, before transference PVDF membranes were activated for 5 minutes in methanol and then immersed on transfer buffer until they were used.
7. Once electrophoresis had finished, stacking gel was removed. The resolving gel was then placed in the transference sandwich. This was formed by the gel, the PVDF membrane upon it, and both of them between two pieces of Whatmann paper and two foam pads.
8. The sandwich was placed on the transference system (Mini Trans-Blot Electrophoretic Transfer Cell form Bio-Rad) and the transference buffer and a cooling unit of ice is added.
9. Transference was run at a voltage of 90V for 90 minutes.

### 6.3.4 Immunodetection assay.

1. Once the transference had finished PVDF membranes were blocked with 10% skim milk in PBS Tween 0.1% for 1 hour.

2. Incubation of primary antibodies (table 14) was performed in PBS Tween 0.1% BSA2% overnight at 4°C on a shaker.
3. Next day, after primary antibody solution was removed, membranes were washed in PBS Tween 0.1% three times 10 minutes each on a shaker.
4. For secondary antibody incubation, HRP-conjugated secondary antibodies (Table 14) were dissolved in PBS Tween 0.1% and 0.01% skim milk and added to the membranes for 1 hour at room temperature on a shaker.
5. Again, after secondary antibody incubation, membranes were washed 3 times in PBS tween 0.1% for 10 minutes on a shaker.
6. EZ-ECL mix was prepared according to the instructions provided by the manufacturer (mixing equal proportions of solution A and solution B).
7. ECL mix was then added to the membranes for 2 minutes.
8. Visualization of luminiscence was done in a dark room using Carestream® BioMax® light films from Kodak and developing and fixer reactives.
9. When necessary membranes were stored at 4°C. For doing new protein detection the former antibody was removed by incubating the membrane in stripping solution 1X for 10 minutes. Then membranes were washed with PBS tween 0.1%. Next, the protocol continued as noted in step 1 of this section.

### 6.3.5 Film scanning and densidometry.

1. Films were scanned using a photo scanner.
2. Analysis of the films was performed using ImageJ[326] by a densidometry analysis. These analyses were carried in the following way.
3. Scanned films were open with ImageJ software.
4. Images were converted to 8 bit images.
5. Converted images were then inverted in the gray scale.
6. The intensity of each band was quantified using the same area for every band. Using the same area to analyse bright intensity, a background measure was taken.
7. Background measure was subtracted to all other measures. Then the value of the analysed protein was normalized using the charge control of every sample. Finally each sample was normalized with respect to control sample.

| Antibody | Dilution | Description | Manufacturer |
|---|---|---|---|
| WT1 | 1:1000 | Rabbit | Abcam ab89901 |
| GAPDH | 1:1000 | Mouse | Santa Cruz sc-32233 |
| pSMAD 1/5 | 1:1000 | Rabbit | Cell Signaling 41D10 |
| SMAD 1/5/8 | 1:1000 | Rabbit | Santa Cruz sc-6031-R |
| Anti-Rabbit IgG | 1:2000 | Goat | Sigma A6154 |
| Anti-Mouse IgG | 1:2000 | Goat | Sigma A4416 |

**Table 14.** Antibodies used for Western blot experiments.

## 6.4 Gene expression analysis.

For gene expression analysis qRT-PCR technique has been used. To perform these analyses RNA was extracted from tissues and cells, then reverse ranscribed to cDNA and finally the levels of each gene expression were measured using qRT-PCR.

### 6.4.1 RNA extraction.

For RNA extraction from cultured cells or tissues, PureLink™ RNA Mini Kit was used according the manufacturer instructions. Briefly:

1. Lysis buffer complemented with β-mercaptoethanol (10µl/ml of lysis buffer) was poured into the plates were cells were cultured. The surface was then scrapped with a tip. Then the lysis buffer was recovered and placed on a new tube.
2. Lysates were mixed with ethanol 70% RNAse free (1:1 proportion) by vortexing.
3. Next, purified RNA was poured into the kit columns.
4. Columns were then washed with the solutions provided by the manufacturer.
5. RNA was eluted in RNAse free water.
6. RNA concentration in ng/ml was quantified using a NanoQuant plate (TECAN) and the reader 200 PRO (TECAN).

For RNA extraction from FACS sorted cells, Single Cell RNA Purification Kit was used according the manufacturer instructions. Briefly:

1. Lysis buffer complemented with β-mercaptoethanol (10µl/ml of lysis buffer) was poured into the tube were cells had been FACS-sorted. To extract the RNA cells were mechanically lysed using a pipette.
2. Lysates were mixed with ethanol 100% RNAse free (1:1 proportion) by vortexing.
3. Next, RNA was poured into the kit columns.

4. Columns were then washed with the solutions provided by the manufacturer and according to its instructions.
5. RNA was eluted in RNAse free water.
6. RNA concentration in ng/ml was quantified using a NanoQuant plate (TECAN) and the reader 200 PRO (TECAN)

### 6.4.2 cDNA sinthesis.

Purified RNA was reverse transcribed to obtain cDNA. For this purpose *SuperscriptTM III First-Strand Synthesis SuperMix* kit was used:

1. For each reaction up to 1000ng of RNA in a maximum volume of 20 µl were transcribed. Reaction mix was prepared as follows:

| Reactives | Volume |
|---|---|
| Rt enzyme | 1.5 µl |
| Mix | 10 µl |
| Sample | 1000ng |
| $H_2O$ RNAse free | Necessary to complete the 20 µl |

**Table 15.** Retrotranscrition reaction mix.

When the concentration of the RNA elution was too low to reach 1000ng in 8.5µl, 8.5µl of the sample with the lowest concentration marked the concentration for the rest of the samples of the experiment. For every reverse transcription one of the samples was also transcribed in absence of the Rt enzyme as a negative control for the qRT-PCR experiments.

2. Samples were the placed into a thermocycler and rtPCR was performed under the following conditions:

| Temperature | Time |
|---|---|
| 25°C | 10 minutes |
| 50°C | 30 minutes |
| 85°C | 5 minutes |
| 4°C | - |

3. When this protocol had finished 1µl of RNAseH was added to every sample and tubes were incubated during 20 minutes at 37°C.

### 6.4.3 qRT-PCR.

Quantitative real time PCR (qRT-PCR) allows the quantification of a gene of interest in a sample. qRT-PCRs were performed according the next protocol:

1. For each reaction a 15µl volume reaction mix was prepared. For each sample that was tested for every gene, triplicates were done. Each reaction mix consisted of:

| Reactive | Volume |
|---|---|
| goTaq master mix | 7.5µl |
| $H_2O$ nuclease free water | 6.6µl |
| Primers 50 µM | 0.45µl/ primer |

**Table 16.** qRT-PCR reaction mix.

2. Once the reaction mix was ready the sample was added. Then each reaction was added into the wells of 96 well plates.
3. The plates were then run in a thermocycler under the following cycling conditions:

| Step | Cycles | Temperature | Time |
|---|---|---|---|
| 1. Pre incubation | 1 | 95°C | 10 minutes |
| 2. Amplification | 40 | 95°C | 30 seconds |
| | | 60°C | 40 seconds |
| | | 72°C | 30 seconds |
| 3. Melt curve | 1 | 95°C | 15 seconds |
| | | 60°C | 1 minute |
| | | 95°C | 15 seconds |

4. For each reaction an amplification curve was obtained. For each curve the StepOne software obtained a threshold cycle (Ct) value. These values were used to calculate gene expression in the following way:
   4.1. The mean of the Ct replicates was calculated.
   4.2. Gene of interest Ct (iCt) was normalized by the gene of reference Ct (rCt). And a ΔCt was obtained: $\Delta Ct = iCt - rCt$
   4.3. Each ΔCt was then normalized to the reference sample ΔCt (rΔCt): $\Delta\Delta Ct = r\Delta Ct - \Delta Ct$
   4.4. As amplifying curves are a logarithmic expression of the measured expression values. ΔΔCt were used to calculate the lineal values: $Gene\ expression\ value = 2^{-\Delta\Delta Ct}$

In this thesis 18S rRNA expression was used as a reference gene. The primers used for qRT-PCR analysis can be found in table 16.

| Gene | Primer | Sequence 5'-3' |
|---|---|---|
| *Wt1* | F | TTCAAGGACTGCGAGAGAAG |
| | R | GGGAAAACTTTCGCTGACAA |
| *Bmp4* | F | GAGGAGTTTCCATCACGAAGA |
| | R | GCTCTGCCGAGGAGATCA |
| *Wnt4* | F | AGACGTGCGAGAAACTCAAAG |
| | R | GGAACTGGTATTGGCACTCCT |
| *Sox9* | F | CAGCAAGACTCTGGGCAAG |
| | R | TCCACGAAGGGTCTCTTCTC |
| *Sry* | F | GCTGGGATGCAGGTGGAAAA |
| | R | CCCTCCGATGAGGCTGATATT |
| *Fgf9* | F | GGGGAGCTGTATGGATCAGA |
| | R | TCCCGTCCTTATTTAATGCAA |
| *Rspo1* | F | CGACATGAACAAATGCATCA |
| | R | CTCCTGACACTTGGTGCAGA |
| *Podxl* | F | TCCTTGTTGCTGCCCTCT |
| | R | CTCTGTGAGCCGTTGCTG |
| *Tbx18* | F | CCGAGACTCTAGGAAC |
| | R | TGATGGCCTCGAATGC |
| *Krt8* | F | AGTTCGCCTCCTTCATTGAC |
| | R | GCTGCAACAGGCTCCACT |
| *Msln* | F | CTGCAGACCCAGACTACAAAGA |
| | R | GAGGCCTGTGGGGAGACT |
| *Smpd3* | F | GATTGACGGCTGTCATTACCT |
| | R | ATGTAATCGCCCTTGAATGC |
| *Cdkn1c* | F | TCTCCTTTGCTCGTTT |
| | R | GGCATTGTGGGTGTTG |
| *18S* | F | CGATTGGATGGTTTAGTGAGG |
| | R | AGTTCGACCGTCTTCTCAGC |

| | | |
|---|---|---|
| *Fst* | F | TGGATTAGCCTATGAGGGAAAG |
| | R | TGGAATCCCATAGGCATTTT |
| *Amh* | F | CCACACCTCTCTCCACTGGTA |
| | R | GGCACAAAGGTTCAGGGGG |
| *Runx1* | F | GCAGGCAACGATGAAAACTACT |
| | R | GCAACTTGTGGCGGATTTGTA |
| *Foxl2* | F | ACAACACCGGAGAAACCAGAC |
| | R | CGTAGAACGGGAACTTGGCTA |
| *Sf1* | F | CCTCGATGTGAAATTCCTGAACA |
| | R | TCCTGGGCGTCCTTTACG |
| *Cbx2* | F | AGGCCGAGGAAACACACAG |
| | R | TCTCTTGGAGTCTAGGTCGCT |
| *Hsd3b1* | F | CTCAGTTCTTAGGCTTCAGCAATTAC |
| | R | CCAAAGGCAAGATATGATTTAGGA |
| *Star* | F | CCGGAGCAGAGTGGTGTCA |
| | R | CAGTGGATGAAGCACCATGC |
| *Cyp11a1* | F | CCAGTGTCCCCATGCTCAAC |
| | R | TGCAGTGTCCTTCCAGGTCT |
| *Ddx4* | F | AGGGGATGAAAGAACTATGGT |
| | R | AGCAACAAGAACTGGGCACT |
| *Stra8* | F | CTCCTCCTCCACTCTGTTGC |
| | R | GCGGCAGAGACAATAGGAAG |
| *Dppa3* | F | GACCCAATGAAGGACCCTGAA |
| | R | GCTTGACACCGGGGTTTAG |
| *Nanog* | F | AGGCTTTGGAGACAGTGAGGTG |
| | R | TGGGTAAGGGTGTTCAAGCACT |
| *Ppargc1a* | F | GGAGCCGTGACCACTGACA |
| | R | TGGTTTGCTGCATGGTTCTG |

**Table 17.** qRT-PCR primer list.

### 6.4.4 RNAscope.

To validate *Bmp4* expression in the epicardium, a RNAscope *in situ* hybridisation was performed. *In situ* hybridisation uses labelled probes to localize a DNA or RNA sequence (RNA in this case) in a tissue section. For this technique, mouse heart cryosections with a thickness of 12µm and stored at −80°C, were used. RNAscope for *Bmp4* was performed on a Leica Biosystems BOND RX research staining robot (Leica Biosystems), as follows:

1. Frozen sections were removed from storage at −80°C and fixed immediately in pre-cooled ice cold 4% neutral buffered formaldehyde.
2. Next, sections werw washed with 5min incubations of 50%, 70% and 100% ethanol at room temperature.
3. Slides were then placed onto an RX staining robot and stained using the ACD Bio LS 2.5 Brown RNAscope assay kit, following manufacturer's recommendations.

4. Appropriate control probes (PPIB and DapB) were used to determine that the optimal pre-treatment conditions were 20 min incubation with protease only. The *Bmp4* probe was stained under identical conditions.
5. RNAscope staining slides were then counterstained with Haematoxylin, dehydrated in graded ethanol, cleared in xylene and coverslipped with Pertex.

### 6.4.5 Chromatin immunoprecipitation (ChIP).

Chromatin IP allows the isolation of sequences bound by a specific protein. Using antibodies against that protein, DNA bound by the selected protein in separated using magnetic beads. Then, the presence of the region of interest is analysed through a qRT-PCR. Chromatin IP was performed as follows:

1. Immortalised epicardial cells were dissociated with 1:10 diluted trypsin and fixed with 1% formaldehyde 10 min at room temperature.
2. Crosslinking was stopped by adding 0.125M glycine.
3. Cells were then centrifuged and washed in ice-cold PBS.
4. Ten ml of ChIP lysis buffer were added for 10min, in ice, to cells.
5. Cells were again centrifuged and the pellet was resuspended in 0.3ml of sonication buffer ($2*10^6$ cells).
6. Next, DNA was sonicated into 200–500 bp fragments using a Diagenode Bioruptor.
7. After centrifugation (10 min, 13000rpm, 4°C), chromatin lysates were centrifuged and supernatants used for immunoprecipitation.
8. Magnetic Dynabeads Protein A were used for immunoprecipitations with 10µg of antibodies against WT1 (Abcam, ab89901) and rabbit IgG (Sigma-Aldrich, I8140) as a control. Immunoprecipitations with crosslinked chromatin were carried out ON at 4°C using antibody prebound magnetic beads.
9. Next day, beads were washed with ChIP washing buffer six times.
10. Bound complexes were eluted with 0.3 ml of 50 mM Tris–HCl, 10 mM EDTA, 1% SDS and proteinase-K. Immunoprecipitated and input DNA were isolated by phenol: chloroform extraction followed by ethanol precipitation
11. Eluted DNA was quantified by qRT-PCR as previously described, using the primers of table 18.

| Region | Primer | Sequence 5'-3' |
|---|---|---|
| *Bmp4 promoter* | F | CCCCGCCTCGAAAACTGG |
| | R | TGTTCTAACCTCGGAAGCGC |
| UTR negative control | F | AAGACTGGGGAGGAAGGGAA |
| | R | AGGGACGGAGACCAGATACT |

Table 18. ChIP primer list.

## 6.5 Histological techniques.

### 6.5.1 Histological analysis.

Mice used for the histological analysis were sacrificed with carbon dioxide gas. After weighing the animals a complete necropsy was performed.

And the following selected tissues were collected and processed for histopatological evaluation: genitourinary organs, liver, lung, heart, kidney, adrenal glands, brain, gastrointestinal tissue and brown adipose tissue.

All sampled tissues were fixed in 10% neutral-buffered formalin, for approximately 24 hours, processed, and embedded in paraffin. Embedded tissues were cut into 4 to 5 µm sections, stained with haematoxylin and eosin (H&E) and reviewed by light microscopy by a certified pathologist from the Histopahologt facility of the Institute for research in Biomedicine (IRB).

### 6.5.2 Haematoxylin and Eosin staining .

1. Slides were dewaxed in xylene (3x 5 minute washes), before being rehydrated in a series of ethanol washes (3x 5 minutes in 100% EtOH, followed by 2 minutes each in 90%, 70%, 50% and 30% EtOH).
2. Slides were washed in tap water
3. Then slides were stained for 5 minutes with Mayer's Haematoxylin.
4. After another wash with tap water,
5. sections were differentiated in 1% HCl in 70% EtOH for a few seconds and washed with tap water.
6. Slides were then placed in Saturated Lithium Carbonate solution for a few seconds and washed in running tap water for 5 minutes.
7. After staining with Eosin for 2-5 minutes, slides were rinsed in tap water again before placing into 100% EtOH.

8. Following 3 more washes in 100% EtOH (1-2 minutes each), the slides were cleared in xylene (3x 5 minute washes)
9. and mounted using DPX mounting medium. Eosin stain: 3 parts 1% aqueous Eosin and 1 part 1% EtOH, with Acetic Acid 0.05% final concentration.

### 6.5.3 Immunohistochemistry.

#### *Sample fixation and paraffinization*

Embryos were washed in PBS and then fixed in fixation solution (PFA 4%). Embryos were then whashed in a graded series of ethanol, buthanol and finally in paraffin. Then, samples were embedded in paraffin wax. The times of PFA fixation and alcohol washes depended on the stage of embryo development. These times can be found in table 19.

| Embryo stage | PFA 4% | PBS | EtOH 70 % | EtOH 80 % | EtOH 90 % | EtOH 96 % | EtOH 100 % | BuOH | Paraffin |
|---|---|---|---|---|---|---|---|---|---|
| E9.5-10.5 | 1 h | 20 min | 15 min | 15 min | 15 min | 15 min | 10 min + 10 min | 10 min + 10 min | 3x30min |
| E11.5-12.5 | 2h | 20 min | 25 min | 25 min | 25 min | 25 min | 15min +15 min | 15min +15 min | 3x30min |
| E13.4-14.5 | 3h | 20 min | 30 min | 30 min | 30 min | 30 min | 20 min + 20 min | 20 min + 20 min | 1h +2x30min |
| E15.5-16.5 | 4h | 20 min | 45 min | 45 min | 45 min | 45 min | 30 min + 30 min | 30 min + 30 min | 2h +1h +1h |

**Table 19.** Fixation and deshidratation times.

When the procedure was too long, fixed embryos could be stored in Et0H 70% at 4°C for several weeks. Once embryos were embedded in paraffin they were stored at room temperature until they were used to generate the sections used for immunohistochemistry.

Paraffin sections were cut 5-7µm thick using a microtome. Sections were mounted on Superfrost PlusTM slides.

#### *Immunofluorescence staining of paraffin sections*

1. Slides were washed 5 times, 10 minutes each, in xylene. These washes were done in agitation
2. Then slides were rehydrated with a series of ethanol washes in agitation:

2.1. EtOH 100%: 2 x 5 minutes.

2.2. EtOH 96 %: 2 x 5 minutes.

2.3. EtOH 70%: 2 x 5 minutes.

2.4. EtOH 50%: 5 minutes.

2.5. EtOH 30%: 5 minutes.

3. Next the slides were washed in distillate water for at least 5 minutes.
4. For a better staining, an antigen retrieval process was performed. For this, slides were incubated in citrate buffer in a pressure cooker and boiled for 15 minutes. Using the Sapore 30622 electric pressure cooker, the porridge function was used for antigen retrieval.
5. Following antigen retrieval, slides were let to cool down until they were at room temperature.
6. As primary antibody incubation was done directly over the slide, around the sample was drawn a circle with a hydrophobic solution using a Super PAP Pen. Additionally to avoid evaporation of the different solution during the whole process, slides were kept in a humidified chamber.
7. Slides were then incubated with blocking solution (2% FBS, 0.1% gelatin in PBS) for 2 hours at room temperature.
8. When blocking was finished sections were incubated with primary antibodies in blocking solution overnight at 4°C in a humid chamber. Primary antibodies used and their concentrations can be found in table 20.
9. Next day slides were washed with PBS-Triton 0.1%: 3 hashes of 10 minutes each.
10. Then, secondary antibodies were incubated in PBS at room temperature for 2 hours at dark. The list of secondary antibodies and the used concentrations can be found in table 21. There were two kinds of secondary antibodies used: on one hand Alexa fluor conjugated antibodies and on the other hand biotin conjugated secondary antibodies. When the first were used steps 11 and 12 were not followed and, instead, the protocol directly jumped to step 13.
11. Following secondary antibody incubation 3 more PBS-triton 0.1% washes, 10 minutes each one, were done.
12. Next slices incubated with biotin antibodies were incubated with 1:400 streptavidin-conjugated fluorophores for 2 hours at dark and room temperature in PBS.
13. Slides were washed 3 more times with PBS-triton 0.1% for 10 minutes.
14. Then slides were incubated with DAPI 1:500 in PBS for 5 minutes.
15. Slides were finally mounted with fluoromont mounting medium.

16. Before storing the slides at 4°C until microscope visualization, they were left to dry at room temperature.
17. Immunofluorescence experiments were visualized using a… microscope.

| Antibody | Dilution | Description | Manufacturer | Biotin-Streptovidin |
|---|---|---|---|---|
| WT1 | 1:100 | Rabbit | Abcam ab89901 | Yes |
| MF20 | 1:50 | Mouse | DSHB MF20-s | No |
| EMCN | 1:100 | Rat | Santa Cruz sc-65495 | No |
| GFP | 1:200 | Goat | Abcam ab6673 | No |
| SOX9 | 1:100 | Rabbit | Millipore AB5535-25UG | No |
| FOXL2 | 1:100 | Goat | Novus Biologicals NB100-1277ss | Yes |

**Table 20.** Primary antibodies used for immunofluorescence experiments.

| Antibody | Dilution | Description | Manufacturer |
|---|---|---|---|
| Anti-rabbit AF-488 | 1:400 | Donkey | Invitrogen A21206 |
| Anti-goat AF-488 | 1:400 | Donkey | Invitrogen A11055 |
| Anti-mouse AF-546 | 1:400 | Donkey | Invitrogen A21203 |
| Biotin Anti-Rabbit IgG | 1:400 | Donkey | Jackson 711-065-152 |
| Biotin Anti-Goat IgG | 1:400 | - | Jackson 715-065-150 |
| Streptavdin, Alexa 488 | 1:400 | - | Invitrogen S11223 |
| Streptavidin, Cy™3 | 1:400 | - | Jackson 016-160-084 |

**Table 21.** Secondary antibodies used for immunofluorescence experiments.

### *Compact myocardium thickness analysis*

Compact myocardium thickness was used as a quantifiable measure of *Wt1* reduction effect on heart morphology. To delimit compact myocardial zone, Endomucin-1 and MF20 stainings were used. MF20 stains all myocardium, Endomucin-1 is expressed in the endocardium and therefore allows to identificate trabecular myocardium: the section stained by MF20 but not Endomucin was considered the compact myocardium.

1. Myocardial wall thickness widely varies at different heart sections. To select comparable heart sections the next parameter was used: only those sections were the atria and the valves connecting ventricles and atria were present, were used.

2. Compact myocardium thickness was quantified using ImageJ[326]. This analysis was carried in the following way.
3. Using the straight line tool, a line was drawn between the extern border of compact myocardium and the inside border (where Endomucin-1 staining started). The length of this line was automatically provided by ImageJ.
4. From the top of the ventricle wall (where it joins the atria), to the opposite extreme (where it reaches the interventricular septum surface) 6 measures as the one described in the previous point, were taken at regular intervals.

## 6.6 Flow citometry and cell sorting (FACS).

Flow citometry allows the analysis of cell surface or intracellular molecules of a cell populations in a single-cell manner. This allows the identification of different cell types in an heterogeneous population. In this thesis we have taken advantage of the fluorescence emitted by the *Wt1*$^{GFP/+}$ knockin and by the two reporters used in this thesis, the *R26R*$^{mTmG}$ and *R26R*$^{tdRFP}$, to characterize and isolate *Wt1* and *Wt1*$^{Cre}$ expressing populations.

### 6.6.1 Sample preparation.

We have used two different protocols for hearts and the rest of the organs. The reason is because, previously, our group had identified two populations of GFP positive cells in *Wt1*$^{GFP/+}$ mice. One of them are epicardial cells and the other, presumably, a subset of cardiomyocytes. When hearts were dissected with collagenase these two populations were not identifiable avoiding us to characterize or isolate our population of main interest.

1. Embryos were dissected using in PBS under a magnifying glass using needles.
2. Dissected organs were placed on a tube with PBS until the enzyme solution was added.
3. Then organs dissected were incubated with and enzyme solution, either trypsin or collagenase depending on the experiment.

a) In the case of hearts of figure 28.

3.1. PBS was removed from tubes containg heart ventricles and 300µl of trypsine solution (1:10 in PBS EDTA) were added.
3.2. Hearts were incubated for 10 min at 37°C at 1000 rpm in a shaker.
3.3. After these 10 minutes, trypsine solution was collected, without collecting the remains of the heart, and added to a new eppendorf with 400µl of DMEM medium.

3.4. Then 200 additional µl of the trypsine solution were added to hearts. This process was repeated for approximately 40 minutes until all heart was disaggregated.

b) In the case of all other organs and hearts from figure 27.

3.1. PBS was removed from tubes containg organs and 400µl of collagenase solution (0,01% in HBSS) was added.

3.2. Cells were incubated in collagenase solution for 30min, 37 °C at 1000rpm in a shake. When necessary disaggregation was completed using mechanical disaggregation with a pipette.

4. Cell solutions were then centrifugued 5 minutes at 1000rpm.
5. Cell pellets were resuspended in PBS.
6. Just before bringing the cells to flow citometry 1µl of DAPI was added in order to discard death cells.

### 6.6.2 Flow citometry and cell sorting.

Flow citometry and cell sorting experiments were performed on a BD Bioscience FACSAria II and data was analysed using BD FACSDiva software (v6.1.3). FACS sorting of GFP or RFP populations was carried out by gating against their respective negative control littermates.

## 6.7 Electronic microscopy.

For a proper measurement of cell shape parameters, hearts and lungs were analysed using Scanning Electron Microscopy (SEM) and Transmission Electron Microscopy (TEM). Hearts and lungs were analysed at indicated developmental stages.

### 6.7.1 Transmission electron micrscopy.

1. Immediately after dissection, hearts and lungs were placed in a 2% paraformaldehyde, 2.5% glutaraldehyde in 0.1 M cacodylate buffer and fixed overnight at 4°C.
2. Next day tissues were washed 4 times with 0.1 M cacodylate buffer for 10 minutes each wash at 4°C in a gentle shaking.
3. Then the samples were post-fixed in 1% osmium tetroxide, 0.8% potassium ferrocyanide in 0.1 M phosphate buffer for 2 hours at 4°C and at dark.
4. After post-fixation, samples were washed 4 times with mq water 10 minutes each wash. Then water was discarted and samples were stored in PB 0,1M at 4°C.

5. Samples were then dehydratated. To this, tissues were washed in agitation and at 4°C with the following alcohols:
   5.1. Ethanol 50%: 3 x 10 minutes.
   5.2. Ethanol 70%: 3 x 10 minutes.
   5.3. Ethanol 90%: 3 x 10 minutes.
   5.4. Ethanol 96%: 3 x 10 minutes.
   5.5. Ethanol 100%: 3 x 10 minutes.
6. Tissues were then transitioned into an EPON resin.
7. Next, samples were embbeded in moulds containing fresh resin and were polymerised for two days at 65°C.
8. Sections of 0.5µm thick were stained with Methylene Blue to determine the area for thin sectioning (70nm) with a diamond knife.
9. Thin sections were placed onto formvar on 100-mesh copper grids and stained with aqueous uranyl acetate and lead citrate.
10. Grids were examined using a Tecnai Spirit TWIN TEM (FEI) 120 kV LaB6 and CCD Megaview 1Kx1K digital camera.

### 6.7.2 Scanning electron microscopy.

1. For SEM samples were processed as explained for SEM until dehidratation.
2. Dehidratation was performed as follows:
   2.1. Ethanol 50%: 3 x 10 minutes.
   2.2. Ethanol 70%: 3 x 10 minutes.
   2.3. Ethanol 90%: 3 x 10 minutes.
   2.4. Ethanol 96%: 3 x 10 minutes.
   2.5. Ethanol 100%: 3 x 10 minutes.
3. After dehidratation a critical point drying procedure was performed.
4. Images were taken on a JEOL JSM 7100F.

### 6.7.3 Determination of cell shape parameters.

The morphological parameters of cell shapes were measured using ImageJ (National Institutes of Health). Morphological analyses were performed as described previously[327] and three parameters were calculated for each cell:

1. Cell lenght length

2. Circularity index ($4\pi \times area/perimeter^2$), which assumes values between 1 for a circular shape and 0 for an elongated morphology.
3. Aspect ratio (length of major axis/length of minor axis) (AR). The AR of a perfect circle will be 1 and its value becomes greater than 1 with increased elongation.

For each stage a minimum of 3 hearts or lungs were analysed. Also, for each stage a minimum of 25 cells were analysed.

## 6.8 Epicardial cell culture.

Immortalized epicardial have been described previously[190]. Briefly: *Wt1*$^{GFP/+}$ mice were crossed with 'Immorto' mice carrying the *Tg(H2-K1-tsA58)* transgene (Jackson Laboratory) carrying a temperature-sensitive simian virus 40 large T antigen[328]. Hearts from E11.5 *Wt1*$^{GFP}$; *Tg(H2-K1-tsA58)*$^{+/-}$ mice were placed in 24-well gelatinized dishes. After 24 hours, hearts were removed, and the epicardial monolayer of cells attached to the gelatin-coated surface was grown until confluent. Cells were propagated at 33 °C in DMEM with 10% heat-inactivated FBS.

Manipulation of epicardial cells was performed on sterile conditions in a class II biosafety cabinet. Prior to its use, it was sterilized each time with UV light and the surface was cleaned with ethanol 70%. All material used in the cabinet was previously sterilized.

### 6.8.1 Cell thawing.

Cells were stored at -80°C until thawed. Thawing process was performed as fast as possible in the following conditions:

1. Crio-tubes where cells were stored where placed in a 37°C bath for thwaing.
2. Just before thawing was complete, cells where transferred to a tube containing 9 ml of DMEM suplemented medium (10% FBS, 1% Glutamine, 1% P/S).
3. The tube with the cells was then centrifuged at 1000 rpm for 5 min.
4. The supernatant was removed and the pellet was resuspended on 5ml of new DMEM suplemented medium.
5. Resuspended cells were seeded in a T25-flask and cultured at 33°C and a 5% volume of $CO_2$.
6. Next day, once cells had adhered to the T-flask surface, old medium was removed and replaced by 5ml of new DMEM suplemented medium.

### 6.8.2 Cell propagation.

Cells were cultured and propagated in T75-flasks. Before cells reached confluence they were trypsinized and propagated to a new T75 as follows:

1. Medium is carefully removed.
2. Cells are washed with PBS, previously warmed at 37°C for 5 minutes at 33°C.
3. PBS is aspirated and 3ml of trypsine are added to cells.
4. Cells are incubated with trypsine for 5 minutes at 37°C. After this 5 minutes, cells are helped to detach from T-flask surface with a few gentle Knocks.
5. 7 ml of DMEM 10%FBS are added to the cells.
6. When cells were going to be used in a experiment they were counted with a Neubauer chamber and then the needed volume was transferred to the plates where the experiment was performed. When cells were trypsinized for maintenance purposes 1ml of the cells was placed on a new T-75 flask and then 9ml of new DMEM 10FBS medium were added.
7. Cells were then returned to the incubator at 37°C and 5% $CO_2$.

### 6.8.3 Cell freezing.

When cells were not being used they were frozen and stored in crio-tubes at -80°C.

1. Cells are trypsinized as explained in 6.10.2 section.
2. Cell suspension is centrifugued at 100rpm for 5 minutes.
3. The supernatant is discarded and cells are resuspended in freezing solution.
4. Cells in freezing solution are distrubuted in cryo-tubes (1ml/cryotube).
5. Cryotubes are stored in a Cryo 1°C freezing container at -80°C
6. Next day cryotubes can be stored in normal boxes at -80°C.

### 6.8.4 Western blot or qRT-PCR.

For western blot or qPCR experiments, $1.5\times10^5$ epicardial cells were seeded into 6-well plastic culture plates. Cells were left to grow On and then the medium was changed to 2% FBS supplemented with dorsomorphin (4µM) or LDN-193189 (0.5µM). For the time-course experiment of BMP4, immortalized epicardial cells were pretreated ON with dorsomorphin before BMP4 stimulation (100 ng/ml).

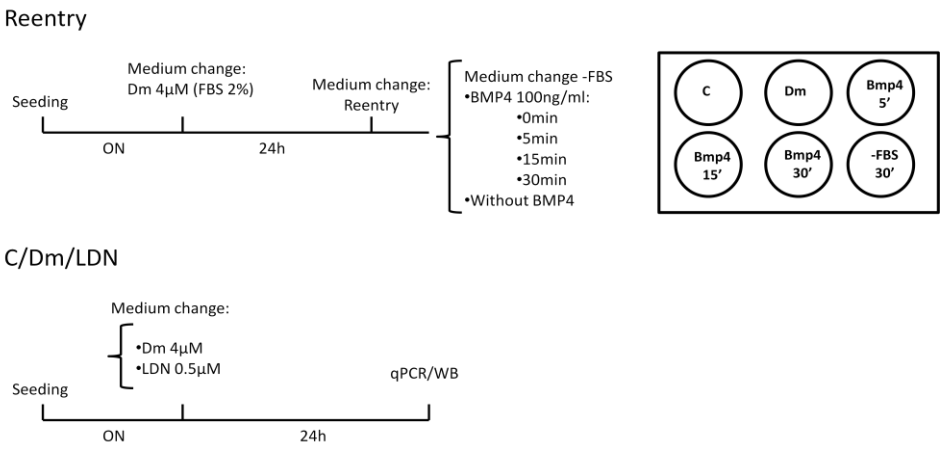


**Figure 14. *In vitro* experimental design schemes.**

## 6.8.5 Immunofluorescence.

For *in vitro* immunofluorescence analyses, $4\times10^4$ epicardial cells were cultured into 24-well plates for 18 h, followed by treatment with or without BMP4 (100 ng/ml) for 48 h.

1. Glass coverslips were coated with gelatin 0.1% for this a brief wash with gelatin was performed before cells were cultured.
2. After the experiment treatment was performed confluent epicardial cell monolayers were washed with PBS.
3. Then, cells were fixed at room temperature with 4% PFA in PBS for 12 minutes.
4. After fixation cells were permeabilized using 0.1% Triton X-100 in PBS for 7 minutes.
5. Cells were next washed with PBS 3 times 5 minutes each wash.
6. After that cells were blocked using BSA 1% in PBS for 30 minutes at room temperature.
7. Cells were then incubated with primary antibodies (anti β-catenin 1:400) at 4°C overnight.
8. The next day cells were washed 3 times (10 minutes each wash) with PBS.
9. Next, cells were labelled with secondary antibodies for 1 hour in the dark at room temperature.
10. Nuclei were stained with DAPI) for 5 minutes.
11. After staining coverslips were mounted in Fluoromount.
12. Images were acquired using a Leica TCS SP5 confocal laser scanning microscope (Leica Microsystems) equipped with a DMI6000 inverted microscope, and Argon (458/476/488/ 514), diode-pumped solid-state (561 nm) and HeNe (633) lasers. The Alexa 488 and Alexa 546 images were acquired sequentially using 488 and 561 laser lines, an acoustic optical beam splitter (AOBS) and emission detection ranges of 500-

555 and 571-625, respectively. Confocal z-stack xy plane images were taken at 0.21 µm intervals at a total depth of 7 µm. The xy or xz section images were generated from z-stack images with Leica software. Images for direct comparison were obtained under identical parameters and were representative of three different assays.

13. The final analysis of all images was performed using ImageJ software. Cell height was measured by reconstructing the monolayer as a z-stack and drawing a line from the basal border of the monolayer to the bottom of the coverslip. Cell area was measured in xy sections by drawing a line around the circumference of each cell at its midsection.

## 6.9 *Ex vivo* and *in vivo* BMP4 signaling inhibition experiments.

### 6.9.1 *Ex vivo* heart culture experiments.

1. First, the wells that were going to be used for ex vivo experiments were coated for 24 hours with an agarose 1% solution. Agarose was allowed to solidify in the hood and then the excess of agarose was removed.
2. Wells were then washed several times with DMEM.

a) For TEM analysis:

1. Dissected heart ventricles from control and *epiWt1KO* E13.5 embryos were cultured in agarose coated wells In the presence of Dm 4µM or DMSO as vehicle controls.
2. Hearts were kept at 37°C for 48 hours.
3. After treatment hearts were processed for TEM analysis as mentioned above.

b) For RNA expression analysis

1. Dissected heart ventricles from $Wt1^{GFP/+}$ E11.5 embryos were cultured in agarose coated wells In the presence of with LDN-193189, or endotoxin-free water as vehicle control.
2. Hearts were incubated at 37°C overnight.
3. Hearts were then dissociated into single cell suspensions and $Wt1^{GFP++}$ cells were FACS sorted as mentioned before.7
4. RNA from $Wt1^{GFP}$ FACS sorted cells was obtained using a Total RNA Purification Kit (Norgen, 17200) following manufacturer instructions.

5. RNA was then used for reverse transcription and amplification with a QuantiTect Whole Transcriptome Kit. Real-time PCR experiments were performed as described above.

### 6.9.2 *In vivo* experiments.

1. For in vivo rescue experiments, *Gata5$^{Cre}$; Wt1$^{GFP/+}$* males and *Wt1$^{loxP/loxP}$* female mice were set up for timed matings as described above.
2. Pregnant females were treated with the BMP inhibitor LDN-193189 via intraperitoneal injections from E13.5. LDN-193189 was dissolved in endotoxin-free water (Sigma-Aldrich, 95289) at 1.5 mg/ml and neutralised at pH 6.8. The dosage per injection was 6 mg/kg, twice per day. Control females received an equivalent volume of endotoxin-free water via intraperitoneal injections.
3. Embryos were collected at E15.5 and fixed for TEM, WB or immunostaining analysis, as described above.

## 6.10 Proliferation assays.

One of the most used ways to quantify cell proliferation is BrdU incorporation assay. 5-bromo-2'-deoxyuridine (BrdU) is a thymidine analog. Its incorpotation to newly synthesized DNA can be detected by an anti-BrdU antibody. This allows for a tracking of the rates of new produced cells and therefore, proliferation. In this thesis we have used the cell proliferation *Elisa BrdU kit* according manufacturer instructions. Briefly:

1. Cells were cultured in 96 well plates with a final volume of 100µl. For each condition 3 replicates per experiment were analysed.
2. Once treatment had finished 10µl/well of BrdU labelling solution were added. Cells were incubated with labelling solution for 2 hours at 37°C.
3. Labelling solution was removed by tapping off the plates.
4. Then 200µl/well of FixDenat solution was added to the cells, which were incubated for 30 min at room temerature.
5. After removing FixDenat solution 100µl/well of anti-BrdU-POD working solution were added and cells were incubated with this solution for 90min at room temperature.
6. Antibody conjugate was removed and cells were washed 3 times with PBS.
7. Next 100µl of substrate solution was added to each well. Cells were incubated at dark and at room temperature until colour appeared (about 30min).

8. Lectures were taken in a 200 PRO (TECAN) reader and measures were done by measuring the absorbance of the samples at 370nm.

## 6.11 Cell transfection and luciferase assay.

To analyse transcriptional activity we used a luciferase reporter assay. In these experiments cells were transfeceted with a plasmid containing a luciferase gene, followed by the promoter of the gene of interest (in this case *Wt1*). Luciferase activity allowed us to track *Wt1* transcriptional activity under different conditions.

For this experiment, we used Hek293 cells. The reason for using this cell line, instead of inmortalized epicardial cells, is the low transfection efficiency of the last.

### 6.11.1 Cell transfection.

1. Hek293 cells were cultured on 24 well plates and let grow until reaching 70-80% confluence, as recommended by the manufacturer.
2. Before transfection, cell medium was changed to OptiMeM.
3. For each well, 100µl of OptiMeM medium with DNA mix was prepared. Mix consisted of 250ng of *Wt1*-promotor plasmid and 50ng of Renilla luciferase plasmid.
4. For each well, 100µl of OptiMeM medium with lipofectamin were prepared (3 µl/µg of DNA).
5. Lipofectamin mix was added to DNA eppendorf and mixed by gentle pippeting.
6. Mix was left 20 minutes at room temperature.
7. 200µl of the mix were added to each well.
8. Cells were left ON with the OptiMeM mix and then the medium was changed to DMEM 2% FBS and treated according to experimental purposes.

### 6.11.1 Luciferase assay.

For luciferase activity detection, the *Dual-Glo® Luciferase Assay System* kit was used. The protocol followed manufacturer instructions. Briefly:

1. Just before the lecture was going to be performed medium was removed.
2. 120µl/well of luciferase reagent was added to cells.
3. The plate was left 10 minutes in agitation at dark to allow for cell lysis.
4. 90µl of the lysate was added to a 96 well plate.
5. Luciferase luminescence was measured in a TECAN.

6. 40 µl of Stop and Glove buffer were added to each well. Then we waited 5 minutes to let it act.
7. Renilla luminescence was measured in a TECAN. Renilla luminescence was used as a transfection control.
8. Luciferase lectures were normalized using Renilla lectures.

For each condition and experiment triplicates were done.

## 6.12 Statistical analysis.

Data are presented as mean ± s.e.m (standard error mean). Statistical significance between two groups was determined by unpaired, two-tailed Student's *t*-tests. When more than one group was analysed it was applied a nonparametric one-way ANOVA followed by Tukey's posthoc test to evaluate the differences among multiple groups of samples. For the BrdU experiment, due to the intrinsic differences among experiments, a matched one-way Anova followed by Dunnett's multiple comparision test was applied. When more than one factor was analysed (sex-genotype; genotype-treatment) a nonparametric two-way ANOVA followed by Tukey's posthoc test was applied. Two-tailed Chi-square ($\chi^2$) test was performed in pair comparisions when proportions of a whole where compared.

## 6.13 Contributions.

Figure 15 was performed by Víctor Velecela. TEM analysis from figures 16, 17, 20 and 21 were performed by Ana García Melero.

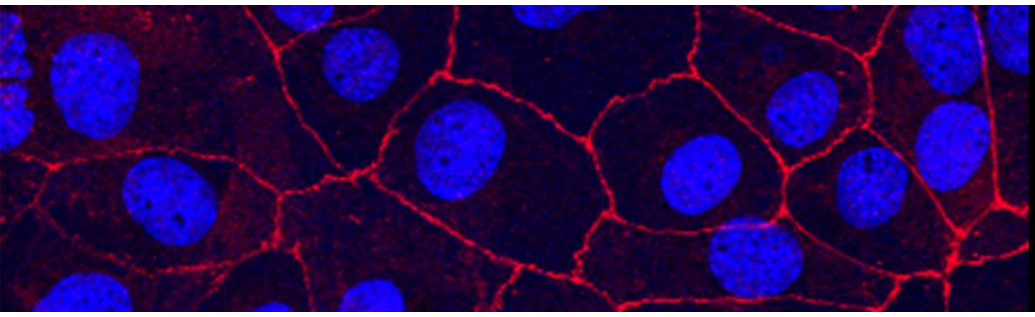

# OBJECTIVES

The main objective of this work is to improve the knowlegde about *Wt1* role in embryonic development. More specifically, our intention was to get a more detailed comprehension of WT1 function in two systems where *Wt1* has been previously investigated: the epicardium and gonad development. Therefore, the objectives of this work are:

**1** To elucidate the function of BMP4 in the epicardium maturation

**2** To investigate if WT1 regulates the BMP4 pathway.

**3** To investigate whether the processes observed during epicardial maturation can be extrapolated to the development of mesothelium covering other organs.

**4** To characterize $Wt1^{Cre}$ activity in the urogenital organs.

**5** To generate a new *Wt1KO* mouse that allows the study of sexual organs until adulthood ($Wt1^{Cre};Wt1^{Loxp/GFP}$ mouse).

**6** To study *Wt1* downregulation effect in adult $Wt1^{Cre};Wt1^{Loxp/GFP}$ gonads and genital tracts.

**7** To identificate the molecular mechanisms behind the phenotype oserved in $Wt1^{Cre};Wt1^{Loxp/GFP}$ mice.

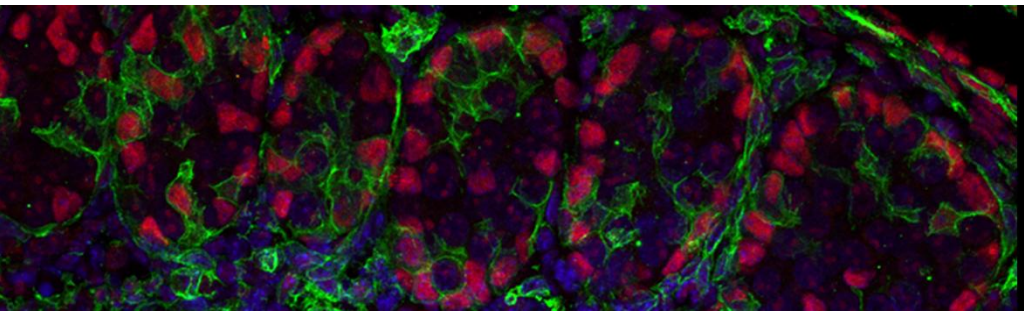

# RESULTS

## 8.1 WT1 regulates BMP4 expression during epicardium development.

The embryonic epicardial program during development and the effect of WT1 loss on its molecular signature have been previously characterized (Fig. 10,11)[230]. One of the pathways highlighted in both transcriptomic data, was the BMP4 pathway. BMP4 is an extracellular signaling protein with several roles during development and disease[267]. It has been described that BMP4 is required for the proepicardium formation and specification in zebrafish and chicken[162,164], but the *Bmp4* role in the mammal epicardium has not been studied.

To validate the transcriptomic analysis, *Wt1* GFP$^{++}$ cells from Wt1$^{GFP/+}$ embryos were FACS-sorted at different stages of development (from E11.5 to E16.5). *Bmp4* mRNA expression was analysed in these cells using qRT-PCR. *Bmp4* expression was downregulated during development (Fig. 15A), confirming the transcriptomic results. Control and *Gata5$^{Cre}$; Wt1$^{GFP/LoxP}$* (*epiWt1KO*) epicardial cells, FACS-sorted from E13.5 ventricles, were analysed following the same procedure. As in the transcriptomic data, *Bmp4* expression was upregulated in *epiWt1KO* cells (Fig. 15B). To further validate these results, we performed an RNAscope for *Bmp4* on heart sections of E13.5 embryos. Results indeed indicated an upregulation and a specific *Bmp4* expression in the epicardium (Fig. 15C).

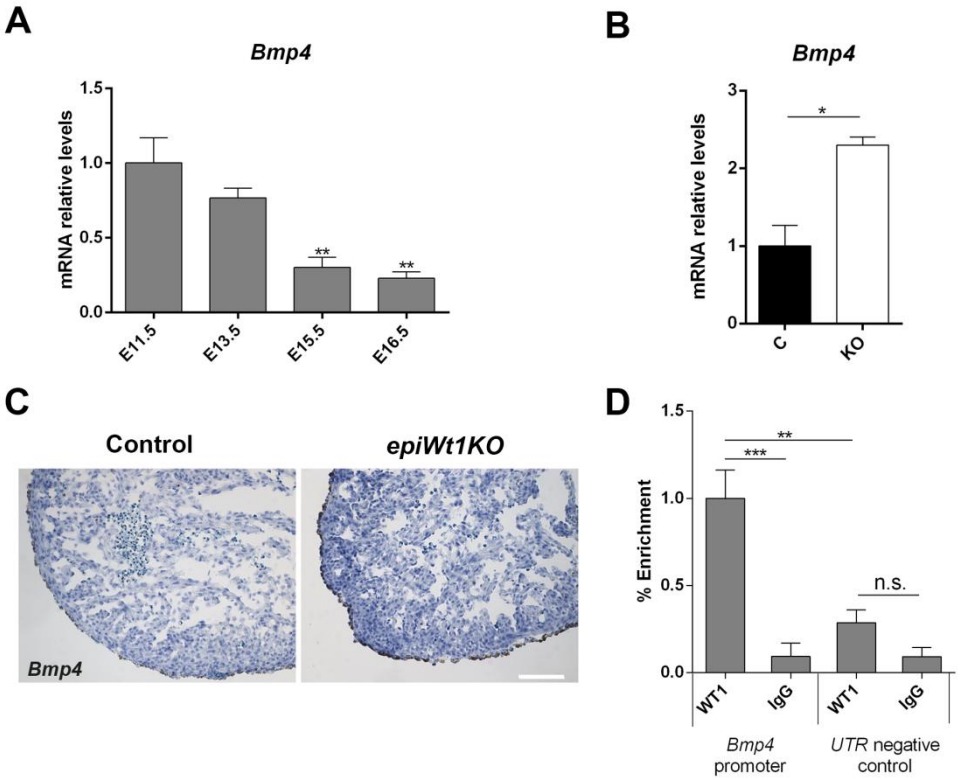

**Figure 15. WT1 regulates BMP4 expression during epicardial development.** (A) qRT-PCR analysis of *Bmp4* expression in *Wt1*-GFP$^{++}$ FACS-sorted epicardial cells from *Wt1*$^{GFP/+}$ mice at different days of development. (B) qRT-PCR analysis of *Bmp4* in *Wt1*-GFP$^{++}$ FACS-sorted epicardial cells from control and *epiWt1KO* mice. (C) RNAscope *in situ* hybridisation analyses of *Bmp4* in hearts from control and e*piWt1KO* at E13.5. (D) WT1 binding to a *Bmp4* regulatory region was examined by ChIP with a WT1 antibody and control IgG using immortalised epicardial cells. qRT-PCR of the immunoprecipitated DNA was conducted using primers flanking the *Wt1* binding site and a 3'UTR region as a negative control. Values represent mean ± s.e.m. *P<0.05, **P<0.01, ***P<0.001, n.s. not significant, one-way ANOVA followed by Tukey's posthoc test (A,C), or two tailed t-test (B). Three replicates per condition were used for the analysis. Scale bar, 100µm.

Finally, to investigate whether WT1 was directly regulating *Bmp4* expression, we performed a ChIP with an antibody against WT1 in immortalized epicardial cells. Results indicated that WT1 occupies the *Bmp4* regulatory region in epicardial cells (Fig. 15D).

## 8.2 *Wt1* deletion abrogates epicardial cell flattening during development.

### 8.2.1 Epicardial cells undergo a cell flattening process throughout development.

One of the most relevant aspects of development is the morphological change that cells undergo during their maturation from an embryonic to an adult phenotype[329]. Interestingly, BMP4 action has been described to regulate proliferation and cell shape changes in different contexts, like epithelial invagination in chick, or ovarian follicle development[330,331]. Therefore, we wondered whether *Bmp4* downregulation was correlating with changes in epicardial cell shape.

To assess this question, scanning electron microscopy (SEM) and transmission electron microscopy (TEM) were used to analyse mice embryonic hearts from E11.5 to E18.5. Epicardial cells at E11.5 showed a cuboidal cell shape with large, centrally located nuclei. From this morphology, epicardial cells change until acquiring, at E18.5, a flattened phenotype with flattened nuclei (Fig. 16A,B). In order to quantify this transformation, the length, aspect ratio (AR), circularity, and the area of epicardial cells, was measured. These values are indicative of cell morphology: a circularity value close to 1 indicates that the shape is similar to a perfect circle. AR values, on the other hand, increases with the degree of cell flattening.

Obtained values indicated that cell length from epicardial cells increases during development and E18.5 epicardial cells presented a 5 times higher cell length than E11.5 cells. A similar pattern was described for epicardial AR during development, and the opposite one for epicardial cell circularity (Fig. 16C-F).

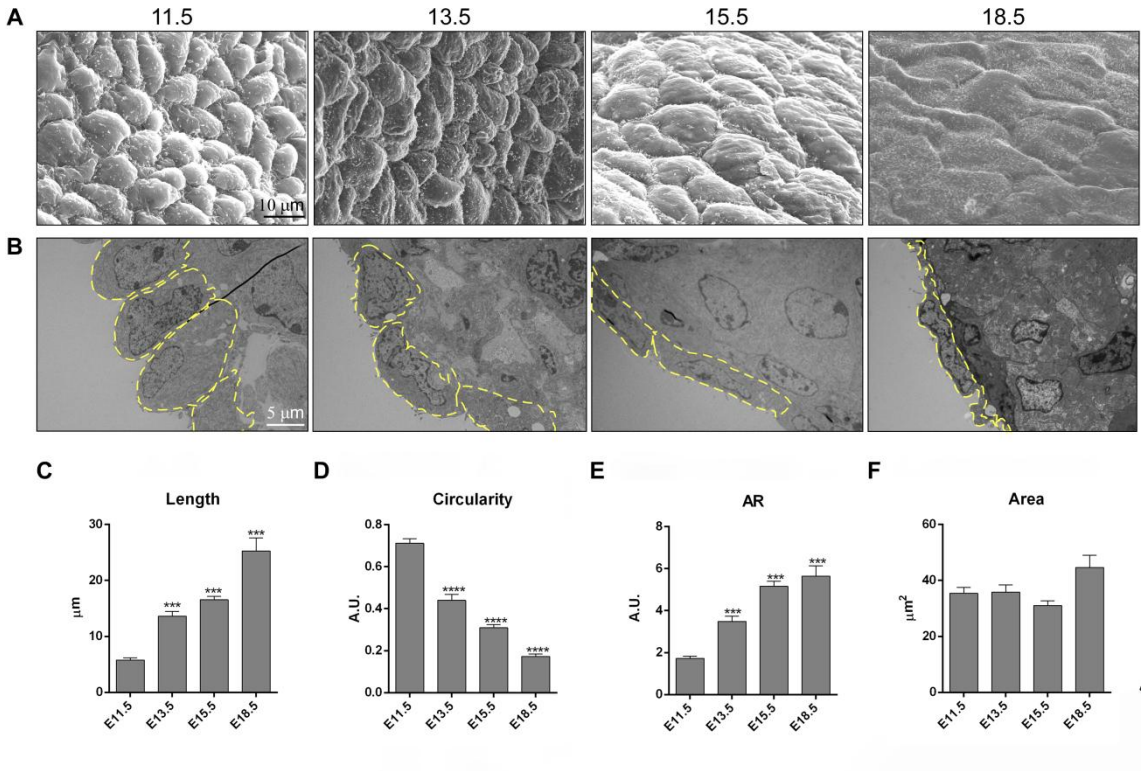


**Figure 16. Epicardial cell shape flattens through embryonic development.** (A) SEM analysis of the epicardium at different days of embryonic development. (B). TEM analysis of epicardial cells at indicated days of development. (C-F) Quantification of epicardial cell length, cell area, circularity, and cell aspect ratio (AR), at different days of development, in TEM images. Values represent mean ± s.e.m. ***P<0.001, ****P<0.0001, one-way ANOVA followed by Tukey's posthoc test. Three independent embryos were assessed per condition, and at least 25 epicardial cells were quantified. Yellow dashed lines outline the shape of the epicardial cells in B. Scale bar, 10µm (A), 5 µm (B).

### 8.2.2 *Wt1* deletion in the epicardium results in a cell shape deffect.

*Bmp4* expression is upregulated in the *epiWt1KO (*Fig. 15B). Therefore, we decided to investigate whether epicardial cells from *epiWt1KO* hearts showed an impairment in cell shape changes observed during development.

Using SEM and TEM, epicardial cells from control and *epiWt1KO* E15.5 embryos were examined. SEM and TEM analysis showed flattened epicardial cells were present in control hearts, whereas most *epiWt1KO* cells presented a cuboidal phenotype (Fig. 17A,B). To confirm this observation, cell length, AR, circularity, and cell area of control and *epiWt1KO* cells (Fig. 17C-F) were calculated. *EpiWt1KO* cell length presented a 32% reduction, while AR from *epiWt1KO* cells was 44% lower than AR from control epicardial cells. In contrast, *epiWt1KO* cell circularity was 60% higher than that measured in control cells.

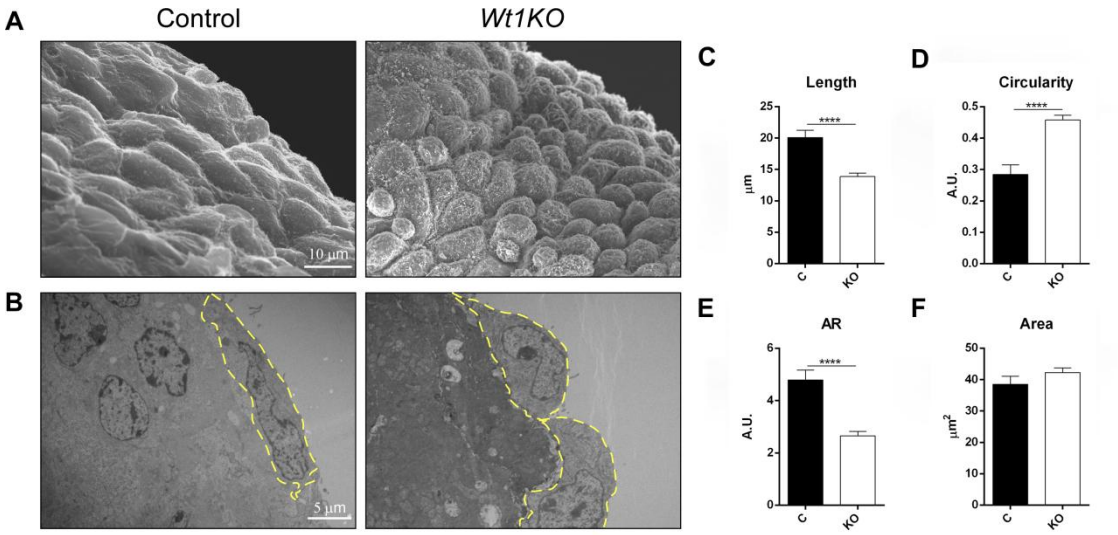


**Figure 17. *Wt1* expression is required for epicardial cell flattening.** (A) SEM analysis of the epicardium from E15.5 control and *epiWt1KO* hearts. (B) TEM analysis of the epicardium from E15.5 control and *epiWt1KO* hearts. (C-F) Quantification of epicardial cell length, AR, circularity and cell area in TEM images from control and *epiWt1KO* hearts. Values represent mean ± s.e.m. ****P<0.0001, two-tailed t-tests. Three independent embryos were assessed per condition, and at least 25 epicardial cells were quantified. Yellow dashed lines outline the shape of the epicardial cells. Scale bar, 10µm (A), 5 µm (B).

The comparison between the analysis of control and *epiWt1KO* cells (Fig. 17), and the description of epicardial cell shape changes in development (Fig. 16) indicated that *epiWt1KO* cells at E15.5 showed a similar phenotype than control cells at early stages of development. This took us to hypothesize *Wt1* deletion arrests epicardial cells in an early embryonic state.

## 8.3 BMP4 pathway modulates epicardial cell shape.

### 8.3.1 BMP4 regulates epicardial cell shape.

We realized that the early stage-cuboidal phenotype correlates with the higher levels of *Bmp4* expression both during the epicardium development (Fig. 15A) and in *epiWt1KO* cells (Fig. 15B). Therefore, we decided to investigate whether this correlation implied causality.

Cultured epicardial cells were treated with recombinant BMP4 (rBMP4) for 48 hours. To measure cell morphology *in vitro,* β-CATENIN staining was analysed using confocal imaging. Control and treated cells showed a uniform staining pattern at the cell-cell contact (Fig. 18A). According to what we expected, cell AR of rBMP4 treated cells was reduced almost to half, indicating they were closer to a cuboidal cell shape. (Fig. 18B).

This change followed the same pattern observed *in vivo,* suggesting BMP4 is responsible for epicardial cell shapes observed during development and in *epiWt1KO* hearts.

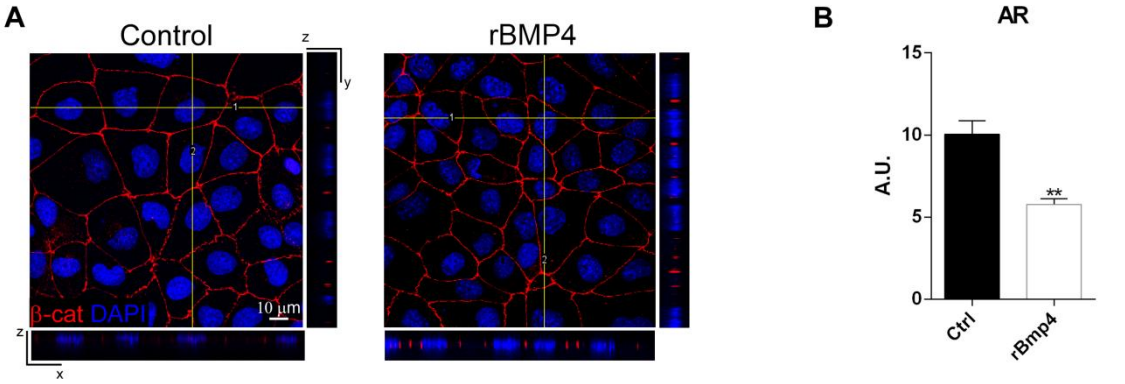


**Figure 18. BMP4 regulates epicardial cell shape.** (A) Immunofluorescence analysis for β-CATENIN (β-cat) in immortalized epicardial cells cultured in the presence of recombinant BMP4 (rBMP4). Orthogonal *xz* and *yz* projections of 3D confocal image stacks of epicardial cells stained for β-cat (red) and DAPI (blue) are shown to illustrate the morphology of the cells. Scale bar: 10µm. (B) Quantification of epicardial aspect ratio (AR) in epicardial cells cultured In the presence of rBMP4. Values represent mean ± s.e.m. **P<0.01, two-tailed t-test. At least 35 cells were analysed per condition in four independent experiments.

### 8.3.2 BMP4 acts through its canonical pSMAD pathway to regulate epicardial cell shape.

To understand the underlying mechanisms of *Bmp4* regulation of epicardial cell shape, first, we proceeded to test whether we were able to modulate the BMP4 pathway in epicardial cells. For this reason, we decided to use two different known inhibitors of the canonical BMP pathway: Dorsomorphin (Dm) and LDN-193189 (LDN), which are two chemical compounds that abrogate SMAD1/5/8 phosphorylation[332,333]. The action of these inhibitors abrogates the capacity of the SMAD complex of being translocated to the nuclei, where they act as a transcription factor.

First, to test if BMP4 acts through its canonical pathway in the epicardium, epicardial cells were pretreated *in vitro* with Dm overnight (ON) and then treated with rBMP4 (Fig. 19). Cell lysates were extracted at increasing times of rBMP4 treatment and SMAD phosphorylation was evaluated using WB, demonstrating that rBMP4 activates the canonical BMP4/pSMAD pathway in epicardial cells (Fig. 19).

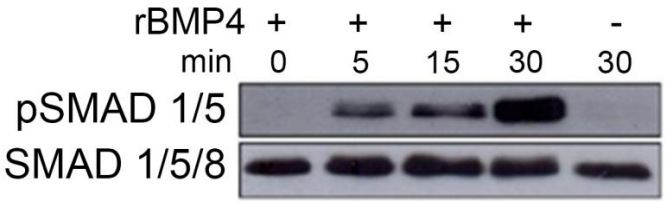


**Figure 19. BMP4 induces the phosphorylation of SMAD1 and SMAD5 in epicardial cells**. Immortalized epicardial cells were pre-treated for 18 hours with dorsomorphin before rBMP4 stimulation for indicated time points. Cell lysates were analysed by Western blotting with antibodies against phosphorylated SMAD1/5 (pSMAD1/5) and SMAD1/5/8 as a loading control. Three independent experiments were assessed.

Once we had determined our ability to modulate the BMP4 pathway, we decided to try to rescue the *epiWt1KO* phenotype by injecting an inhibitor of the BMP pathway, LDN-193189 (LDN), in pregnant mice (Fig. 20A). First, we demonstrated that LDN treatment effectivley abrogated SMAD1/5 phosphorylation *in vivo* (Fig. 20B). Then, hearts of control and treated and untreated *epiWt1KO* embryos were analysed by TEM (Fig. 20C). Next, epicardial cell length, AR, circularity, and area were calculated. *EpiWt1KO* cells treated with LDN presented a flattened phenotype similar to that observed in epicardial cells from control hearts. Also, cell length, AR, and circularity values from *epiWt1KO* treated cells were similar to those obtained from control cells, in contrast to those obtained from *epiWt1KO* untreated cells(Fig. 20D-G). In resume, our *in vivo* results demonstrated that the BMP4 pathway is involved in the regulation of epicardial cell morphology.

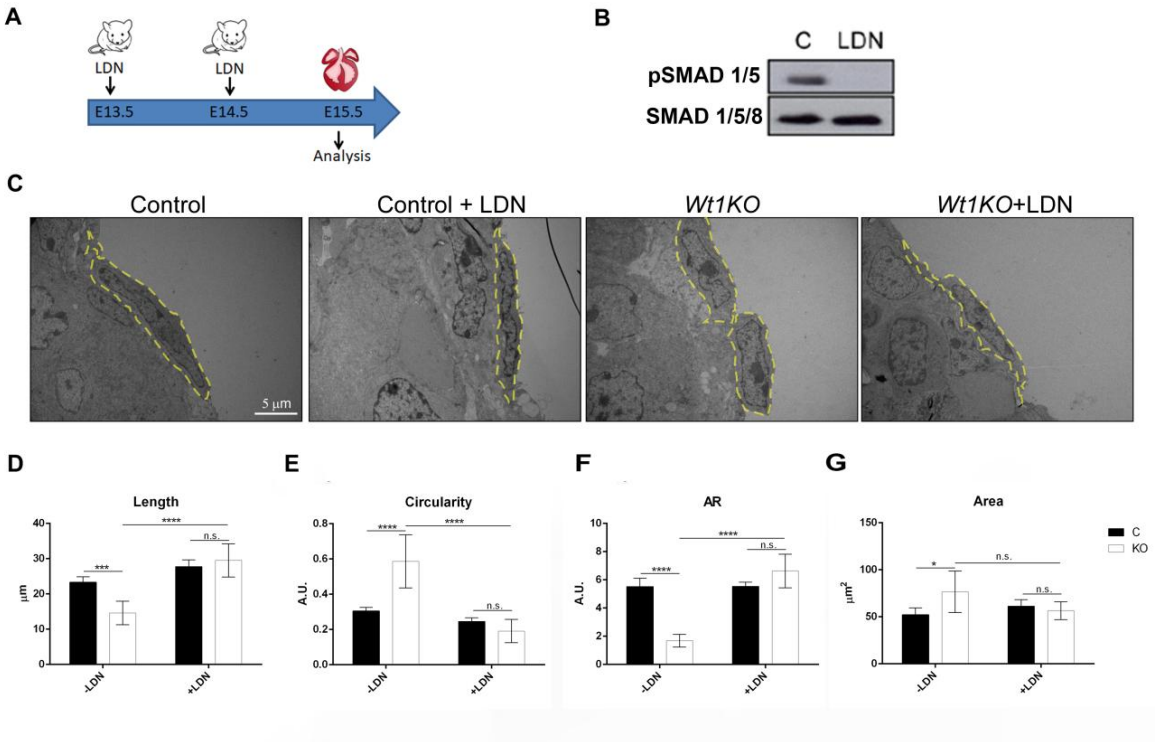

**Figure 20. BMP4 pathway inhibition rescues epicardial flattening in *epiWt1KO* cells *in vivo*.** (A) Schematic of the experimental design: pregnant females were injected with LDN at E13.5 and E14.5. Hearts were then analysed at E15.5. (B) Heart extracts from control and LDN-193189 (LDN)-treated pregnant mice, were analysed by Western Blotting with indicated antibodies. (C) TEM analysis of E15.5 control and *epiWt1KO* hearts treated with LDN or vehicle, indicating that flattening was rescued in epicardial *epiWt1KO* cells in the presence of LDN. (D-G) Quantification of epicardial cell lenght, AR, circularity and area, in TEM images. Values represent mean ± s.e.m. *P<0.05, ***P<0.001,**** P<0.0001 one-way ANOVA followed by Tukey's posthoc test. Three independent experiments or embryos per condition were assessed per condition, and at least 20 epicardial cells were quantified. Yellow dashed lines in C outline the shape of the epicardial cells. Scale bar, 5µm.

Although SMAD pathway inhibition resulted in a clear rescue of epicardial cell shape in *epiWt1KO* hearts, there was still the possibility for this result to be a secondary effect of LDN on treated embryos. To face this option, we decided to repeat the experiment on *ex vivo* cultured hearts (Fig. 21A) in the presence of Dorsomorphin (Dm), a BMP pathway inhibitor that efficiently inhibited SMAD1/5 phosphorylation in epicardial cells(Fig. 21B). After 48 hours, TEM analysis revealed that Dm treatment rescued *epiWt1KO* cuboidal phenotype to the flattened shape observed in control littermates (Fig. 21C). Analysis of epicardial cell length, AR, circularity and cell area confirmed this observation (Fig. 21D-G).

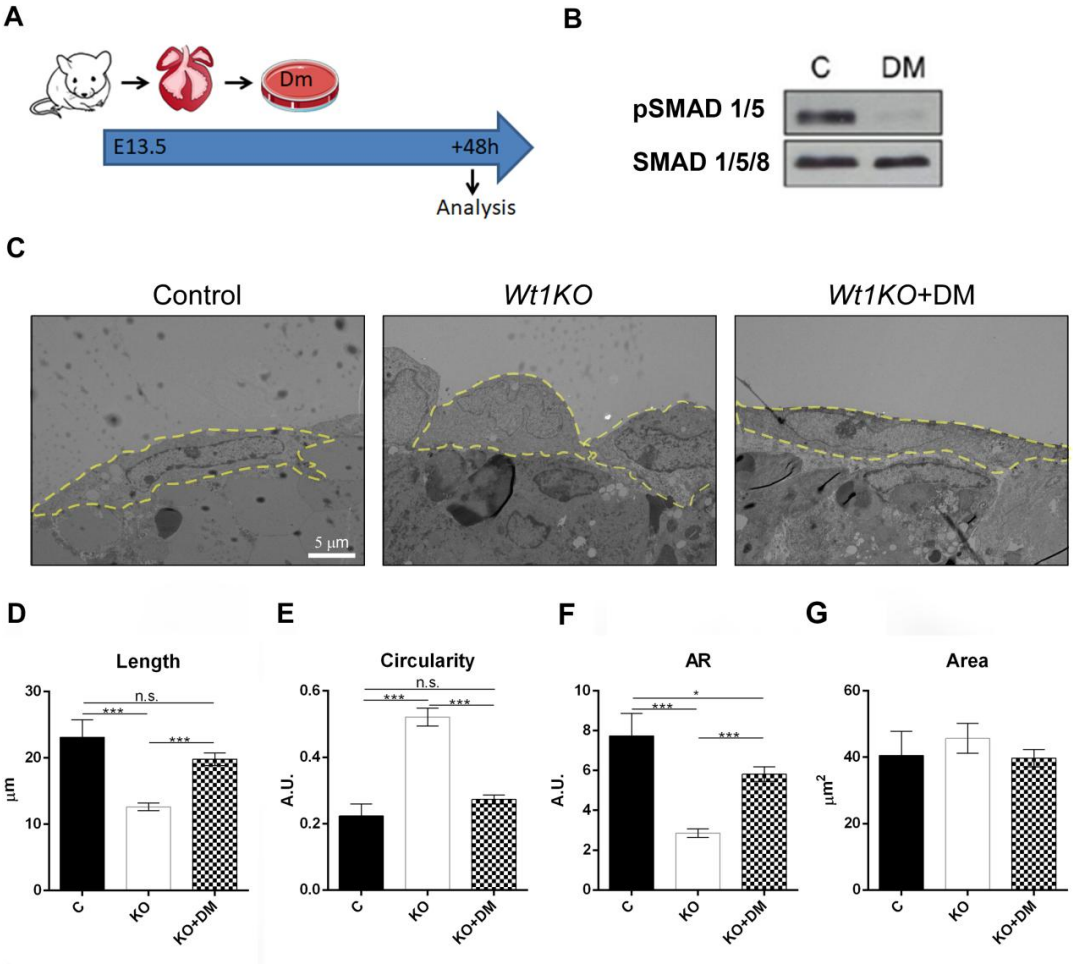

**Figure 21. BMP4 pathway inhibition rescues epicardial flattening in *epiWt1KO* cells *ex vivo*.** (A) Schematic of the experimental design: hearts from E13.5 embryos were cultured *ex vivo* in presence or abscence of Dm. Hearts were then analysed 48 hours later. (B) Heart extracts from control and *epiWt1KO* untreated or Dm-treated hearts were analysed by Western blotting with indicated antibodies. (C) TEM analysis of control and *epiWt1KO* hearts treated with DM or vehicle. Rescue of the flattening phenotype in epicardial *epiWt1KO* cells in the presence of DM can be observed. (D-G) Quantification of epicardial cell length AR, circularity and area in TEM images. Values represent mean ± s.e.m. *P<0.05, *** P<0.001, n.s. no significance, one-way ANOVA followed by Tukey's posthoc test. Three independent embryos were assessed per condition, and at least 20 epicardial cells were quantified. Yellow dashed lines in C outline the shape of the epicardial cells. Scale bar, 5µm.

These results confirm BMP4 acts through its canonical pathway to modulate epicardial cell shape. Interestingly, our results suggest that inhibition of the BMP4 pathway is sufficient to rescue the cell morphology phenotype observed in *epiWt1KO* epicardial cells.

## 8.4 BMP4 molecular mechanisms underlying *epiWt1KO* cell morphology phenotype.

Previous results demonstrate that WT1 regulates *Bmp4* expression (Fig. 15B) and that BMP4 is responsible for modulating epicardial cell shape through its canonical pathway (Fig. 18-21). However, we wanted to decipher the molecular mechanisms of this process.

### 8.4.1 BMP4 modulates epicardial cell proliferation *in vitro*.

*Wt1* has been described to be implicated in proliferation regulation. *In vitro* studies have shown that WT1 regulates the mitotic checkpoint complex by interacting with MAD2, a component of the spindle assembly checkpoint[334]. Moreover, WT1 has also been described to regulate Cycline E, implicated in G1 to S cell cycle progression[335]. In the epicardium, early stage epicardial cells show higher proliferation rates, which decrease with development progression[209]. Accordingly, in the transcriptomic data previously generated in our group, C*dk4* and *Ccnd2* expression is downregulated during epicardium development (Fig. 10 and Table 2). Therefore, we wondered whether BMP4 could be regulating epicardial proliferation.

Epicardial cell proliferation was evaluated using a BrdU (Bromodeoxyuridine) incorporation kit. First, we analysed whether inhibition of the BMP4 pathway, which is the expected process during development, resulted in reduced epicardial proliferation. Indeed, cells treated with Dm for 24 hours showed a significant reduction in BrdU incorporation levels compared to control cells (Fig. 22A). Then, we wondered whether BMP4 could modulate epicardial proliferation. To test this idea, epicardial cells pretreated with Dm ON were then treated rBMP4. Epicardial proliferation showed a BMP4 positive response. Cotreatment of rBMP4 with its downstream

inhibitor, Dm, consistently abrogated rBMP4 proliferation induction (Fig. 22B). These results suggest that the BMP4 pathway regulates epicardial proliferation *in vitro*.

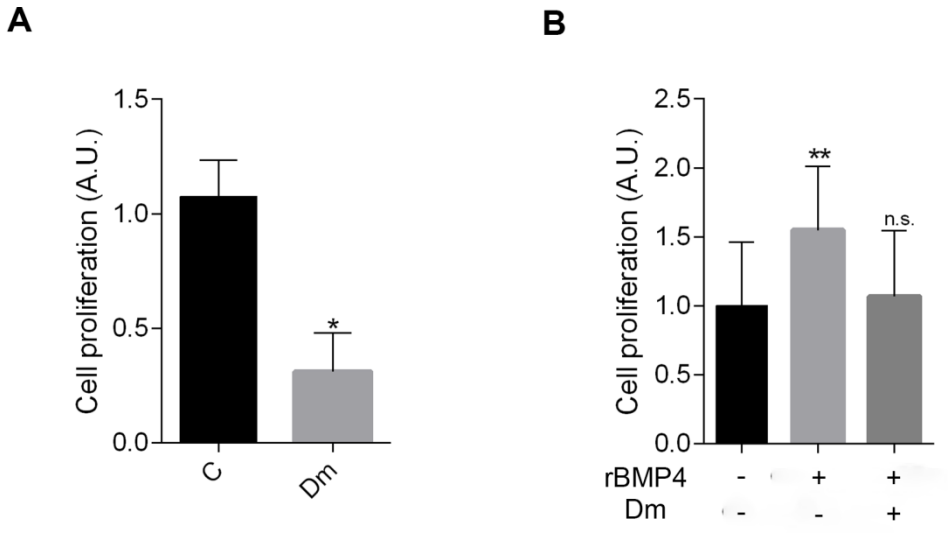


**Figure 22. BMP4 pathway positively regulates epicardial cell proliferation.** (A) BrDU incorporation in Control (C) and Dm-treated (Dm) immortalized epicardial cell proliferation demonstrated BMP pathway inhibition reduces cell proliferation. (B) BrDU incorporation in epicardial cells treated in presence or abscence of rBMP4 or/and Dm shows that rBMP4 induces cell proliferation *in vitro*. Values represent mean ± s.e.m. *P<0.05, **P<0.01 matched one-way ANOVA followed by Dunett's posthoc test.

### 8.4.2 BMP4 pathway downregulation results in the acquisition of a late stage genetic signature of epicardial cells.

Described results show how BMP4 induces the acquisition of a cuboidal cell shape and an increase in proliferation rates in epicardial cells (Fig. 18 and 22). These two properties are both typical of an early stage epicardium. Therefore, our interest focused on how the BMP4 pathway participates in regulating the embryonic epicardial program previously described (Fig. 10)[230].

As *Bmp4* is mainly expressed in the early stages of development, we decided to analyse the expression of genes whose expression was upregulated at these stages and then downregulated during development. These genes, as *Bmp4,* belong to cluster 1 genes of the transcriptomic data of the embryonic epicardial program (Fig. 10). Included in this cluster are *Tbx18, Podxl, Krt8, Cdkn1c or Smpd3* genes.

Epicardial cells were treated with Dm for 24h and then, the expression of the specified genes was measured using qRT-PCR. *Tbx18* is a classical marker of the embryonic epicardium[226]. *Podxl* gene encodes a cell adhesion and cell morphology protein that acts as an anti-adhesive protein[336]. *Krt8* encodes a cytoskeletal protein present in many epithelial cells[337]. *Cdkn1c* and

*Smpd3* are two genes previously described to be modulated by the BMP pathway in hair follicles stem cells[338]. Additionally, both of them are upregulated in *epiWt1KO* epicardial cells and downregulated during epicardium development. The expression of all of them was downregulated in the presence of Dm (Fig. 23). This downregulation follows the expected shift taking place in the embryonic epicardium signature and correlates with *Bmp4* downregulation during development.

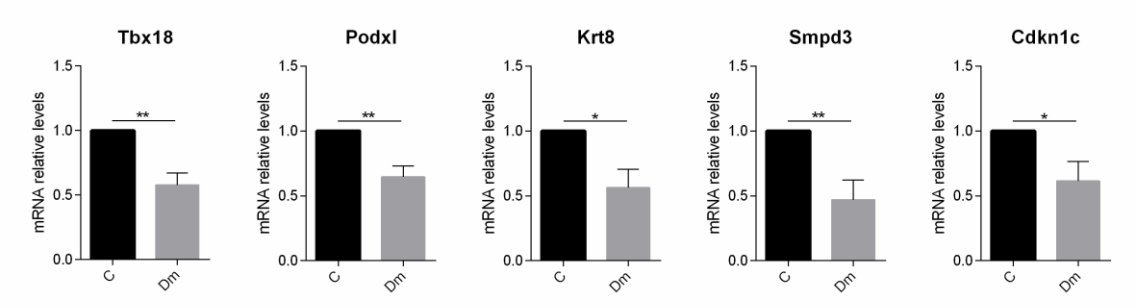


**Figure 23. BMP4 pathway inhibition causes the acquisition of an epicardial mature genetic signature.** qRT-PCR analysis of the indicated genes in control (C) and Dm-treated (Dm) immortalized epicardial cells. A downregulation of early stage genes from the epicardial embryonic program can be observed. Values represent mean ± s.e.m. *P<0.05 ** P<0.01, two-tailed t-test. Three independent experiments were performed.

These results suggest that the modulation of the BMP4 pathway inhibition modulated the expression of early stage epicardial genes.

### 8.4.3 pSMAD 1/5 regulates *Wt1* expression in epicardial cells.

WT1 is one of the key transcription factors required for epicardium development[190,194]. How WT1 regulates genetic programs responsible for these events has been widely studied and is well characterized. However, the mechanisms regulating *Wt1* expression are not so well defined. Importantly *Wt1* expression is also modulated during the epicardium development, and, as *Bmp4*, its expression is downregulated during development (Fig. 15). As we had observed that BMP4 pathway inhibition with Dm resulted in the modulation of genes abundantly express at early stages of the epicardium development (Fig. 23), we wanted to analyse whether this effect could be applied to *Wt1* expression.

Indeed, exposure of epicardial cells to Dm correlated with a downregulation of WT1 expression levels (Fig. 24A). A ChIP-sequencing experiment performed in hair follicles demonstrated that *Wt1* is a target of pSMAD 1/5[338]. Therefore, we decided to investigate whether BMP4 signaling could be regulating *Wt1* promoter activity. Hek293 cells were transfected with the *Wt1* promoter and then cultured In the presence of BMP4 or BMP4 and Dm. Luciferase activity was

reduced when Dm was present in the medium (Fig. 24B). These results prove that *Wt1* expression is regulated by BMP4 effectors pSMAD1/5.

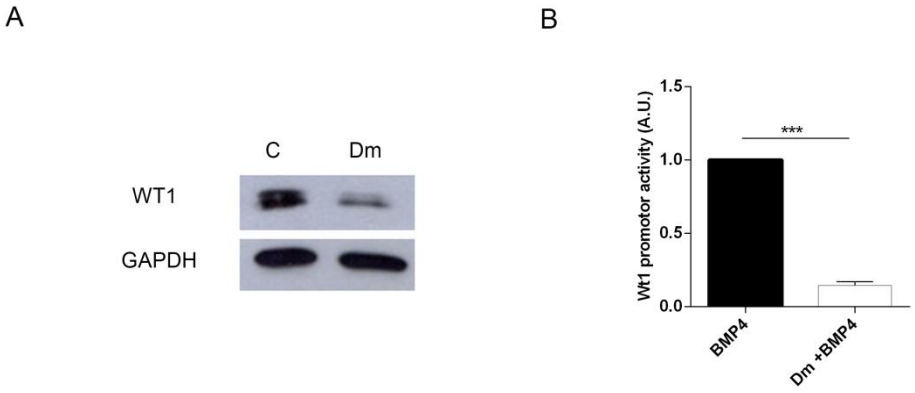


**Figure 24. BMP4 pathway modulation regulates WT1 expression.** (A) Western blot analysis for WT1 was performed using lysates of control (C) and Dm-treated (Dm) immortalized epicardial cells. GAPDH is shown as a loading control. (B) Luciferase reporter assay of mouse *Wt1* promoter in the presence of rBMP4 or rBMP4 and Dm. *** P<0.001, two-tailed t-test. Three independent experiments were performed.

## 8.5 *Bmp4* downregulation correlates with lung mesothelial flattening.

The epicardium is the mesothelium covering the heart. In addition to the epicardium, *Wt1* is also expressed in mesotheliums of other organs[339]. Therefore, we wondered whether the mechanisms and events described so far could be extrapolated to other organs, specifically in the lung.

We again used TEM to analyse mice lung mesothelial cells morphology at E11.5 and E18.5. The results revealed that lung mesothelial cells also transition from a cuboidal cell shape to a flattened phenotype during maturation (Fig. 25A). AR, length, circularity and area measurements of these cells showed a similar tendency to that observed in epicardial cells (Fig. 25B-E). In order to elucidate if the similarity of the morphological changes observed both in epicardial and lung mesothelial cells could be extended to transcriptional changes, we analysed the expression of genes regulated during epicardial development in freshly isolated lung mesothelial cells at E11.5 and E18.5. Results showed that the expression of genes downregulated during the epicardium development (*Wt1*, *Bmp4*, *Podxl*, *Tbx18*, *Krt7*) is also reduced during lung mesothelium development, and also that genes upregulated during the same period in the epicardium, follow the same pattern in lung mesothelial cells (*Msln)* (Fig. 25F).

Therefore, our results suggest that mesothelial cell flattening is a process that could be happening, in the terms described for the epicardium, in other mesotheliums as well.

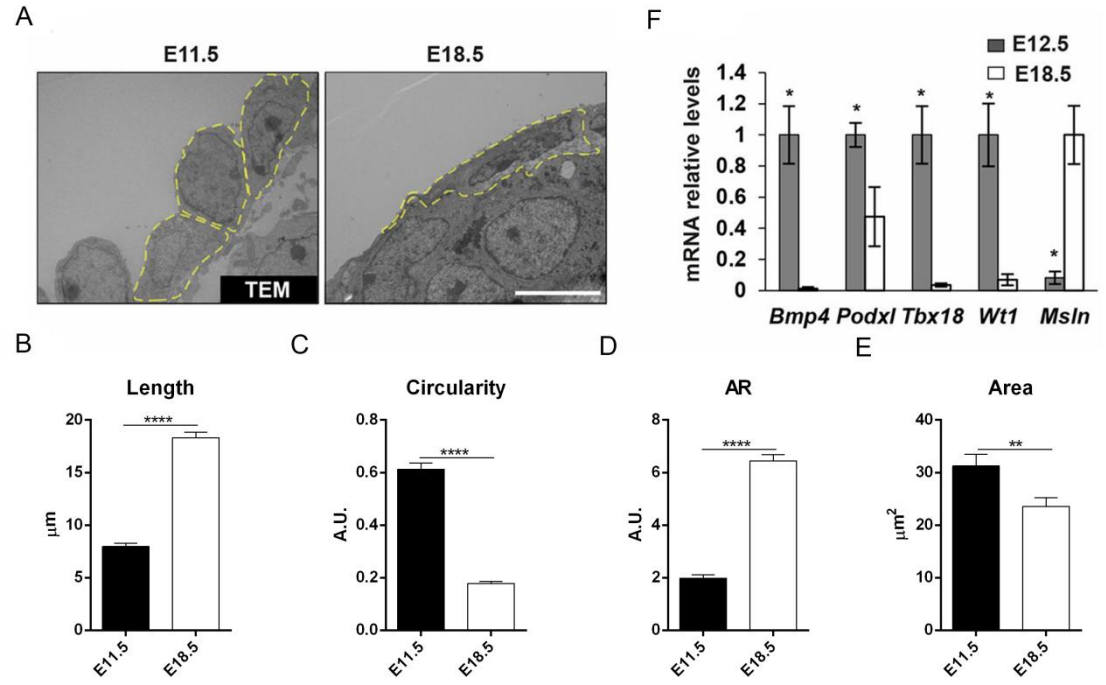


**Figure 25. *Bmp4* expression inversely correlates with a cuboidal-to-squamous transition during lung mesothelial maturation.** (A) Representative TEM of lung sections at E11.5 and E18.5. (B-E) Quantification of lung mesothelial cell length, cell area, circularity, and cell aspect ratio (AR), at E11.5 and E18.5 days of development, in TEM images. (F) qRT-PCR analyses of the indicated genes in *Wt1-GFP* sorted mesothelial cells at different days of development. Values represent mean±s.e.m. and *P*-values are based on one-tailed *t*-tests. **P*<0.05, ** *P*<0.01,**** *P*<0.0001. Three independent embryos were assessed per condition, and at least 40 mesotheliall cells were quantified. . Yellow dashed lines in A outline the shape of lung mesothelial cells. Scale bar: 5 µm

## 8.6 *Wt1$^{Cre}$* is expressed in the gonads.

### 8.6.1 *Wt1$^{Cre}$* traces gonad, but neither kidney nor adrenal gland lineages.

*Gata5$^{Cre}$* expression pattern limited our study spectrum to the epicardium[184]. Therefore, we decided to shift to another model: the Tg(WT1-cre)#Jbeb (*Wt1$^{Cre}$*) mouse model. The *Wt1$^{Cre}$* transgenic mouse has been widely used as a tool for tracing *Wt1* positive cells during the development of several organs, especially in the cardiovascular field[166,221]. However, it has never been used for the organs of the urogenital system, where *Wt1* plays a key role during development[75,76,262,317]. To characterize *Wt1$^{Cre}$* expression in the urogenital system, we crossed *Wt1$^{Cre}$* males with reporter *R26R$^{mTmG/mTmg}$* females. In the *Wt1$^{Cre}$; R26R$^{mTmG/+}$* mouse model, after Cre-mediated LoxP recombination, membranous GFP is expressed. Embryos were collected at E14.5 and WT1 and GFP expression was analysed using immunofluorescence staining in heart and urogenital sections. As previously described, *Wt1$^{Cre}$* activated GFP was

present in the epicardium and the subepicardial layer. On the other hand, organs derived from the urogenital ridge showed different degrees of GFP staining: gonads (G) presented abundant GFP cells whereas kidney (K) and adrenal gland (AG) showed no GFP cells, with the exception of some sparse cells surrounding its surface, despite endogenous WT1 is abundantly expressed in both organs (Fig. 26A). A more detailed examination with higher magnification images of gonads of both sexes and kidneys confirmed these appreciations (Fig. 26B).

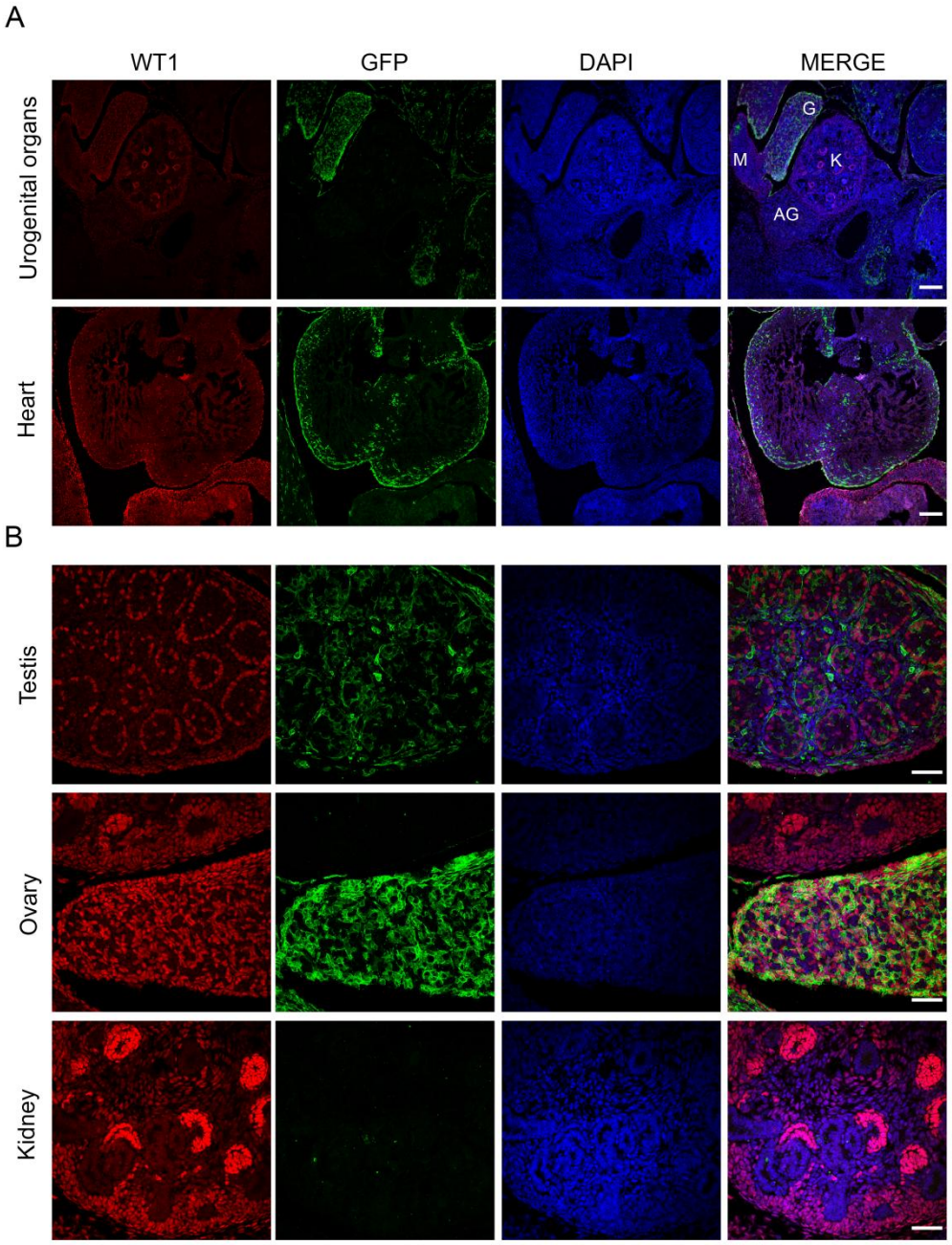


**Figure 26. *Wt1*$^{Cre}$ efficiently recombines in the gonads but neither in the kidney nor in the adrenal gland**. Immunofluorescent staining for WT1 (red), GFP reporter of the *Wt1*$^{Cre}$ lineage (green) and nuclear DAPI stain (blue) using sections from E14.5 control and *Wt1*$^{Cre}$;*R26R*$^{mTmG/+}$, XX and XY littermates. (A) shows heart and urogenital organs sections, (B) shows testis, ovary and kidney sections. WT1 actual expression is present in all organs but GFP staining is restricted to gonads and a few cells in the adrenal gland. Scale bar, 150µm (A) or 50µm (B). Three embryos per condition were used for the analysis. G; gonads. M; mesonephro; AG; adrenal gland; K; kideny.

### 8.6.2 *Wt1*$^{Cre}$ is not expressed in all *Wt1* cells.

The absence of GFP cells in the kidney and the adrenal gland intrigued us. Therefore, we decided to repeat the analysis in other organs where *Wt1* has been studied, using a more quantitative approach. In order to monitor *Wt1*$^{Cre}$ activity, the % of GFP cells from *Wt1*$^{GFP/+}$ was compared to GFP expression in *Wt1*$^{Cre}$*; R26R*$^{mTmG/+}$ embryos at E14.5 in organs where *Wt1* expression is well characterized. *Wt1*$^{GFP/+}$ is a *knockin (KI)* of *Wt1* exon 1. Thus, in *Wt1*$^{GFP/+}$ embryos all cells expressing *Wt1* are GFP. In *Wt1*$^{Cre}$*; R26R*$^{mTmG/+}$ organs, all cells expressing *Wt1* plus all cells deriving from those and cells that once expressed *Wt1*, are GFP positive. Therefore, in *Wt1*$^{Cre}$*; R26R*$^{mTmG/+}$ embryos, the % of cells expressing GFP should be equal or higher to GFP positive cell % in *Wt1*$^{GFP/+}$ embryos (Fig. 27A). In hearts and lungs, results were as expected: the % of GFP cells was equal or superior in *Wt1*$^{Cre}$*; R26R*$^{mTmG/+}$ embryos than in *Wt1*$^{GFP/+}$. Interestingly, in the liver and kidneys, although a high number of cells are *Wt1* positive (about 40% and 15% respectively), the % of GFP cells in *Wt1*$^{Cre}$*; R26R*$^{mTmG/+}$ organs was below 1% in both cases (Fig. 27B).

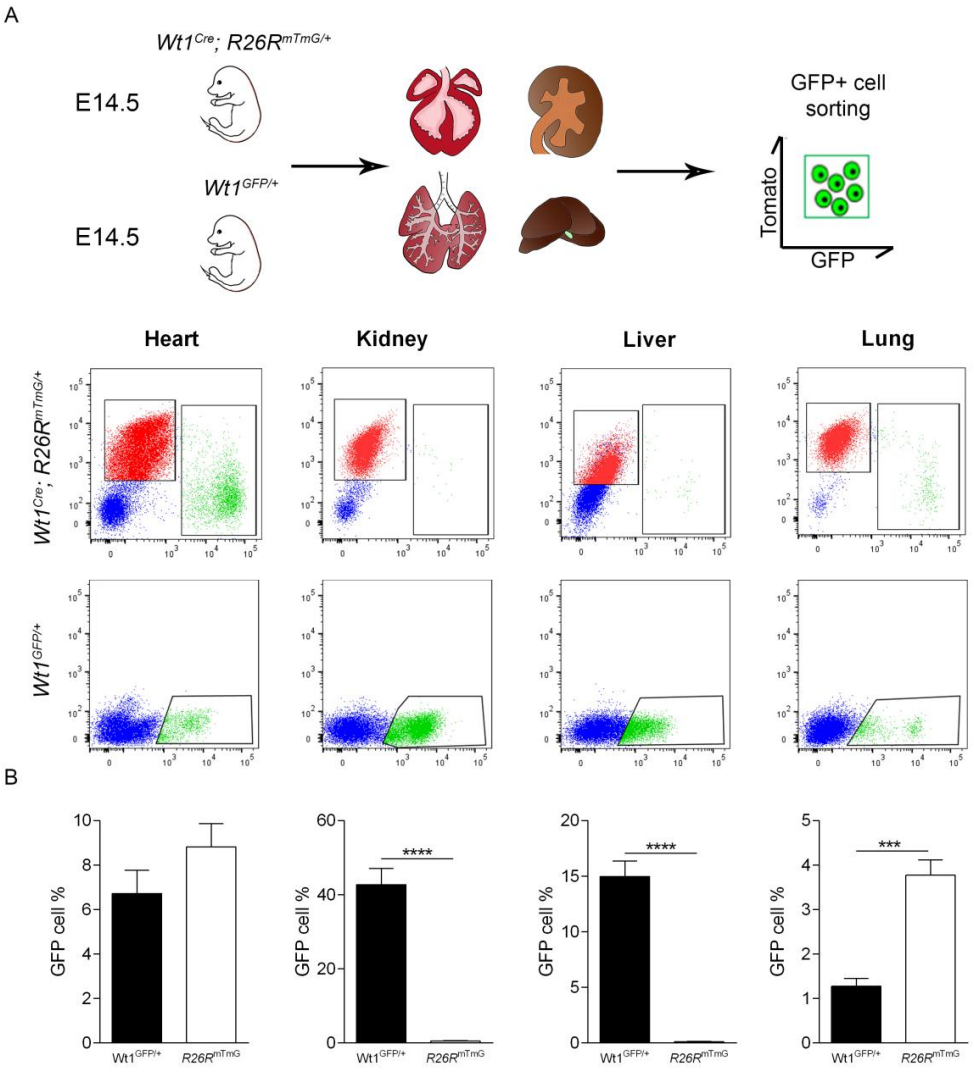

**Figure 27. The percentage of GFP cells does not correlate in *Wt1*$^{GFP/+}$ and *Wt1*$^{Cre}$*; R26R*$^{mTmG/+}$ mouse models**. (A) *Wt1*$^{GFP/+}$ and *Wt1*$^{Cre}$*; R26R*$^{mTmG/+}$ embryos were collected at E14.5 and hearts, lungs, kidneys and livers were then enzymatically dissociated and FACS analysed. Gates encompasses Tomato+, GFP- (red), GFP+ (green) and double negative (blue) populations. (B) GFP positive cell % reveal expression pattern differences between both reporters. GFP cell % in liver and kidneys *Wt1*$^{Cre}$*; R26R*$^{mTmG/+}$ was minimal, whether in hearts and lungs was similar or superior than in *Wt1*$^{GFP/+}$ embryos**.** Values represent mean ± s.e.m. *** P<0.001, **** P<0.0001 two-tailed t-test. Four embryos per condition were used for the analysis.

These results suggested that *Wt1*$^{Cre}$ is expressed in hearts and lungs but barely in livers and kidneys, suggesting a difference in the lineage tracing behaviour of the *Wt1*$^{Cre}$ mouse model in different cell populations.

Despite the evidence of these results, there were still two points needing further clarification. First, although highly improbable (as it is a widely used model), there was the possibility that the reporter was not correctly working despite *Wt1*$^{Cre}$ was active. Second, in the case of the lungs and hearts, we did not actually know exactly if all cells expressing *Wt1* were also expressing the Cre recombinase.

Therefore, to further prove this point, we decided to use a second reporter mouse model and follow a more accurate strategy. We crossed *Wt1*$^{GFP/+}$*; Wt1*$^{Cre}$ males with *R26R*$^{tdRFP/tdRFP}$ females to generate *Wt1*$^{GFP/+}$*; Wt1*$^{Cre}$*; R26R*$^{tdRFP/+}$ embryos. In these embryos, *Wt1* expressing cells are GFP positive while *Wt1*$^{Cre}$ activates RFP expression. Double positive cells are those in which the *Wt1*$^{Cre}$ is active and *Wt1* is expressed. GFP positive cells are those in which the *Wt1*$^{Cre}$ is not active. Finally, RFP positive cells are those that derive from *Wt1*$^{Cre}$ expressing cells.

Using flow cytometry (Fig. 28A) we were able to analyse the exact % of total *Wt1* positive cells (GFP cells) in which *Wt1*$^{Cre}$ was active (RFP cells) (Fig. 28B). The results of this experiment confirmed our previous data for kidneys and livers. In *Wt1*$^{GFP/+}$*; Wt1*$^{Cre}$*; R26R*$^{tdRFP/+}$ kidneys we observed that about of 58% of all cells where GFP positive. However, less than 1% of these cells were RFP positive. A similar pattern was observer in livers: from all the 36% of cells GFP positive, less than 0,3% were RFP positive. On the other hand, in the lung, while only 2.8% were GFP positive, almost three quarters of them were RFP positive (74.10%). Gonads percentages were close to this second situation: 35.3% of all cells were GFP positive, from those, more than a half (63.95%), were RFP positive. This experiment, additionally, unveiled some interesting facts about *Wt1*$^{Cre}$ expression in heart. As mentioned before, there are two *Wt1*$^{GFP}$ populations in the embryonic heart, presumably corresponding to epicardial cells (Wt1$^{GFP++}$) and cardiomyocytes (Wt1$^{GFP+}$)[230]. From all Wt1 $^{GFP++}$ cells, 79.23% were RFP (*Wt1*$^{Cre}$) positive. On the other hand, only a 28.56% of all Wt1$^{GFP+}$ cells were RFP positive (*Wt1*$^{Cre}$ positive). Finally, this experiment, allowed us to distinguish a particular population that is not

easily traceble. In lineage tracing studies, reporter is active not only in derived cells, but also in those still expressing the gene under study. In this case, *Wt1* endogenous GFP expression allowed to distinguish between, $GFP^+$; $RFP^+$ cells (those still expressing the gene), and $GFP^-$; $RFP^+$ cells (cells derived from *Wt1* expressing progenitors). At E13.5, the stage analysed, we detected a large $GFP^-$; $RFP^+$ population in the lung (9.58% of all cells), while in the gonads it represented a negligible fraction (0.85%). The accuracy of this % is of course questionable, especially taking into account the effectiveness of the Cre recombination. However, the frame provided by this experiment might be a useful tool to improve lineage tracing studies in the future.

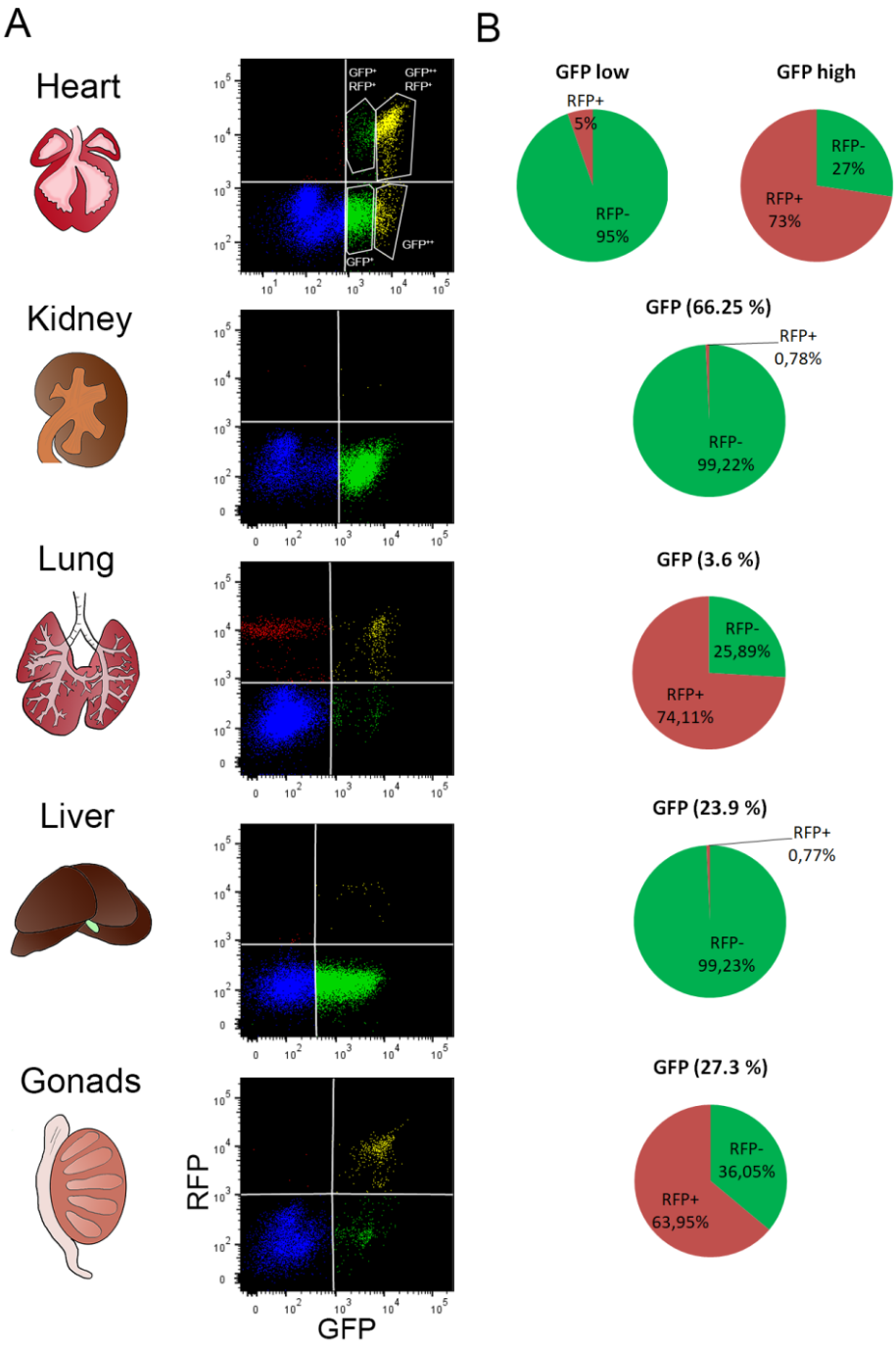

**Figure 28. Percentage of *Wt1*$^{Cre}$ (RFP) cells does not correlate with *Wt1* (GFP) cells in *Wt1*$^{Cre}$; *Wt1*$^{GFP/+}$; *R26R*$^{tdRFP/+}$ mice**. (A) *Wt1*$^{Cre}$; *Wt1*$^{GFP/+}$; *R26R*$^{tdRFP/+}$ embryos were collected at E13.5 and hearts, lungs, kidneys, livers and gonads were then enzymatically dissociated and FACS analysed. Kidney and Grid lanes separate GFP$^-$,RFP$^-$ (blue); GFP$^+$,RFP$^-$ (green); GFP$^-$,RFP$^+$ (red); GFP$^+$,RFP$^+$ (yellow). In the heart FACS, gate encompasses GFP$^+$ and GFP$^{++}$, RFP$^+$ or RFP$^-$ subpopulations. (B) % of *Wt1*-GFP positive, *Wt1*$^{Cre}$-RFP negative (green) and *Wt1*-GFP positive, *Wt1*$^{Cre}$-RFP positive (red) cells in total GFP-*Wt1* cells. In kidneys and livers *Wt1*$^{Cre}$ was expressed in a negligible % of *Wt1*$^{GFP}$ cells. Lungs, heart and gonads showed different grades of *Wt1*$^{Cre}$ and *Wt1*$^{GFP}$ correlation. Three embryos per condition were used for the analysis.

## 8.7 Generation of a new *Wt1KO* model.

*Wt1* conventional KO is lethal around E13.5, preventing the study of *Wt1* deletion effects further from that point[190]. Indeed, the study of the *Wt1* role has always been hampered by the fact that its deletion, even in a conditional way in specific tissues, normally leads to embryonic or postnatal lethality at some point. There are two reasons for this lethality: *Wt1KOs* show aberrant development of coronary vessels and present kidney agenesis[76,190,194].

The results obtained with the *Wt1*$^{Cre}$ reporter analyses lightened one promising possibility: we could use the *Wt1*$^{Cre}$ to generate a *Wt1* gonad KO with an expanded lifespan. For this reason, we generated a new *Wt1* mouse model: *Wt1*$^{Cre}$; *Wt1*$^{Loxp/GFP}$. In these mice, exon 1 of one of the *Wt1* alleles is replaced by a GFP. In the other allele, exon 1 is flanked by loxP sequences. In the presence of a Cre recombinase, the floxed allele is deleted, ending in both alleles being Wt1 null. In these mice, the BAC containing the *Wt1* gene and part of its regulatory regions, followed by an IRES cassette and a Cre is inserted in an unknown position in the genome (Fig. 29A,B). The contribution of the BAC to total amount of *Wt1* levels was almost null.

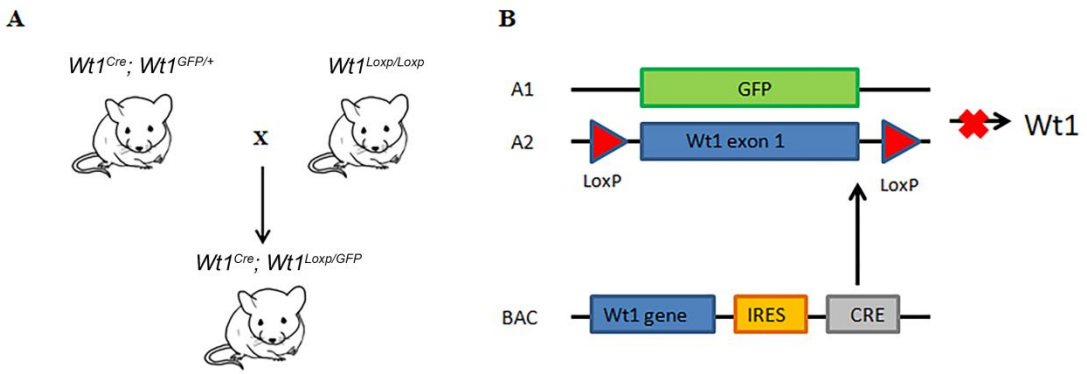


**Figure 29. *Wt1*$^{Cre}$; *Wt1*$^{loxP/GFP}$ mouse, a new *Wt1KO* model.** (A) Breeding strategy used to generate *Wt1*$^{Cre}$; *Wt1*$^{loxP/GFP}$ mice. (B) Genetic landscape of alleles and *Wt1*$^{Cre}$ BAC in *Wt1*$^{Cre}$; *Wt1*$^{loxP/GFP}$ mice. GFP knockin allele does not express *Wt1*. In the presence of the Cre recombinase, the *Wt1* floxed allele is deleted.

## 8.8 *Wt1$^{Cre}$; Wt1$^{LoxP/GFP}$* mice show a partial embryonic lethality.

*Wt1$^{Cre}$;Wt1$^{Loxp/GFP}$* mice were born and reached adulthood with no signs of an apparent phenotype compared to control mice (Fig. 30A). To test whether there was any range of lethality, we decided to count the number of mice from each of the four genotypes resulting from the previously explained crossing (Fig. 30B). The genotyping of adult mice at 6 months of age revealed a sub-Mendelian distribution of the *Wt1$^{Cre}$;Wt1$^{Loxp/GFP}$* mice (14,63%) genotype This difference was also observed in the group of mice that reached 1 year of life (10,34%). Our interest then was to elucidate the moment when the observed lethality was happening. Therefore, we analysed the proportions of all the offsprings used to perform the different embryonic experiments. Neither at E11.5 nor at E14,5, the disparity observed in adult mice proportions was appreciated (31.82% and 23.08%, respectively).

It is challenging to settle whether the % observed in adult mice is the result of some lethality that occurs between E14.5 and birth. However, it is interesting to consider that once *Wt1$^{Cre}$;Wt1$^{Loxp/GFP}$* mice were born, they showed the same survival capacity as the other genotype mice. In conclusion, these results suggest that at a certain stage during embryonic development, there is a critical point that marks *Wt1$^{Cre}$;Wt1$^{Loxp/GFP}$* survival.

A


B

| | *Wt1$^{Loxp/+}$* | *Wt1$^{Cre}$; Wt1$^{Loxp/+}$* | *Wt1$^{Loxp/GFP}$* | ***Wt1$^{Cre}$; Wt1$^{Loxp/GFP}$*** |
|---|---|---|---|---|
| E11.5 | 24/132 (18.18%) | 30/132 (22.73%) | 37/132 (28.03%) | 42/132 (31.82%) |
| E14.5 | 19/78 (24.36%) | 18/78 (23.08%) | 23/78 (29.49%) | 18/78 (23.08%) |
| 6 months | 24/82 29.72% | 26/82 31.71% | 20/82 24.39% | 12/82 (14.63%) |
| 12 months | 8/29 (27.59%) | 9/29 (31.03%) | 9/29 (31.03%) | 3/29 (10.34%) |

**Figure 30. *Wt1$^{Cre}$;Wt1$^{Loxp/GFP}$* mutant mice reach adulthood.** (A) No visible difference was observed between control and *Wt1$^{Cre}$;Wt1$^{Loxp/GFP}$* mice. Scale bar: 1cm. (B) Distribution of the different genetic combinations resulted from the intercross of *Wt1$^{Cre}$; Wt1$^{GFP/+}$* males with *Wt1$^{loxP/loxP}$* females.

## 8.9 *Wt1$^{Cre}$;Wt1$^{Loxp/GFP}$* mice show ambiguous genitalia.

An interesting finding of the analysis of adult *Wt1$^{Cre}$;Wt1$^{Loxp/GFP}$* mice was that all the mutant mice were, externally, phenotipically females. In addition, detailed external examinations revelead the presence of a micropenis in all *Wt1$^{Cre}$;Wt1$^{Loxp/GFP}$* mice. Quantification of anogenital distance confirmed these appreciations (Fig. 31A,B) and suggested a feminization of some of the "externally females" XY *Wt1$^{Cre}$;Wt1$^{Loxp/GFP}$* mice. To test this, Y chromosome

presence was analysed by genotyping these mice for the *Rbm31* gene. This gene has the particularity that it is shorter in the Y chromosome than in the X chromosome. Therefore, a PCR of the *Rbm31* gene of XY mice would produce 2 different bands[340]. Indeed, this was the case of some $Wt1^{Cre};Wt1^{Loxp/GFP}$ mice (Fig. 31C). As we had observed a difference between the expected and the observed proportions of $Wt1^{Cre};Wt1^{Loxp/GFP}$ mice, we decided to test whether this potential lethality could be linked to sex. However, almost half of $Wt1^{Cre};Wt1^{Loxp/GFP}$ (45.45%) were XY mice, suggesting that this is not the case (Fig. 31D). When a necropsy was performed on control and $Wt1^{Cre};Wt1^{Loxp/GFP}$ mice, we observed that internal genitalia from XX and XY $Wt1^{Cre};Wt1^{Loxp/GFP}$ presented two small structures compatible with gonads at the lower pole of both kidneys and atrophied genital tracts (Fig. 31E).

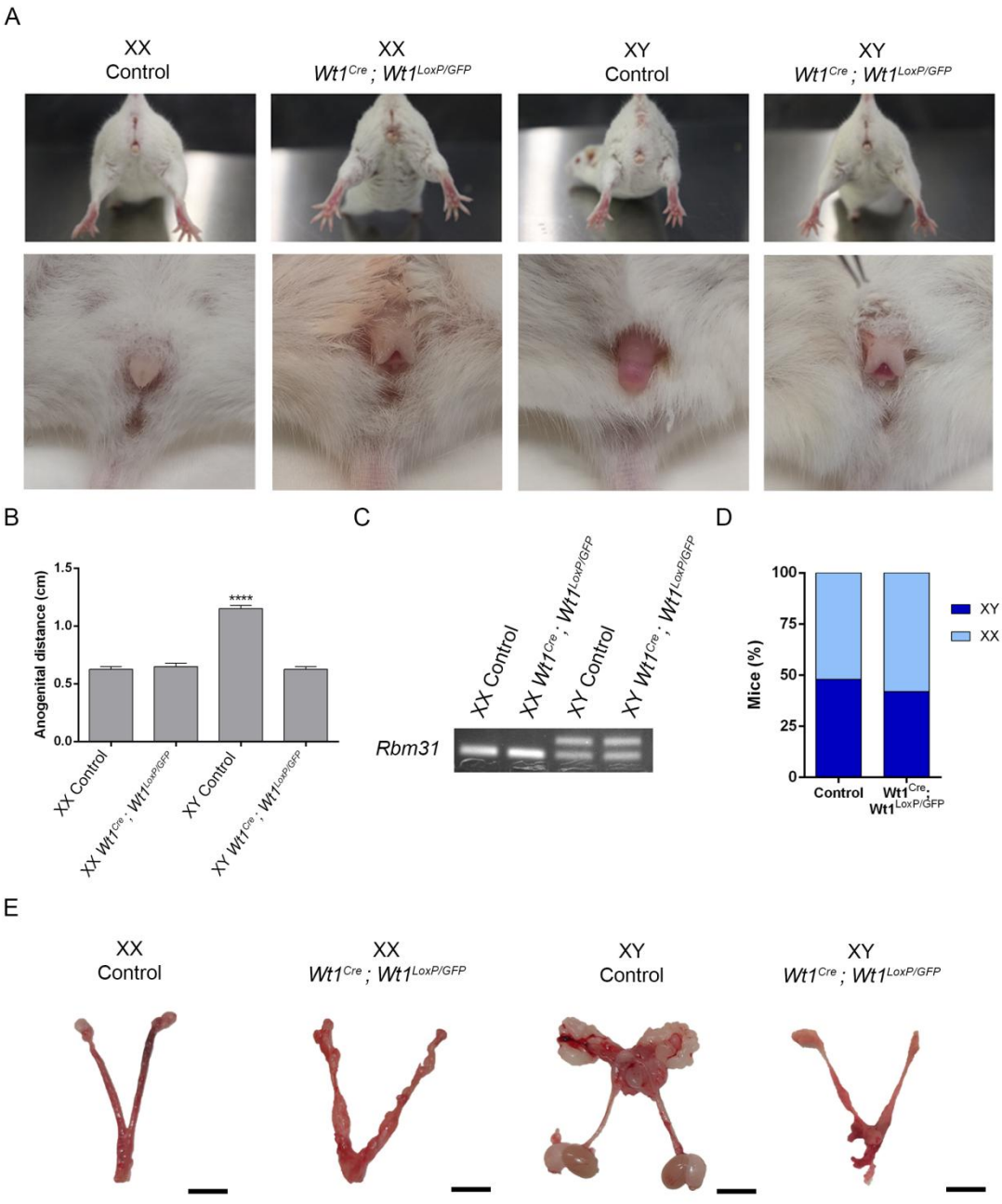

**Figure 31. *Wt1$^{Cre}$;Wt1$^{Loxp/GFP}$* mice present ambiguous genitalia.** (A) External genitalia of XX and XY, control and *Wt1$^{Cre}$;Wt1$^{Loxp/GFP}$* mice. Top panel shows mice anogenital view. Below panel shows the presence of micropenis in all *Wt1$^{Cre}$;Wt1$^{Loxp/GFP}$* mice. (B) Anogenital distance quantification of the indicated phenotypes indicated a feminization of XY *Wt1$^{Cre}$;Wt1$^{Loxp/GFP}$* mice. **** P<0.0001, one-way ANOVA followed by Tukey's posthoc test. (C) Sexual genotyping of XY and XX, control and *Wt1$^{Cre}$;Wt1$^{Loxp/GFP}$* mice using *Rbm31* primers. (D) Lethality is not sex-associated. No significant differences were observed in frequencies of XY and XX between control and *Wt1$^{Cre}$;Wt1$^{Loxp/GFP}$* mice ($\chi^2$, p=0,3938).(E) Internal genitalia of XX and XY, control and *Wt1$^{Cre}$;Wt1$^{Loxp/GFP}$* mice. *Wt1$^{Cre}$;Wt1$^{Loxp/GFP}$* mice show reduced gonads and atrophic genital tracts. Scale bar, 1cm.

The histopathological analysis of *Wt1$^{Cre}$;Wt1$^{Loxp/GFP}$* mice revealed all KO mice showed structures compatible with gonads at the lower pole of both kidneys. Moreover, both XX and XY *Wt1$^{Cre}$;Wt1$^{Loxp/GFP}$* showed other tissue structures compatible with both male and female genital organs in the abdominal/retroperitoneal cavity. The comparison between *Wt1$^{Cre}$;Wt1$^{LoxpP/+}$* and Wt1$^{Loxp/GFP}$ controls presented no relevant macroscopic alterations (Fig. 32,33).

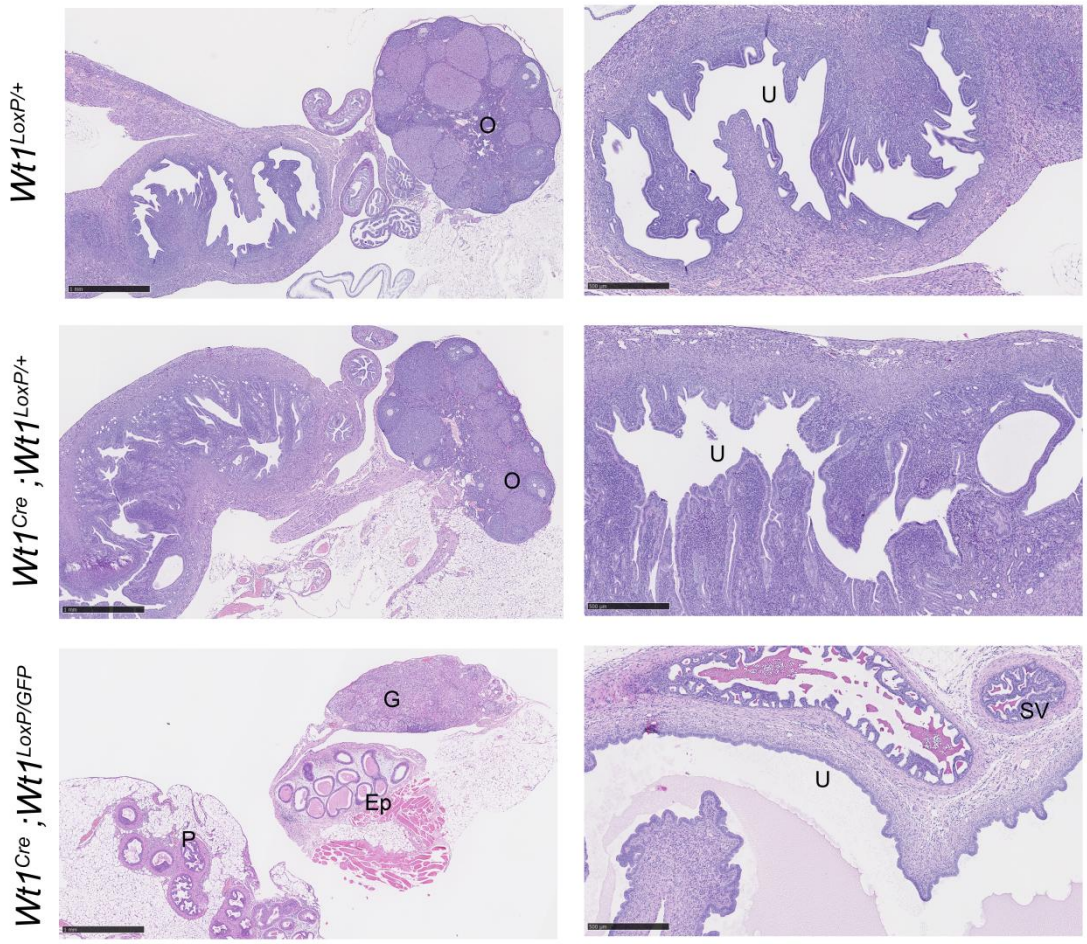


**Figure 32. *Wt1$^{Cre}$;Wt1$^{Loxp/GFP}$* adult XX gonads present streak gonads and an hermaprhodyte genital tract.** Left panel shows histological analysis of ovaries from controls (*Wt1$^{Loxp/+}$* and *Wt1$^{Cre}$;Wt1$^{Loxp/+}$*) and gonads from XX *Wt1$^{Cre}$;Wt1$^{Loxp/GFP}$* adult mice by *H&E* staining. Right panel shows histological analysis from genital tracts from controls and XX *Wt1$^{Cre}$;Wt1$^{Loxp/GFP}$* adult mice by *H&E* staining. Scale bar, 500µm. G; gonad. Ep; Epididymys. O; Ovary. P; Prostate. SV; seminal vesicles. U; uterus. Scale bar, 1mm.

In both XX and XY *Wt1*$^{Cre}$;*Wt1*$^{Loxp/GFP}$ mice, no mature gonads were present. Instead, both showed atrophic gonads. No testicular tissue was present in any of the XY *Wt1*$^{Cre}$;*Wt1*$^{Loxp/GFP}$ mice, and only the epididymis was seen and located near the primitive gonad in the lumbar area. In all XY and XX *Wt1*$^{Cre}$;*Wt1*$^{Loxp/GFP}$ mice, the remaining genital tract consisted of the simultaneous presence of male and female genital structures (Fig. 32,33). Therefore, male accessory sex glands, including seminal vesicles, coagulating glands, prostate glands were identified histologically in both female and male *Wt1*$^{Cre}$;*Wt1*$^{Loxp/GFP}$ mice. Moreover, in two of the *Wt1*$^{Cre}$;*Wt1*$^{Loxp/GFP}$ mice (XY and XX), dilated uterus/cystic uterus with a material compatible with fluid content that had not yet progressed to macroscopically evident cystic dilation, was also observed (Fig. 32,33).

The necropsy and histological changes at the level of the genital system suggested that *Wt1*$^{Cre}$;*Wt1*$^{Loxp/GFP}$ mice had undergone a sexual transformation that might be compatible with hermaphroditism of the genital tract, as both XY and XX *Wt1*$^{Cre}$;*Wt1*$^{Loxp/GFP}$ mice present masculine and feminine genital tract structures (Fig. 32,33).

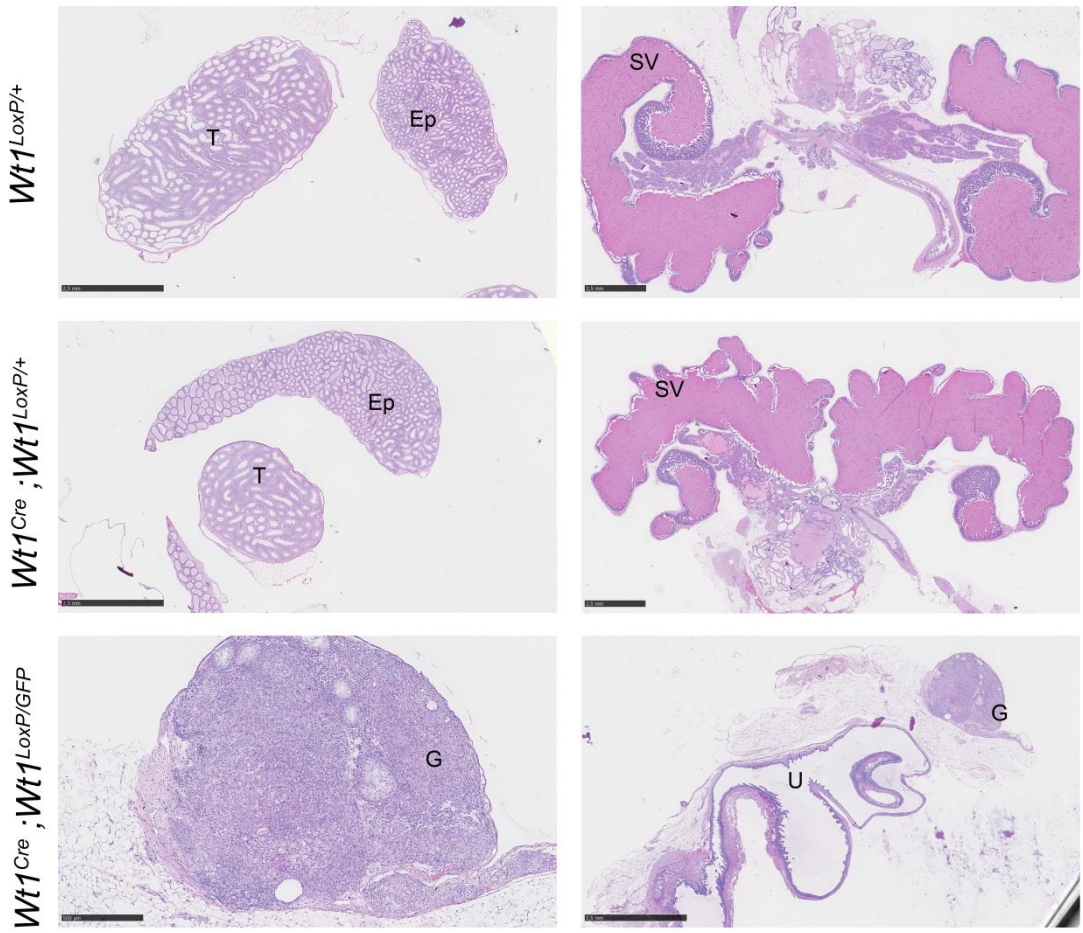


**Figure 33. *Wt1*$^{Loxp/GFP}$ adult XY gonads present streak gonads and an hermaprhodyte genital tract.** Left panel shows histological analysis testis and epididymys from controls and gonad from XY *Wt1*$^{Cre}$;*Wt1*$^{Loxp/GFP}$ adult mice by

*H&E* staining. Scale bar, 2.5mm (500µm for $Wt1^{Cre};Wt1^{Loxp/GFP}$ image). Right panel shows histological analysis from genital tracts from controls and XY $Wt1^{Cre};Wt1^{Loxp/GFP}$ adult mice by *H&E* staining. Scale bar, 2.5mm. G; gonad. Ep; Epididymys. P; Prostate. SV; seminal vesicles. T; testis. U; uterus.

## 8.10 $Wt1^{Cre};Wt1^{Loxp/GFP}$ embryonic gonad development is impaired.

### 8.10.1 *Wt1* expression is downregulated in $Wt1^{Cre};Wt1^{Loxp/GFP}$ gonads.

Having observed such defects in the sexual organs of adult $Wt1^{Cre};Wt1^{Loxp/GFP}$ mice, we decided to perform a series of experiments analyzing the embryological development of $Wt1^{Cre};Wt1^{Loxp/GFP}$ gonads. At E14.5 bright-field images of $Wt1^{Cre};Wt1^{Loxp/GFP}$ embryos gonads revealed an abnormal embryonic development. $Wt1^{Cre};Wt1^{Loxp/GFP}$ XY gonads were smaller than control littermate gonads and did not present normal testis cords structures. In addition, no apparent differences were observed between XY and XX $Wt1^{Cre};Wt1^{Loxp/GFP}$ and XX control gonads (Fig. 34A). At E12.5, when bipotential gonad is still present, qRT-PCR analysis of *Wt1* expression in $Wt1^{Cre};Wt1^{Loxp/GFP}$ gonads revealed a dramatic reduction of *Wt1* levels(Fig. 34B), confirming an efficient deletion of the floxed allele. Additionally, we did not find differences among *Wt1* mRNA levels in the different control genotypes of $Wt1^{Cre};Wt1^{Loxp/GFP}$ littermates ($Wt1^{Loxp/+}$ , $Wt1^{Cre};Wt1^{Loxp/+}$ and $Wt1^{Loxp/GFP}$) (Fig. 34C). These results indicate the observed phenotype is only attributable to the efficient deletion of both alleles and not to a possible heterozygosity effect.

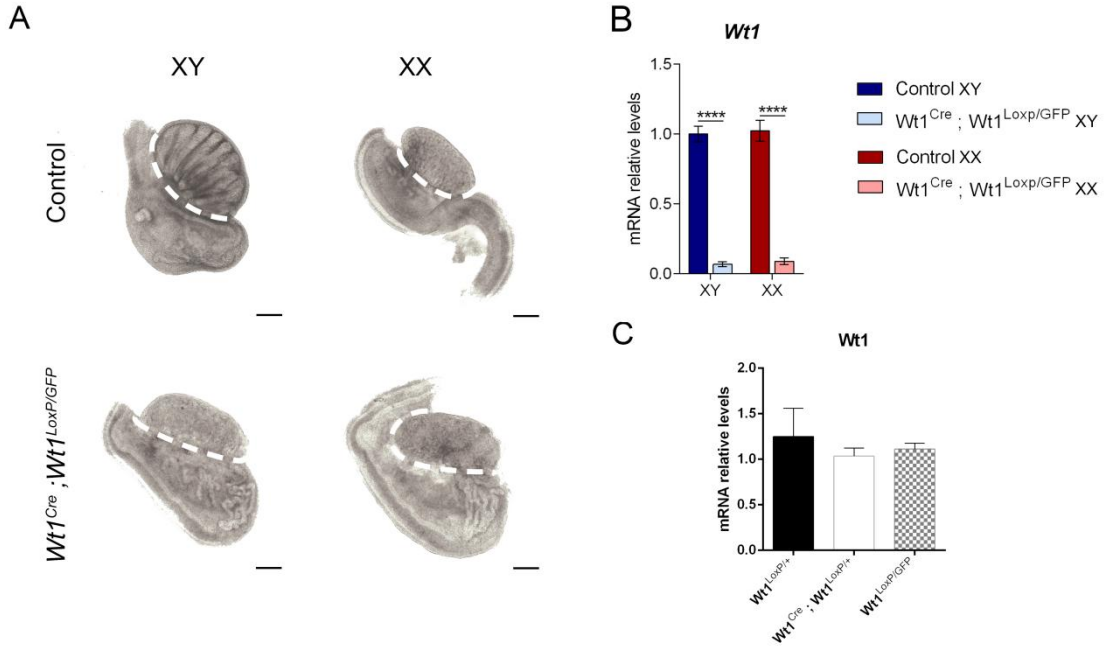


**Figure 34. *Wt1* is downregulated in $Wt1^{Cre};Wt1^{Loxp/GFP}$ XX and XY embryonic gonads.** (A) Bright-field images of E14.5 control and $Wt1^{Cre};Wt1^{Loxp/GFP}$ XY and XX gonads and mesonephros revealed an aberrant phenotype of mutant gonads.(B) qRT-PCR analysis in gonads from E12.5 control and $Wt1^{Cre};Wt1^{Loxp/GFP}$ littermates, showed *Wt1* mRNA levels were downregulated in $Wt1^{Cre};Wt1^{Loxp/GFP}$ embryos. (C) No significative differences were observed between

*Wt1* mRNA levels in control $Wt1^{LoxP/+}$, $Wt1^{Cre};Wt1^{LoxP/+}$ and $Wt1^{GFP/+}$ gonads using a qRT-PCR analysis. **** P<0.0001 two-way (B) or one-way (C) ANOVA followed by Tukey's posthoc test. Three embryos per condition were used for the analysis. Dashed lines in D separate gonads from mesonephros. Scale bar, 250µm.

*Wt1* is implicated in gonad development and participates in the decision between male and female differentiation[99]. In gonads, *Wt1* is expressed first in the coelomic epithelium covering them, and later also in somatic cells from both male and female organs [74,99]. To verify WT1 protein downregulation we decided to analyse WT1 expression pattern in E14.5 $Wt1^{Cre};Wt1^{Loxp/GFP}$ gonads. WT1 and GFP staining in E14.5 gonads showed a WT1 expression downregulation in gonads from XX and XY $Wt1^{Cre};Wt1^{Loxp/GFP}$ embryos. In our model, mutant cells remain GFP positive despite functional WT1 is absent. Therefore, GFP staining indicated the presence of $Wt1^{GFP}$ cells in the gonad. Moreover, in XY $Wt1^{Cre};Wt1^{Loxp/GFP}$ gonads, no testis cords structures were present, suggesting an aberrant differentiation of somatic cells (Fig. 35).

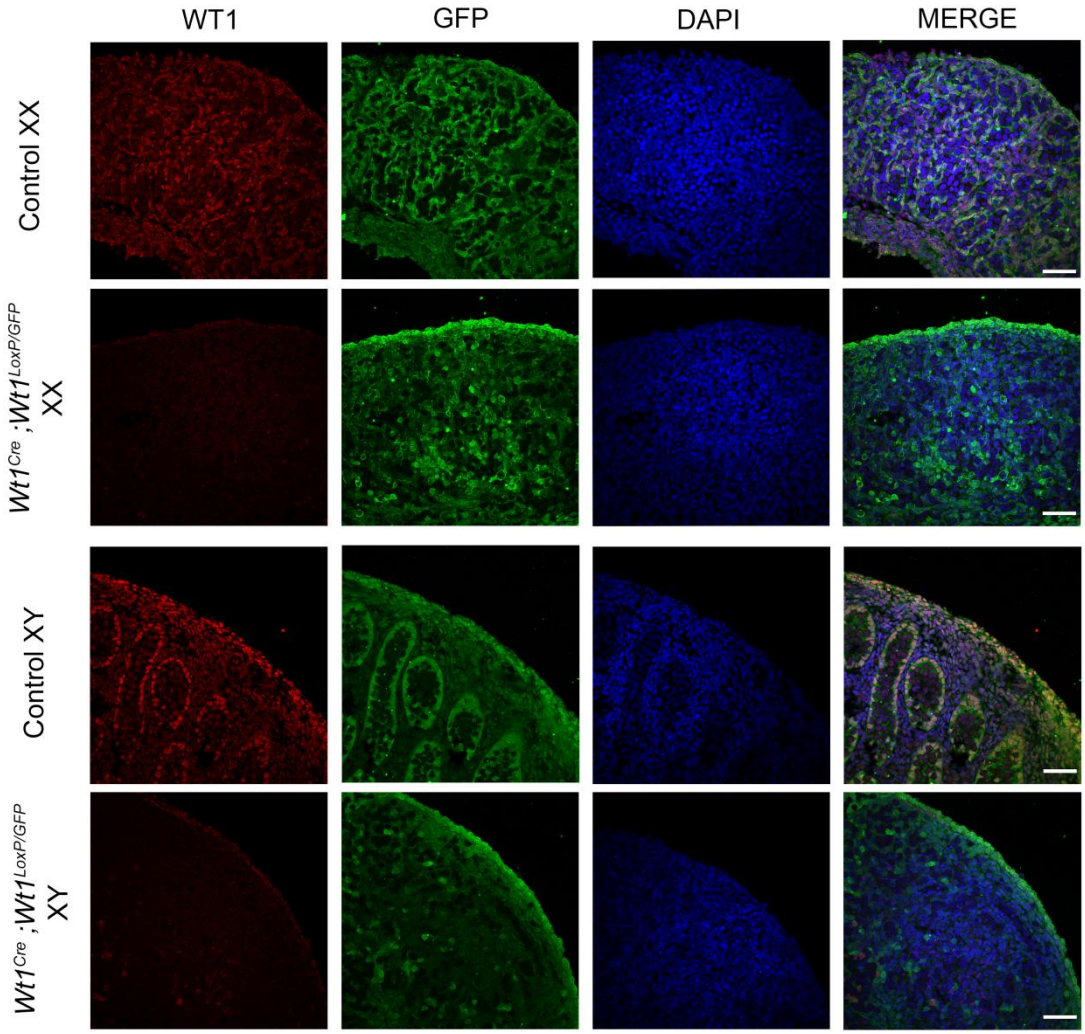


**Figure 35. Immunofluorescence analysis of WT1 and GFP in gonad sections of control and $Wt1^{Cre};Wt1^{Loxp/GFP}$ mice**. Immunofluorescent staining for WT1 (red), GFP(green) and nuclear DAPI stain (blue) using sections from E14.5 control and $Wt1^{Cre};Wt1^{Loxp/GFP}$, XX and XY littermates showed reduced WT1 protein levels in mutant gonads. Scale bar, 50µm. Three embyos per condition were used for the analysis.

### 8.10.2 Supportive lineage differentiation is impaired in *Wt1$^{Cre}$;Wt1$^{Loxp/GFP}$* gonads.

Sexual differentiation in the gonads starts with the differentiation of gonad progenitors into the supportive lineage cells of XY and XX embryos (Sertoli and Granulosa cells, respectively). To corroborate the absence of somatic cells suggested by WT1 and GFP staining in *Wt1$^{Cre}$;Wt1$^{Loxp/GFP}$* embryos(Fig. 35), we performed a staining, in gonads of these embryos, against two well-described markers of supporting cells from either XY or XX gonads, SOX9 (Sertoli cells) and FOXL2 (Granulosa cells)[86,121]. We were not able to detect the expression of none of the mentioned proteins in *Wt1$^{Cre}$;Wt1$^{Loxp/GFP}$* gonads(Fig. 36), suggesting a defective differentiation of both Sertoli and Granulosa cells.

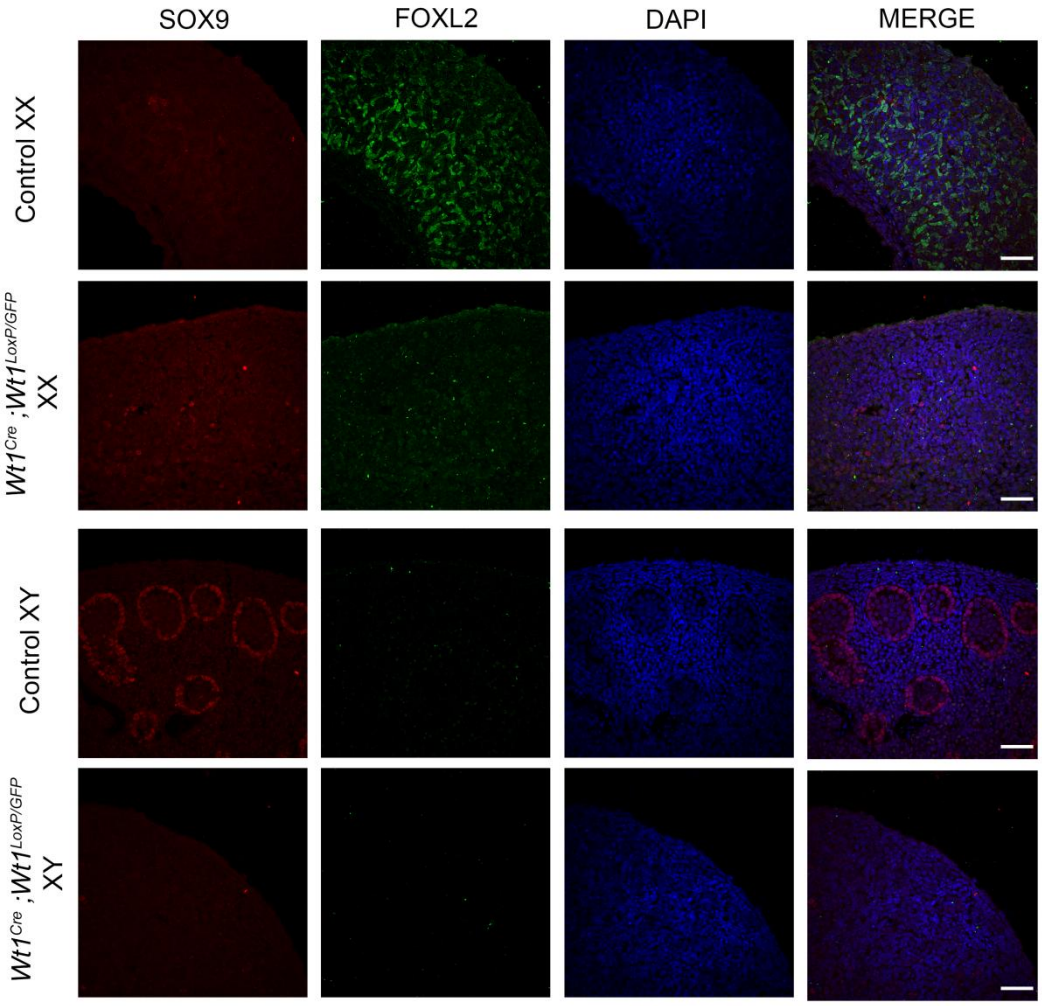


**Figure 36. Sertoli and Granulosa cells are not present in *Wt1$^{Cre}$;Wt1$^{Loxp/GFP}$* gonads**. Immunofluorescent staining for SOX9 (red), FOXL2 (green) and nuclear DAPI stain (blue) using sections from E14.5 control and *Wt1$^{Cre}$;Wt1$^{Loxp/GFP}$*, XX and XY littermates indicated no supportive cells were present in *Wt1$^{Cre}$;Wt1$^{Loxp/GFP}$* gonads. Three embryos per condition were used for the analysis.

The aberrant embryonic phenotype in *Wt1*$^{Cre}$;*Wt1*$^{Loxp/GFP}$ embryos lead us to investigate whether the phenotype correlated with genetic changes in the specific programs. For this, we isolated gonads at E12.5 and analysed the expression of genes implicated in gonadal differentiation both in male and female control and *Wt1*$^{Cre}$;*Wt1*$^{Loxp/GFP}$ embryos.

*Wt1* has been previously described to participate both in Sertoli and Granulosa cells differentiation[99]. Therefore, we decided to analyse a set of genes that are upregulated in Sertoli or pre-Granulosa cells (Fig. 37A,B). *Wt1*$^{Cre}$;*Wt1*$^{Loxp/GFP}$ XY gonads showed reduced expression of *Sox9*, *Fgf9* and *Sry* classical male genes (Fig. 37A). In XX *Wt1*$^{Cre}$;*Wt1*$^{Loxp/GFP}$ gonads, the expression of *Wnt4, Rspo1 Foxl2*, and *Fst* classical Granulosa cell signature genes were downregulated (Fig. 37B). Additionally, we also analysed the expression of *Runx1*, a recently described pro-granulosa gene[341].

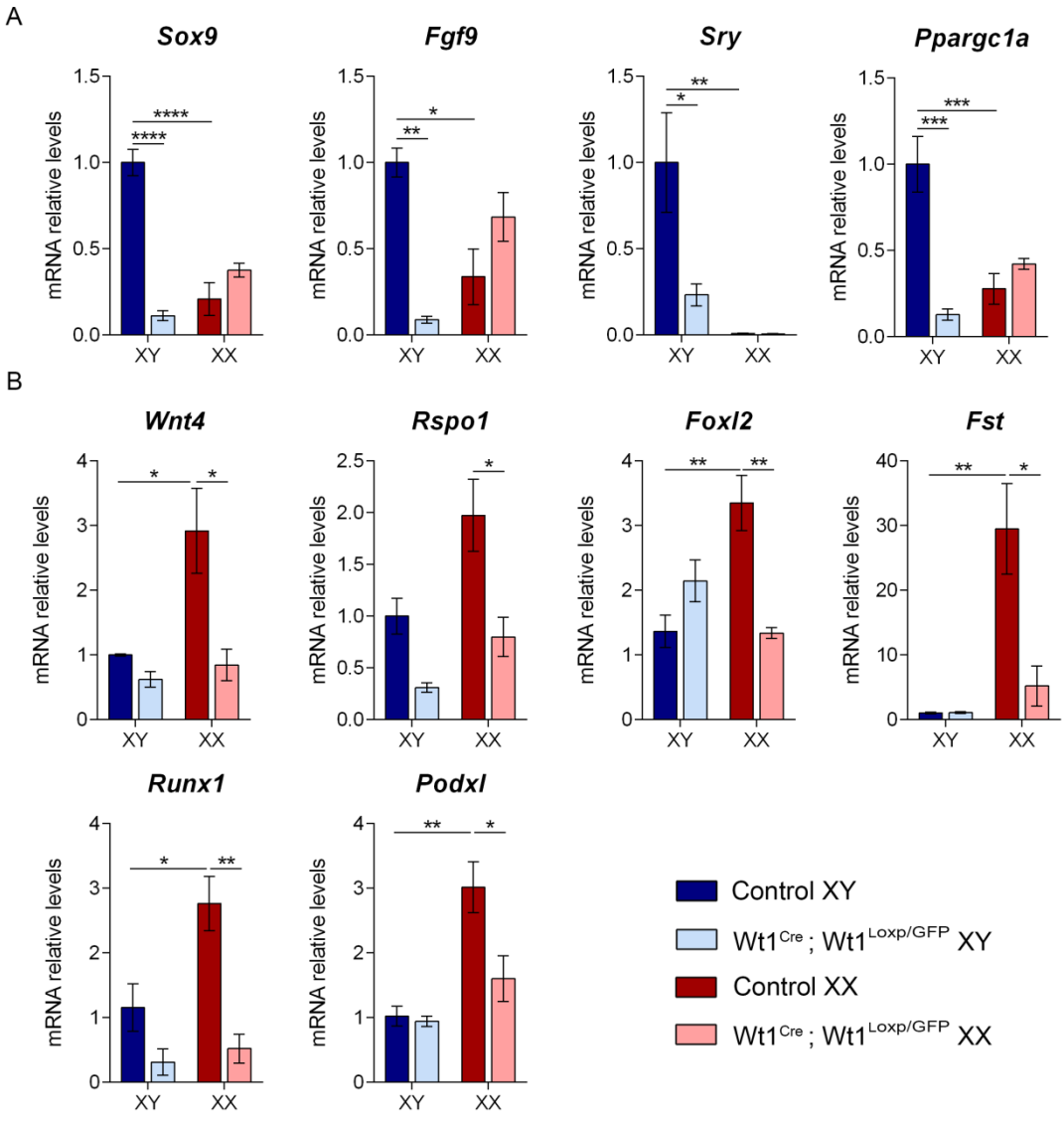

**Figure 37. Supportive lineage embryonic differentiation is impaired in both XY and XX *Wt1$^{Cre}$;Wt1$^{Loxp/GFP}$* mice.** qRT-PCR of the indicicated genes show that genes implicated in Sertoli (A) and Granulose (B) development are downregulated in XX and XY *Wt1$^{Cre}$;Wt1$^{Loxp/GFP}$* embryos, respectively. Values represent mean ± s.e.m. *P<0.05, ** P<0.01, *** P<0.001, **** P<0.0001, two-way ANOVA followed by Tukey's posthoc test. Three embryos per condition were used for the analysis.

In this study, we have analysed several genes previouslly identified as key players in gonad development but, in addition, we have also included new genes like *Ppargc1a* and *Podxl* that display a dimporphic pattern of expression with an unknown role during development. qRT-PCR analysis validated the dimorphic pattern of expression of both genes (*Ppargc1a* is upregulated in XY and *Podxl* in XX gonads)[78,342]. Moreover, we found a downregulation of both genes in XY and XX gonads respectively (Fig. 37A,B).

### 8.10.3 *Wt1$^{Cre}$;Wt1$^{Loxp/GFP}$* gonads show aberrant steroidogenic and primordial germ cell development.

*Wt1* has been described to be implicated in supportive versus steroidogenic fate decision[99,103,343]. Indeed, in absence of WT1, steroidogenic fate is promoted and *Wt1KO* supportive cells can reprogram to steroidogenic cells[99,103]. As the steroidogenic program is engaged after suportive program, we decided to analyse steroidogenic gene expression at E14.5. We found that in XY *Wt1$^{Cre}$;Wt1$^{Loxp/GFP}$* mice, steroidogenic gene expression (*Hsd3b1*, *Cyp11a1, Star*) was downregulated in absence of WT1. However, we did observe the opposite profile in females (Fig. 38A). WT1 has been proposed to inhibit steroidogenic cell fate by repressing *steroidogenic factor 1* (*Sf1)* expression[99]. Therefore we analysed *Sf1* expression in control and in *Wt1$^{Cre}$;Wt1$^{Loxp/GFP}$* mice. Interestingly we found that *Sf1* epression correlated with sterodiogenic profile in XY mice, but it was not increased in XX in *Wt1$^{Cre}$;Wt1$^{Loxp/GFP}$* mice. Finally, we analysed the expression of *Amh.* AMH is one of the first hormones generated by the testis and it is responsible for Müllerian duct regression in males[134]. We observed a clear downregulation of *Amh* levels in XY *Wt1$^{Cre}$;Wt1$^{Loxp/GFP}$* gonads (Fig. 38A), indicating a mechanism for the phenotype observed in adults.

The other main lineage implicated in gonad development is formed by primordial germ cells (PGCs)[65]. XY PGCs are stuck in mitotic arrest while XX PGCs shift to meiosis[65].To investigate the effect of *Wt1* deletion on PGCs we analysed the expression of some PGCs hallmark genes. *Dppa3*, *Ddx4* and *Nanog* expression was downregulated in XY *Wt1$^{Cre}$;Wt1$^{Loxp/GFP}$* gonads. *Stra8* is the main responsible for meiosis initiation in XX gonads[344]. *Stra8* expression was downregulated in XX *Wt1$^{Cre}$;Wt1$^{Loxp/GFP}$* gonads (Fig. 38B). Interestingly, in XY *Wt1$^{Cre}$;Wt1$^{Loxp/GFP}$*

embryos we observed an upregulation tendency, suggesting meiosis is actively blocked in XY wild type gonads.

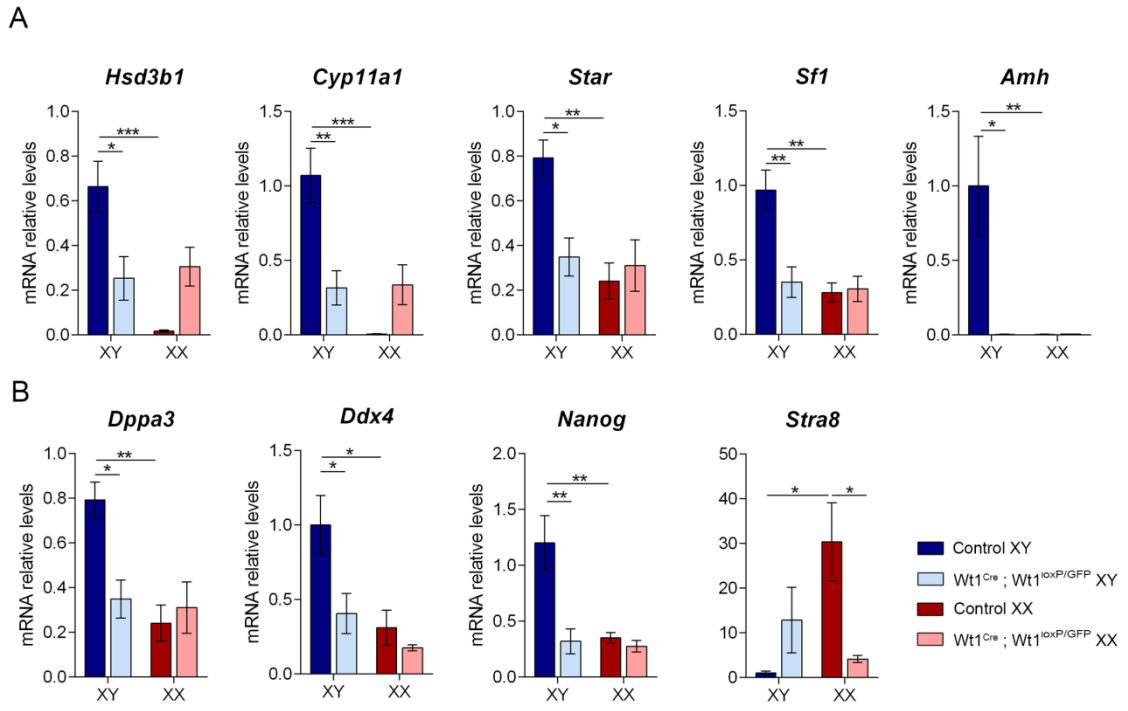


**Figure 38. Gonadal steroidogenic and PGC differentiation is impaired in both XY and XX *Wt1$^{Cre}$;Wt1$^{Loxp/GFP}$* mice.** (A) mRNA levels of H*sd3b1*, *Cyp11a1, Star, Sf1* and *Amh* in control and *Wt1$^{Cre}$;Wt1$^{Loxp/GFP}$* gonads. (B) mRNA levels of *Dppa3, Ddx4, Nanog and Stra8* in control and *Wt1$^{Cre}$;Wt1$^{Loxp/GFP}$* gonads. Values represent mean ± s.e.m. *P<0.05, ** P<0.01, *** P<0.001, two-way ANOVA followed by Tukey's posthoc test. Four replicates per condition were used for the analysis.

In conclusion, our results indicate all main gonad lineages: supportive, steroidogenic and PGCs affected in *Wt1$^{Cre}$;Wt1$^{Loxp/GFP}$* mice.

## 8.11 Deficient deletion of *Wt1* in *Wt1$^{Cre}$;Wt1$^{Loxp/GFP}$* hearts.

*Wt1$^{Cre}$* mouse line has been used previously to study the proepicardium, the epicardium and coronary development[166,221]. *Wt1* expression is crucial for correct heart development and previous *Wt1KO* show severe defects in heart development including smaller ventricles, a thinner epicardium and a much reduced coronary vascular system[190]. We had proved *Wt1$^{Cre}$* was actually expressed in most epicardial cells in the heart (Fig. 27,28) . Therefore we decided to look at more detail *Wt1$^{Cre}$;Wt1$^{Loxp/GFP}$* embryonic hearts.

First we decided to further check if *Wt1$^{Cre}$* is correctly expressed. Using an immunofluorescence staining against GFP in *Wt1$^{Cre}$; R26R$^{mTmG/+}$* mouse heart sections, we confirmed a correct spatial expression of *Wt1$^{Cre}$* (Fig. 39A).

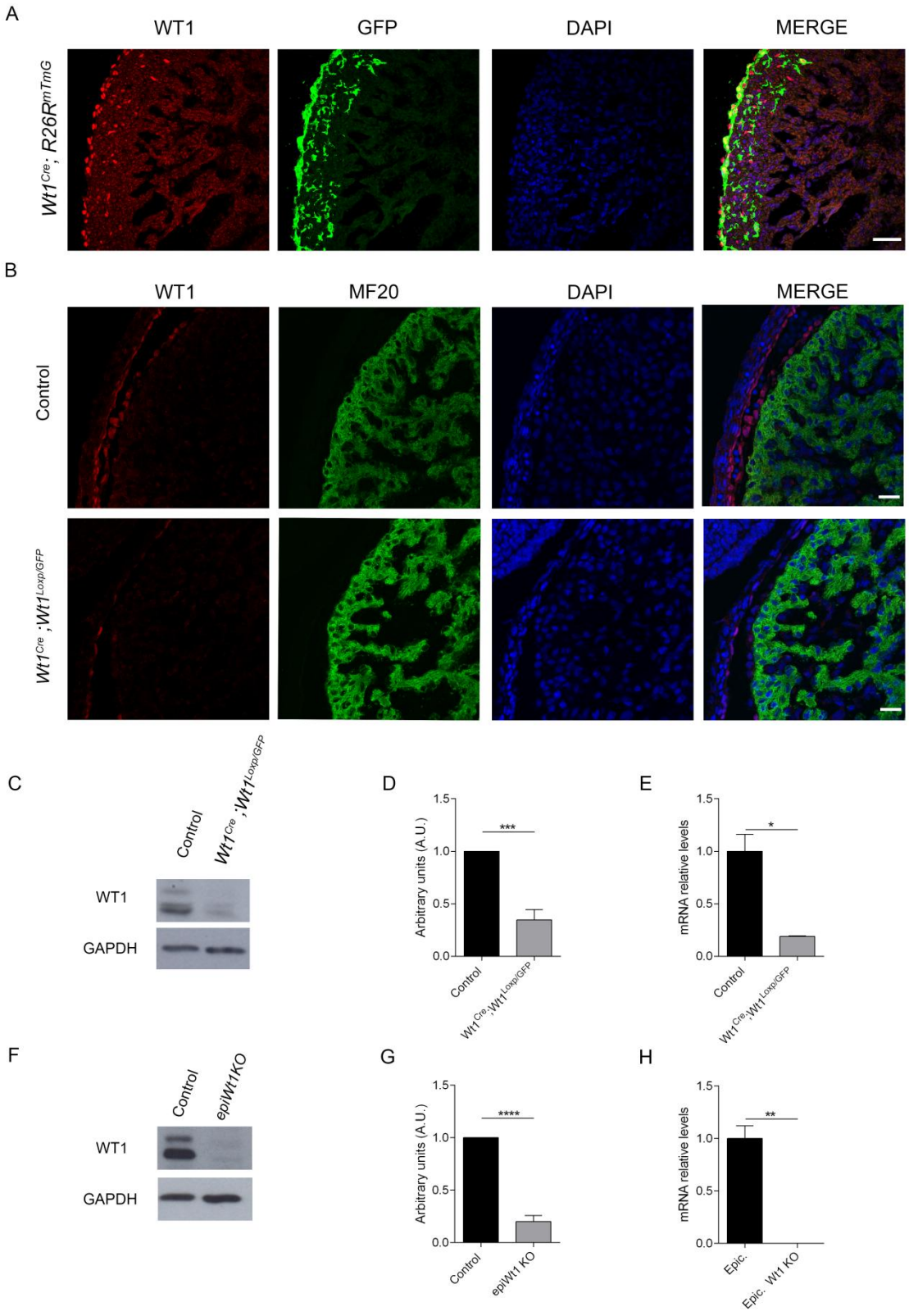


**Figure 39. The epicardium from *Wt1$^{Cre}$;Wt1$^{Loxp/GFP}$* mice show reduced WT1 expression levels**. (A) Immunofluorescent staining for WT1 (red), GFP reporter of the *Wt1$^{Cre}$* lineage (green) and nuclear DAPI stain (blue) using sections from E14.5 *Wt1$^{Cre}$; R26R$^{mTmG/+}$* heart. *Wt1$^{Cre}$* is expressed in most cells expressing WT1. (B) Immunofluorescent staining for WT1 (red), MF20 (green) and nuclear DAPI stain (blue) using sections from E11.5 control and *Wt1$^{Cre}$;Wt1$^{Loxp/GFP}$* littermates indicated WT1 protein is reduced in epicardial cells. (C) Whole hearts

lysates form *control* and *Wt1*$^{Cre}$;*Wt1*$^{Loxp/GFP}$ mice were analysed by western blotting with WT1 antibodies and GAPDH as loading control and then quantified. (D) WB densidometry of WT1 levels in "C". (E) qRT-PCR analysis of *Wt1* expression in *Wt1*GFP$^{++}$ sorted cells of control and *Wt1*$^{Cre}$;*Wt1*$^{Loxp/GFP}$ mice indicated a clear reduction of *Wt1* in mutant hearts. (F) Whole hearts lysates from control and *Gata5*$^{Cre}$; *Wt1*$^{loxP/GFP}$ (*epiWt1KO*) were analysed by western blotting with WT1 antibodies and GAPDH as loading control and then quantified. (G) WB densidometry of WT1 levels in "F". (H) qRT-PCR analysis of *Wt1* expression in control and *Wt1KO* immortalized epicardial cells indicated the downregulation of *Wt1* levels in a conventional *Wt1KO*. Values represent mean±s.e.m. *P<0.05, ** P<0.01, *** P<0.001, **** P<0.0001 two-tailed-t-test. Three replicates or embryos per condition were used for the analysis. Scale bar, 50µm (A), 25µm (B).

To analyse the expression of WT1 in the *Wt1*$^{Cre}$;*Wt1*$^{Loxp/GFP}$ epicardium, we used a WT1 immunofluorescence staining in E11.5 heart sections. We observed a clear downregulation of WT1 levels in the *Wt1*$^{Cre}$;*Wt1*$^{Loxp/GFP}$ epicardium compared to control (Fig. 39B). To quantify WT1 levels, we performed a Western blot analysis using whole heart lysates from control and *Wt1*$^{Cre}$;*Wt1*$^{Loxp/GFP}$ mice at E11.5 (Fig. 39C). WT1 protein levels in *Wt1*$^{Cre}$;*Wt1*$^{Loxp/GFP}$ mice were 60% lower than those expressed by controls (Fig. 39D). To better quantify *Wt1* levels in epicardial cells we FACS sorted *Wt1-GFP*$^{++}$ cells from *Wt1*$^{Cre}$;*Wt1*$^{Loxp/GFP}$ and control E11.5 hearts and analysed *Wt1* mRNA levels. *Wt1* mRNA levels in *Wt1*$^{Cre}$;*Wt1*$^{Loxp/GFP}$ sorted epicardial cells were 80% lower than control cells (Fig. 39E). Differents studies have investigated the effects of *Wt1* downregulation in the epicardium[190,194]. Therefore, to obtain a better understanding of our mouse model we decided to compare this downregulation with other *Wt1KO* models. WT1 levels in whole heart lysates from *Gata5*$^{Cre}$ *Wt1KO* were 80% lower than in control (Fig. 39F,G). Additionally, *Wt1* mRNA levels reduction in immortalized *Wt1KO* epicardial cells obtained from a conventional *Wt1KO*, compared to control cells was also higher than that observed in *Wt1*$^{Cre}$;*Wt1*$^{Loxp/GFP}$ epicardial cells (Fig. 39H).

These results suggest that *Wt1* downregulation degree in *Wt1*$^{Cre}$;*Wt1*$^{Loxp/GFP}$ is not enough to cause an embryonic phennotype similar to that observed in another *Wt1KO* model like the *Gata5*$^{Cre}$ ; *Wt1*$^{Loxp/GFP}$ (*epiWt1KO*).

Previous *Wt1* constitutive and conditional KOs show a thin myocardium phenotype[76,190]. Therefore, we decided to analyse myocardial thickness in control and *Wt1*$^{Cre}$;*Wt1*$^{Loxp/GFP}$ embryos. For this purpose we performed a double staining against Endomucin-1 and sarcomeric myosin (MF20). Ventricular myocardium can be divided in two well delimited zones: the compact and the trabecular myocardium. Trabecular myocardium constitutes the inside luminal heart wall. The formation of the trabecular myocardium allows heart growth without need of coronary vasculature. On the other side, compact myocardium constitutes the exterior walls of heart ventricles. The increase of compact myocardium thickness requires the formation of vasculature to avoid the consequent hypoxia[345]. As I have previously described,

myocardial vasculature formation highly depends on a correct epicardium development. Endomucin-1 is a transmembrane sialomucin expressed in capillary and venous but not arterial endothelial cells. Endomucin-1 is a marker of endocardium, the layer surrounding the interior of myocardium, allowing for visualization of both endocardium and trabecular myocardium state. *Wt1*$^{Cre}$;*Wt1*$^{Loxp/GFP}$ showed no apparent phenotype: endocardium was well formed, and normal trabeculation was observed (Fig. 40A). Quantification of compact myocardium thickness showed no significance difference between control and *Wt1*$^{Cre}$;*Wt1*$^{Loxp/GFP}$ (Fig. 40B).

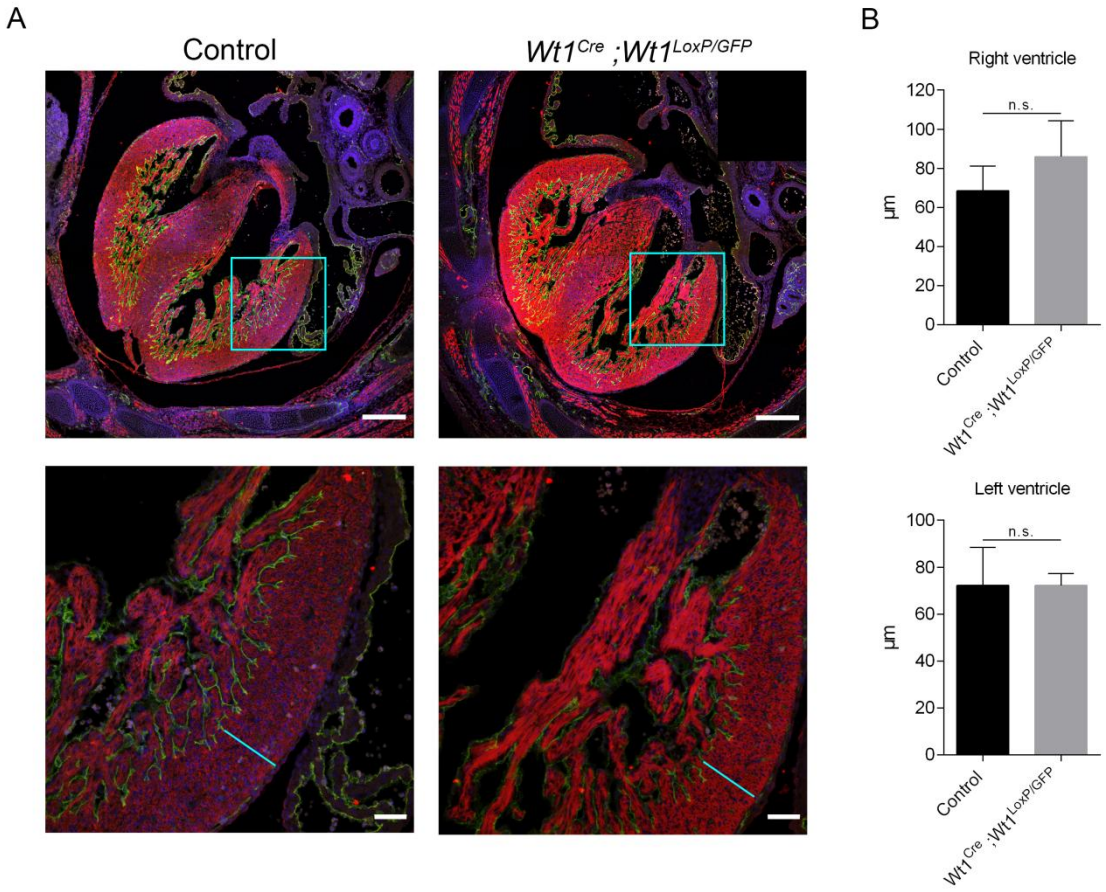


**Figure 40. *Wt1*$^{Cre}$;*Wt1*$^{Loxp/GFP}$ embryonic hearts show a normal heart morphology**. (A) Immunofluorescent staining for MF20 (red), Endomucin-1 (green) and nuclear DAPI stain (blue) using sections from E14.5 control and *Wt1*$^{Cre}$;*Wt1*$^{Loxp/GFP}$ littermates. (B) Quantification of compact myocardium thickness. Values represent mean ± s.e.m. n.s. (no significant), P>0.05, two-tailed t-test. Three embryos per condition were used for the analysis. Scale bar, 250µm (top panel), 50µm (below panel).

## 8.12 Defects in heart development are responsible for *Wt1*$^{Cre}$;*Wt1*$^{Loxp/GFP}$ partial lethality.

Expected mendelian percentages of *Wt1*$^{Cre}$;*Wt1*$^{Loxp/GFP}$ observed at E14.5, opposed to the sub-Mendelian values obtained at adult stages, indicated some *Wt1*$^{Cre}$;*Wt1*$^{Loxp/GFP}$ mice could be dying between E14.5 and birth (Fig. 30). Therefore, we decided to analyse a stage between

both days: at E18.5, percentages of the four different genotypes were similar to those expected from a Mendelian distribution. However, one of the embryos presented a pronounced aberrant heart development (Fig. 41). This result suggests that a fraction of *Wt1*$^{Cre}$;*Wt1*$^{Loxp/GFP}$, similarly to other *Wt1KO* models[190], dies due to defects in heart development.

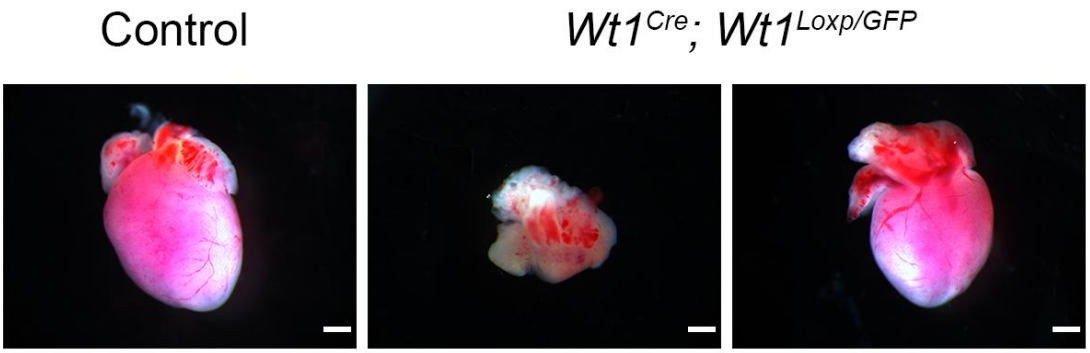


**Figure 41. A *Wt1*$^{Cre}$;*Wt1*$^{Loxp/GFP}$ heart showed an aberrant heart morphology**. Bright-field images of control and two different *Wt1*$^{Cre}$;*Wt1*$^{Loxp/GFP}$ littermates. One of the hearts from *Wt1*$^{Cre}$;*Wt1*$^{Loxp/GFP}$ embryos showed an aberreant morphology. Scale bar, 500µm.

## 8.13 *Wt1*$^{Cre}$;*Wt1*$^{Loxp/GFP}$ kidney development is not impaired.

*Wt1* plays a role in the development of a large number of tissues[4]. Conventional *Wt1KO* shows defects in kidneys, gonads, the heart or the spleen[76]. Additionally, different *Wt1KOs* have demonstrated that WT1 participates in the development or adult homeostasis of organs like the pancreas, the liver, the lungs or fat[309–312]. Although lineage tracing results in this work show that *Wt1*$^{Cre}$ expression does not totally recapitulate WT1 embryonic expression, we wondered whether *Wt1*$^{Cre}$;*Wt1*$^{Loxp/GFP}$ could be suffering from defects in any of the other organs where WT1 plays a role.

To this, we analysed *Wt1* mRNA levels of three organs where WT1 has been described to participate: kidneys, spleen and lungs[76,309]. The results obtained agreed with those showed before (Fig. 27,28): in kidneys, where *Wt1*$^{Cre}$ could activate neither RFP nor Tomato expression, no differences were observed between control and *Wt1*$^{Cre}$;*Wt1*$^{Loxp/GFP}$, *Wt1* mRNA levels. On the other hand, *Wt1* expression levels in *Wt1*$^{Cre}$;*Wt1*$^{Loxp/GFP}$ lungs and spleen were reduced compared to control, in accordance with the % of RFP positive cells observed before (Fig. 42A). As *Wt1* has been widely studied in kidney development and *Wt1* deletion in the kidney has been traditionally considered one of the principal causes of *Wt1KOs* lethality[76,262], we performed WT1 staining in E14.5 *Wt1*$^{Cre}$;*Wt1*$^{Loxp/GFP}$ to analyse WT1 protein expression. As

expected, we observed no differences between control and *Wt1*$^{Cre}$;*Wt1*$^{Loxp/GFP}$ embryos (Fig. 42B).

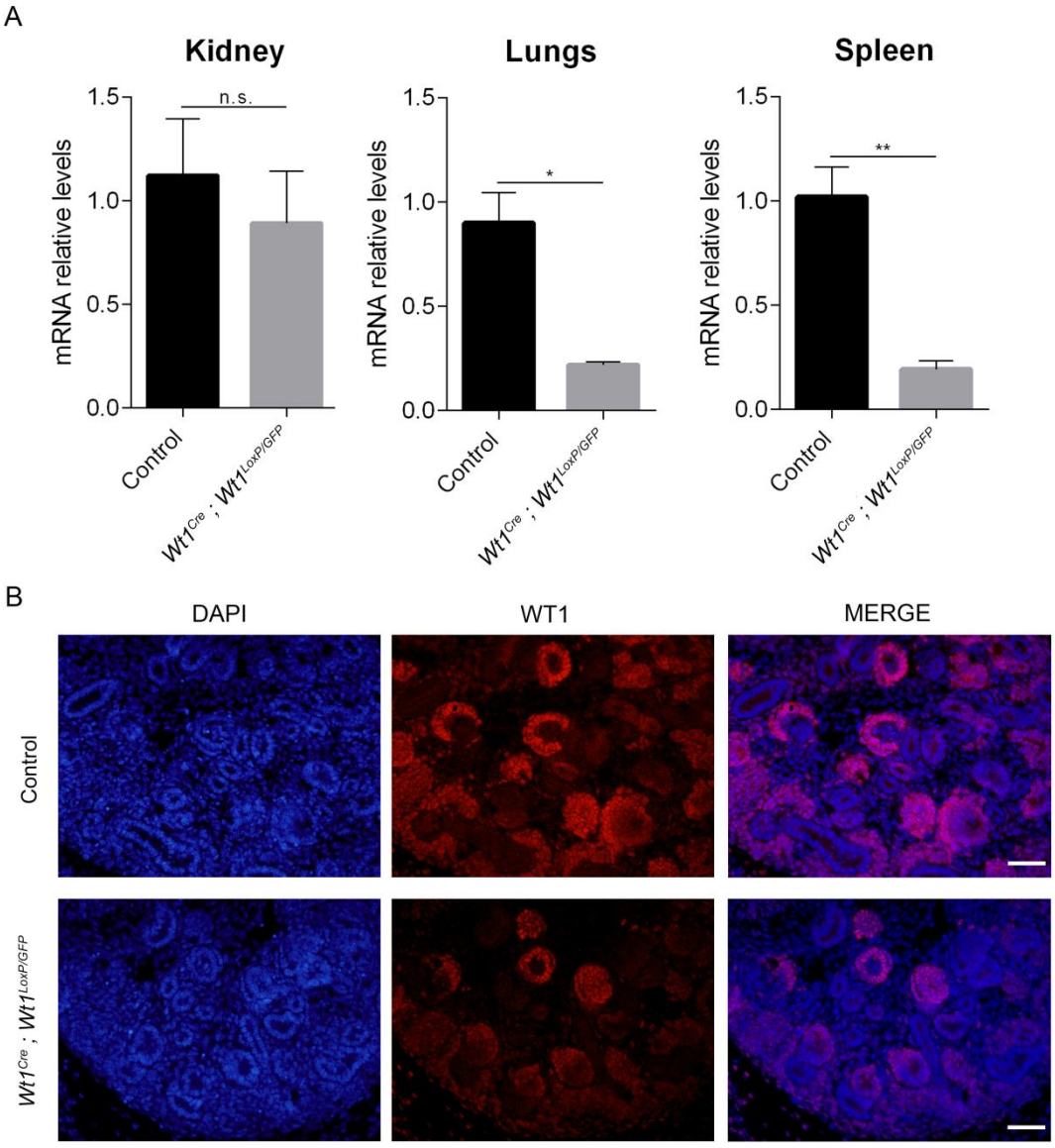


**Figure 42. *Wt1* expression is not affected in the kidneys from *Wt1*$^{Cre}$; *Wt1*$^{Loxp/GFP}$ mice.** (A) qRT-PCR analysis of *Wt1* expression in control and *Wt1*$^{Cre}$; *Wt1*$^{Loxp/GFP}$ kidneys, spleen and lungs. mRNA Wt1 levels are reduced in lungs and spleen but not in kidneys. Values represent mean ± s.e.m. * P<0.05, ** P<0.01 two-tailed t-test. (B) Immunofluorescent staining for WT1 (red) and nuclear DAPI stain (blue) using sections from E14.5 control and *Wt1*$^{Cre}$; *Wt1*$^{Loxp/GFP}$ littermates. WT1 protein levels were similar in control and *Wt1*$^{Cre}$; *Wt1*$^{Loxp/GFP}$ kidneys. Scale bar, 100µm. Three embryos per condition were used for the analysis.

The *Wt1*$^{Cre}$ mouse model has been previously used to study the development of some of the organs where *Wt1* is expressed (Visceral white adipose tissue[313], pancreas [310] or lungs[309]). Besides, as I mentioned during the introduction, *WT1KOs* show defects in those and other organs, including the kidneys, the adrenal gland or the spleen[76,262].

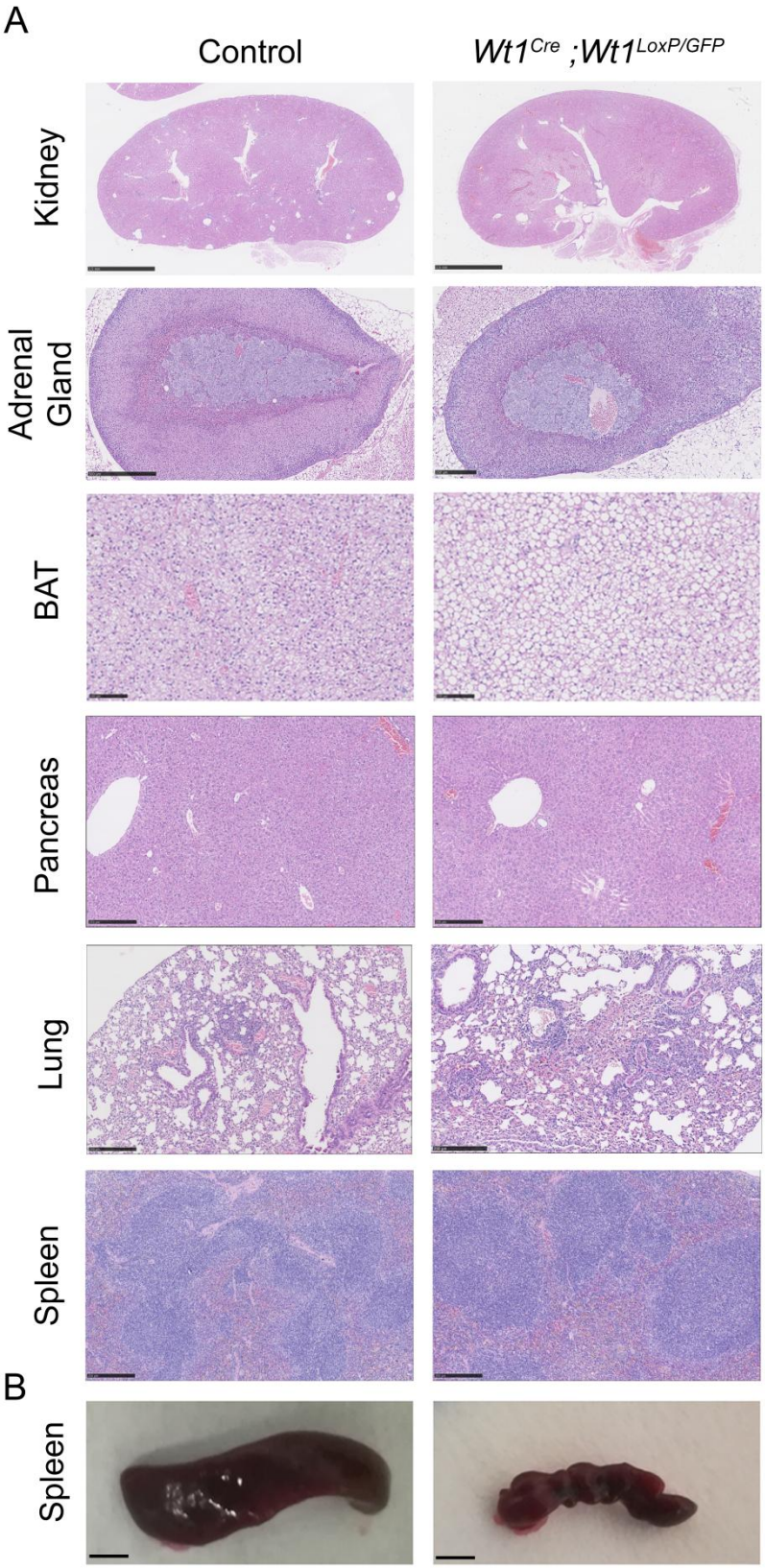


**Figure 43. Histology of control and *Wt1$^{Cre}$;Wt1$^{Loxp/GFP}$* adult organs.** (A) H&E images of the indicated organs in control and *Wt1$^{Cre}$;Wt1$^{Loxp/GFP}$* mice. No major changes were observed in the histology of the kidney, the adrenal gland, the spleen, the pancreas and the lungs. Brown adipose tissue (BAT) cells showed increased cell size (B) Pictures of spleens from control and *Wt1$^{Cre}$;Wt1$^{Loxp/GFP}$* mice. *Wt1$^{Cre}$;Wt1$^{Loxp/GFP}$* were smaller than control spleens

and presented a polylobulated apperance. Scale bar, 2.5mm (kidney). Scale bar, 250µm, the rest of images. Three animals per genotype were used for the analysis.

Therefore, to assess posible changes in those tissues in *Wt1*$^{Cre}$*;Wt1*$^{Loxp/GFP}$ mice, an histological study was performed on adult *Wt1*$^{Cre}$*;Wt1*$^{Loxp/GFP}$ mice. Spleen from *Wt1*$^{Cre}$*;Wt1*$^{Loxp/GFP}$ mice showed a polylobulated appearance. However, the architecture of the spleen was unaffected and *Wt1*$^{Cre}$*;Wt1*$^{Loxp/GFP}$ spleens showed normal white and red pulp tissue (Fig. 43A,B). In the brown adipose tissue, *Wt1*$^{Cre}$*;Wt1*$^{Loxp/GFP}$ mice presented an increase in size of the brown adipocytes and/or their lipid cytoplasmic droplets. Pancreas from *Wt1*$^{Cre}$*;Wt1*$^{Loxp/GFP}$ demonstrated an slight pancreatomegaly. No relevant changes were appreciated in the other organs analysed by a certified pathologist: eyes, brain, bone marrow, urinary bladder, lungs, kidneys, intestines or adult hearts.

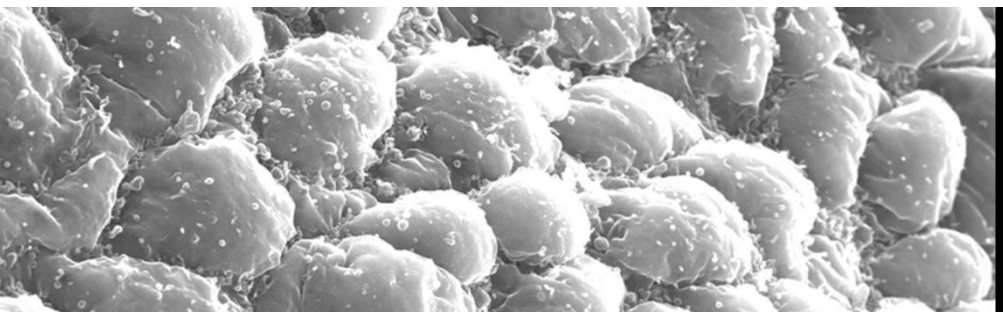

# DISCUSSION

## 9.1 WT1 regulates epicardial maturation through *Bmp4* regulation.

The epicardium plays a crucial role in heart development[145]. Additionally, different works support an important function of the epicardium in the heart healing following myocardial infarction (MI)[280,281,287,293]. However, the pathways implicated in the epicardium development are still a matter of investigation. In this thesis we have tried to elucidate the mechanisms of epicardium development, specifically how the BMP4 pathway regulates different aspects of epicardium biology like cell morphology or proliferation (Fig. 44).

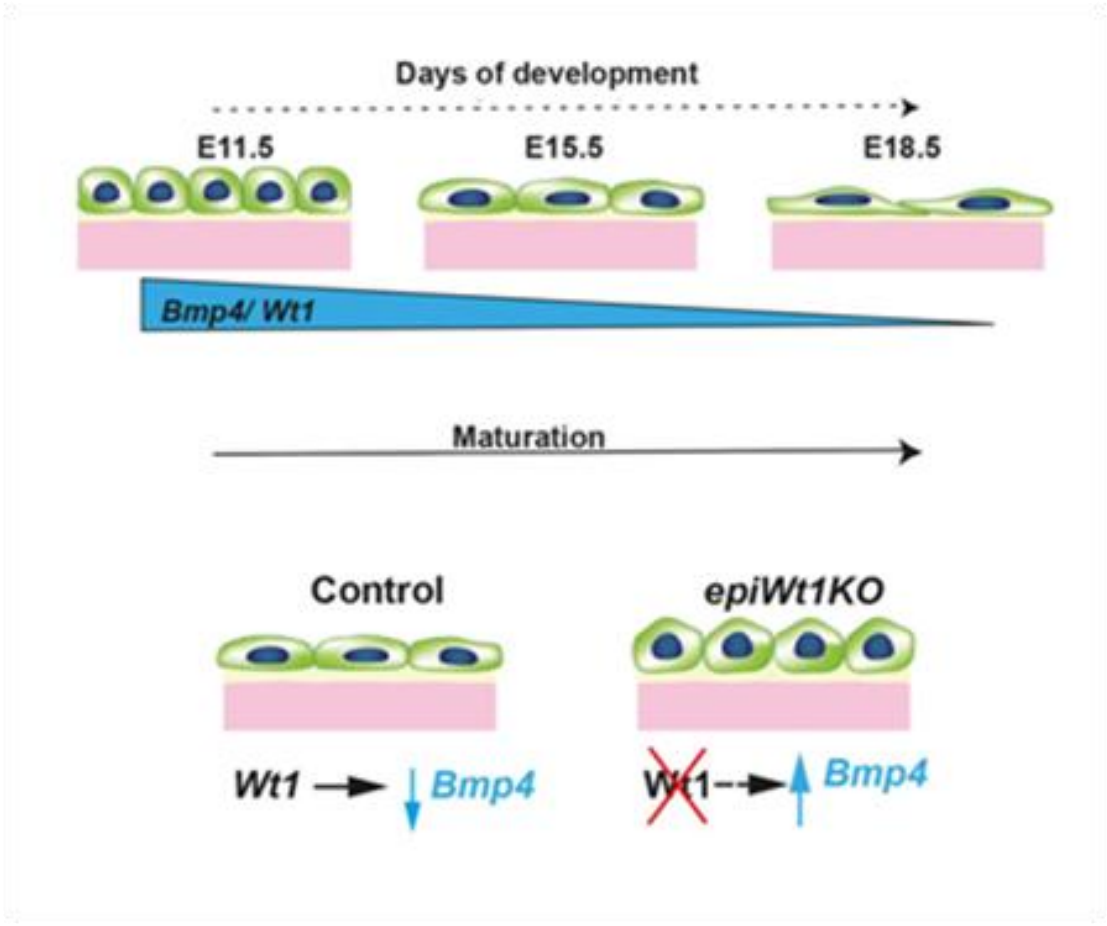


**Figure 44. Model of the cuboidal-to-squamous transition taking place during epicardial maturation**. During embryonic heart development, epicardial cells undergo a change from a cuboidal to a flattened phenotype to form a mature squamous epicardium. The epicardium maturation process inversely correlates with *Bmp4* expression levels. *Bmp4* expression is repressed by WT1 and can therefore orchestrate the described transition, which is affected in *epiWt1KO* mice. Modified from Velecela et al., 2019.

It is known that *Bmp4* is expressed in the PE and that BMP signaling cooperates with other signaling pathways in the decision that drives some mesodermal cells to become proepicardial cells[162,164,165]. Indeed, in zebrafish embryos, BMP signaling is implicated in the mechanism driving some dorsal pericardial cells extrusion to form the proepicardium[346]. However, it has not been investigated the function of BMP4 once the epicardium is formed. Additionally, all

results relating to *Bmp4* in PE have been obtained in chick embryos or zebrafish, while BMP4 role in mammal epicardium has not yet been studied[162,164,165,179].

*Bmp4* has multiple roles during development and it is crucial for the differentiation of several cell types[267]. We have demonstrated that *Bmp4* expression is downregulated during epicardium development (Fig. 15A). Moreover, our data indicate that *Bmp4* downregulation is a crucial step in the epicardium maturation: high levels of *Bmp4* correlate with the cell morphology typical from early stages of embryonic development: *epiWt1KO* embryos present *Bmp4* upregulated levels and a cuboidal morphology (Fig. 15-17) and rBMP4 supplemented cells *in vitro* show a more cuboidal morphology than control cells (Fig. 18). Accordingly, inhibition of the BMP4 pathway rescued epicardial *Wt1KO* cell morphology, both *in vivo* and *ex vivo,* to a mature, squamous phenotype (Fig. 20,21).

Early-stage epicardial cells also show higher rates of proliferation[209]. Following this logic, rBMP4 induced proliferation, whereas inhibition of BMP signaling reduced it (Fig. 22). Furthermore, when we inhibited the BMP4 pathway, we observed how genes whose expression pattern correlate with *Bmp4* during the epicardium development follow the same changes they undergo during development, as stated by our group transcriptomic data (Fig. 10, 23)[230]. During development, the heart grows, increasing its volume and, therefore, its surface. On the other hand, it has been described that epicardial cell proliferation rates diminish during this process[209]. These two seemingly contradictory facts can be understood by the flattening of epicardial cells during development, as described in this thesis (Fig. 16).

Apart from WT1 and BMP4, there are other transcription factors and molecules implicated in epicardium development[145]. The question then is: what happens when we inhibit or modulate those other genes? Do we observe a similar phenotype? Most of the studies related to the epicardium have focused on the formation of EPDCs[145]. However, similar phenotypes can be observed in other models where epicardium has been studied. In a *Wt1$^{CreERT2}$ ; Lats1/2 KO* (LATS 1 and 2 are mediators of the HIPPO pathway), the heart presents a less compacted myocardium due to a defective coronary remodeling[207]. The authors described how *Lats1/2* epicardial KO cells undergo a defective EMT fibroblast differentiation and remain halted on an intermediate state between epicardial and fibroblast cells. It is interesting to notice that, although they did not mention it, epicardial cells from their E14.5 KO show a cell shape resembling our cuboidal *epiWt1KO* phenotype (Fig. 45)[207].

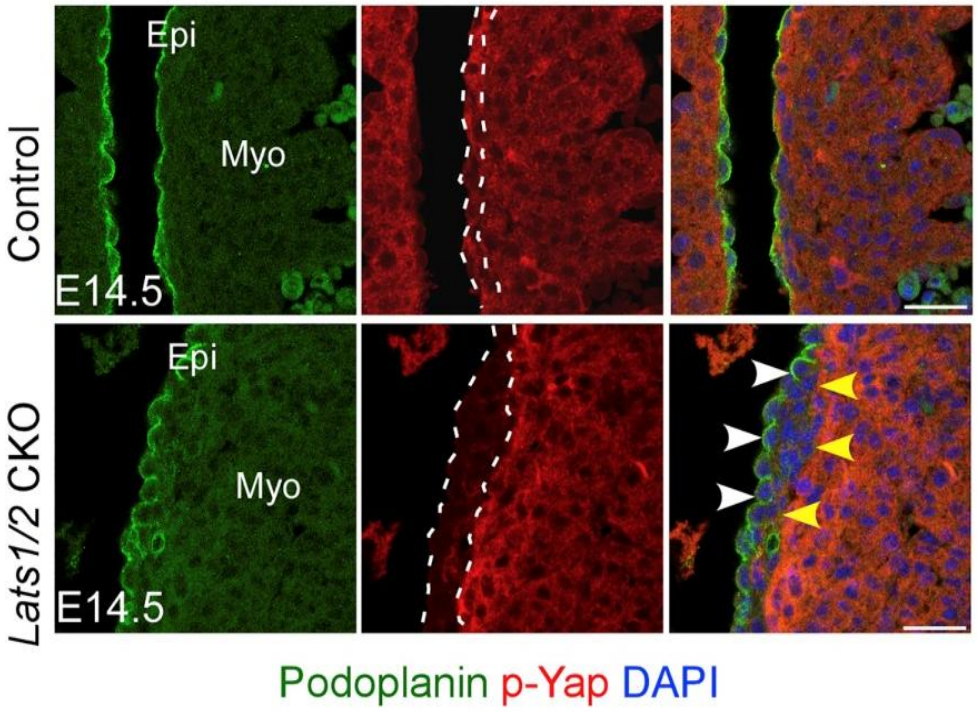


**Figure 45. *Lats1/2* deficiency in epicardial cells results in a cuboidal phenotype**. Scale bar: 50µm. Modified from Xiao et al., 2018.

Another example is *Crim1*. CRIM1 is a transmembrane protein expressed in epicardial cells and EPDC. *Crim1 KO* mice show a reduced ventricular size and epicardial defects, including an abnormal epicardial cell morphology at E13.5 (Fig. 46). In the authors' words: "*findings supported by scanning electron microscopic analysis of* $Crim1^{\Delta flox/\Delta flox}$ *hearts, which revealed a loss of the regular, cobblestone appearance of the epicardium*"[202].

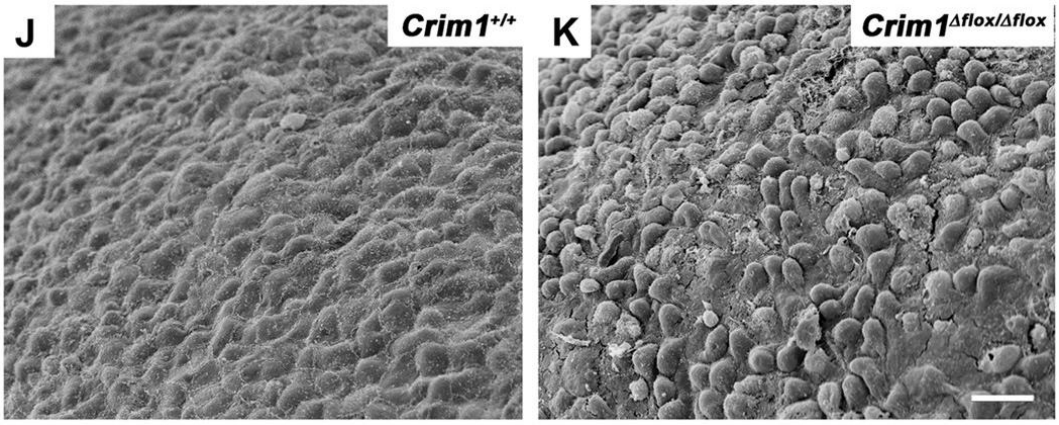


**Figure 46. *Crim1KO* show an epicardial cuboidal phenotype**. Scanning electron micrographs of the ventricular surface of 13.5 dpc $Crim1^{+/+}$ (**J**) and $Crim1^{\Delta flox/\Delta flox}$ (**K**) hearts. Scale bar: 20 µm. Modified from Iyer et al., 2016.

It is interesting to mention that CRIM1 is a homolog of CHORDIN, a BMP-regulating protein. Indeed, CRIM1 has 6 chordin-like cysteine-rich repeats that can directly bind to BMP4[347,348]. These results, in accordance with our data, suggest that an alteration of a member of the BMP

pathway in the epicardium results in a defective epicardial development, which can be noticed by its abnormal morphology.

In conclusion, the cuboidal morphology observed in these two KOs suggests that, in both cases, the observed phenotype might be caused by the arrest of epicardial cells in a more primitive stage, closer to proepicardial cells.

The epicardial cell shape changes we have characterized during development are accompanied by changes in nuclear cell morphology (Fig. 16,17). Lamin-B1 (B1) is a lamin protein belonging to type V intermediate filament proteins[349–351]. Although the way lamins work is not fully understood, it is well-known they influence nuclear shape[352]. *Lb1* null embryos show a reduced compact myocardium and discontinuous smooth muscle surrounding coronary vessels. Moreover, epicardial *Lb1* null cells show reduced migration and rounder cell nuclei. Interestingly, one of the genes downregulated in *Lb1* null embryos is *Noggin,* an inhibitor of BMP signaling[353].

Despite these data, one might still think that epicardial cell morphology defects are a secondary effect of the impaired epicardial development caused by a BMP4 pathway defect. However, two pieces of evidence oppose this possibility: the first of them is our *in vitro* data; the other is a wide bibliography linking *Bmp4* to changes in cell morphology. The change of cellular morphology is a common process observed in several different model animals, tissues and, importantly, other mesotheliums. In many of these cases, BMP plays an important role. In Drosophila dorsal closure, for example, BMP signaling causes a reduction of apical surface area in the amnioserosa simple epithelium[354]. In the chick embryo, epithelial invagination of olfactory, lens, otic and hypophyseal placodes, is regulated by BMP activity[330]. The follicles within the ovary need to transform their cell shape in order to assure the correct development of the follicle[331]. Ovarian mesothelial flattened cells display an increased cell surface, but also, this increase in cell size is accompanied by a reduction of cell proliferation and migration[331]. Interestingly, all of these mentioned changes are also controlled in the follicles by BMP signaling[355].

The next question is how the BMP4 pathway regulates cell shape. Our data suggest BMP4 directly regulates cell shape by modulating the expression of structural genes like *Podxl* or *Krt8* (Fig. 23). However, the genes or combination of genes implicated in this regulation remains to be determined. Interestingly, in zebrafish embryos, the morphological changes undergone by the subset of cells giving rise to PE, are controlled by BMP signaling[346]. The authors of that work demonstrated that the mechanism behind those changes is BMP regulation of

actomyosin dynamics[346]. To further clarify the mechanism orchestrating the changes described in this work, the study of a BMP4 gain of function mouse may be useful: preventing *Bmp4* physiological downregulation during epicardial development and analyzing the genetical changes observed could allow identifying genes directly implicated in cell shape changes or epicardial proliferation.

Using WB and luciferase assay data (Fig. 24), we have suggested *Wt1* expression might be regulated by the BMP4 pathway. This suggests a feedback loop in which BMP4 induces *Wt1* expression while WT1 represses *Bmp4* expression. As I have mentioned before, *Wt1* appears as a pSMAD1/5/8 target in a recent ChIP-seq experiment performed in hair follicle stem cells[338]. Moreover, in the data presented in this thesis, there is an apparent contradiction that might be solved by the proposed feedback loop. If WT1 inhibits *Bmp4* expression, as *epiWt1KO* data suggests, then, how is it possible that *Bmp4* expression directly correlates with *Wt1* downregulation during development? Should not *Bmp4* follow the opposite pattern? As I have explained during the introduction, *Bmp4* expression is necessary for PE induction, indicating its expression may precede *Wt1* expression. I propose that BMP4 induces *Wt1* expression. Then, as it is necessary that BMP signaling is abrogated to continue with the epicardium development, WT1 inhibits *Bmp4*. As *Bmp4* is downregulated, so it is *Wt1*. Of course, for this hypothesis to be true, there is a need for a third actor, one that keeps *Bmp4* expression inhibited in later stages of development, or maybe the inhibition of the one, that, in the beginning, firstly induced *Bmp4* expression.

We have demonstrated that similarly to the epicardium, the lung mesothelium also undergoes a flattening process that correlates with *Bmp4* downregulation (Fig. 25). The question is whether this is happening in other mesotheliums. In a single-cell sequencing experiment performed on the embryonic pancreas, the mesothelial pancreatic population was defined[356]. The authors described that, similar to our findings, early-stage pancreatic mesothelium is characterized by high expression levels of *Bmp4*, whereas the mature stage displays high expression levels of *Nbl1*[356]. Moreover, deletion of *Wt1* in the adult pancreas mesothelium using a $Wt1^{CreERT2}$ resulted in the reduction of intercellular junctions leading to changes in cellular shape[357].

Following MI, the epicardium is reactivated and it seems to play an important role in the healing of the scar[145]. As the epicardium after MI recovers some of its embryonic characteristics, it would be interesting to know if epicardial cells post-MI also recover the cuboidal cell morphology of early embryonic stages. And also, just as *Wt1* is reexpressed in

epicardial cells post-MI, it would be informative to investigate whether *Bmp4* is also reexpressed. So far, it has been described that pSMAD1/5/8 expression is observed in the epicardium following MI[287]. Interestingly, in a study performed on cryoinjured hearts on zebrafish, it was demonstrated that in the region bordering the injured area, there was an enrichment for the expression of some BMP target genes like *Id1*, *Smad1* or *Alk8*. Additionally, cardiomyocytes in the wound border area showed increased expression of pSMAD1/5/8[358]. Moreover, in a second study performed on zebrafish, injured hearts showed an increase of *Bmp4* in the outermost layer, the epicardium[359]. These data suggest that BMP signaling is important in heart regeneration. It would be interesting to investigate if BMP4 and WT1 cooperate during the epicardium reactivation following MI. However, regarding heart injury, we know that whatever happens "naturally" we know it is not enough to fully regenerate the heart. It is possible that the recovery of *all* embryonic properties is not the best option. In a study published in 2010, the authors demonstrated that, because BMP4 induces cellular apoptosis, *Bmp4*$^{+/-}$ hearts present a reduced infarct size and less myocardial apoptosis. Moreover, treatment of injured mice with Noggin or Dm reduced infarct size[360]. Whether these observations are related to BMP4 produced by the epicardium or whether reactivation of BMP signaling in the epicardium is or not beneficial remains to be clarified.

In this thesis, I have proposed some of the roles *Bmp4* might be playing during epicardium development. However, it is everyday clearer that signaling pathways do not exert their functions in a well clustered binary way, meaning that each pathway has a specific role and it is active or not. It is closer to reality a vision in which a network of pathways, ligands and receptors collaborate, and also a paradigm in which different levels or concentrations can lead to different results. In this sense, in an elegant article, it was demonstrated how, *in vitro,* the combination of BMP4 with other ligands, and the modulation of both ligands concentrations, results in different outputs of BMP pathway activation[361]. In the epicardium, there is a wide number of signaling pathways operating. Additionally, epicardial cells are subjected to a large number of stimuli[145]. How they all cooperate for a correct development is far from being understood. If we focus on BMP4 and the roles here investigated, there are a couple of other proteins or molecules or even physical events implicated. For example, in the case of cell shape, there is a crescent number of articles investigating how the physical properties of the environment influence cellular morphology[362,363]. Mechanical stimuli coming from the environment can be generated by neighbor cells, ECM or fluid flow. During heart development, cardiac ECM stiffness increases at a regular rate until it reaches adult heart values at E14[364]. The effect of substrate stiffness in cellular volume or cell morphology has been largely studied,

and, as a very general formulation, it can be stated that as stiffness increases, cells tend to spread, reduce cell high and gain volume[365]. Indeed, this is the pattern followed by epicardial cells during development. Additionally, two more aspects can be added to this topic: first, cell morphology can influence genetical and metabolical cellular properties and second, the epicardium is a source of different components of ECM. Whether one process precedes another or whether we are talking about a group of factors cooperating is a question that needs to be tackled: how all these events influence each other? Are there feedback loops implicated? Is there a triggering phenomenon? Does the epicardium participate in heart development by modulating the physical properties of the heart? The answers to these questions shall help to understand the events described in this thesis.

*Wt1* expression is a hallmark of the embryonic epicardium and *Wt1* expression is essential for heart formation. Accordingly, *epiWt1KO* (*Gata5$^{Cre}$; Wt1$^{LoxP/GFP}$*) mice are embryonically lethal between E16.5 and E18.5[190]. *EpiWt1KO* embryos develop the epicardium, but the formation of EPDCs in these KO is affected. The genetic signature of *epiWt1KO* is altered (Fig. 11) and one of the pathways affected is the BMP4 pathway.

There are several pieces of evidence suggesting that WT1 inhibition of *Bmp4* is a common event in the development of several organs. WT1 has already been described to control *Bmp4* expression during kidney and tongue development[127,366]. We hypothesize that *Bmp4* inhibition is necessary for the differentiation of lateral plate mesoderm (LPM) progenitors into different cell types of the organs that originate from the LPM. Indeed, BMP signaling is implicated in LPM specification and *Bmp4* is one of the markers that have been used to track the LPM[167,367]. There are a group of organs and tissues that develop from the LPM. Among them, we find the heart, kidneys, gonads, the spleen and other structures derived from the coelomic epithelium[367]. Interestingly, in chicken embryos, the specification of the region that will give rise to the gonads, depends on BMP4 regulation by Sonic Hedgehog signaling[67]. Decisions leading to each of those lineages have been studied using different kinds of techniques, including stem cells, lineage tracing or singlecell-seq experiments[367]. In an exhaustive article using iPSCs, the authors tried to map the decisions leading from the primitive streak to different fates of mesodermal origin. BMP signaling was crucial in the first of these decisions, promoting lateral mesoderm and inhibiting paraxial mesoderm[368]. From lateral mesoderm progenitors, authors followed the differentiating road until they obtained cardiomyocytes. Interestingly, using a BMP inhibitor, authors concluded that BMP activation promoted cardiomyocytes at the expense of (pro)epicardium or endocardium[368]. In addition, the modulation of BMP signaling is a common point in other protocols trying to generate

epicardial cells from stem cells[369,370]. We have characterized how WT1 inhibits *Bmp4* expression in the epicardium (Fig. 15) and also we have shown that *Bmp4* expression is downregulated during lung mesothelium development (Fig. 25). Further work will be necessary to clarify whether this is a general mechanism guiding LPM specification.

## 9.2 *Wt1$^{Cre}$*, a tool revisited.

In this work, I have used two *Wt1KO* models. The *Wt1$^{Cre}$; Wt1$^{LoxP/GFP}$* allowed us to partially circumvent *Wt1KO* embryonic lethality and reach adulthood in a downregulated *Wt1* context (Fig. 29,30) The second one, *Gata5$^{Cre}$;Wt1$^{Loxp/GFP}$*, allowed us to explore a new aspect in the epicardium biology: regulation of the epicardium maturity through WT1 control of the BMP4 pathway.

About the *Wt1$^{Cre}$; Wt1$^{LoxP/GFP}$,* there are two major aspects I would like to comment on. The first one refers to the Cre expression. The *Wt1$^{Cre}$* mouse model has been used in the past for several lineage tracing studies in many tissues, and also to generate different KOs (Tables 22 and 23). The conclusions obtained by those studies, taking into account our results, should be relooked very carefully, especially in those cases where a negative phenotype was observed. The same happens with lineage tracing experiments, in which at least a set of cells is not being traced. It is worth mentioning at least one of those studies: in an *Alk3 Wt1$^{Cre}$* mediated KO the authors observed no phenotype in the epicardium and the heart[371]. ALK3 is a BMP receptor expressed in the epicardium and, possibly, one among others by which BMP4 acts. Therefore, it is a result that contradicts our *epiWt1KO* data. Besides the possibility of BMP4 acting through other receptors, our data indicate that probably *Alk3* deletion was not effective enough to generate a phenotype.

| Tissue | Reference |
|---|---|
| Pancreas | Ariza et al. 2019[315] |
| Pancreas | Ariza et al. 2018[310] |
| Septum Transversum | Carmona et al., 2016[372] |
| Heart | Villa Del Campo et al., 2016[373] |
| Septum Transversum | Cano et al., 2016[215] |
| Lungs | Cano et al., 2013[309] |
| Gastrointestinal tissues | Carmona et al., 2013[374] |
| The epicardium | Del Monte et al., 2011[166] |
| The epicardium | Wessels et al., 2012[221] |
| The epicardium | Casanova et al., 2013[375] |
| Perycites heart liver | Yamazaki et al., 2017[376] |
| Heart | Durst et al., 2015[377] |
| Heart | Dorr. et al., 2015[378] |

| | |
|---|---|
| Heart | Moore-Morris et al., 2014[379] |
| Fat | Chau et al., 2014[313] |

Table 22. Articles and tissues where *Wt1*$^{Cre}$ has been used for lineage tracing experiments.

| Deleted gene | Presence of of phenotype | Reference |
|---|---|---|
| *Mrtfb/ Mrtfa* | + | Quijada et al., 2019[208] |
| *Wnt11* | - | Van Vliet. et al., 2017[380] |
| *Fat4* | - | Ragni et al., 2017[381] |
| *Mrtfb/Mrtfa* | +(not shown) | Trembley. et al., 2015[223] |
| *Alk3* | +* | Lockhart. et al., 2015[371] |
| *Tbx5* | + | Diman et al., 2014[382] |
| *Notch1* | + | Del Monte et al., 2011[166] |
| *Sna1* | - | Casanova et al., 2013[375] |

Table 23. Articles where *Wt1*$^{Cre}$ has been used to generate KOs.

However, these same caveats in *Wt1*$^{Cre}$ expression raise one possibility: in those organs where *Wt1*$^{Cre}$ is active, the fact that some *Wt1*$^{Cre}$*; Wt1*$^{LoxP/GFP}$ reach adulthood, allows the study of WT1 functions in the long term, maybe allowing to formulate questions for WT1 role in posterior stages of development or in the progression of diseases that appear during adulthood.

The second of these aspects is how *Wt1* expression levels influence the severity of the phenotype. As stated by a wide range of *Wt1*KOs, including our *Gata5*$^{Cre}$ *epiWt1KO*, *Wt1* deletion leads to severe defects in heart development[76,190,194,262]. In *Wt1*$^{Cre}$ *; Wt1*$^{LoxP/GFP}$ GFP++ sorted epicardial cells, we quantified a reduction of 80% in *Wt1* mRNA expression levels (Fig. 39E). This reduction can be considered as a successful KO and, indeed, it causes severe defects in heart development of some *Wt1*$^{Cre}$*; Wt1*$^{LoxP/GFP}$ embryos (Fig. 41), potentially leading to a lethal phenotype. However, some of these embryos manage to survive. What is this telling to us? There is a group of factors to consider to answer this question. The first one opens a dichotomy: either the small group of cells in which the Cre is not expressed is enough to drive a correct heart development or the low, but higher than in other *Wt1*KOs levels of *Wt1* are. Epicardial cells give rise to epicardial derived cells (EPDC), which, in turn, differentiate into different cell types needed for heart development as smooth muscle cells or cardiac fibroblasts[145]. There have been a lot of efforts to elucidate whether there was a group of cells that are fated since the beginning to become EPDC and about deciphering if the epicardium is composed of different subtypes of cells. Our results could be suggesting that this last is the correct answer. This idea, indeed, is supported by very recent studies using single-seq technology: in zebrafish, two independent studies have described the presence of three epicardium populations with specific functions[214,359]. In mice, a population of epicardial cells,

along with a cardiomyocyte population, has been traced back to a common progenitor in the proximity of the cardiac crescent, the juxta-cardiac field[383]. As we have described how, in a significant % of GFP$^{+}$ (potentially cardiomyocytes) cells from *Wt1$^{Cre}$; Wt1$^{GFP/+}$; R26R$^{tdRFP/+}$* hearts, *Wt1$^{Cre}$* is not active (Fig. 28), it is tempting to hypothesize that it is precisely this population the one maintaining *Wt1* expression and, as a consequence, driving a correct heart development in our model.

Another possibility is that, in our mutant, *Wt1* is not deleted in the other WT1-positive cell types in the heart (endothelial cells or cardiomyocytes), and that *Wt1* deletion in those cells is the main cause for the phenotypes observed in other models. The existance of different *Wt1* positive cell types differentiated by the expression of the *Wt1$^{Cre}$* leads to the second part of this thesis. Indeed, although the adrenal gland and gonads derive from a common primordium, in *Wt1$^{Cre}$* mice, as will be further discussed below, the Cre is only active in the gonads and a small subset of cells of adrenal glands (Fig. 26 ).

## 9.3 *Wt1$^{Cre}$; Wt1$^{LoxP/GFP}$*, a gonad *Wt1KO* from the bipotential gonad to adulthood.

Gonad development starts with the formation of the biopotential gonads[384]. The events driving this structure to fully developed testis and ovaries, as well as female and male genital tracts, are still a matter of investigation[384]. In the past decades, the discovery of several genes implicated in this process has broadened our perspective about sexual differentiation[385]. Moreover, the understanding of the molecular mechanisms implicated in the pathways determining sex has helped to explain the causes beyond several disorders of sex development (DSD)[386].

In this thesis, we have characterized a developmental impairment in *Wt1$^{Cre}$; Wt1$^{LoxP/GFP}$* gonads. We have also shown how this embryonic defect leads to unfunctional atrophied sexual gonads both in male and female adult mice. Thus, our model provides a complete panoramic of how a developmental defect results in an adult phenotype (Fig. 47).

*Wt1* role in gonad development has been previously studied and different mouse models have been generated to study it. *Amh$^{Cre}$* and *Foxl2$^{Cre}$* mice have been used to generate *Wt1KOs* in Sertoli and Granulosa cells[101,343]. In addition, a constitutive *CreER* has been used to delete *Wt1* prior to sexual determination[99]. Furthermore, mice with different mutations resembling those found in human syndromes, such as Frasier syndrome, have been generated to understand

*Wt1* role in those syndromes[58]. Our *Wt1*$^{Cre}$*; Wt1*$^{LoxP/GFP}$ model, however, is the first adult *Wt1KO* model in which *Wt1* deletion is accomplished since the bipotential gonad stage.

The deletion of *Wt1* before the formation of the gonadal primordium prevents gonad formation[387]. Therefore, the study of *Wt1* role in sexual development has been hampered by this limitation. In our case, although *Wt1* is supposed to be deleted since the first moment of *Wt1* expression, *Wt1*$^{Cre}$*; Wt1*$^{LoxP/GFP}$ gonads are formed. The cause underlying this phenotype is the particular pattern of *Wt1*$^{Cre}$ expression. To better understand this, it is useful to recapitulate the initial events of gonad morphogenesis. The earliest event of gonad development is the swelling of the coelomic epithelium covering the surface of the mesonephros, giving rise to the adrenogonadal primordium (AGP)[388]. This structure later divides and originates the adrenal primordium and the bipotential gonad (Fig. 47)[389]. WT1 is required for genital ridge survival, and WT1 plays a crucial role in the definition of the AGP identity[317]. If *Wt1* deletion in *Wt1*$^{Cre}$ *; Wt1*$^{LoxP/GFP}$ mice occurred in the AGP, we would expect to observe a phenotype in the adult adrenal gland, but we do not (Fig. 43). Moreover, in *Wt1*$^{Cre}$*;R26R*$^{mTmG/+}$*,* reporter activity was only observed in a small subset of adrenal capsular cells (Fig. 26A)

The conclusion obtain from these observations is that *Wt1* is downregulated only in the bipotential gonad but not in the other organs derived from the urogenital ridge (kidney or adrenal gland). There are some possibilities or reasons underlying this particular phenotype. One possibility is that the *Wt1*$^{Cre}$ is activated after the separation of both organs. Another could suggest the existence of two different progenitors in the AGP: adrenal progenitors would be *Wt1*$^{Cre}$ negative whereas gonad progenitor would be *Wt1*$^{Cre}$ positive. Interestingly, in the chicken embryo, the coelomic epithelium giving rise to the adrenal gland and the gonads is formed by two layers[390]. The outer layer is the origin of the gonads whereas the inner layer derives into adrenocortical precursors[390]. Thus, our results may indicate that in mice, gonad and adrenocortical cells also have two different progenitors that form separated populations in the coelomic epithelium.

Once bipotential gonad is present, *Wt1* plays pivotal roles in the decisions determining the fate of gonad progenitor cells. The two main cell types in the gonad belong to either supportive or steroidogenic lineage. In two articles where single-cell sequencing was used to trace the fate or trajectory of somatic cell differentiation, the authors concluded that "*gonadal supporting cells are specified from Nra5a1 early progenitors by a non-sex-specific transcriptomic program before pre-Granulosa and Sertoli cells acquire their sex-specific*

*identity*"[77,78]. Steroidogenic cells will later differentiate from these same progenitors[77,78]. To understand the differentiation point that *Wt1*$^{Cre}$*; Wt1*$^{LoxP/GFP}$ gonad progenitors reach, we characterized the expression of several genes implicated or used as markers of the different main gonad cell types (Fig. 38,39).

WT1 is required for sex determination and differentiation of Sertoli and Granulosa cells[99]. Indeed, *Wt1*$^{Cre}$*; Wt1*$^{LoxP/GFP}$ mice show no presence of neither of these cell types (Fig. 37). Additionally, *Wt1*$^{Cre}$*; Wt1*$^{LoxP/GFP}$ gonads present an altered expression of a set of genes implicated in sexual differentiation (Fig. 38). So far, *Wt1* has been mostly implicated in male sexual differentiation: direct WT1 regulation of *Sry* has been described[83,84] and several key "male genes" are downregulated in *Wt1KOs*, including our model (*Sox*, *Amh* or *Fgf9*) (Fig. 38B)[99,101,137]. In the past recent years, WT1 participation in female fate commitment has also been suggested[99,343]. In our model, in the absence of WT1, *FoxL2*, *Fst*, *Rspo1* or *Wnt4* expression is downregulated (Fig. 38C). Here, we have additionally described how *Runx1*, which has been recently described as a crucial gene for maintaining female identity[341], is also affected when *Wt1* is deleted.

Steroidogenic cell differentiation is also a crucial event during gonad development[65]. *Wt1* has been implicated in the decision that leads either to supporting or steroidogenic lineage, meaning that *Wt1* needs to be downregulated to allow for steroidogenic cell differentiation. Accordingly, when *Wt1* is deleted, an increase in the steroidogenic cell program is observed[99,103]. This process has been described to be regulated by WT1 repression of *Sf1* expression[99]. However, in *Wt1*$^{Cre}$*; Wt1*$^{LoxP/GFP}$ XY gonads, we observed the exact opposite phenotype: steroidogenic genes like *Hsd3b1*, *Star* and *Cyp11a1* are downregulated, and so it is *Sf1*. On the other hand, in XX gonads we do observe an upregulation tendency of those genes expression. However, this increase does not reach male expression levels (Fig. 39A). There are some ideas we may get from this data:

As I mentioned before, supportive and steroidogenic cells arise from a common progenitor [77,78]. Taking into account this proposal, depending on the point where differentiation is halted, detection of the different cell types will be or not possible in the gonads. Fei Gao and colleagues used a *Cre-ER*$^{TM}$ to delete *Wt1* from E9.5 onward. They detect some SOX9 and FOXL2 positive cells in their *Wt1KO* gonads and also an increase of steroidogenic cells[99]. In that case, probably, *Wt1* is deleted when lineage specification has surpassed or at least reached the crossroad between supportive and steroidogenic program. Supportive lineage, in which *Wt1* expression is maintained, fails to differentiate in absence of WT1, and some cells reprogram to

steroidogenic cells, which, as *Wt1* expression is downregulated in them, can normally differentiate. In our *Wt1*$^{Cre}$; *Wt1*$^{LoxP/GFP}$, we hypothesize that progenitor cells fail to differentiate, remaining at a point before the intersection of both lineages. Indeed, both supportive and steroidogenic differentiation is blocked (Fig. 37,38). The difference between the point in which the path of differentiation ends could explain the differences between the phenotype of two, *a priori*, similar *Wt1KO* models.

Another way to look at it is through the expression of *Sf1*. *Sf1* is the key orchestrator of steroidogenesis but also a gene crucial for early gonad formation[74,99]. WT1 has been described to activate *Sf1* at early stages and to repress it later[74,99]. In males, steroidogenic differentiation occurs earlier than in females[78]. Accordingly, *Sf1* expression is increased in E14.5 control males compared to females(Fig 38A). In XX and XY *Wt1*$^{Cre}$; *Wt1*$^{LoxP/GFP}$ gonads, *Sf1* expression remain at control XX levels. If *Wt1* downregulation does not result in *Sf1* upregulation, it suggests progenitor cells in *Wt1*$^{Cre}$; *Wt1*$^{LoxP/GFP}$ gonads remain in the genetic background typical of earlier stages, in which WT1 activates *Sf1*.

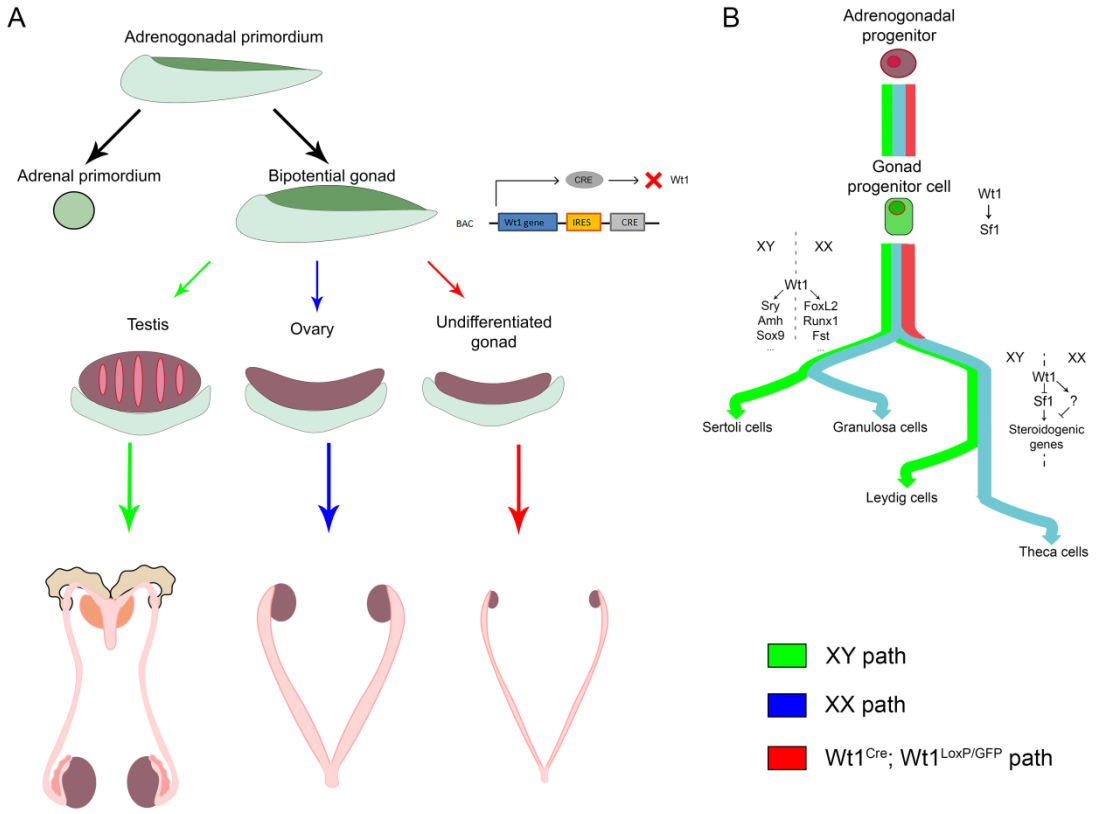


**Figure 47. Model of *Wt1*$^{Cre}$; *Wt1*$^{LoxP/GFP}$ development.** (A) Adrenogonadal primordium gives rise to the adrenal primordium and the bipotential gonad. At this stage, the *Wt1*$^{Cre}$ is activated. Bipotential gonads undergo sex differentiation becoming testis in XY mice, and ovaries in XX mice. *Wt1*$^{Cre}$; *Wt1*$^{LoxP/GFP}$ XX and XY gonads fail to differentiate and give rise to streak gonads in the adult. (B) Adrenogonadal progenitors differentiate into gonadal progenitors. In these cells, *Wt1* is deleted and control and *Wt1*$^{Cre}$; *Wt1*$^{LoxP/GFP}$ development starts diverging.

Gonadal progenitors give rise to supportive cells, which differentiate into Sertoli in XY mice, and to Granulose cells in XX mice. Depending on the presence of chromosome Y, *Wt1* either participates in the male path (regulating genes like *Sry*, *Amh* or *Sox9*); or in the female path (regulating genes like *Foxl2*, *Fst* or *Runx1*). Later, gonadal progenitors give rise to steroidogenic cells. *Wt1* downregulation in control mice upregulates *Sf1* expression, leading to an increase in steroidogenesis. In $Wt1^{Cre}$; $Wt1^{LoxP/GFP}$ mice, cells do not reach the stage where *Wt1* downregulation implies an *Sf1* upregulation. *Wt1* deletion results in an independent, and unknown mechanism of steroidogenesis upregulation. Green indicates the XY path; blue indicates the XX path; red indicates the $Wt1^{Cre}$; $Wt1^{LoxP/GFP}$ path.

Interestingly, in XX $Wt1^{Cre}$; $Wt1^{LoxP/GFP}$, we observe an increase in steroidogenic cell expression. However, *Sf1* expression is not upregulated in XX $Wt1^{Cre}$ ; $Wt1^{LoxP/GFP}$ gonads (Fig. 38A). Therefore, the increase in steroidogenic gene expression observed in $Wt1^{Cre}$ ; $Wt1^{LoxP/GFP}$ XX embryos is independent of *Sf1*. These results indicate that there is an unknown player in female gonads that keeps repressed steroidogenic cell linage, a factor that is altered in $Wt1^{Cre}$; $Wt1^{LoxP/GFP}$ embryos.

In females, androgens synthesized by Theca cells need to be transformed into estrogens in Granulosa cells[391]. Therefore, steroidogenic lineage differentiation in females must wait until Granulosa cells differentiate to prevent undesired virilization caused by ectopic androgen expression[391]. Indeed, in the single-cell-seq article I mentioned before, the authors claimed; "*XX stromal cells commit to steroidogenic progenitor cells from E16.5 onward*"[78]. Therefore, there must be something in females, but not in males, that keeps steroidogenic lineage blocked between the beginning of sexual differentiation and E16.5, something affected in $Wt1^{Cre}$; $Wt1^{LoxP/GFP}$ mice. The most plausible candidate may be a gene or genes upregulated during the beginning of Granulosa cell differentiation. In the adrenal gland, WNT signaling has been described to suppress steroidogenesis, suggesting this can also be the case of ovaries[392].

## 9.4 $Wt1^{Cre}$; $Wt1^{LoxP/GFP}$, a model for Disorders of Sex Development.

Disorders of sex development (DSD) comprehend a large group of syndromes characterized by discordant chromosomal, gonadal, or anatomical sex[386]. Despite the considerable research that has been made to understand the mechanisms underlying DSD, genetic causes remain unknown for most cases[386]. Different mutations in the *WT1* gene have been related to DDS, Frasier syndrome and Meacham syndrome, in which 46,XY individuals show ambiguous or female external genitalia and gonadal dysgenesis, among other characteristics[4]. In addition, a few cases of 46, XX patients showing ovaries lack or streak dysgenic ovaries. Interestingly, all these syndromes and cases were present in association with one or another kind of renal phenotype[51,52]. Recently, in a study analyzing children with testicular (TDSD) or ovotesticular DSD of unknown etiology, a small group was linked to WT1 mutations in ZF4. The authors of

this work demonstrate how a *Wt1* mutation causes an embryonic gonadal defect leading to a phenotype described in 46, XX patients with patients[58]. However, this is not the common case: although the role of *Wt1* during embryonic development has been widely studied, not much is known about the impact of *Wt1* defects on adult sex development.

Conditional *Wt1*KO either on Sertoli or Granulosa cell has shed some light on this topic. However, these KOs do not share the wide range of DSD observed in DDS and Frasier syndromes or the XX patients with TDSD or ovotesticular DSD linked to WT1 mutations. Gonadal sex determination is a critical step in the development of sexually dimorphic internal and external reproductive organs. Our mouse model is the first to accomplish the deletion of *Wt1* since the early formation of the bipotential gonads in both XX and XY mice through the adult stage and produce an ambiguous genitalia phenotype in $Wt1^{Cre}; Wt1^{LoxP/GFP}$ mice (Fig. 31-34).

Adult $Wt1^{Cre}; Wt1^{LoxP/GFP}$ gonads do not show male or female histological structures (neither testis cords nor female follicles were observed) (Fig. 32,33). Therefore it would not be appropriate to define $Wt1^{Cre}; Wt1^{LoxP/GFP}$ as hermaphrodites, which would present ovotestis (in which both male and female structures would be shown). It is probably more precise to say that they are asexual, at least in the sense they do not have developed sexual structures. However, adult $Wt1^{Cre}; Wt1^{LoxP/GFP}$ mice, both XX and XY, showed male and female structures in the genital tract: epididymis, uterus, vas deferens or seminal vesicles (Fig. 32,33). Reduction in *Amh* expression levels in XY $Wt1^{Cre}; Wt1^{LoxP/GFP}$ mice might explain the presence of a uterus in them (Fig. 38A). Indeed, AMH XY deficient mice develop male reproductive organs[94]. Additionally, $Amh^{Cre}$ XY *Wt1KOs* mice also show a uterus, confirming *Wt1* expression is needed for Müllerian duct regression[101]. Currently, we know that WT1 has been described to directly regulate *Amhr2* and *Amh* genes, suggesting the mechanism of the observed phenotype[137,393].

The presence of male structures like epididymis in XX $Wt1^{Cre}; Wt1^{LoxP/GFP}$ mice indicates the Wolffian duct has not regressed. For Wolffian duct retention and differentiation, androgens are required[133]. In $Foxl2^{Cre}$ *Wt1KO* mice, Wolffian duct degeneration was delayed but not blocked[343]. We observe an increase in the steroidogenic genetic program in our XX KO mice (Fig. 38A). However, as I mentioned before, steroidogenic gene upregulation did not reach male control levels. Therefore, this may indicate an androgen-independent mechanism of Wolffian duct retention. Deletion of COUP-TFII in female embryos has been described to lead to Wolffian duct retention independently of androgen production[394]. We have not quantified androgen production in $Wt1^{Cre}; Wt1^{LoxP/GFP}$ mice. However, the measurement of testosterone

levels in *Wt1*$^{Cre}$*; Wt1*$^{LoxP/GFP}$ mice could help to understand the phenotype observed and to better comprehend the importance of androgens in the formation of the genital tract.

The characterization of *Wt1*$^{Cre}$*; Wt1*$^{LoxP/GFP}$ lead us to propose it as a useful model to study *DSD*. In the past decades, several genes involved in DSD have been identified[386]. Traditionally, *WT1* mutations have been linked to XY DSD[4]. However, recently, *WT1* has also been associated to XX DSD[58,395]. Interestingly, in both cases, WT1 mutations were found in the ZF4 of the protein. Our model, however, represents a different case not yet identified in humans: the total absence of the gene/protein specifically in the reproductive organs.

Another use for our model could be the study of direct sex chromosome effects. Differences between sexes in non-gonadal tissues can be caused by the effect of sexual differentiation in the gonads (hormones) but also by the direct contribution of sexual chromosomes[396]. The discrimination of these factors has gained relevance in the past years/decades, as a way to better understand sexual differentiation, especially in the brain[397]. To investigate this topic, XX/XY- testis/ovaries combinations of mice have been used[398]. Additionally, mice without gonads (*Sf1KO* mice) have been also proposed and used to study this[399]. Therefore, *Wt1*$^{Cre}$*; Wt1*$^{LoxP/GFP}$ mice, which never develop gonadal tissues but reach adulthood, could be a useful and informative model.

## 9.5 *Wt1* in cell plasticity and differentiation, a crossroad gene.

As a final recapitulation, in this work, I have described one of the roles played by *Wt1* during the development of the epicardium. Additionally, I have characterized a new *Wt1KO* model to study sexual organs development. Despite the differences of both processes, some similarities are present. In both cases, we have encountered with cells with multipotent potential. Epicardial cells can either maturate to quiescent epicardial cells or differentiate to EPDC and its descendant's lineages. Cells from the coelomic epithelium of the gonad can also differentiate and give rise to different cell types as Sertoli/Granulosa cells or cells from the steroidogenic lineage. A second aspect is the apparent contradictory mechanisms implicated in these events. *Bmp4* is upregulated in *Wt1KO* cells but also correlates with *Wt1* downregulation during development. In the gonads, WT1 induces *Sf1* expression to allow for bipotential gonad formation. Then, *Wt1* must be downregulated to allow for steroidogenic cell differentiation. Additionally, we have characterized how *Wt1* modulation is necessary to correct drive male and female programs in the genital tract. The idea of *Wt1* playing oppossing roles depending on the context is not new: oncogene/tumor suppressor or pro-EMT/pro-MET roles have been

linked to *Wt1*. All these pieces of evidence support the idea of *Wt1* as a hallmark of high cell plasticity and differentiation potential. The implications and possibilities of this statement will certainly keep *Wt1* as a relevant and interesting matter of study as it has been until now.

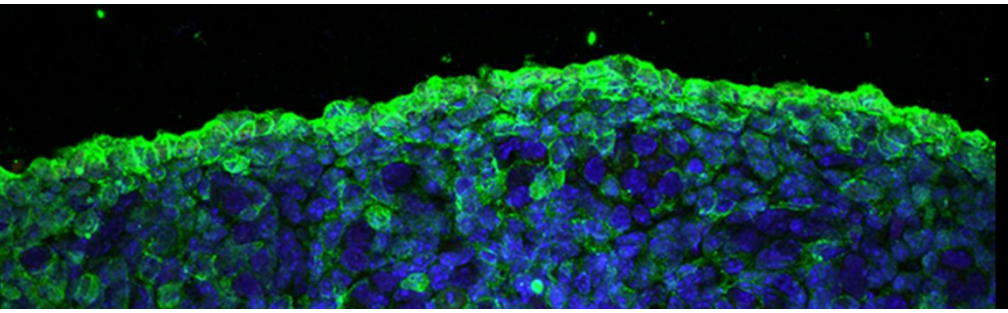

# CONCLUSIONS

The results obtained in this work led us to formulate the following conclusions:

**1** Epicardial cells undergo a cell flattening process during the epicardium development.

**2** WT1 expression is necessary for epicardial cell shape flattening.

**3** WT1 regulates BMP4 pathway in epicardial cells.

**4** BMP4 pathway regulates epicardial cell morphology.

**5** Mesothelial cell flattening may be a common process in the different tissues where mesothelium is present.

**6** *Wt1*$^{Cre}$ expression differs from WT1 expression pattern.

**7** *Wt1*$^{Cre}$; *Wt1*$^{loxp/GFP}$ mice present an ambiguous genitalia phenotype.

**8** *Wt1*$^{Cre}$; *Wt1*$^{loxp/GFP}$ mice present an impaired gonad differentiation.

**9** *Wt1*$^{Cre}$; *Wt1*$^{loxp/GFP}$ show a sub-lethal phenotype caused by defects in heart development in some embryos.

**10** *Wt1*$^{Cre}$; *Wt1*$^{loxp/GFP}$ mice do not show the kidney defects present in other *Wt1KO* mouse models.

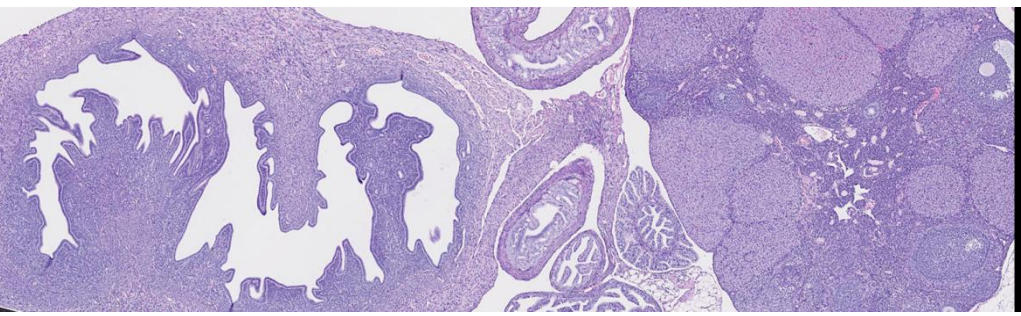

# BIBLIOGRAPHY

1. Call, K. M. *et al.* Isolation and characterization of a zinc finger polypeptide gene at the human chromosome 11 Wilms' tumor locus. *Cell* **60,** 509–520 (1990).

2. Gessler, M. *et al.* Homozygous deletion in Wilms tumours of a zinc-finger gene identified by chromosome jumping. *Nature* **343,** 774–778 (1990).

3. Haber, D. A. *et al.* An internal deletion within an 11p13 zinc finger gene contributes to the development of Wilms' tumor. *Cell* **61,** 1257–1269 (1990).

4. Hastie, N. D. Wilms' tumour 1 (WT1) in development, homeostasis and disease. *Dev.* **144,** 2862–2872 (2017).

5. Haber, D. A. *et al.* Alternative splicing and genomic structure of the Wilms tumor gene WT1. *Proc. Natl. Acad. Sci. U. S. A.* **88,** 9618–9622 (1991).

6. Gessler, M., König, A. & Bruns, G. A. P. The genomic organization and expression of the WT1 gene. *Genomics* **12,** 807–813 (1992).

7. Dallosso, A. R. *et al.* Genomic imprinting at the WT1 gene involves a novel coding transcript (AWT1) that shows derugulation in Wilm's tumours. *Hum. Mol. Genet.* **13,** 405–415 (2004).

8. Dechsukhum, C., Ware, J. L., Ferreira-Gonzalez, A., Wilkinson, D. S. & Garrett, C. T. Detection of a novel truncated WT1 transcript in human neoplasia. *Mol. Diagn.* **5,** 117–128 (2000).

9. Tatsumi, N. *et al.* Identification of a novel C-terminal truncated WT1 isoform with antagonistic effects against major WT1 isoforms. *PLoS One* **10,** (2015).

10. Wang, Z. Y., Qiu, Q. Q., Enger, K. T. & Deuel, T. F. A second transcriptionally active DNA-binding site for the Wilms tumor gene product, WT1. *Proc. Natl. Acad. Sci. U. S. A.* **90,** 8896–8900 (1993).

11. Madden, S. L., Cook, D. M. & Rauscher, F. J. A structure-function analysis of transcriptional repression mediated by the WT1, Wilms' tumor suppressor protein. *Oncogene* **8,** 1713–1720 (1993).

12. Holmes, G. *et al.* Two N-terminal self-association domains are required for the dominant negative transcriptional activity of WT1 Denys-Drash mutant proteins. *Biochem. Biophys. Res. Commun.* **233,** 723–728 (1997).

13. Smolen, G. A., Vassileva, M. T., Wells, J., Matunis, M. J. & Haber, D. A. SUMO-1 modification of the Wilms' tumor suppressor WT1. *Cancer Res.* **64,** 7846–7851 (2004).

14. Ye, Y., Raychaudhuri, B., Gurney, A., Campbell, C. E. & Williams, B. R. Regulation of WT1 by phosphorylation: inhibition of DNA binding, alteration of transcriptional activity and cellular translocation. *EMBO J.* **15,** 5606–5615 (1996).

15. Sakamoto, Y., Yoshida, M., Semba, K. & Hunter, T. Inhibition of the DNA-binding and transcriptional repression activity of the Wilms' tumor gene product, WT1, by cAMP-

dependent protein kinase-mediated phosphorylation of Ser-365 and Ser-393 in the zinc finger domain. *Oncogene* **15,** 2001–2012 (1997).

16. Toska, E. & Roberts, S. G. E. Mechanisms of transcriptional regulation by WT1 (Wilms' tumour 1). *Biochem. J.* **461,** 15–32 (2014).

17. Essafi, A. *et al.* A Wt1-Controlled chromatin switching mechanism underpins tissue-specific wnt4 activation and repression. *Dev. Cell* **21,** 559–574 (2011).

18. Maheswaran, S. *et al.* Physical and functional interaction between WT1 and p53 proteins. in *Proceedings of the National Academy of Sciences of the United States of America* **90,** 5100–5104 (1993).

19. Idelman, G., Glaser, T., Roberts, C. T. & Werner, H. WT1-p53 interactions in insulin-like growth factor-I receptor gene regulation. *J. Biol. Chem.* **278,** 3474–3482 (2003).

20. Scharnhorst, V., Dekker, P., Van Der Eb, A. J. & Jochemsen, A. G. Physical interaction between Wilms tumor 1 and p73 proteins modulates their functions. *J. Biol. Chem.* **275,** 10202–10211 (2000).

21. Carpenter, B. *et al.* BASP1 Is a Transcriptional Cosuppressor for the Wilms' Tumor Suppressor Protein WT1. *Mol. Cell. Biol.* **24,** 537–549 (2004).

22. Srichai, M. B. *et al.* A WT1 Co-regulator Controls Podocyte Phenotype by Shuttling between Adhesion Structures and Nucleus. *J. Biol. Chem.* **279,** 14398–14408 (2004).

23. Wang, W., Lee, S. B., Palmer, R., Ellisen, L. W. & Haber, D. A. A Functional Interaction with CBP Contributes to Transcriptional Activation by the Wilms Tumor Suppressor WT1. *J. Biol. Chem.* **276,** 16810–16816 (2001).

24. Johnstone, R. W. *et al.* A novel repressor, par-4, modulates transcription and growth suppression functions of the Wilms' tumor suppressor WT1. *Mol. Cell. Biol.* **16,** 6945–6956 (1996).

25. Richard, D. J., Schumacher, V., Royer-Pokora, B. & Roberts, S. G. E. Par4 is a coactivator for a splice isoform-specific transcriptional activation domain in WT1. *Genes Dev.* **15,** 328–339 (2001).

26. Stoll, R. *et al.* Structure of the Wilms Tumor Suppressor Protein Zinc Finger Domain Bound to DNA. *J. Mol. Biol.* **372,** 1227–1245 (2007).

27. Bickmore, W. A. *et al.* Modulation of DNA binding specificity by alternative splicing of the wilms tumor wt1 gene transcript. *Science (80-. ).* **257,** 235–237 (1992).

28. Laity, J. H., Dyson, H. J. & Wright, P. E. Molecular basis for modulation of biological function by alternate splicing of the Wilms' tumor suppressor protein. *Proc. Natl. Acad. Sci. U. S. A.* **97,** 11932–11935 (2000).

29. Kann, M. *et al.* Genome-wide analysis of Wilms' tumor 1-controlled gene expression in podocytes reveals key regulatory mechanisms. in *Journal of the American Society of Nephrology* **26,** 2097–2104 (2015).

30. Lefebvre, J. *et al.* Alternatively spliced isoforms of WT1 control podocyte-specific gene expression. *Kidney Int.* **88,** 321–331 (2015).

31. Dong, L. *et al.* Integration of cistromic and transcriptomic analyses identifies Nphs2, Mafb, and Magi2 as Wilms' tumor 1 target genes in podocyte differentiation and maintenance. *J. Am. Soc. Nephrol.* **26,** 2118–2128 (2015).

32. Caricasole, A. *et al.* RNA binding by the Wilms tumor suppressor zinc finger proteins. *Proc. Natl. Acad. Sci. U. S. A.* **93,** 7562–7566 (1996).

33. Bardeesy, N. & Pelletier, J. Overlapping RNA and DNA binding domains of the wt1 tumor suppressor gene product. *Nucleic Acids Res.* **26,** 1784–1792 (1998).

34. Kennedy, D., Ramsdale, T., Mattick, J. & Little, M. An RNA recognition motif in Wilms' tumour protein (WT1) revealed by structural modelling. *Nat. Genet.* **12,** 329–332 (1996).

35. Larsson, S. H. *et al.* Subnuclear localization of WT1 in splicing or transcription factor domains is regulated by alternative splicing. *Cell* **81,** 391–401 (1995).

36. Davies, R. C. *et al.* WT1 interacts with the splicing factor U2AF65 in an isoform-dependent manner and can be incorporated into spliceosomes. *Genes Dev.* **12,** 3217–3225 (1998).

37. Niksic, M., Slight, J., Sanford, J. R., Caceres, J. F. & Hastie, N. D. The Wilms' tumour protein (WT1) shuttles between nucleus and cytoplasm and is present in functional polysomes. *Hum. Mol. Genet.* **13,** 463–471 (2004).

38. Bharathavikru, R. *et al.* Transcription factor Wilms' tumor 1 regulates developmental RNAs through 3' UTR interaction. *Genes Dev.* **31,** 347–352 (2017).

39. Rampal, R. *et al.* DNA Hydroxymethylation Profiling Reveals that WT1 Mutations Result in Loss of TET2 Function in Acute Myeloid Leukemia. *Cell Rep.* **9,** 1841–1855 (2014).

40. Wang, Y. *et al.* WT1 recruits TET2 to regulate its target gene expression and suppress leukemia cell proliferation. *Mol. Cell* **57,** 662–673 (2015).

41. Miller-Hodges, E. & Hohenstein, P. WT1 in disease: Shifting the epithelial-mesenchymal balance. *Journal of Pathology* **226,** 229–240 (2012).

42. Charlton, J. & Pritchard-Jones, K. WT1 mutation in childhood cancer. *Methods Mol. Biol.* **1467,** 1–14 (2016).

43. Treger, T. D., Chowdhury, T., Pritchard-Jones, K. & Behjati, S. The genetic changes of Wilms tumour. *Nature Reviews Nephrology* **15,** 240–251 (2019).

44. Huff, V. Wilms' tumours: About tumour suppressor genes, an oncogene and a chameleon gene. *Nature Reviews Cancer* **11,** 111–121 (2011).

45. Oka, Y. *et al.* in *Immunotherapy of Cancer: An Innovative Treatment Comes of Age* 159–185 (2016). doi:10.1007/978-4-431-55031-0_12

46. Riccardi, V. M., Sujansky, E., Smith, A. C. & Francke, U. Chromosomal imbalance in the aniridia-Wilms' tumor association: 11p interstitial deletion. *Pediatrics* **61,** 604–61O (1978).

47. Francke, U., Holmes, L. B., Atkins, L. & Riccardi, V. M. Aniridia-Wilms' tumor association: evidence for specific deletion of 11p13. *Cytogenet. Cell Genet.* **24,** 185–192 (1979).

48. Fischbach, B. V., Trout, K. L., Lewis, J., Luis, C. A. & Sika, M. WAGR syndrome: A clinical review of 54 cases. *Pediatrics* **116,** 984–988 (2005).

49. Little, M. & Wells, C. A clinical overview of Wt1 gene mutations. *Human Mutation* **9,** 209–225 (1997).

50. Pelletier, J. *et al.* Germline mutations in the Wilms' tumor suppressor gene are associated with abnormal urogenital development in denys-drash syndrome. *Cell* **67,** 437–447 (1991).

51. Jeanpierre, C. *et al.* Identification of constitutional WT1 mutations, in patients with isolated diffuse mesangial sclerosis, and analysis of genotype/phenotype correlations by use of a computerized mutation database. *Am. J. Hum. Genet.* **62,** 824–833 (1998).

52. Lipska, B. S. *et al.* Genotype-phenotype associations in WT1 glomerulopathy. *Kidney Int.* **85,** 1169–1178 (2014).

53. Barbaux, S. *et al.* Donor splice-site mutations in WT1 are responsible for Frasier syndrome. *Nat. Genet.* **17,** 467–470 (1997).

54. Meacham, L. R., Winn, K. J., Culler, F. L. & Parks, J. S. Double vagina, cardiac, pulmonary, and other genital malformations with 46,XY karyotype. *Am. J. Med. Genet.* **41,** 478–481 (1991).

55. Toriello, H. V. & Higgins, J. V. Report of another child with sex reversal and cardiac, pulmonary, and diaphragm defects [5]. *American Journal of Medical Genetics* **44,** 252 (1992).

56. Killeen, O. G., Kelehan, P. & Reardon, W. Double vagina with sex reversal, congenital diaphragmatic hernia, pulmonary and cardiac malformations - Another case of Meacham syndrome. *Clin. Dysmorphol.* **11,** 25–28 (2002).

57. Suri, M. *et al.* WT1 mutations in Meacham syndrome suggest a coelomic mesothelial origin of the cardiac and diaphragmatic malformations. *Am. J. Med. Genet. Part A* **143,** 2312–2320 (2007).

58. Eozenou, C. *et al.* Testis formation in XX individuals resulting from novel pathogenic variants in Wilms' tumor 1 (WT1) gene. *Proc. Natl. Acad. Sci. U. S. A.* **117,** 13680–13688 (2020).

59. Richeldi, L., Collard, H. R. & Jones, M. G. Idiopathic pulmonary fibrosis. *The Lancet* **389,** 1941–1952 (2017).

60. Sontake, V. *et al.* Fibrocytes Regulate Wilms Tumor 1–Positive Cell Accumulation in Severe Fibrotic Lung Disease. *J. Immunol.* **195,** 3978–3991 (2015).

61. Sontake, V. *et al.* Wilms' tumor 1 drives fibroproliferation and myofibroblast transformation in severe fibrotic lung disease. *JCI insight* **3,** (2018).

62. Asahina, K., Zhou, B., Pu, W. T. & Tsukamoto, H. Septum transversum-derived mesothelium gives rise to hepatic stellate cells and perivascular mesenchymal cells in developing mouse liver. *Hepatology* **53,** 983–995 (2011).

63. Kendall, T. J. *et al.* Embryonic mesothelial-derived hepatic lineage of quiescent and heterogenous scar-orchestrating cells defined but suppressed by WT1. *Nat. Commun.* **10,** (2019).

64. Mariottini, C. *et al.* Wilm's tumor 1 promotes memory flexibility. *Nat. Commun.* **10,** (2019).

65. DeFalco, T. & Capel, B. Gonad Morphogenesis in Vertebrates: Divergent Means to a Convergent End. *Annu. Rev. Cell Dev. Biol.* **25,** 457–482 (2009).

66. Karl, J. & Capel, B. Sertoli cells of the mouse testis originate from the coelomic epithelium. *Dev. Biol.* **203,** 323–333 (1998).

67. Yoshino, T., Murai, H. & Saito, D. Hedgehog-BMP signalling establishes dorsoventral patterning in lateral plate mesoderm to trigger gonadogenesis in chicken embryos. *Nat. Commun.* **7,** (2016).

68. Hu, Y. C., Okumura, L. M. & Page, D. C. Gata4 Is Required for Formation of the Genital Ridge in Mice. *PLoS Genet.* **9,** (2013).

69. Miyamoto, N., Yoshida, M., Kuratani, S., Matsuo, I. & Aizawa, S. Defects of urogenital development in mice lacking Emx2. *Development* **124,** 1653–1664 (1997).

70. Birk, O. S. *et al.* The LIM homeobox gene Lhx9 is essential for mouse gonad formation. *Nature* **403,** 909–913 (2000).

71. Val, P., Lefrançois-Martinez, A. M., Veyssière, G. & Martinez, A. SF-1 a key player in the development and differentiation of steroidogenic tissues. *Nuclear Receptor* **1,** (2003).

72. Luo, X., Ikeda, Y. & Parker, K. L. A cell-specific nuclear receptor is essential for adrenal and gonadal development and sexual differentiation. *Cell* **77,** 481–490 (1994).

73. Katoh-Fukul, Y. *et al.* Male-to-female sex reversal in M33 mutant mice. *Nature* **393,** 688–692 (1998).

74. Wilhelm, D. & Englert, C. The Wilms tumor suppressor WT1 regulates early gonad development by activation of Sf1. *Genes Dev.* **16,** 1839–1851 (2002).

75. Val, P., Martinez-Barbera, J. P. & Swain, A. Adrenal development is initiated by Cited2 and Wt1 through modulation of Sf-1 dosage. *Development* **134,** 2349–2358 (2007).

76. Kreidberg, J. A. *et al.* WT-1 is required for early kidney development. *Cell* **74,** 679–691 (1993).

77. Stévant, I. *et al.* Deciphering Cell Lineage Specification during Male Sex Determination with Single-Cell RNA Sequencing. *Cell Rep.* **22,** 1589–1599 (2018).

78. Stévant, I. *et al.* Dissecting Cell Lineage Specification and Sex Fate Determination in Gonadal Somatic Cells Using Single-Cell Transcriptomics. *Cell Rep.* **26,** 3272–3283.e3 (2019).

79. Gubbay, J. *et al.* A gene mapping to the sex-determining region of the mouse Y chromosome is a member of a novel family of embryonically expressed genes. *Nature* **346,** 245–250 (1990).

80. Hacker, A., Capel, B., Goodfellow, P. & Lovell-Badge, R. Expression of Sry, the mouse sex determining gene. *Development* **121,** 1603–1614 (1995).

81. Koopman, P., Münsterberg, A., Capel, B., Vivian, N. & Lovell-Badge, R. Expression of a candidate sex-determining gene during mouse testis differentiation. *Nature* **348,** 450–452 (1990).

82. Katoh-Fukui, Y. *et al.* Cbx2, a polycomb group gene, is required for Sry gene expression in mice. *Endocrinology* **153,** 913–924 (2012).

83. Bradford, S. T. *et al.* A cell-autonomous role for WT1 in regulating Sry in vivo. *Hum. Mol. Genet.* **18,** 3429–3438 (2009).

84. Hossain, A. & Saunders, G. F. The Human Sex-determining Gene SRY Is a Direct Target of WT1. *J. Biol. Chem.* **276,** 16817–16823 (2001).

85. Sekido, R., Bar, I., Narváez, V., Penny, G. & Lovell-Badge, R. SOX9 is up-regulated by the transient expression of SRY specifically in Sertoli cell precursors. *Dev. Biol.* **274,** 271–279 (2004).

86. Chaboissier, M. C. *et al.* Functional analysis os Sox8 and Sox9 during sex determination in the mouse. *Development* **131,** 1891–1901 (2004).

87. Vidal, V. P. I., Chaboissier, M. C., De Rooij, D. G. & Schedl, A. Sox9 induces testis development in XX transgenic mice. *Nat. Genet.* **28,** 216–217 (2001).

88. Barrionuevo, F. *et al.* Homozygous Inactivation of Sox9 Causes Complete XY Sex Reversal in Mice1. *Biol. Reprod.* **74,** 195–201 (2006).

89. Bishop, C. E. *et al.* A transgenic insertion upstream of Sox9 is associated with dominant XX sex reversal in the mouse. *Nat. Genet.* **26,** 490–494 (2000).

90. Schmahl, J., Kim, Y., Colvin, J. S., Ornitz, D. M. & Capel, B. Fgf9 induces proliferation and nuclear localization of FGFR2 in Sertoli precursors during male sex determination. *Development* **131,** 3627–3636 (2004).

91. Schmahl, J., Eicher, E. M., Washburn, L. L. & Capel, B. Sry induces cell proliferation in the mouse gonad. *Development* **127,** 65–73 (2000).

92. Brennan, J., Karl, J. & Capel, B. Divergent vascular mechanisms downstream of sry establish the arterial system in the XY gonad. *Dev. Biol.* **244,** 418–428 (2002).

93. Combes, A. N. *et al.* Endothelial cell migration directs testis cord formation. *Dev. Biol.* **326,** 112–120 (2009).

94. Behringer, R. R., Finegold, M. J. & Cate, R. L. Müllerian-inhibiting substance function during mammalian sexual development. *Cell* **79,** 415–425 (1994).

95. Meeks, J. J., Weiss, J. & Jameson, J. L. Dax1 is required for testis determination. *Nat. Genet.* **34,** 32–33 (2003).

96. Swain, A., Narvaez, V., Burgoyne, P., Camerino, G. & Lovell-Badge, R. Dax1 antagonizes Sry action in mammalian sex determination. *Nature* **391,** 761–767 (1998).

97. Tevosian, S. G. *et al.* Gonadal differentiation, sex determination and normal Sry expression in mice require direct interaction between transcription partners GATA4 and FOG2. *Development* **129,** 4627–4634 (2002).

98. Bouma, G. J., Washburn, L. L., Albrecht, K. H. & Eicher, E. M. Correct dosage of Fog2 and Gata4 transcription factors is critical for fetal testis development in mice. *Proc. Natl. Acad. Sci. U. S. A.* **104,** 14994–14999 (2007).

99. Chen, M. *et al.* Wt1 directs the lineage specification of sertoli and granulosa cells by repressing Sf1 expression. *Dev.* **144,** 44–53 (2017).

100. Rao, M. K. *et al.* Tissue-specific RNAi reveals that WT1 expression in nurse cells controls germ cell survival and spermatogenesis. *Genes Dev.* **20,** 147–152 (2006).

101. Gao, F. *et al.* The Wilms tumor gene, Wt1, is required for Sox9 expression and maintenance of tubular architecture in the developing testis. *Proc. Natl. Acad. Sci. U. S. A.* **103,** 11987–11992 (2006).

102. Chang, H. *et al.* Wt1 negatively regulates B-catenin signaling during testis development. *Development* **135,** 1875–1885 (2008).

103. Zhang, L. *et al.* Reprogramming of Sertoli cells to fetal-like Leydig cells by Wt1 ablation. *Proc. Natl. Acad. Sci. U. S. A.* **112,** 4003–4008 (2015).

104. Buehr, M., Gu, S. & McLaren, A. Mesonephric contribution to testis differentiation in the fetal mouse. *Development* **117,** 273–281 (1993).

105. Tilmann, C. & Capel, B. Mesonephric cell migration induces testis cord formation and Sertoli cell differentiation in the mammalian gonad. *Development* **126,** 2883–2890 (1999).

106. Romereim, S. M. & Cupp, A. S. Mesonephric cell migration into the gonads and vascularization are processes crucial for testis development. *Results Probl. Cell Differ.* **58,** 67–100 (2016).

107. Coveney, D., Cool, J., Oliver, T. & Capel, B. Four-dimensional analysis of vascularization during primary development of an organ, the gonad. *Proc. Natl. Acad. Sci. U. S. A.* **105,** 7212–7217 (2008).

108. Capel, B., Albrecht, K. H., Washburn, L. L. & Eicher, E. M. Migration of mesonephric cells into the mammalian gonad depends on Sry. *Mech. Dev.* **84,** 127–131 (1999).

109. Jeays-Ward, K. *et al.* Endothelial and steroidogenic cell migration are regulated by WNT4 in the developing mammalian gonad. *Development* **130,** 3663–3670 (2003).

110. Combes, A. N. *et al.* Gonadal defects in Cited2-mutant mice indicate a role for SF1 in both testis and ovary differentiation. *Int. J. Dev. Biol.* **54,** 683–689 (2010).

111. Caruso, M. *et al.* R-spondin 1/Dickkopf-1/beta-catenin machinery is involved in testicular embryonic angiogenesis. *PLoS One* **10,** (2015).

112. Cool, J., DeFalco, T. J. & Capel, B. Vascular-mesenchymal cross-talk through Vegf and Pdgf drives organ patterning. *Proc. Natl. Acad. Sci. U. S. A.* **108,** 167–172 (2011).

113. Bott, R. C. *et al.* KDR-LacZ-expressing cells are involved in ovarian and testis-specific vascular development, suggesting a role for VEGFA in the regulation of this vasculature. *Cell Tissue Res.* **342,** 117–130 (2010).

114. Brennan, J., Tilmann, C. & Capel, B. Pdgfr-α mediates testis cord organization and fetal Leydig cell development in the XY gonad. *Genes Dev.* **17,** 800–810 (2003).

115. Cupp, A. S., Uzumcu, M. & Skinner, M. K. Chemotactic role of neurotropin 3 in the embryonic testis that facilitates male sex determination. *Biol. Reprod.* **68,** 2033–2037 (2003).

116. Ross, A. J., Tilman, C., Yao, H., MacLaughlin, D. & Capel, B. AMH induces mesonephric cell migration in XX gonads. in *Molecular and Cellular Endocrinology* **211,** 1–7 (2003).

117. Bowles, J. *et al.* Retinoid signaling determines germ cell fate in mice. *Science (80-. ).* **312,** 596–600 (2006).

118. Yao, H. H. C. *et al.* Follistatin operates downstream of Wnt4 in mammalian ovary organogenesis. *Dev. Dyn.* **230,** 210–215 (2004).

119. Pepling, M. E. & Spradling, A. C. Mouse ovarian germ cell cysts undergo programmed breakdown to form primordial follicles. *Dev. Biol.* **234,** 339–351 (2001).

120. Eggers, S., Ohnesorg, T. & Sinclair, A. Genetic regulation of mammalian gonad development. *Nature Reviews Endocrinology* **10,** 673–683 (2014).

121. Ottolenghi, C. *et al.* Foxl2 is required for commitment to ovary differentiation. *Hum. Mol. Genet.* **14,** 2053–2062 (2005).

122. Uhlenhaut, N. H. *et al.* Somatic Sex Reprogramming of Adult Ovaries to Testes by FOXL2 Ablation. *Cell* **139,** 1130–1142 (2009).

123. Tomizuka, K. *et al.* R-spondin1 plays an essential role in ovarian development through positively regulating Wnt-4 signaling. *Hum. Mol. Genet.* **17,** 1278–1291 (2008).

124. Chassot, A. A. *et al.* Activation of β-catenin signaling by Rspo1 controls differentiation of the mammalian ovary. *Hum. Mol. Genet.* **17,** 1264–1277 (2008).

125. Vainio, S., Heikkilä, M., Kispert, A., Chin, N. & McMahon, A. P. Female development in mammals is regulated by Wnt-4 signalling. *Nature* **397,** 405–409 (1999).

126. Maatouk, D. M. *et al.* Stabilization of β-catenin in XY gonads causes male-to-female sex-reversal. *Hum. Mol. Genet.* **17,** 2949–2955 (2008).

127. Motamedi, F. J. *et al.* WT1 controls antagonistic FGF and BMP-pSMAD pathways in early renal progenitors. *Nat. Commun.* **5,** 4444 (2014).

128. Takasawa, K. *et al.* FOXL2 transcriptionally represses Sf1 expression by antagonizing WT1 during ovarian development in mice. *FASEB J.* **28,** 2020–2028 (2014).

129. Kim, Y. *et al.* Fgf9 and Wnt4 act as antagonistic signals to regulate mammalian sex determination. *PLoS Biol.* **4,** 1000–1009 (2006).

130. Jameson, S. A., Lin, Y. T. & Capel, B. Testis development requires the repression of Wnt4 by Fgf signaling. *Dev. Biol.* **370,** 24–32 (2012).

131. Matson, C. K. *et al.* DMRT1 prevents female reprogramming in the postnatal mammalian testis. *Nature* **476,** 101–105 (2011).

132. Minkina, A. *et al.* DMRT1 protects male gonadal cells from retinoid-dependent sexual transdifferentiation. *Dev. Cell* **29,** 511–520 (2014).

133. Shaw, G. & Renfree, M. B. Wolffian duct development. *Sex. Dev.* **8,** 273–280 (2014).

134. Roly, Z. Y. *et al.* The cell biology and molecular genetics of Müllerian duct development. *Wiley Interdisciplinary Reviews: Developmental Biology* **7,** (2018).

135. Gouédard, L. *et al.* Engagement of bone morphogenetic protein type IB receptor and Smad1 signaling by anti-Mullerian hormone and its type II receptor. *J. Biol. Chem.* **275,** 27973–27978 (2000).

136. Orvis, G. D. *et al.* Functional redundancy of TGF-beta family type i receptors and receptor-smads in mediating anti-müllerian hormone-induced müllerian duct regression in the mouse. *Biol. Reprod.* **78,** 994–1001 (2008).

137. Klattig, J., Sierig, R., Kruspe, D., Besenbeck, B. & Englert, C. Wilms' Tumor Protein Wt1 Is an Activator of the Anti-Müllerian Hormone Receptor Gene Amhr2. *Mol. Cell. Biol.* **27,** 4355–4364 (2007).

138. Parr, B. A. & McMahon, A. P. Sexually dimorphic development of the mammalian reproductive tract requires Wnt-7a. *Nature* **395,** 707–710 (1998).

139. Yeh, S. *et al.* Generation and characterization of androgen receptor knockout (ARKO) mice: An in vivo model for the study of androgen functions in selective tissues. *Proc. Natl. Acad. Sci. U. S. A.* **99,** 13498–13503 (2002).

140. Welsh, M., Sharpe, R. M., Walker, M., Smith, L. B. & Saunders, P. T. K. New insights into the role of androgens in wolffian duct stabilization in male and female rodents. *Endocrinology* **150,** 2472–2480 (2009).

141. Kobayashi, A. & Behringer, R. R. Developmental genetics of the female reproductive tract in mammals. *Nature Reviews Genetics* **4,** 969–980 (2003).

142. Ma, L., Benson, G. V., Lim, H., Dey, S. K. & Maas, R. L. Abdominal B (AbdB) Hoxa genes: Regulation in adult uterus by estrogen and progesterone and repression in Mullerian duct by the synthetic estrogen diethylstilbestrol (DES). *Dev. Biol.* **197,** 141–154 (1998).

143. Miquerol, L. & Kelly, R. G. Organogenesis of the vertebrate heart. *Wiley Interdiscip. Rev. Dev. Biol.* **2,** 17–29 (2013).

144. Clowes, C. *et al.* The functional diversity of essential genes required for mammalian cardiac development. *Genesis* **52,** 713–737 (2014).

145. Quijada, P., Trembley, M. A. & Small, E. M. The Role of the Epicardium during Heart Development and Repair. *Circulation Research* 377–394 (2020). doi:10.1161/CIRCRESAHA.119.315857

146. KURKIEWICZ & T. O histogenezie miesna sercowego zwierzat kregowych-Zur Histogenese des Herzmuskels der Wirbeltiere. *Bull Int Acad Sci Cracovie* (1909). at <https://ci.nii.ac.jp/naid/10015099297>

147. Hirakow, R. Epicardial formation in staged human embryos. *Kaibogaku Zasshi.* **67,** 616–622 (1992).

148. Jahr, M., Schlueter, J., Brand, T. & Männer, J. Development of the proepicardium in Xenopus laevis. *Dev. Dyn.* **237,** 3088–3096 (2008).

149. Viragh, S. & Challice, C. E. The origin of the epicardium and the embryonic myocardial circulation in the mouse. *Anat. Rec.* **201,** 157–168 (1981).

150. Serluca, F. C. Development of the proepicardial organ in the zebrafish. *Dev. Biol.* **315,** 18–27 (2008).

151. Männer, J. Experimental study on the formation of the epicardium in chick embryos. *Anat. Embryol. (Berl).* **187,** 281–289 (1993).

152. Pombal, M. A. *et al.* Epicardial development in lamprey supports an evolutionary origin of the vertebrate epicardium from an ancestral pronephric external glomerulus. *Evol. Dev.* **10,** 210–216 (2008).

153. Cano, E., Carmona, R., Velecela, V., Martínez-Estrada, O. & Muñoz-Chápuli, R. The proepicardium keeps a potential for glomerular marker expression which supports its evolutionary origin from the pronephros. *Evol. Dev.* **17,** 224–230 (2015).

154. Männer, J., Pérez-Pomares, J. M., Macías, D. & Muñoz-Chápuli, R. The origin, formation and developmental significance of the epicardium: A review. *Cells Tissues Organs* **169,** 89–103 (2001).

155. Schlueter, J. & Brand, T. Origin and fates of the proepicardium. *Aswan Hear. Cent. Sci. Pract. Ser.* **2,** 11 (2011).

156. Muñoz-Chápuli, R., Macías, D., Ramos, C., Gallego, A. & De Andrés, V. Development of the subepicardial mesenchyme and the early cardiac vessels in the dogfish (Scyliorhinus canicula). *J. Exp. Zool.* **275,** 95–111 (1996).

157. Zhou, B., Gise, A. von, Ma, Q., Rivera-Feliciano, J. & Pu, W. T. Nkx2-5- and Isl1-expressing cardiac progenitors contribute to proepicardium. *Biochem. Biophys. Res. Commun.* **375,** 450–453 (2008).

158. Barnes, R. M., Firulli, B. A., Conway, S. J., Vincentz, J. W. & Firulli, A. B. Analysis of the Hand1 cell lineage reveals novel contributions to cardiovascular, neural crest, extra-embryonic, and lateral mesoderm derivatives. *Dev. Dyn.* **239,** 3086–3097 (2010).

159. Saga, Y., Kitajima, S. & Miyagawa-Tomita, S. Mesp1 expression is the earliest sign of cardiovascular development. *Trends in Cardiovascular Medicine* **10,** 345–352 (2000).

160. Watt, A. J., Battle, M. A., Li, J. & Duncan, S. A. GATA4 is essential for formation of the proepicardium and regulates cardiogenesis. *Proc. Natl. Acad. Sci. U. S. A.* **101,** 12573–12578 (2004).

161. Barnes, R. M. *et al.* Hand2 loss-of-function in hand1-expressing cells reveals distinct roles in epicardial and coronary vessel development. *Circ. Res.* **108,** 940–949 (2011).

162. Liu, J. & Stainier, D. Y. R. Tbx5 and Bmp signaling are essential for proepicardium specification in zebrafish. *Circ. Res.* **106,** 1818–1828 (2010).

163. Ishii, Y., Langberg, J. D., Hurtado, R., Lee, S. & Mikawa, T. Induction of proepicardial marker gene expression by the liver bud. *Development* **134,** 3627–3637 (2007).

164. Schlueter, J., M??nner, J. & Brand, T. BMP is an important regulator of proepicardial identity in the chick embryo. *Dev. Biol.* **295,** 546–558 (2006).

165. Kruithof, B. P. T. *et al.* BMP and FGF regulate the differentiation of multipotential pericardial mesoderm into the myocardial or epicardial lineage. *Dev. Biol.* **295,** 507–522 (2006).

166. Del Monte, G. *et al.* Differential notch signaling in the epicardium is required for cardiac inflow development and coronary vessel morphogenesis. *Circ. Res.* **108,** 824–836 (2011).

167. Rojas, A. *et al.* Gata4 expression in lateral mesoderm is downstream of BMP4 and is activated directly by Forkhead and GATA transcription factors through a distal enhancer element. *Development* **132,** 3405–3417 (2005).

168. Grieskamp, T., Rudat, C., Lüdtke, T. H. W., Norden, J. & Kispert, A. Notch signaling regulates smooth muscle differentiation of epicardium-derived cells. *Circ. Res.* **108,** 813–823 (2011).

169. Torlopp, A., Schlueter, J. & Brand, T. Role of fibroblast growth factor signaling during proepicardium formation in the chick embryo. *Dev. Dyn.* **239,** 2393–2403 (2010).

170. Urness, L. D., Bleyl, S. B., Wright, T. J., Moon, A. M. & Mansour, S. L. Redundant and dosage sensitive requirements for Fgf3 and Fgf10 in cardiovascular development. *Dev. Biol.* **356,** 383–397 (2011).

171. Van Wijk, B. *et al.* Epicardium and myocardium separate from a common precursor pool by crosstalk between bone morphogenetic protein- and fibroblast growth factor-signaling pathways. *Circ. Res.* **105,** 431–441 (2009).

172. Buermans, H. P. J. *et al.* Comprehensive gene-expression survey identifies Wif1 as a modulator of cardiomyocyte differentiation. *PLoS One* **5,** (2010).

173. Phillips, M. D., Mukhopadhyay, M., Poscablo, C. & Westphal, H. Dkk1 and Dkk2 regulate epicardial specification during mouse heart development. *Int. J. Cardiol.* **150,** 186–192 (2011).

174. Ho, E. & Shimada, Y. Formation of the epicardium studied with the scanning electron microscope. *Dev. Biol.* **66,** 579–585 (1978).

175. Rodgers, L. S., Lalani, S., Runyan, R. B. & Camenisch, T. D. Differential growth and multicellular villi direct proepicardial translocation to the developing mouse heart. *Dev. Dyn.* **237,** 145–152 (2008).

176. Hirose, T. *et al.* PAR3 is essential for cyst-mediated epicardial development by establishing apical cortical domains. *Development* **133,** 1389–1398 (2006).

177. Sengbusch, J. K., He, W., Pinco, K. A. & Yang, J. T. Dual functions of α4β1 integrin in epicardial development: Initial migration and long-term attachment. *J. Cell Biol.* **157,** 873–882 (2002).

178. Nahirney, P. C., Mikawa, T. & Fischman, D. A. Evidence for an extracellular matrix bridge guiding proepicardial cell migration to the myocardium of chick embryos. *Dev. Dyn.* **227,** 511–523 (2003).

179. Ishii, Y., Garriock, R. J., Navetta, A. M., Coughlin, L. E. & Mikawa, T. BMP signals promote proepicardial protrusion necessary for recruitment of coronary vessel and epicardial progenitors to the heart. *Dev. Cell* **19,** 307–316 (2010).

180. Hatcher, C. J. *et al.* A role for Tbx5 in proepicardial cell migration during cardiogenesis. *Physiol. Genomics* **18,** 129–140 (2004).

181. Yang, J. T., Rayburn, H. & Hynes, R. O. Cell adhesion events mediated by α4 integrins are essential in placental and cardiac development. *Development* **121,** 549–560 (1995).

182. Kwee, L. *et al.* Defective development of the embryonic and extraembryonic circulatory systems in vascular cell adhesion molecule (VCAM-1) deficient mice. *Development* **121,** 489–503 (1995).

183. Peralta, M. *et al.* Heartbeat-driven pericardiac fluid forces contribute to epicardium morphogenesis. *Curr. Biol.* **23,** 1726–1735 (2013).

184. Merki, E. *et al.* Epicardial retinoid X receptor α is required for myocardial growth and coronary artery formation. *Proc. Natl. Acad. Sci. U. S. A.* **102,** 18455–18460 (2005).

185. Zamora, M., Männer, J. & Ruiz-Lozano, P. Epicardium-derived progenitor cells require β-catenin for coronary artery formation. *Proc. Natl. Acad. Sci. U. S. A.* **104,** 18109–18114 (2007).

186. Mellgren, A. M. *et al.* Platelet-derived growth factor receptor β signaling is required for efficient epicardial cell migration and development of two distinct coronary vascular smooth muscle cell populations. *Circ. Res.* **103,** 1393–1401 (2008).

187. Sridurongrit, S., Larsson, J., Schwartz, R., Ruiz-Lozano, P. & Kaartinen, V. Signaling via the Tgf-β type I receptor Alk5 in heart development. *Dev. Biol.* **322,** 208–218 (2008).

188. Zeini, M. *et al.* Spatial and temporal regulation of coronary vessel formation by calcineurin-NFAT signaling. *Development* **136,** 3335–3345 (2009).

189. Zhou, B. *et al.* Fog2 is critical for cardiac function and maintenance of coronary vasculature in the adult mouse heart. *J. Clin. Invest.* **119,** 1462–1476 (2009).

190. Martínez-Estrada, O. M. *et al.* Wt1 is required for cardiovascular progenitor cell formation through transcriptional control of Snail and E-cadherin. *Nat. Genet.* **42,** 89–93 (2010).

191. Singh, M. K., Lu, M. M., Massera, D. & Epstein, J. A. MicroRNA-processing enzyme dicer is required in epicardium for coronary vasculature development. *J. Biol. Chem.* **286,** 41036–41045 (2011).

192. Combs, M. D., Braitsch, C. M., Lange, A. W., James, J. F. & Yutzey, K. E. NFATC1 promotes epicardium-derived cell invasion into myocardium. *Development* **138,** 1747–1757 (2011).

193. Smith, C. L., Baek, S. T., Sung, C. Y. & Tallquist, M. D. Epicardial-derived cell epithelial-to-mesenchymal transition and fate specification require PDGF receptor signaling. *Circ. Res.* **108,** (2011).

194. Von Gise, A. *et al.* WT1 regulates epicardial epithelial to mesenchymal transition through β-catenin and retinoic acid signaling pathways. *Dev. Biol.* **356,** 421–431 (2011).

195. Vega-Hernández, M., Kovacs, A., de Langhe, S. & Ornitz, D. M. FGF10/FGFR2b signaling is essential for cardiac fibroblast development and growth of the myocardium. *Development* **138,** 3331–3340 (2011).

196. Tallquist, M. D. & Baek, S. T. Nf1 limits epicardial derivative expansion by regulating epithelial to mesenchymal transition and proliferation. *Development* **139,** 2040–2049 (2012).

197. Rudat, C., Norden, J., Taketo, M. M. & Kispert, A. Epicardial function of canonical Wnt-, Hedgehog-, Fgfr1/2-, and Pdgfra-signalling. *Cardiovasc. Res.* **100,** 411–421 (2013).

198. Wei, K. *et al.* Developmental origin of age-related coronary artery disease. *Cardiovasc. Res.* **107,** 287–294 (2015).

199. Trembley, M. A., Velasquez, L. S., de Mesy Bentley, K. L. & Small, E. M. Myocardin-related transcription factors control the motility of epicardium-derived cells and the maturation of coronary vessels. *Dev.* **142,** 21–30 (2015).

200. Singh, A. *et al.* Hippo signaling mediators Yap and Taz are required in the epicardium for coronary vasculature development HHS Public Access. *Cell Rep* **15,** 1384–1393 (2016).

201. Arora, H. *et al.* Prokineticin receptor-1 signaling promotes Epicardial to Mesenchymal Transition during heart development. *Sci. Rep.* **6,** (2016).

202. Iyer, S. *et al.* Crim1 has cell-autonomous and paracrine roles during embryonic heart development. *Sci. Rep.* **6,** (2016).

203. Greulich, F., Rudat, C., Farin, H. F., Christoffels, V. M. & Kispert, A. Lack of genetic interaction between Tbx18 and Tbx2/Tbx20 in mouse epicardial development. *PLoS One* **11,** (2016).

204. Vieira, J. M. *et al.* BRG1-SWI/SNF-dependent regulation of the Wt1 transcriptional landscape mediates epicardial activity during heart development and disease. *Nat. Commun.* **8,** (2017).

205. Ramjee, V. *et al.* Epicardial YAP/TAZ orchestrate an immunosuppressive response following myocardial infarction. *J. Clin. Invest.* **127,** 899–911 (2017).

206. Liu, X. *et al.* Wdpcp promotes epicardial EMT and epicardium-derived cell migration to facilitate coronary artery remodeling. *Sci. Signal.* **11,** (2018).

207. Xiao, Y. *et al.* Hippo Signaling Plays an Essential Role in Cell State Transitions during Cardiac Fibroblast Development. *Dev. Cell* **45,** 153–169.e6 (2018).

208. Quijada, P. *et al.* Pre-existing fibroblasts of epicardial origin are the primary source of pathological fibrosis in cardiac ischemia and aging. *J. Mol. Cell. Cardiol.* **129,** 92–104 (2019).

209. Wu, M. *et al.* Epicardial Spindle Orientation Controls Cell Entry into the Myocardium. *Dev. Cell* **19,** 114–125 (2010).

210. Simões, F. C. & Riley, P. R. The ontogeny, activation and function of the epicardium during heart development and regeneration. *Development (Cambridge)* **145,** (2018).

211. Braitsch, C. M., Combs, M. D., Quaggin, S. E. & Yutzey, K. E. Pod1/Tcf21 is regulated by retinoic acid signaling and inhibits differentiation of epicardium-derived cells into smooth muscle in the developing heart. *Dev. Biol.* **368,** 345–357 (2012).

212. Katz, T. C. *et al.* Distinct Compartments of the Proepicardial Organ Give Rise to Coronary Vascular Endothelial Cells. *Dev. Cell* **22,** 639–650 (2012).

213. Plavicki, J. S. *et al.* Multiple modes of proepicardial cell migration require heartbeat. *BMC Dev. Biol.* **14,** (2014).

214. Weinberger, M., Simões, F. C., Patient, R., Sauka-Spengler, T. & Riley, P. R. Functional Heterogeneity within the Developing Zebrafish Epicardium. *Dev. Cell* **52,** 574–590.e6 (2020).

215. Cano, E. *et al.* Extracardiac septum transversum/proepicardial endothelial cells pattern embryonic coronary arterio-venous connections. *Proc. Natl. Acad. Sci. U. S. A.* **113,** 656–661 (2016).

216. Cai, C. L. *et al.* A myocardial lineage derives from Tbx18 epicardial cells. *Nature* **454,** 104–108 (2008).

217. Volz, K. S. *et al.* Pericytes are progenitors for coronary artery smooth muscle. *Elife* **4,** (2015).

218. Guimarães-Camboa, N. *et al.* Pericytes of Multiple Organs Do Not Behave as Mesenchymal Stem Cells In Vivo. *Cell Stem Cell* **20,** 345–359.e5 (2017).

219. Acharya, A. *et al.* The bHLH transcription factor Tcf21 is required for lineagespecific EMT of cardiac fibroblast progenitors. *Dev.* **139,** 2139–2149 (2012).

220. Acharya, A., Baek, S. T., Banfi, S., Eskiocak, B. & Tallquist, M. D. Efficient inducible Cre-mediated recombination in Tcf21cell lineages in the heart and kidney. *Genesis* **49,** 870–877 (2011).

221. Wessels, A. *et al.* Epicardially derived fibroblasts preferentially contribute to the parietal leaflets of the atrioventricular valves in the murine heart. *Dev. Biol.* **366,** 111–124 (2012).

222. Zhou, B., von Gise, A., Ma, Q., Hu, Y. W. & Pu, W. T. Genetic fate mapping demonstrates contribution of epicardium-derived cells to the annulus fibrosis of the mammalian heart. *Dev. Biol.* **338,** 251–261 (2010).

223. Trembley, M. A., Velasquez, L. S., de Mesy Bentley, K. L. & Small, E. M. Myocardin-related transcription factors control the motility of epicardium-derived cells and the maturation of coronary vessels. *Dev.* **142,** 21–30 (2015).

224. Zhou, B. & Pu, W. T. Genetic Cre-loxP assessment of epicardial cell fate using Wt1-Driven cre alleles. *Circulation Research* **111,** (2012).

225. Rudat, C. & Kispert, A. Wt1 and epicardial fate mapping. *Circ. Res.* **111,** 165–169 (2012).

226. Wu, S. P., Dong, X. R., Regan, J. N., Su, C. & Majesky, M. W. Tbx18 regulates development of the epicardium and coronary vessels. *Dev. Biol.* **383,** 307–320 (2013).

227. Lupu, I. E., Redpath, A. N. & Smart, N. Spatiotemporal Analysis Reveals Overlap of Key Proepicardial Markers in the Developing Murine Heart. *Stem Cell Reports* **14,** 770–787 (2020).

228. Carmona, R., Barrena, S., López Gambero, A. J., Rojas, A. & Muñoz-Chápuli, R. Epicardial cell lineages and the origin of the coronary endothelium. *FASEB J.* **34,** 5223–5239 (2020).

229. Zhou, B. *et al.* Epicardial progenitors contribute to the cardiomyocyte lineage in the developing heart. *Nature* **454,** 109–13 (2008).

230. Velecela, V. *et al.* Epicardial cell shape and maturation are regulated by Wt1 via transcriptional control of Bmp4. *Dev.* **146,** (2019).

231. Yamaguchi, Y. *et al.* Adipogenesis and epicardial adipose tissue: A novel fate of the epicardium induced by mesenchymal transformation and PPARγ activation. *Proc. Natl. Acad. Sci. U. S. A.* **112,** 2070–2075 (2015).

232. Le Jemtel, T. H., Samson, R., Ayinapudi, K., Singh, T. & Oparil, S. Epicardial Adipose Tissue and Cardiovascular Disease. *Current Hypertension Reports* **21,** (2019).

233. Stevens, S. M., von Gise, A., VanDusen, N., Zhou, B. & Pu, W. T. Epicardium is required for cardiac seeding by yolk sac macrophages, precursors of resident macrophages of the adult heart. *Dev. Biol.* **413,** 153–159 (2016).

234. Balmer, G. M. *et al.* Dynamic haematopoietic cell contribution to the developing and adult epicardium. *Nat. Commun.* **5,** (2014).

235. Velecela, V. *et al.* WT1 regulates the expression of inhibitory chemokines during heart development. *Hum. Mol. Genet.* **22,** 5083–5095 (2013).

236. Shen, H. *et al.* Extracardiac control of embryonic cardiomyocyte proliferation and ventricular wall expansion. *Cardiovasc. Res.* **105,** 271–278 (2015).

237. Li, P. *et al.* IGF signaling directs ventricular cardiomyocyte proliferation during embryonic heart development. *Development* **138,** 1795–1805 (2011).

238. Lavine, K. J. *et al.* Endocardial and epicardial derived FGF signals regulate myocardial proliferation and differentiation in vivo. *Dev. Cell* **8,** 85–95 (2005).

239. Pennisi, D. J. & Mikawa, T. Normal patterning of the coronary capillary plexus is dependent on the correct transmural gradient of FGF expression in the myocardium. *Dev. Biol.* **279,** 378–390 (2005).

240. Kastner *et al.* Genetic analysis of RXR alpha developmental function: convergence of RXR and RAR signaling pathways in heart and eye morphogenesis. *Cell* **78,** 987–1003 (1994).

241. Sucov, H. M. *et al.* RXRα mutant mice establish a genetic basis for vitamin A signaling in heart morphogenesis. *Genes Dev.* **8,** 1007–1018 (1994).

242. Niederreither, K. *et al.* Embryonic retinoic acid synthesis is essential for heart morphogenesis in the mouse. *Development* **128,** 1019–1031 (2001).

243. Guadix, J. A. *et al.* Wt1 controls retinoic acid signalling in embryonic epicardium through transcriptional activation of Raldh2s. *Development* **138,** 1093–1097 (2011).

244. Nieto, M. A., Huang, R. Y. Y. J., Jackson, R. A. A. & Thiery, J. P. P. EMT: 2016. *Cell* **166,** 21–45 (2016).

245. Pei, D., Shu, X., Gassama-Diagne, A. & Thiery, J. P. Mesenchymal–epithelial transition in development and reprogramming. *Nature Cell Biology* **21,** 44–53 (2019).

246. Yang, J. *et al.* Guidelines and definitions for research on epithelial–mesenchymal transition. *Nature Reviews Molecular Cell Biology* **21,** 341–352 (2020).

247. Von Gise, A. & Pu, W. T. Endocardial and epicardial epithelial to mesenchymal transitions in heart development and disease. *Circ. Res.* **110,** 1628–1645 (2012).

248. Carmona, R., Ariza, L., Cano, E., Jiménez-Navarro, M. & Muñoz-Chápuli, R. Mesothelial-mesenchymal transitions in embryogenesis. *Seminars in Cell and Developmental Biology* **92,** 37–44 (2019).

249. Zhang, Y. & Weinberg, R. A. Epithelial-to-mesenchymal transition in cancer: complexity and opportunities. *Frontiers of Medicine* **12,** 361–373 (2018).

250. Shaw, T. J. & Martin, P. Wound repair: A showcase for cell plasticity and migration. *Current Opinion in Cell Biology* **42,** 29–37 (2016).

251. Lamouille, S., Xu, J. & Derynck, R. Molecular mechanisms of epithelial-mesenchymal transition. *Nature Reviews Molecular Cell Biology* **15,** 178–196 (2014).

252. Lamouille, S., Subramanyam, D., Blelloch, R. & Derynck, R. Regulation of epithelial-mesenchymal and mesenchymal-epithelial transitions by micrornas. *Current Opinion in Cell Biology* **25,** 200–207 (2013).

253. Warzecha, C. C. & Carstens, R. P. Complex changes in alternative pre-mRNA splicing play a central role in the epithelial-to-mesenchymal transition (EMT). *Seminars in Cancer Biology* **22,** 417–427 (2012).

254. Compton, L. A., Potash, D. A., Brown, C. B. & Barnett, J. V. Coronary vessel development is dependent on the type III transforming growth factor β receptor. *Circ. Res.* **101,** 784–791 (2007).

255. Molin, D. G. M. *et al.* Expression patterns of Tgfβ1-3 associate with myocardialisation of the outflow tract and the development of the epicardium and the fibrous heart skeleton. *Dev. Dyn.* **227,** 431–444 (2003).

256. Morabito, C. J., Dettman, R. W., Kattan, J., Collier, J. M. & Bristow, J. Positive and negative regulation of epicardial-mesenchymal transformation during avian heart development. *Dev. Biol.* **234,** 204–215 (2001).

257. Craig, E. A., Austin, A. F., Vaillancourt, R. R., Barnett, J. V. & Camenisch, T. D. TGFβ2-mediated production of hyaluronan is important for the induction of epicardial cell differentiation and invasion. *Exp. Cell Res.* **316,** 3397–3405 (2010).

258. Pennisi, D. J. & Mikawa, T. FGFR-1 is required by epicardium-derived cells for myocardial invasion and correct coronary vascular lineage differentiation. *Dev. Biol.* **328,** 148–159 (2009).

259. Smart, N. *et al.* Thymosin β4 induces adult epicardial progenitor mobilization and neovascularization. *Nature* **445,** 177–182 (2007).

260. Bax, N. A. M. *et al.* Cardiac malformations in Pdgfrα mutant embryos are associated with increased expression of WT1 and Nkx2.5 in the second heart field. *Dev. Dyn.* **239,** 2307–2317 (2010).

261. Smith, C. L., Baek, S. T., Sung, C. Y. & Tallquist, M. D. Epicardial-derived cell epithelial-to-mesenchymal transition and fate specification require PDGF receptor signaling. *Circ. Res.* **108,** (2011).

262. Moore, A. W., McInnes, L., Kreidberg, J., Hastie, N. D. & Schedl, A. YAC complementation shows a requirement for Wt1 in the development of epicardium, adrenal gland and throughout nephrogenesis. *Development* **126,** 1845–57 (1999).

263. Shikama, N. *et al.* Essential function of p300 acetyltransferase activity in heart, lung and small intestine formation. *EMBO J.* **22,** 5175–5185 (2003).

264. Urist, M. R. Bone: Formation by autoinduction. *Science (80-. ).* **150,** 893–899 (1965).

265. Wozney, J. M. *et al.* Novel regulators of bone formation: molecular clones and activities. *Science (80-. ).* **242,** 1528–1534 (1988).

266. Mueller, T. D. & Nickel, J. Promiscuity and specificity in BMP receptor activation. *FEBS Letters* **586,** 1846–1859 (2012).

267. Wang, R. N. *et al.* Bone Morphogenetic Protein (BMP) signaling in development and human diseases. *Genes and Diseases* **1,** 87–105 (2014).

268. De Caestecker, M. The transforming growth factor-β superfamily of receptors. *Cytokine and Growth Factor Reviews* **15,** 1–11 (2004).

269. Zhang, Y. E. Non-Smad signaling pathways of the TGF-β family. *Cold Spring Harb. Perspect. Biol.* **9,** (2017).

270. Winnier, G., Blessing, M., Labosky, P. A. & Hogan, B. L. M. Bone morphogenetic protein-4 is required for mesoderm formation and patterning in the mouse. *Genes Dev.* **9,** 2105–2116 (1995).

271. Lawson, K. A. *et al.* Bmp4 is required for the generation of primordial germ cells in the mouse embryo. *Genes Dev.* **13,** 424–436 (1999).

272. Furuta, Y. & Hogan, B. L. M. BMP4 is essential for lens induction in the mouse embryo. *Genes Dev.* **12,** 3764–3775 (1998).

273. Selever, J., Liu, W., Lu, M. F., Behringer, R. R. & Martin, J. F. Bmp4 in limb bud mesoderm regulates digit pattern by controlling AER development. *Dev. Biol.* **276,** 268–279 (2004).

274. Bergmann, O. *et al.* Evidence for cardiomyocyte renewal in humans. *Science (80-. ).* **324,** 98–102 (2009).

275. Menasché, P. Cell therapy trials for heart regeneration — lessons learned and future directions. *Nature Reviews Cardiology* **15,** 659–671 (2018).

276. Lien, C. L., Harrison, M. R., Tuan, T. L. & Starnes, V. A. Heart repair and regeneration: Recent insights from zebrafish studies. *Wound Repair and Regeneration* **20,** 638–646 (2012).

277. Porrello, E. R. *et al.* Transient regenerative potential of the neonatal mouse heart. *Science (80-. ).* **331,** 1078–1080 (2011).

278. Haubner, B. J. *et al.* Functional Recovery of a Human Neonatal Heart after Severe Myocardial Infarction. *Circ. Res.* **118,** 216–221 (2016).

279. Wang, J., Cao, J., Dickson, A. L. & Poss, K. D. Epicardial regeneration is guided by cardiac outflow tract and Hedgehog signalling. *Nature* **522,** 226–230 (2015).

280. Lepilina, A. *et al.* A Dynamic Epicardial Injury Response Supports Progenitor Cell Activity during Zebrafish Heart Regeneration. *Cell* **127,** 607–619 (2006).

281. Ruiz-Villalba, A. *et al.* Interacting resident epicardium-derived fibroblasts and recruited bone marrow cells form myocardial infarction scar. *J. Am. Coll. Cardiol.* **65,** 2057–2066 (2015).

282. Van Wijk, B., Gunst, Q. D., Moorman, A. F. M. & van den Hoff, M. J. B. Cardiac Regeneration from Activated Epicardium. *PLoS One* **7,** (2012).

283. Cao, J. *et al.* Tension Creates an Endoreplication Wavefront that Leads Regeneration of Epicardial Tissue. *Dev. Cell* **42,** 600–615.e4 (2017).

284. González-Rosa, J. M., Peralta, M. & Mercader, N. Pan-epicardial lineage tracing reveals that epicardium derived cells give rise to myofibroblasts and perivascular cells during zebrafish heart regeneration. *Dev. Biol.* **370,** 173–186 (2012).

285. Marro, J., Pfefferli, C., De Charles, A. S. P., Bise, T. & Jaźwińska, A. Collagen XII contributes to epicardial and connective tissues in the zebrafish heart during ontogenesis and regeneration. *PLoS One* **11,** (2016).

286. Wang, J., Karra, R., Dickson, A. L. & Poss, K. D. Fibronectin is deposited by injury-activated epicardial cells and is necessary for zebrafish heart regeneration. *Dev. Biol.* **382,** 427–435 (2013).

287. Zhou, B. *et al.* Adult mouse epicardium modulates myocardial injury by secreting paracrine factors. *J. Clin. Invest.* **121,** 1894–1904 (2011).

288. Kikuchi, K. *et al.* Retinoic Acid Production by Endocardium and Epicardium Is an Injury Response Essential for Zebrafish Heart Regeneration. *Dev. Cell* **20,** 397–404 (2011).

289. Wei, K. *et al.* Epicardial FSTL1 reconstitution regenerates the adult mammalian heart. *Nature* **525,** 479–485 (2015).

290. Kikuchi, K. *et al.* Tcf21+ epicardial cells adopt non-myocardial fates during zebrafish heart development and regeneration. *Development* **138,** 2895–2902 (2011).

291. Zhou, B. & Pu, W. T. Epicardial epithelial-to-mesenchymal transition in injured heart. *J. Cell. Mol. Med.* **15,** 2781–2783 (2011).

292. Liu, Q. *et al.* Epicardium-to-fat transition in injured heart. *Cell Research* **24,** 1367–1369 (2014).

293. Huang, G. N. *et al.* C/EBP transcription factors mediate epicardial activation during heart development and injury. *Science (80-. ).* **338,** 1599–1603 (2012).

294. Bock-Marquette, I. *et al.* Thymosin β4 mediated PKC activation is essential to initiate the embryonic coronary developmental program and epicardial progenitor cell activation in adult mice in vivo. *J. Mol. Cell. Cardiol.* **46,** 728–738 (2009).

295. Smart, N. *et al.* Thymosin β4 facilitates epicardial neovascularization of the injured adult heart. in *Annals of the New York Academy of Sciences* **1194,** 97–104 (2010).

296. Smart, N. *et al.* De novo cardiomyocytes from within the activated adult heart after injury. *Nature* **474,** 640–644 (2011).

297. Costantini, F. & Kopan, R. Patterning a complex organ: Branching morphogenesis and nephron segmentation in kidney development. *Developmental Cell* **18,** 698–712 (2010).

298. Donovan, M. J. *et al.* Initial differentiation of the metanephric mesenchyme is independent of WT1 and the ureteric bud. *Dev. Genet.* **24,** 252–262 (1999).

299. Davies, J. A. *et al.* Development of an siRNA-based method for repressing specific genes in renal organ culture and its use to show that the Wt1 tumour suppressor is required for nephron differentiation. *Human Molecular Genetics* **13,** 235–246 (2004).

300. Hu, Q. *et al.* Wt1 ablation and Igf2 upregulation in mice result in Wilms tumors with elevated ERK1/2 phosphorylation. *J. Clin. Invest.* **121,** 174–183 (2011).

301. Sim, E. U. H. *et al.* Wnt-4 regulation by the Wilms' tumour suppressor gene, WT1. *Oncogene* **21,** 2948–2960 (2002).

302. Berry, R. L. *et al.* Deducing the stage of origin of Wilms' tumours from a developmental series of Wt1-mutant mice. *DMM Dis. Model. Mech.* **8,** 903–917 (2015).

303. Hammes, A. *et al.* Two splice variants of the wilms' tumor 1 gene have distinct functions during sex determination and nephron formation. *Cell* **106,** 319–329 (2001).

304. Menke, A. L. *et al.* Thewt1-heterozygous mouse; a model to study the development of glomerular sclerosis. *J. Pathol.* **200,** 667–674 (2003).

305. Guo, J.-K. WT1 is a key regulator of podocyte function: reduced expression levels cause crescentic glomerulonephritis and mesangial sclerosis. *Hum. Mol. Genet.* **11,** 651–659 (2002).

306. Gao, F. *et al.* The Wt1+/R394W Mouse Displays Glomerulosclerosis and Early-Onset Renal Failure Characteristic of Human Denys-Drash Syndrome. *Mol. Cell. Biol.* **24,** 9899–9910 (2004).

307. Ratelade, J. *et al.* A murine model of Denys-Drash syndrome reveals novel transcriptional targets of WT1 in podocytes. *Hum. Mol. Genet.* **19,** 1–15 (2009).

308. Que, J. *et al.* Mesothelium contributes to vascular smooth muscle and mesenchyme during lung development. *Proc. Natl. Acad. Sci. U. S. A.* **105,** 16626–16630 (2008).

309. Cano, E., Carmona, R. & Muñoz-Chápuli, R. Wt1-expressing progenitors contribute to multiple tissues in the developing lung. *Am. J. Physiol. - Lung Cell. Mol. Physiol.* **305,** (2013).

310. Ariza, L., Cañete, A., Rojas, A., Muñoz-Chápuli, R. & Carmona, R. Role of the Wilms' tumor suppressor gene Wt1 in pancreatic development. *Dev. Dyn.* **247,** 924–933 (2018).

311. Ijpenberg, A. *et al.* Wt1 and retinoic acid signaling are essential for stellate cell development and liver morphogenesis. *Dev. Biol.* **312,** 157–170 (2007).

312. Chau, Y. Y. *et al.* Acute multiple organ failure in adult mice deleted for the developmental regulator Wt1. *PLoS Genet.* **7,** (2011).

313. Chau, Y. Y. *et al.* Visceral and subcutaneous fat have different origins and evidence supports a mesothelial source. *Nat. Cell Biol.* **16,** 367–375 (2014).

314. Cohen, P. *et al.* Ablation of PRDM16 and beige adipose causes metabolic dysfunction and a subcutaneous to visceral fat switch. *Cell* **156,** 304–316 (2014).

315. Ariza, L., Rojas, A., Muñoz-Chápuli, R. & Carmona, R. The Wilms' tumor suppressor gene regulates pancreas homeostasis and repair. *PLoS Genet.* **15,** (2019).

316. Gebeshuber, C. A. *et al.* Focal segmental glomerulosclerosis is induced by microRNA-193a and its downregulation of WT1. *Nat. Med.* **19,** 481–487 (2013).

317. Bandiera, R. *et al.* WT1 Maintains Adrenal-Gonadal Primordium Identity and Marks a Population of AGP-like Progenitors within the Adrenal Gland. *Dev. Cell* **27,** 5–18 (2013).

318. GTEx Portal. at <https://gtexportal.org/home/gene/WT1>

319. Hoess, R. H., Wierzbicki, A. & Abremski, K. The role of the loxP spacer region in PI site-specific recombination. *Nucleic Acids Res.* **14,** 2287–2300 (1986).

320. Sauer, B. & Henderson, N. Targeted insertion of exogenous DNA into the eukaryotic genome by the Cre recombinase. *New Biol.* **2,** 441–449 (1990).

321. Lakso, M. *et al.* Targeted oncogene activation by site-specific recombination in transgenic mice. *Proc. Natl. Acad. Sci. U. S. A.* **89,** 6232–6236 (1992).

322. Orban, P. C., Chui, D. & Marth, J. D. Tissue- and site-specific DNA recombination in transgenic mice. *Proc. Natl. Acad. Sci. U. S. A.* **89,** 6861–6865 (1992).

323. Hosen, N. *et al.* The Wilms' tumor gene WT1-GFP knock-in mouse reveals the dynamic regulation of WT1 expression in normal and leukemic hematopoiesis. *Leukemia* **21,** 1783–1791 (2007).

324. Muzumdar, M. D., Tasic, B., Miyamichi, K., Li, N. & Luo, L. A global double-fluorescent cre reporter mouse. *Genesis* **45,** 593–605 (2007).

325. Luche, H., Weber, O., Rao, T. N., Blum, C. & Fehling, H. J. Faithful activation of an extra-bright red fluorescent protein in 'knock-in' Cre-reporter mice ideally suited for lineage tracing studies. *Eur. J. Immunol.* **37,** 43–53 (2007).

326. Abràmoff, M. D., Magalhães, P. J. & Ram, S. J. Image processing with imageJ. *Biophotonics International* **11,** 36–41 (2004).

327. Trescos, Y., Tessier, E., Rougeaux, C., Goossens, P. L. & Tournier, J. N. Micropatterned macrophage analysis reveals global cytoskeleton constraints induced by Bacillus anthracis edema toxin. *Infect. Immun.* **83,** 3114–3125 (2015).

328. Jat, P. S. *et al.* Direct derivation of conditionally immortal cell lines from an H-2Kb-tsA58 transgenic mouse. *Proc. Natl. Acad. Sci. U. S. A.* **88,** 5096–5100 (1991).

329. Perez-Vale, K. Z. & Peifer, M. Orchestrating morphogenesis: building the body plan by cell shape changes and movements. *Development (Cambridge, England)* **147,** (2020).

330. Jidigam, V. K., Srinivasan, R. C., Patthey, C. & Gunhaga, L. Apical constriction and epithelial invagination are regulated by BMP activity. *Biol. Open* 1–10 (2015). doi:10.1242/bio.015263

331. Da Silva-Buttkus, P. *et al.* Effect of cell shape and packing density on granulosa cell proliferation and formation of multiple layers during early follicle development in the ovary. *J. Cell Sci.* **121 ,** 3890–3900 (2008).

332. Yu, P. B. *et al.* Dorsomorphin inhibits BMP signals required for embryogenesis and iron metabolism. *Nat. Chem. Biol.* **4,** 33–41 (2008).

333. Cuny, G. D. *et al.* Structure-activity relationship study of bone morphogenetic protein (BMP) signaling inhibitors. *Bioorganic Med. Chem. Lett.* **18,** 4388–4392 (2008).

334. Shandilya, J., Toska, E., Richard, D. J., Medler, K. F. & Roberts, S. G. E. WT1 interacts with MAD2 and regulates mitotic checkpoint function. *Nat. Commun.* **5,** 4903 (2014).

335. Loeb, D. M. *et al.* Cyclin E is a target of WT1 transcriptional repression. *J. Biol. Chem.* **277,** 19627–19632 (2002).

336. Strilić, B. *et al.* Electrostatic cell-surface repulsion initiates lumen formation in developing blood vessels. *Curr. Biol.* **20,** 2003–2009 (2010).

337. Magin, T. M., Vijayaraj, P. & Leube, R. E. Structural and regulatory functions of keratins. *Experimental Cell Research* **313,** 2021–2032 (2007).

338. Genander, M. *et al.* BMP Signaling and Its pSMAD1/5 Target Genes Differentially Regulate Hair Follicle Stem Cell Lineages. *Cell Stem Cell* **15,** 619–633 (2014).

339. Kawanishi, K. Diverse properties of the mesothelial cells in health and disease. *Pleura and Peritoneum* **1,** 79–89 (2016).

340. Tunster, S. J. Genetic sex determination of mice by simplex PCR. *Biol. Sex Differ.* **8,** (2017).

341. Nicol, B. *et al.* RUNX1 maintains the identity of the fetal ovary through an interplay with FOXL2. *Nat. Commun.* **10,** (2019).

342. Bouma, G. J., Hudson, Q. J., Washburn, L. L. & Eicher, E. M. New candidate genes identified for controlling mouse gonadal sex determination and the early stages of granulosa and Sertoli cell differentiation. *Biol. Reprod.* **82,** 380–389 (2010).

343. Cen, C. *et al.* Inactivation of Wt1 causes pre-granulosa cell to steroidogenic cell transformation and defect of ovary development. *Biol. Reprod.* **103,** 60–69 (2020).

344. Anderson, E. L. *et al.* Stra8 and its inducer, retinoic acid, regulate meiotic initiation in both spermatogenesis and oogenesis in mice. *Proc. Natl. Acad. Sci. U. S. A.* **105,** 14976–14980 (2008).

345. Sedmera, D., Pexieder, T., Vuillemin, M., Thompson, R. P. & Anderson, R. H. Developmental patterning of the myocardium. *Anatomical Record* **258,** 319–337 (2000).

346. Andrés-Delgado, L. *et al.* Actin dynamics and the Bmp pathway drive apical extrusion of proepicardial cells. *Dev.* **146,** (2019).

347. Wilkinson, L. *et al.* CRIM1 Regulates the Rate of Processing and Delivery of Bone Morphogenetic Proteins to the Cell Surface. *J. Biol. Chem.* **278,** 34181–34188 (2003).

348. Larraín, J. *et al.* BMP-binding modules in chordin: A model for signalling regulation in the extracellular space. *Development* **127,** 821–830 (2000).

349. Dechat, T., Adam, S. A., Taimen, P., Shimi, T. & Goldman, R. D. Nuclear lamins. *Cold Spring Harbor perspectives in biology* **2,** (2010).

350. Burke, B. & Stewart, C. L. The nuclear lamins: Flexibility in function. *Nature Reviews Molecular Cell Biology* **14,** 13–24 (2013).

351. Gruenbaum, Y. & Foisner, R. Lamins: Nuclear Intermediate Filament Proteins with Fundamental Functions in Nuclear Mechanics and Genome Regulation. *Annu. Rev. Biochem.* **84,** 131–164 (2015).

352. Dahl, K. N., Ribeiro, A. J. S. & Lammerding, J. Nuclear shape, mechanics, and mechanotransduction. *Circulation Research* **102,** 1307–1318 (2008).

353. Tran, J. R., Zheng, X. & Zheng, Y. Lamin-B1 contributes to the proper timing of epicardial cell migration and function during embryonic heart development. *Mol. Biol. Cell* **27,** 3956–3963 (2016).

354. Fernández, B. G., Arias, A. M. & Jacinto, A. Dpp signalling orchestrates dorsal closure by regulating cell shape changes both in the amnioserosa and in the epidermis. *Mech. Dev.* **124,** 884–897 (2007).

355. Nilsson, E. E. & Skinner, M. K. Bone morphogenetic protein-4 acts as an ovarian follicle survival factor and promotes primordial follicle development. *Biol. Reprod.* **69,** 1265–1272 (2003).

356. Byrnes, L. E. *et al.* Lineage dynamics of murine pancreatic development at single-cell resolution. *Nat. Commun.* **9,** (2018).

357. Ariza, L., Rojas, A., Muñoz-Chápuli, R. & Carmona, R. The Wilms' tumor suppressor gene regulates pancreas homeostasis and repair. *PLoS Genet.* **15,** (2019).

358. Wu, C. C. *et al.* Spatially Resolved Genome-wide Transcriptional Profiling Identifies BMP Signaling as Essential Regulator of Zebrafish Cardiomyocyte Regeneration. *Dev. Cell* **36,** 36–49 (2016).

359. Cao, J. *et al.* Single epicardial cell transcriptome sequencing identifies caveolin 1 as an essential factor in zebrafish heart regeneration. *Dev.* **143,** 232–243 (2016).

360. Pachori, A. S. *et al.* Bone morphogenetic protein 4 mediates myocardial ischemic injury through JNK-dependent signaling pathway. *J. Mol. Cell. Cardiol.* **48,** 1255–1265 (2010).

361. Antebi, Y. E. *et al.* Combinatorial Signal Perception in the BMP Pathway. *Cell* **170,** 1184–1196.e24 (2017).

362. Petridou, N. I., Spiró, Z. & Heisenberg, C. P. Multiscale force sensing in development. *Nature Cell Biology* **19,** 581–588 (2017).

363. Heisenberg, C. P. & Bellaïche, Y. XForces in tissue morphogenesis and patterning. *Cell* **153,** 948 (2013).

364. Majkut, S. *et al.* Heart-specific stiffening in early embryos parallels matrix and myosin expression to optimize beating. *Curr. Biol.* **23,** 2434–2439 (2013).

365. Rens, E. G. & Merks, R. M. H. Cell Shape and Durotaxis Explained from Cell-Extracellular Matrix Forces and Focal Adhesion Dynamics. *iScience* **23,** (2020).

366. Gao, Y., Toska, E., Denmon, D., Roberts, S. G. E. & Medler, K. F. WT1 regulates the development of the posterior taste field. *Development* **141,** 2271–2278 (2014).

367. Prummel, K. D., Nieuwenhuize, S. & Mosimann, C. The lateral plate mesoderm. *Dev.* **147,** (2020).

368. Loh, K. M. M. *et al.* Mapping the Pairwise Choices Leading from Pluripotency to Human Bone, Heart, and Other Mesoderm Cell Types. *Cell* **166,** 451–467 (2016).

369. Iyer, D. *et al.* Robust derivation of epicardium and its differentiated smooth muscle cell progeny from human pluripotent stem cells. *Dev.* **142,** 1528–1541 (2015).

370. Witty, A. D. *et al.* Generation of the epicardial lineage from human pluripotent stem cells. *Nat. Biotechnol.* **32,** 1026–35 (2014).

371. Lockhart, M. M. *et al.* Alk3 mediated Bmp signaling controls the contribution of epicardially derived cells to the tissues of the atrioventricular junction. *Dev. Biol.* **396,** 8–18 (2014).

372. Carmona, R. *et al.* Conditional deletion of WT1 in the septum transversum mesenchyme causes congenital diaphragmatic hernia in mice. *Elife* **5,** (2016).

373. Villa Del Campo, C. *et al.* Myc overexpression enhances of epicardial contribution to the developing heart and promotes extensive expansion of the cardiomyocyte population. *Sci. Rep.* **6,** (2016).

374. Carmona, R., Cano, E., Mattiotti, A., Gaztambide, J. & Muñoz-Chápuli, R. Cells Derived from the Coelomic Epithelium Contribute to Multiple Gastrointestinal Tissues in Mouse Embryos. *PLoS One* **8,** (2013).

375. Casanova, J. C., Travisano, S. & De la Pompa, J. L. Epithelial-to-mesenchymal transition in epicardium is independent of snail1. *Genesis* **51,** 32–40 (2013).

376. Yamazaki, T. *et al.* Tissue Myeloid Progenitors Differentiate into Pericytes through TGF-β Signaling in Developing Skin Vasculature. *Cell Rep.* **18,** 2991–3004 (2017).

377. Durst, S. *et al.* Mutations in DCHS1 cause mitral valve prolapse. *Nature* **525,** 109–113 (2015).

378. Dorr, K. M. *et al.* Casz1 is required for cardiomyocyte G1-to-S phase progression during mammalian cardiac development. *Dev.* **142,** 2037–2047 (2015).

379. Moore-Morris, T. *et al.* Resident fibroblast lineages mediate pressure overload-induced cardiac fibrosis. *J. Clin. Invest.* **124,** 2921–2934 (2014).

380. Van Vliet, P. P. *et al.* Tissue specific requirements for WNT11 in developing outflow tract and dorsal mesenchymal protrusion. *Dev. Biol.* **429,** 249–259 (2017).

381. Ragni, C. V. *et al.* Amotl1 mediates sequestration of the Hippo effector Yap1 downstream of Fat4 to restrict heart growth. *Nat. Commun.* **8,** (2017).

382. Diman, N. Y. S. G. *et al.* Tbx5 is required for avian and mammalian epicardial formation and coronary vasculogenesis. *Circ. Res.* **115,** 834–844 (2014).

383. Tyser, R. C. V *et al.* Characterization of a common progenitor pool of the epicardium and myocardium. *Science (80-. ).* **2986,** eabb2986 (2021).

384. Stévant, I. & Nef, S. Genetic Control of Gonadal Sex Determination and Development. *Trends in Genetics* **35,** 346–358 (2019).

385. Ainsworth, C. Sex redefined. *Nature* **518,** 288–291 (2015).

386. Witchel, S. F. Disorders of sex development. *Best Practice and Research: Clinical Obstetrics and Gynaecology* **48,** 90–102 (2018).

387. Wilhelm, D. & Englert, C. The Wilms tumor suppressor WT1 regulates early gonad development by activation of Sf1. *Genes Dev.* **16,** 1839–1851 (2002).

388. Piprek, R. P., Kloc, M. & Kubiak, J. Z. Early development of the gonads: Origin and differentiation of the somatic cells of the genital ridges. *Results Probl. Cell Differ.* **58,** (2016).

389. Hatano, O., Takakusu, A., Nomura, M. & Morohashi, K. I. Identical origin of adrenal cortex and gonad revealed by expression profiles of Ad4BP/SF-1. *Genes to Cells* **1,** 663–671 (1996).

390. Saito, D., Tamura, K. & Takahashi, Y. Early segregation of the adrenal cortex and gonad in chicken embryos. *Dev. Growth Differ.* **59,** 593–602 (2017).

391. Young, J. M. & McNeilly, A. S. Theca: The forgotten cell of the ovarian follicle. *Reproduction* **140,** 489–504 (2010).

392. Walczak, E. M. *et al.* Wnt signaling inhibits adrenal steroidogenesis by cell-autonomous and non-cell-autonomous mechanisms. *Mol. Endocrinol.* **28,** 1471–1486 (2014).

393. Hossain, A. & Saunders, G. F. Role of Wilms Tumor 1 (WT1) in the Transcriptional Regulation of the Mullerian-Inhibiting Substance Promoter. *Biol. Reprod.* **69,** 1808–1814 (2003).

394. Zhao, F. *et al.* Elimination of the male reproductive tract in the female embryo is promoted by COUP-TFII in mice. *Science (80-. ).* **357,** 717–720 (2017).

395. Gomes, N. L. *et al.* A 46,XX testicular disorder of sex development caused by a Wilms' tumour Factor-1 (WT1) pathogenic variant. *Clin. Genet.* **95,** 172–176 (2019).

396. Arnold, A. P. in *Current Topics in Developmental Biology* **134,** 289–315 (2019).

397. Arnold, A. P. Sexual differentiation of brain and other tissues: Five questions for the next 50 years. *Hormones and Behavior* **120,** (2020).

398. Arnold, A. P. Four Core Genotypes and XY* mouse models: Update on impact on SABV research. *Neuroscience and Biobehavioral Reviews* **119,** 1–8 (2020).

399. Büdefeld, T., Grgurevic, N., Tobet, S. A. & Majdic, G. Sex differences in brain developing in the presence or absence of gonads. *Dev. Neurobiol.* **68,** 981–995 (2008).

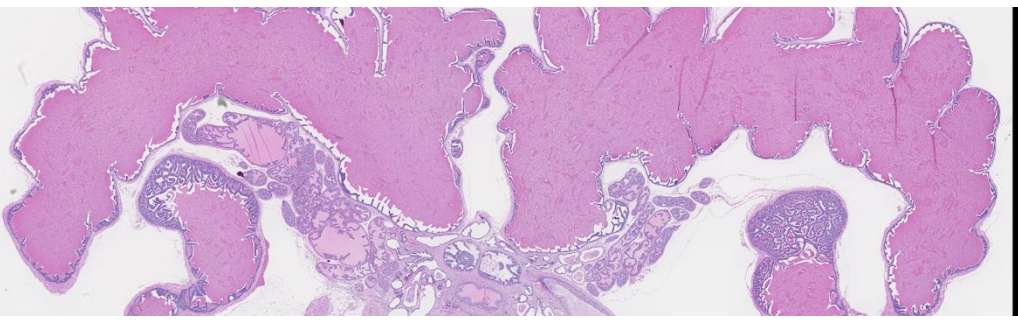

# ANNEX

## Publications derived from this thesis

- Víctor Velecela**, Alejo Torres-Cano**, Ana García-Melero, Marina Ramiro-Pareta, Claudia Müller-Sánchez, Marc Segarra-Mondejar, You-Ying Chau, Begoña Campos-Bonilla, Manuel Reina, Francesc X. Soriano, Nicholas D. Hastie, Fernando O. Martínez, Ofelia M. Martínez-Estrada. Epicardial cell shape and maturation are regulated by Wt1 via transcriptional control of *Bmp4.* Development 2019 146: dev178723.

- **Alejo Torres-Cano**, Marina Ramiro-Pareta, You-Ying Chau, Manuel Reina, Francesc X. Soriano and Ofelia M. Martínez Estrada. Deletion of *Wt1* in bipotential gonad leads to disorders of sex development in adult mice. Manuscript under preparation.